



**HAL**  
open science

# Kinematic analysis of reconfigurable parallel manipulators

Abhilash Nayak

► **To cite this version:**

Abhilash Nayak. Kinematic analysis of reconfigurable parallel manipulators. Automatic. École centrale de Nantes, 2018. English. NNT : 2018ECDN0057 . tel-02056505

**HAL Id: tel-02056505**

**<https://theses.hal.science/tel-02056505>**

Submitted on 4 Mar 2019

**HAL** is a multi-disciplinary open access archive for the deposit and dissemination of scientific research documents, whether they are published or not. The documents may come from teaching and research institutions in France or abroad, or from public or private research centers.

L'archive ouverte pluridisciplinaire **HAL**, est destinée au dépôt et à la diffusion de documents scientifiques de niveau recherche, publiés ou non, émanant des établissements d'enseignement et de recherche français ou étrangers, des laboratoires publics ou privés.

# THESE DE DOCTORAT DE

L'ÉCOLE CENTRALE DE NANTES  
COMUE UNIVERSITE BRETAGNE LOIRE

ECOLE DOCTORALE N° 602  
*Sciences pour l'Ingénieur*  
Spécialité : *Robotique - Mécanique*

Par

**Abhilash NAYAK**

## **L'analyse cinématique de manipulateurs parallèles et reconfigurables**

Thèse présentée et soutenue à Nantes, le 14 décembre 2018  
Unité de recherche : **Laboratoire des Sciences du Numérique de Nantes (LS2N)**

### **Rapporteurs avant soutenance :**

Guangbo HAO  
Belhassen Chedli BOUZGARROU

Senior Lecturer, University College Cork, Irlande  
Maître de Conférences, HDR, Sigma-Clermont, Clermont-Ferrand

### **Composition du Jury :**

Président : Manfred HUSTY

Professeur d'université, Université d'Innsbruck, Autriche

Examineurs : Manfred HUSTY  
Guangbo HAO  
Coralie GERMAIN  
Belhassen Chedli BOUZGARROU

Professeur d'université, Université d'Innsbruck, Autriche  
Senior Lecturer, University College Cork, Irlande  
Professeur agrégée SII (PRAG), Agrocampus-Ouest  
Maître de Conférences, HDR, Sigma-Clermont

Dir. de thèse : Stéphane CARO  
Co-dir. de thèse : Philippe WENGER

Directeur de recherche, CNRS, LS2N, Nantes  
Directeur de recherche, CNRS, LS2N, Nantes



# Résumé

Un manipulateur parallèle à mobilité réduite a moins de six degrés de liberté et présente généralement différents types de mouvement connus sous le nom de modes d'opération. Ainsi, ce type de manipulateur peut être classifié comme reconfigurable selon sa capacité de transition entre les différents modes d'opération. Cette thèse de doctorat s'articule principalement autour de l'analyse cinématique de manipulateurs parallèles à mobilité réduite, de manipulateurs parallèles en série obtenus à partir de leur empilement en série et de mécanismes conformes conçus à partir de leurs configurations singulières à contraintes. La transformation cinématique de Study est utilisée pour dériver les équations algébriques de contraintes. Ensuite, elles sont interprétées à l'aide d'outils de géométrie algébrique pour effectuer des analyses de mobilité, de cinématique et de singularité. Les techniques de "screw theory" et "line geometry" sont utilisées à côté de l'approche algébrique au besoin.

Cette thèse de doctorat est composée de six chapitres. Le premier chapitre présente l'état de l'art des manipulateurs parallèles, des manipulateurs parallèles en série et des mécanismes conformes. Il explique également les outils et concepts fondamentaux utilisés dans ce travail.

Dans le deuxième chapitre, l'analyse des modes d'opération de certains manipulateurs parallèles à mobilité réduite est présentée. La décomposition primaire de l'idéal des polynômes à contraintes conduit à la caractérisation des modes d'opération et des transitions entre eux. De plus, un manipulateur parallèle 4-rRUU doublement reconfigurable est analysé et des dimensions optimales sont synthétisées afin de construire un prototype fonctionnel. Le deuxième chapitre traite l'influence des paramètres de conception sur le nombre de modes d'opération d'un manipulateur parallèle de type 3-RPS.

Le troisième chapitre présente la comparaison d'une famille de manipulateurs parallèles à trois membres. Chaque membre est composé d'articulations aboutissant à deux translations coplanaires suivies d'une liaison sphérique. Ils sont comparés en fonction de leur espace de travail d'orientation sans singularité, leurs mouvements parasites et leurs complexités.

Un manipulateur parallèle en série 3-RPS-3-SPR avec un arrangement en série de deux modules manipulateurs parallèles à mobilité réduite est étudié dans le quatrième chapitre. Sa mobilité globale est calculée en tant que la dimension d'Hilbert de sa variété de contraintes. La matrice jacobienne cinématique série est formulée. De plus, les singularités sérielles sont énumérées en utilisant les conditions de dégénérescence de son tétraèdre caractéristique.

Le cinquième chapitre expose une procédure de synthèse des mécanismes conformes reconfigurables qui se basent sur les singularités de contraintes de leurs homologues rigides. Cette approche permet de concevoir un mécanisme reconfigurable conforme à quatre barres. De plus, une pince reconfigurable et conforme est conçue avec plusieurs modes de préhension.

**Mots-clés:** manipulateurs parallèles, manipulateurs série-parallèle, mécanismes conformes, transformation de Study, singularités.



# Abstract

A lower mobility parallel manipulator has less than six degrees of freedom and usually exhibits different motion types known as operation modes. Thus, it can be classified as reconfigurable on account of its ability to transition between different operation modes. This doctoral thesis mainly revolves around the kinematic analysis of some lower-mobility parallel manipulators, series-parallel manipulators obtained from their serial stacking and compliant mechanisms designed using their constraint singular configurations. Study's kinematic mapping is used to derive the algebraic constraint equations. They are further interpreted using algebraic geometry tools to perform mobility, kinematic and singularity analysis. Screw theory and line geometry techniques are used adjacent to algebraic approach wherever necessary.

This doctoral thesis is composed of six chapters. The first chapter presents the state of the art related to parallel manipulators, series-parallel manipulators and compliant mechanisms. It also explains the key fundamental tools and concepts put to use herein.

In the second chapter, operation mode analysis of some lower mobility parallel manipulators is presented. The primary decomposition of the ideal of constraint polynomials leads to the characterization of the operation modes and transitions between them. Furthermore, a dual reconfigurable 4-rRUU parallel manipulator is analyzed for some configurations whose optimal design is done in order to build a working prototype. The second chapter also discusses the influence of design parameters on the number of operation modes of a 3-RPS parallel manipulator.

Third chapter deals with the comparison of a family of parallel manipulators with three limbs, each consisting of joints resulting in two coplanar translations followed by a spherical joint. They are compared with respect to their singularity-free orientation workspace, parasitic motions and complexity indices.

A 3-RPS-3-SPR series-parallel manipulator with an in-series arrangement of two lower mobility parallel manipulator modules is studied in the fourth chapter. Its global mobility is calculated as Hilbert's dimension of its constraint variety. The serial kinematic Jacobian matrix is formulated and serial singularities are enumerated by listing the conditions for the degeneracy of its characteristic tetrahedron.

Fifth chapter introduces a procedure to synthesize reconfigurable compliant mechanisms based on the constraint singularities of their rigid counterparts. Using this approach, a reconfigurable compliant mechanisms is designed, further leading to the design of a reconfigurable compliant gripper with multiple grasping modes.

**Keywords:** parallel manipulators, series-parallel manipulators, compliant mechanisms, Study's kinematic mapping, singularities.

*Dedicated to my parents, Uday D. NAYAK and Meena G. GAONKAR.*

# Acknowledgements

I would like to thank my thesis director, Stéphane Caro for offering me this opportunity, giving me the freedom to work on my own and also for being there whenever I needed help in spite of his super-tight schedule. Thanks to his collaborations across the world, I have had the honor to meet and interact with many clever people and learn from them. My co-supervisor, Philippe Wenger for his wonderful insights and ideas, especially for letting me shamelessly drop in English words while explaining him things in French. He has been a great mentor throughout this journey. Manfred Husty, for getting me comfortable in Innsbruck and other higher dimensions. Guangbo Hao, for hosting me in Cork and for his out-of-the box ideas and techniques to deal with compliant mechanisms. The mechanic of our lab, Stéphane Jolivet for his ultimate patience to print a myriad of mechanisms and helping me fix my “plaque d’immatriculation”. All the administrative staff on the third floor of our lab, staff of École doctorale and scolarité who are incredibly nice and friendly, and make it a cakewalk to deal with the otherwise annoying administrative stuff. Shivesh Kumar and Andreas Müller for introducing me to fascinating problems and for the pleasure of working together to crack them.

My parents have always encouraged me to pursue what I like, despite many hardships they had to face. I am eternally grateful to them and my sister Anjani for their love, education and support for I wouldn’t be here without them.

PhD life wouldn’t have been so much fun without my friends. Thanks to my special friend Khaoula for sharing my happy moments by walking along Erdre and helping me through tough times also by walking along Erdre. I am also grateful to my friends and colleagues Misbah, Simon, Thomas, Saman, Haiyang, Tahir, Yassir, Sébastien, Kaëlig, Marie-Anne, Michelle, Marie France, Paco, Maggy, Chandrashekhar, Keerthana, Raghav, Chethan, Srikanth, Aditya, my cousins Srikrishna and Sriram, my office-mates Qiuyue and Joumana, for interesting discussions and beautiful memories that I cherish.



# Contents

Résumé . . . . .	0
Abstract . . . . .	2
Acknowledgements . . . . .	5
List of Figures . . . . .	11
List of Tables . . . . .	15
Glossary . . . . .	16
Nomenclature . . . . .	19

## Introduction

---

Scope of the doctoral thesis . . . . .	21
Summary . . . . .	22

## Chapter 1

### State of the art and theoretical background

---

1.1 Literature review . . . . .	24
1.1.1 Parallel manipulators . . . . .	24
1.1.2 Series-parallel manipulators . . . . .	32
1.1.3 Compliant mechanisms . . . . .	34
1.2 Fundamental concepts and tools . . . . .	36
1.2.1 Line geometry . . . . .	36
1.2.2 Screw theory . . . . .	37
1.2.3 Algebraic geometry . . . . .	41
1.2.4 Study's kinematic mapping . . . . .	46
1.2.5 Transformation axis . . . . .	48
1.2.6 Tilt and Torsion angles . . . . .	48
1.3 Conclusions . . . . .	49

## Chapter 2

### Operation modes of parallel manipulators

---

2.1 Operation mode analysis . . . . .	51
2.1.1 An equilateral four-bar linkage . . . . .	51
2.1.2 3-[PP]S and 3-S[PP] PMs . . . . .	55
2.1.3 3-RUU PM . . . . .	61
2.1.4 4-rRUU dual reconfigurable PM . . . . .	68
2.2 Influence of design parameters on operation modes . . . . .	86
2.2.1 Manipulator Architectures . . . . .	87
2.2.2 Kinematic Modeling . . . . .	87

2.2.3	Operation modes . . . . .	89
2.2.4	Examples . . . . .	94
2.2.5	Example 3: Arbitrary design parameters . . . . .	98
2.3	Conclusions . . . . .	99

### Chapter 3

#### Comparison between parallel manipulators

3.1	Introduction . . . . .	102
3.2	Singularity Analysis and Parasitic Motions . . . . .	103
3.2.1	Kinematic Jacobian Matrix obtained by differentiating the constraint equations . . . . .	103
3.2.2	Kinematic Jacobian Matrix obtained based on Screw Theory . . . . .	103
3.2.3	Singularity loci in the orientation workspace . . . . .	104
3.2.4	Maximum Inscribed Circle Radius (MICR) . . . . .	106
3.2.5	Parasitic Motions . . . . .	106
3.2.6	Internal collisions . . . . .	106
3.3	Example: The 3-RPS PM . . . . .	107
3.4	Comparison of 3-[PP]S-Y PMs based on their MICR and parasitic motions . . . . .	111
3.5	Ranking the Pareto optimal solutions based on complexity indices . . . . .	118
3.5.1	Joint-number complexity $K_N$ . . . . .	118
3.5.2	Joint-type complexity $K_J$ . . . . .	118
3.5.3	Loop complexity $K_L$ . . . . .	118
3.5.4	Link diversity $K_B$ . . . . .	119
3.5.5	Actuator-position complexity $K_P$ . . . . .	119
3.5.6	Operation mode complexity $K_{OM}$ . . . . .	120
3.5.7	Total complexity . . . . .	120
3.6	Conclusions . . . . .	121

### Chapter 4

#### Kinematics and singularity analyses of series-parallel manipulators

4.1	Architecture of the 3-RPS-3-SPR series parallel manipulator . . . . .	124
4.2	Parametric representation of the 3-RPS-3-SPR series-parallel manipulator . . . . .	125
4.3	Singularities of the 3-RPS-3-SPR S-PM . . . . .	127
4.3.1	Forward and inverse kinematic Jacobian matrices . . . . .	128
4.3.2	Twist and wrench systems of the 3-RPS-3-SPR PM . . . . .	129
4.3.3	Enumeration of serial singularities . . . . .	131
4.3.4	Characteristic tetrahedron of serial singularities . . . . .	133
4.4	Direct Kinematics Model(DKM) . . . . .	141
4.5	Inverse Kinematics Model (IKM) . . . . .	143
4.6	Conclusions . . . . .	145

### Chapter 5

#### Synthesis of compliant mechanisms based on constraint singularities of parallel manipulators

5.1	Constraint singularities of an equilateral four-bar mechanism . . . . .	149
5.2	Design and analysis of a compliant four-bar mechanism . . . . .	150
5.2.1	Operation modes of the compliant four-bar mechanism-2 . . . . .	152

5.2.2	Simulations of the operation modes . . . . .	153
5.3	Application as a compliant gripper . . . . .	154
5.3.1	Gripper design 2 . . . . .	154
5.3.2	Kinetostatic model . . . . .	162
5.3.3	Case study . . . . .	165
5.4	Conclusions . . . . .	168

## Conclusions and Future Work

---

Synopsis . . . . .	169
Contributions . . . . .	169
Future work . . . . .	171

## Personal publications

---

## Appendix

---

## Bibliography

---





# List of Figures

1.1	Gough platform . . . . .	25
1.2	Stewart platform . . . . .	25
1.3	Cappel platform . . . . .	25
1.4	Gwinnett's amusement device . . . . .	25
1.5	Pollard's spray painter . . . . .	25
1.6	ABB FlexPicker DELTA robot . . . . .	26
1.7	Agile eye . . . . .	26
1.8	Prototype of the 3-RPS boat simulator . . . . .	27
1.9	Sprint Z3 machining head . . . . .	28
1.10	Wunderlich's mechanism with mobility F . . . . .	28
1.11	DYMO robot with multiple operation modes . . . . .	29
1.12	PARAGRIP robot system . . . . .	29
1.13	3-RER PM . . . . .	30
1.14	3-UPU PMs . . . . .	31
1.15	A 5- <i>dof</i> industrial hybrid manipulator . . . . .	33
1.16	Tricept modular hybrid robot . . . . .	33
1.17	Logabex LX4 S-PM. . . . .	34
1.18	Natural and man-made compliant mechanisms . . . . .	35
1.19	Reciprocal screws . . . . .	39
1.20	Variety corresponding to the ideal $\mathcal{J} = \langle x_1^2 + x_2^2 - 1, x_1 + x_2 - 1 \rangle$ . . . . .	42
1.21	Solution to the system of equations $\{x^2 + y + z = 1, x + y^2 + z = 1, x + y + z^2 = 1\}$ . . . . .	44
1.22	$\mathbf{V}(\langle x^3 - xy^3 \rangle)$ as the union of varieties $\mathbf{V}(\langle x \rangle)$ in green and $\mathbf{V}(\langle x^2 - y^3 \rangle)$ in blue. . . . .	45
1.23	Tilt and Torsion angles . . . . .	49
2.1	An equilateral four bar linkage. . . . .	52
2.2	Constraint manifolds of the four-bar linkage in image space. . . . .	53
2.3	Operation mode 1 : $a^2 + b^2 - al = 0$ . . . . .	54
2.4	Operation mode 2 : $a^2 + b^2 + al = 0$ . . . . .	54
2.5	Operation mode 3 : $a^2 + b^2 - l^2 = 0$ . . . . .	55
2.6	Six parallel manipulators belonging to the 3-[PP]S-Y family . . . . .	56
2.7	Planes containing the limbs of the 3-[PP]S-Y PMs . . . . .	58
2.8	Planes containing the limbs of the 3-S[PP]-Y PMs . . . . .	58
2.9	The 3-RUU- $\Delta$ parallel manipulator in a general configuration . . . . .	62
2.10	A RUU limb . . . . .	65
2.11	Relative position of two lines in space . . . . .	65
2.12	A numerical example: solutions to direct kinematics corresponding to Eq. (2.56). . . . .	68
2.13	A 4-rRUU parallel manipulator . . . . .	69
2.14	Double Hooke's joint . . . . .	69
2.15	Possible orientations of the base revolute joint . . . . .	72

2.16	A 4-rRUU PM with horizontal and intersecting base revolute joint axes . . . . .	76
2.17	A 4-RUU PM with horizontal and parallel base revolute joint axes . . . . .	78
2.18	A dual reconfigurable 4-rRUU PM with vertical base revolute joint axes . . . . .	78
2.19	Workspaces of 4-R <sub>x</sub> UU(a-e), 4-R <sub>y</sub> UU(f-j) and 4-R <sub>z</sub> UU(k-o) PMs . . . . .	80
2.20	Link interferences as collision between two capsules . . . . .	82
2.21	Pareto-optimal solutions to the design optimization of the 4-rRUU PM. . . . .	84
2.22	Milling as a tentative application of the 4-rRUU PM prototype. . . . .	84
2.23	Variation of condition number, $\kappa_m = \max_{ikm=1}^{16}(\min_{ax=1}^3(\kappa))$ . . . . .	85
2.24	Variation of actuated joint torques and velocities through 120 points divided along the distance to be milled . . . . .	85
2.25	Architecture of a 3-RPS parallel manipulator with coplanar revolute joints . . . . .	87
2.26	A RPS limb . . . . .	87
2.27	First condition for two operation modes . . . . .	91
2.28	Second condition for two operation modes . . . . .	91
2.29	A 3-RPS parallel manipulator with $n_{23} = 0$ . . . . .	95
2.30	A 3-RPS parallel manipulator with $n_{13} = 0$ . . . . .	96
2.31	Design parameters influencing operation modes . . . . .	97
2.32	A 3-RPS parallel manipulator with two operation modes . . . . .	98
2.33	DKM solutions of a 3-RPS PM . . . . .	100
3.1	Actuation and constraint wrenches for the 3-RPS PM . . . . .	105
3.2	Actuation and constraint wrenches for the 3-RPS PM . . . . .	105
3.3	3-RPS PM architecture . . . . .	107
3.4	3-RPS singularity surfaces for $\frac{h_2}{h_1} = 2$ . . . . .	108
3.5	3-RPS singularity loci and MICR . . . . .	109
3.6	3-RPS OM1: MICR vs. $\frac{Z}{h_1}$ as a function of $\frac{h_2}{h_1}$ . . . . .	109
3.7	3-RPS OM2: MICR vs. $\frac{Z}{h_1}$ as a function of $\frac{h_2}{h_1}$ . . . . .	110
3.8	3-RPS OM1: $\mu$ vs. $\frac{Z}{h_1}$ as a function of $\frac{h_2}{h_1}$ . . . . .	110
3.9	3-RPS OM2: $\mu$ vs. $\frac{Z}{h_1}$ as a function of $\frac{h_2}{h_1}$ . . . . .	111
3.10	MICR vs. maximum displacement $\frac{h_2}{h_1} = \frac{1}{2}, \frac{Z}{h_1} = 1$ . . . . .	112
3.11	MICR vs. maximum displacement $\frac{h_2}{h_1} = 1, \frac{Z}{h_1} = 1$ . . . . .	112
3.12	MICR vs. maximum displacement $\frac{h_2}{h_1} = 2, \frac{Z}{h_1} = 1$ . . . . .	113
3.13	MICR vs. maximum displacement $\frac{h_2}{h_1} = \frac{1}{2}, \frac{Z}{h_1} = 2$ . . . . .	113
3.14	MICR vs. maximum displacement $\frac{h_2}{h_1} = 1, \frac{Z}{h_1} = 2$ . . . . .	114
3.15	MICR vs. maximum displacement $\frac{h_2}{h_1} = 2, \frac{Z}{h_1} = 2$ . . . . .	114
3.16	Pareto optimal solutions . . . . .	116
3.17	The solutions that do not dominate any other solutions. . . . .	117
4.1	A 3-RPS-3-SPR series-parallel manipulator . . . . .	125

---

4.2	$n$ parallel mechanisms (named modules) arranged in series . . . . .	130
4.3	Serial singular configurations with parallel revolute joint axes . . . . .	132
4.4	The characteristic tetrahedron of the 3-RPS-3-SPR S-PM . . . . .	134
4.5	Serial singularity when all faces of the characteristic tetrahedron meet in a point	136
4.6	Three sides of the characteristic tetrahedron meet in a line . . . . .	137
4.7	Can two sides and base of the characteristic tetrahedron meet? . . . . .	138
4.8	Eight IKM solutions of 3-RPS-3-SPR S-PM . . . . .	147
4.9	Eight solutions to IKM as locating 3 points on 3 lines problem . . . . .	147
5.2	Compliant four-bar mechanism-1. . . . .	151
5.9	A novel reconfigurable compliant gripper. . . . .	159
5.10	Prototype of the reconfigurable compliant gripper. . . . .	159
5.13	Multi mode compliant gripper consisting of compliant slider-crank mechanisms. .	162
5.14	Multi mode compliant gripper prototype . . . . .	163
5.15	Grasping modes of the compliant gripper. . . . .	165
5.16	Analysis and comparison (input displacement non-negative). . . . .	167





# List of Tables

1.1	Reciprocity conditions . . . . .	40
1.2	Mapping between algebra and geometry in algebraic geometry . . . . .	46
2.1	Manipulators belonging to the 3-[PP]S-Y and 3-S[PP]-Y families . . . . .	57
2.2	DH parameters of a RUU limb shown in Fig. 2.10 . . . . .	65
2.3	DH parameters of the double-Hooke's joint . . . . .	70
2.4	$h_1$ and $h_2$ as functions of $v_{13}$ such that $\langle h_1x_1 + h_2x_2 \rangle \in \mathcal{J}_1(I)$ . . . . .	75
2.5	Inputs to calculate actuated joint torques and velocities . . . . .	86
3.1	Pareto-optimal solutions (Fig. 3.16) . . . . .	115
3.2	Solutions that do not dominate any other solutions (Fig. 3.17) . . . . .	115
3.3	Complexity indices of Pareto optimal 3-[PP]S-Y PMs in ascending order . . . . .	121
3.4	Least to most complex Pareto optimal 3-[PP]S-Y PMs . . . . .	122
4.1	Enumeration of serial singularities for the 3-RPS-3-SPR S-PM . . . . .	139
4.2	IKM solutions of the 3-RPS-3-SPR S-PM . . . . .	145
5.1	Geometrical parameters (in mm). . . . .	165



# Glossary

In accordance with the International Federation for the Promotion of Mechanism and Machine Science (IFToMM), Angeles [Ang13] and Merlet [Mer10; MG08], the following terminologies are repeatedly used in this doctoral thesis:

**Definition 1.** A **rigid body** is a body in which deformation is so small that it can be neglected. The word **link** is used as a synonym for a rigid body.

**Definition 2.** A **joint** is a connection between two or more links. It is also known as a **kinematic pair**.

**Definition 3.** A **kinematic linkage** or a **kinematic chain** is a network of links and joints to manage forces and movement. The word **limb** or **leg** is used as a synonym for the kinematic chain.

**Definition 4.** A **mechanism** is a kinematic linkage in which one link is fixed or stationary.

**Definition 5.** **Degree of freedom (dof)** or **mobility** is the number of independent parameters required to define the position of a rigid body in space.

Instantaneous or local mobility corresponds to the mobility at any instant of time whereas a full cycle or global mobility is the mobility defined over a range of motion.

Franz Reuleaux(1829-1905) introduced kinematic pairs and the six types of lower kinematic pairs are defined as follows [Ang13]:

1. A **revolute pair** (R) allows a relative rotation through an angle  $\phi$  about an axis with a unit direction vector  $\mathbf{e}$ .
2. A **prismatic pair** (P) allows a relative translation  $t_u$  in the direction of a unit vector  $\mathbf{e}$ .
3. A **helical pair** (H) allows both a relative rotation through an angle  $\phi$  about an axis with a unit direction vector  $\mathbf{e}$  a relative translation  $t_u$  in the direction of a unit vector  $\mathbf{e}$ . However, the rotation and the translation are not independent but related by the *pitch*  $p$  of the pair such that:  $t_u = p\phi$ .
4. A **cylindrical pair** (C) allows both a relative rotation through an angle  $\phi$  about an axis with a unit direction vector  $\mathbf{e}$  and a relative translation  $t_u$  in the direction of  $\mathbf{e}$  such that the rotation and the translation are independent.
5. A **planar pair** (E) allows any translation perpendicular to a unit vector  $\mathbf{e}$  and any rotation about an axis directed along  $\mathbf{e}$ .
6. A **spherical pair** (S) allows an independent rotation about any axis passing through a point  $O$ . The relative motions allowed by a spherical pair are thus characterized by point  $O$ .

Additionally, a **universal pair** (U) allows two relative rotations about two concurrent axes.

**Definition 6.** A **base** is the link in a mechanism where the first joint(is) is(are) connected and is usually fixed.

**Definition 7.** An **end-effector** or a **moving platform** is a link in a mechanism where the last joint(s) is(are) connected.

**Definition 8.** In a kinematic chain, the **connection degree** of a link is the number of rigid bodies connected to this link by a kinematic joint.

**Definition 9.** A **serial manipulator (SM)** is an open kinematic chain in which the fixed base and the end-effector have a connection degree equal to 1 while the other links have a connection degree equal to 2.

**Definition 10.** A **parallel manipulator (PM)** is made up of an end-effector with  $n$ -dof, and of a fixed base, linked together by at least two independent kinematic chains. Actuation takes place through  $n$  simple actuators. The term parallel manipulator was coined by Hunt [Hun87].

**Definition 11.** A **lower mobility PM** is a parallel manipulator with less than 6-dof.

**Definition 12.** A **hybrid** manipulator is a serial linkage mounted on a parallel manipulator and vice-versa or a serial arrangement of two or more parallel manipulators. The latter has come to be known as a **Series-Parallel Manipulator (S-PM)** [Tan00; Che+95; Sha95; WRR89; ZS94; Rom99; ZBL04], a term proposed in Zoppi et al. [ZZM06].

**Definition 13.** A **compliant mechanism** includes flexible elements whose elastic deformation is utilized in order to transmit a force and/or motion [How01].

There are other terms used in this doctoral thesis which are defined directly in the text for the sake of continuity.

# Nomenclature

IFTToMM	International Federation for the Promotion of Mechanism and Machine Science
PM	Parallel Manipulator
SM	Serial Manipulator
S-PM	Series-Parallel Manipulator
ISA	Instantaneous Screw Axis
FSA	Finite Screw Axis
<i>dof</i>	degree of freedom
OTI	Output Transmission Index
CTI	Constraint Transmission Index
$\mathbb{R}$	The set of real numbers
$\mathbb{C}$	The set of complex numbers
$\mathbb{Q}$	The set of rational numbers
$\mathbb{Z}$	The set of integers
$\mathbb{P}^m$	$m$ -dimensional projective space
$\mathbb{R}^m$	$m$ -dimensional affine space
$\Sigma_0$	Coordinate frame attached to the fixed base
$\Sigma_1$	Coordinate frame attached to the moving platform
$\mathbb{E}^3$	The Euclidean 3-dimensional space
SE(3)	Group of Euclidean displacements in $\mathbb{E}^3$
SO(3)	Group of rotations in $\mathbb{E}^3$
<b>M</b>	Transformation matrix
<b>R</b>	Rotation matrix
<b>d</b>	Displacement vector
R	Revolute joint
P	Prismatic joint
C	Cylindrical joint
E	Planar joint
H	Helical joint
U	Universal joint
S	Spherical joint
[PP]	Joints producing two coplanar translations
$\times$	Cross product
$\cdot$	Scalar product
$\circ$	Reciprocal product
$\forall$	For all
$\in$	Belongs to
$\subset$	Subset

$\cup$	Union
$\cap$	Intersection
$\oplus$	Disjoint union
$\vee$	Span
$\wedge$	Incidence
MICR	Maximum Inscribed Circle Radius

# Introduction

## Scope of the doctoral thesis

In the 80s, a Robotics lab in Lausanne, Switzerland faced a challenge: to develop a high-speed and light-weight robot for automatic packaging of chocolate pralines which led to the conception of DELTA robot by Clavel [Cla88; Cla90]. Ever since its realization, advantages of lower-mobility parallel manipulators over the known benefits of classical parallel manipulators (PMs) have been accentuated. Parallel manipulators are closed-loop linkages with appealing features such as large payload capacity, high precision, rigidity and speed [Mer10]. However, many industrial applications require less than six *dof* that has led to the popularity of lower mobility PMs. Due to their reduced mobility, many of them exhibit different motion types called operation modes making them reconfigurable manipulators. The motion types could be planar, translational, cylindrical, spherical, Schönflies, coupled, etc.

The study of any PM begins by learning its mobility, kinematics and singularities before dealing with its dynamics and control. The reduced mobility of lower mobility PMs relies on the geometrical constraints imposed by their limbs on the moving platform. They can be used to determine the pose and motion of the moving platform with respect to the fixed base as functions of the actuated variables of the PM. Furthermore, singularity analysis must be performed to determine any uncontrolled *dof*.

The theory of reciprocal screws is an efficient tool for kinematic analysis, since it is visual, easy-to-use and well-developed [Bal00; Phi84; Hun87]. However, it can only deal with instantaneous motions. Therefore, it is a local analysis technique and is mainly effective for PMs with simple motion types. On the other hand, the geometrical constraints can be expressed as algebraic equations using Study's kinematic mapping so that algebraic geometry tools can be used to perform a comprehensive kinematic analysis of lower mobility PMs [Hus+97; Hus+07; HS08; HS13]. Nonetheless, it can be computationally expensive.

This doctoral thesis initially focuses on both local and global kinematic analysis of some lower mobility PMs such as an equilateral four-bar linkage, zero-torsion mechanisms belonging to the 3-[PP]S and 3-S[PP] family, a 3-RUU PM and a 4-rRUU PM with a reconfigurable R joint. It is not surprising that the operation modes of a PM depend on design parameters. This fact is explored by determining the influence of design parameters on the number of operation modes of the 3-RPS PM with coplanar R joint axes.

The analysis of a 3-[PP]S family of PMs shows that they all exhibit two operation modes. This raises a question as to which one of these PMs are better for a given application. Thus, they are compared in terms of their singularity-free workspaces, parasitic motions and complexities.

Additionally, lower-mobility PMs also appear as constitute elements of hybrid robots that embody the benefits of both serial and parallel manipulators. They can precede a serial manipulator (SM) like in the Tricept robot [SL04b]. They can also be modules of a series-parallel



manipulator (S-PM), where one or more PMs are stacked in series [Mer10].

The 6-*dof* motions of one such S-PM, a 3-RPS-3-SPR S-PM are parametrized using three *Study parameters* of each module. It is essentially one of the many possible parametrizations of *Study's quadric* in  $\mathbb{P}^7$ . Moreover, the singularities arising due to the serial stacking of the 3-RPS and 3-SPR PMs are listed with the help of screw theory and line geometry.

When two or more constraint equations of a lower mobility PM become dependent, it is said to be in a constraint singularity. These kinds of singularities are also the transitions between operation modes of the PM resulting in an instantaneous gain of a *dof* [ZBG02a]. The common notion that “singularities must be avoided” is overturned by using a constraint singularity of an equilateral four-bar mechanism to design a novel reconfigurable compliant four-bar mechanism. Additionally, a reconfigurable compliant gripper is designed with multiple grasping modes.

## Summary

This doctoral thesis is divided into five chapters and the main objectives are as follows:

### 1. Operation mode analyses of some lower mobility PMs

Chapter 2 starts with the operation mode analysis of the simplest PM, an equilateral planar four-bar linkage. Its constraint equations are derived using Blaschke mapping [BR79] which is a special case of Study's kinematic mapping for planar Euclidean transformations. The constraint polynomials can be split into simpler multiple subsets yielding its three operation modes. In algebraic geometry terms, this is done by primary decomposition of the ideal of constraint polynomials. The transitions between the operation modes are depicted as constraint singular configurations where the equilateral four-bar linkage momentarily exhibits a rotational and a translational *dof* simultaneously. Similarly, a family of 3-*dof* lower mobility PMs with zero torsion are shown to have two operation modes. Furthermore, constraint equations of a 3-RUU PM are derived using the geometrical approach and Linear Implimentation Algorithm [WH10] and the varieties are compared. Finally, the operation modes of a 4-rRUU dual reconfigurable PM are determined for three mutually perpendicular orientations of the base R-joint axes. With an objective to construct a working prototype of a 4-rRUU PM for machining operations, optimal design parameters are determined such that the reconfigurable PM has the smallest size but the largest singularity-free workspace.

Another objective of this doctoral thesis is to study the influence of design parameters on the number of operation modes. This problem is explored at the end of Chapter 2 in the context of the 3-RPS PM with coplanar revolute joint axes. The relationships between design parameters are established for the PM to exhibit two operation modes. This work is conducted in the framework of ANR KAPAMAT project in collaboration with University of Innsbruck, Austria.

### 2. Comparison of a family of zero-torsion PMs

Operation modes of PMs belonging to the 3-[PP]S-Y family are studied in Chapter 2 to realize that they all have similar motion types. However, an industrial application might demand a knowledge of the best among them corresponding to their operation modes and choice of actuation. For this reason, they are compared in Chapter 3 on the basis of their singularity free orientation workspace and parasitic motions. Their kinematic Jacobian matrices are derived using screw theory methods in-order to plot singularity loci in their orientation workspaces. The singularity-free workspace is quantized using a new performance index called Maximum

---

Inscribed Circle Radius (MICR). Pareto front is drawn to choose the PMs with the least MICR and the smallest parasitic motions. They are further ranked based on their complexity.

### 3. Kinematic analysis of an S-PM

Even though there is ample research dedicated to the S-PMs, singularities arising due to the stacking of two or more lower-mobility PMs is often ignored or incomplete. With an objective to solve this problem, the serial kinematic Jacobian matrix of the 3-RPS-3-SPR S-PM is derived using screw theory in Chapter 4. Then, its serial singularities are enumerated by examining the conditions for collapse of its characteristic tetrahedron [EULL02].

### 4. Design of reconfigurable compliant mechanisms

One of the many methods to design a compliant mechanism is the rigid body replacement, where rigid members of a mechanism are replaced by their equivalent compliant members [HMO13]. The final objective of this doctoral thesis is to synthesize a compliant mechanism using the aforementioned method starting from the constraint singular configuration of a lower-mobility PM. Thus, the compliant mechanism will be reconfigurable, thanks to the singular configuration shared by different motion types of the rigid body mechanism used for its conception.

The two constraint singular configurations of an equilateral four-bar linkage that separate its three operation modes are shown in Chapter 2. One of these configurations is chosen in Chapter 5 to design a compliant reconfigurable mechanism such that the output motion is either a rotation or translation depending on the nature of actuation. Furthermore, two such mechanisms are assembled with two compliant slider-crank mechanisms to obtain a reconfigurable compliant gripper. As a consequence, the gripper has two linear inputs that control its angular or parallel grasping mode. Unlike any traditional gripper, the reconfigurability of the designed gripper allows grasping objects with a wider variety of shapes. This work is conducted in the framework of PHC Ulysses project in collaboration with University College Cork, Ireland.

## Collaborations

- KAPAMAT project entitled “Kinematic Analysis of lower-mobility parallel manipulators using algebraic geometry tools”.  
Collaborators: Manfred Husty, Martin Pfurner and Thomas Stigger, University of Innsbruck, Austria.
- PHC Ulysses project entitled “Design and analysis of reconfigurable compliant mechanisms based on the singularities of parallel manipulators”.  
Collaborators: Guangbo Hao and Haiyang Li, University College Cork, Ireland.

# Chapter 1

## State of the art and theoretical background

This chapter is the fabric of this doctoral thesis. It puts forth the state of the art and explains the fundamental concepts used to analyze and understand the behavior of the mechanisms studied herein. First, a brief literature review of these manipulators is presented. Then, the mathematical framework is introduced, starting with concepts from line geometry. Furthermore, the usefulness of screw theory in modeling a parallel manipulator is described. Though screw theory offers a quick way to characterize the kinematic behavior of a PM, it is a local analysis method. To overcome this problem and to globally characterize a given PM, algebraic geometry techniques are exploited whose terminology is given subsequently. Finally, the parametrization of a transformation matrix is recalled, first by using the coordinates of a finite screw axis and then by using tilt and torsion angles.

### 1.1 Literature review

The literature review presented in this chapter focuses mainly on historical developments in the field of PMs, S-PMs and compliant mechanisms most relevant to this doctoral thesis. Additionally, different methodologies adopted for their design and kinematic analysis are discussed. For a detailed history of PMs, the reader is redirected to, e.g., Merlet [Mer10] and Bonev [Bon03].

#### 1.1.1 Parallel manipulators

Interest in parallel manipulators has increased considerably in the past 50 years due to their advantages over serial manipulators [Mer10]. Unlike SMs, the PMs possess a larger load capacity since the load on the moving platform is shared by their limbs. Moreover, in most of the PMs, the joints impose only traction-compression constraints implying smaller flexural deformations and better positioning accuracy.

Indeed the discussion of PMs is incomplete without acknowledging the celebrated 6-*dof* octahedral hexapod also known as the Gough-Stewart platform. Though it is the most popular PM today, its inventors are not adequately recognized. In fact, it was independently invented by Gough [GW62], Stewart [Ste65] and Cappel [Cap67], whose designs are shown in Fig. 1.1, 1.2 and 1.3, respectively. Since then, it has been used in numerous applications like flight simulation, rehabilitation, machining, etc. Another overlooked fact about the hexapod is that it is not the first PM to be built [Bon03].

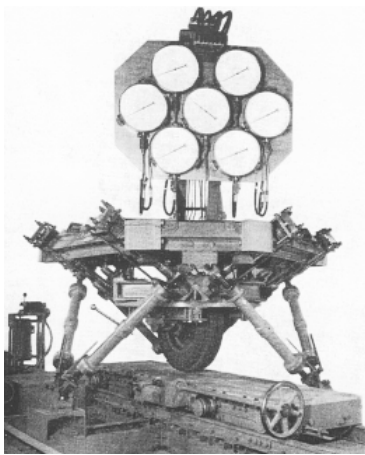


Figure 1.1 – Gough platform [GW62]

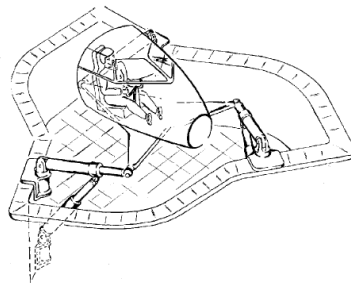


Figure 1.2 – Stewart platform [Ste65]



Figure 1.3 – Cappel platform [Cap67]

The first mention of theoretical problems related to PMs dates back to 1645 by Sir Christopher Wren (1632-1723) and then in the 19th century by Cauchy, Lebesgue, Bricard and Borel [Mer10]. However, probably the first practical application was envisioned and patented by Gwinnett [Gwi31]. It was an amusement device capable of performing a spherical motion as shown in Fig. 1.4. In

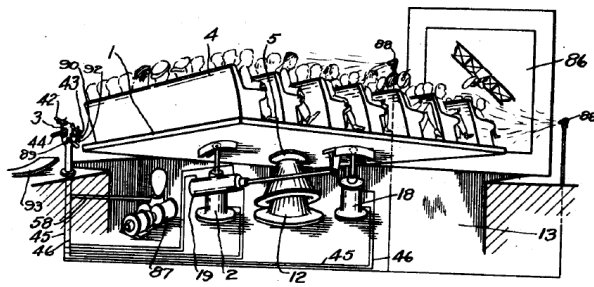


Figure 1.4 – Gwinnett's amusement device [Gwi31].

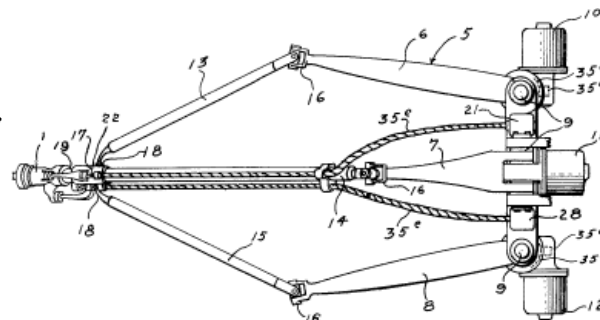


Figure 1.5 – Pollard's spray painter [Pol42].

1942, Pollard patented a spray painting machine. It was a 5-*dof* 2-RUS+1-RUU PM as shown in Fig. 1.5 but was never built. Both these manipulators were lower mobility PMs. Along with the 6-*dof* hexapod, lower mobility PMs have gained a lot of attention lately as six actuators are not required for many applications [LH03].

### Lower mobility PMs

The simplest yet ubiquitous lower mobility planar PM is a four-bar linkage. It could be a planar quadrilateral (RRRR) or slider-crank (RRRP) or double slider linkage (PRRP). Its applications include bicycle suspension, pumpjack, pantograph, steam engines, windshield wiper and so on. When the opposite links of a four-bar linkage are parallel, it's called as a parallelogram linkage (II) where the output link can have a pure translational motion with respect to the input link.

When it comes to spatial lower mobility PMs, three such II-linkages could be placed in such a

way that they completely constrain the orientation of the moving platform to which they are connected. This genius thought led to the most commercially successful robot design known as the DELTA robot as shown in Fig. 1.6. It was designed and patented by the Golden Robot



Figure 1.6 – ABB FlexPicker DELTA robot [Cla88; Cla90].

award winning professor Raymond Clavel [Cla88; Cla90]. It has  $3\text{-}dof$  pure translations and is extensively used in food, medical and electronic and manufacturing industries. On the other hand, many applications require pure rotational motions. Figure 1.7 shows the Agile eye devel-

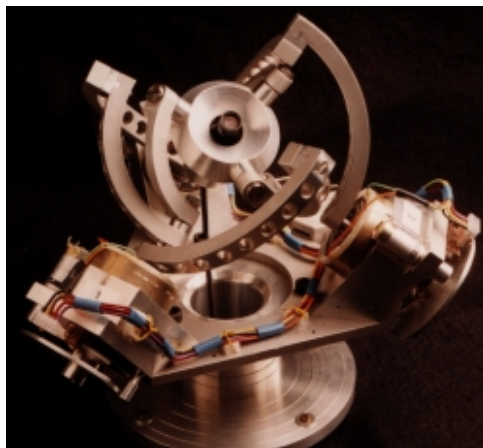


Figure 1.7 – Agile eye [GA89].

oped at Laval University to be used as a camera orienting device [GA89]. It is a  $3\text{-}RRR$  spherical mechanism that belongs to the family of spherical wrists [Kar03]. It has angular velocities superior to  $1000^\circ/s$  as well as a cone vision of  $140^\circ$  with  $\pm 30^\circ$  in torsion. It also exhibits workspace larger than that of human eye although the latter has no torsional motion. As a matter of fact, human wrist and sterno-vascular joint have no torsion either. In fact, there is a whole family of lower mobility PMs without a torsional  $dof$ . This family of PMs are called as *zero torsion mechanisms*.

## Zero-torsion PMs

**Definition 14.** *Zero-torsion PMs* are the class of PMs that always have zero torsion [BZG02; BB08]. In other words, the rotation of their mobile platforms about an axis normal to the latter is always constrained and they display a symmetric motion with respect to the constrained axis.

Accordingly, the local motions of the mobile platform of such mechanisms are two non-pure rotations about horizontal axes and sometimes a pure translational motion along a direction normal to the axes of the rotational motions.

The 3-*dof* 3-RPS PM, introduced by Hunt [Hun83] is one such mechanism that has been studied extensively. Unlike the aforementioned PMs, it generates coupled motions that include both translational and rotational motions. It can be found as the part of a 6-*dof* robot [LS88], as a micro-manipulator wrist subsystem of the ARTISAN manipulator [WRR89] and as a reaction compensation device for space robots [SZ95]. Recently, the 3-RPS PM was used as the rear of a boat simulator as shown in Fig. 1.8 with different actuation modes [LR14]. The 3-RSR PM also

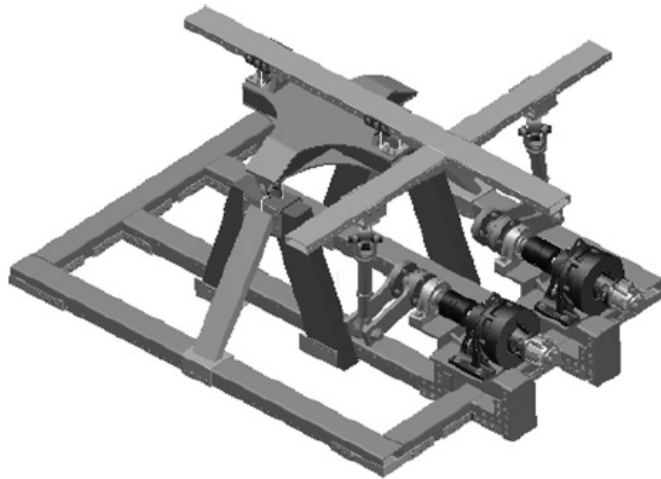


Figure 1.8 – Prototype of the 3-RPS boat simulator [LR14].

belongs to this category of mechanisms. Clemens proposed it to be used as a constant velocity coupling device [Cle69] which later inspired Hunt to propose a reflected tripod [Hun87].

Other examples include the 3-PRS, 3-RRS and 3-PPS PMs. The 3-PRS PM was first proposed for telescopic applications [Car+99]. Another well-known application of the 3-PRS mechanism is a machining head, called the *Sprint Z3* as shown in Fig. 1.9, developed and patented by DS Technology [Wah02]. The 3-RRS PM was analyzed in [Tet+16] to be used as a part of a 6-*dof* hybrid robot for pick-and-place operations. A flexure based 3-PPS PM was used for a nano imprinting tool module in [Yan+11].

## Reconfigurability

The ability of a system to repeatedly change and rearrange the components in a cost-effective way is known as *reconfigurability* [SL04a].

**Definition 15.** A *reconfigurable manipulator* is a robotic system that can reconfigure its architecture to attain different kinematic properties for specific manipulating tasks [CZL14].

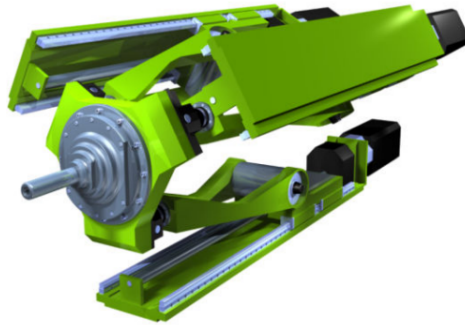


Figure 1.9 – Sprint Z3 machining head [Wah02].

Wohlhart came across a few mechanisms with this behavior in 1996 and named the behaviour as *kinematotropy* [Woh96].

**Definition 16.** *Kinematotropic mechanisms can change their full cycle mobility or dof, while retaining their topological structures.*

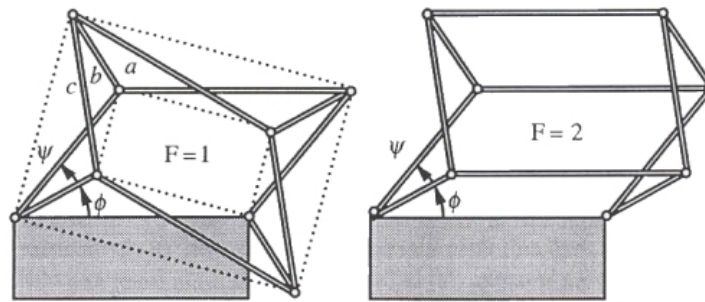


Figure 1.10 – Wunderlich's mechanism with mobility  $F$  [Woh96].

Wohlhart presented two such peculiar mechanisms: Wunderlich's mechanism and Wren's mechanism both of which can exhibit a full mobility of 1 or 2. Wunderlich's mechanism is a planar twelve-bar mechanism with six parallelogram linkages as shown in Fig. 1.10 [Woh96]. Furthermore, Dai *et.al* presented a new class of mechanisms that are able to change their structures and mobilities by changing the link numbers and connectivity and coined the term *metamorphic mechanisms* [DRJ99; ZD09].

**Definition 17.** *Metamorphic mechanisms can exhibit different full cycle mobilities by changing their architectures but retaining the same topology [DRJ99; ZD09].*

Later, in 2002, Zlatanov *et al.* analyzed the DYMO (Double Y-Multi Operational) robot, a 3-URU PM shown in Fig. 1.11 to realize that it can exhibit five distinct 3-*dof* motion types and coined the term *operation modes* [ZBG02a].

**Definition 18.** *A category of reconfigurable manipulators can display distinct regions in their workspace associated with different types of motions. These regions are called **Operation modes** [Nur15].*

A detailed classification of reconfigurable manipulators summarized by Nurahmi in her PhD thesis is briefly recalled here [Nur15]:

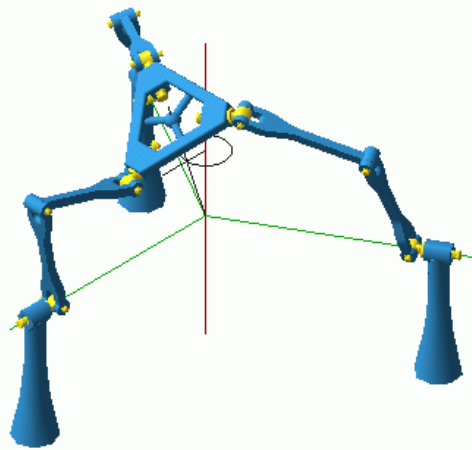
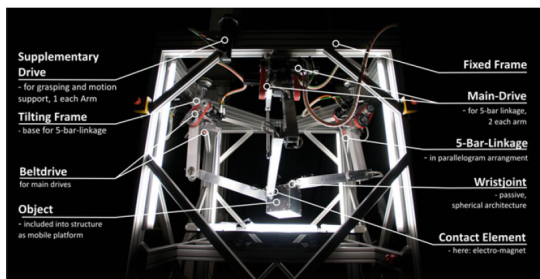
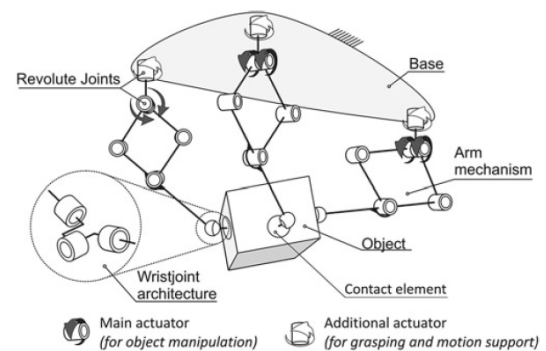


Figure 1.11 – DYMO robot with multiple operation modes [ZBG02a].

1. *Classification based on the presence of multiple operation modes:* PMs can be further classified based on the number of *dofs* in each operation mode [KG07].
  - *Invariable-dof PM:* Same number of *dofs* in every operation mode. Example: Sphe.I.Ro. wrist is a 3-CPU PM that can exhibit fifteen distinct 3-*dof* operation modes [Car+14].
  - *Variable-dof PM:* Do not have the same number of *dofs* in their different operation modes. Some examples: the DYMO robot [ZBG02a] shown in Fig. 1.11, the 4-UPU PM with an extra 3-*dof* operation mode along with the 4-*dof* Schönflies mode [Car+14] and the 4-RUU PM with a 2-*dof* mixed operation mode along with the 4-*dof* Schönflies mode [Nur+16].



(a) Prototype.



(b) Concept sketch

Figure 1.12 – PARAGRIP robot system [Man+13].

2. *Classification based on kinematic architectures:* Based on their structure, the following sub-classifications can be done.
  - *Reconfigurable SM:* Two examples are RMMS robot [PBK96] and MARS manipulator [EK16].
  - *Reconfigurable PM:* Being the focus of this doctoral thesis, some examples are already mentioned. Others include PARAGRIP (Parallel Gripper) robot system, a 3-RIIS PM with 6-*dof* as shown in Fig. 1.12 [Man+13]. It can be used to grasp and manipulate objects by integrating the object as a moving platform. Its reconfigurable architecture



- allows it to change the grasping points adapting it to the requirements of a given task.
- *Reconfigurable hybrid manipulator*: They are a mixture of both serial and parallel architectures. An interesting example is the *Cheope* robot with a RRP spherical wrist over a PM with each leg being a  $P[SS]_2$  or  $3-P[SS]$  configuration [Tos+10]. Thus, the PM can exhibit a  $3-dof$  pure translational motion or a  $4-dof$  Schönflies motion resulting in a  $6-dof$  or a  $7-dof$  hybrid robot.
3. *Classification based on assembly process*: There are two categories of reconfigurable PMs based on whether the structure needs to be disassembled to achieve reconfigurability [SF07].
    - *Dynamic reconfigurable manipulator*: that do not need to be disassembled. All the aforementioned examples belong to this category.
    - *Static reconfigurable manipulator*: that do require disassembly or a change in the basic topology. An example is the MaPaMan (Madras Parallel Manipulator) [SB13]. It can exhibit a  $3-dof$  pure spherical motion or it can behave like a  $3-dof$  zero-torsion PM with only roll, pitch and heave motions.
  4. *Classification based on inactive joints*: An inactive joint is defined as the joint that has no mobility due to the constraints induced by other joints of the manipulator and it has no effect on the overall mobility [KG07].

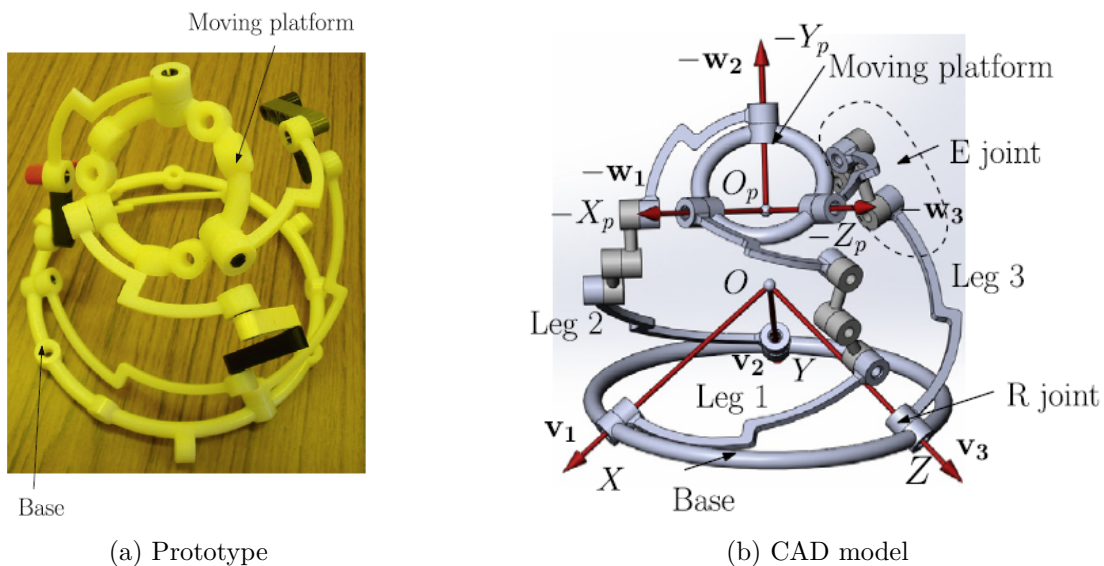


Figure 1.13 – 3-RER PM [Kon14].

- Reconfigurable PMs without any inactive joint in any of their operation modes. The 3-RER PM shown in Fig. 1.13 is one such PM [KGR06; Kon14] with fifteen  $3-dof$  operation modes.
- Reconfigurable PMs with inactive joints in at least one operation mode.

## Kinematics of reconfigurable PMs

The term *kinematics* has Greek origins with *kinein* meaning 'to move'.

**Definition 19.** According to IFToMM, **Kinematics** is defined as a branch of theoretical mechanics dealing with the geometry of motion, irrespective of the causes that produce the motion.

Kinematics is used to describe the motion of links and joints of a system and *kinematic analysis* is the process of measuring the kinematic quantities used to describe this motion. For a PM, it implies to establish relations between the joint coordinates and the moving platform pose (position and orientation) [Mer10].

**Inverse kinematics** consists in establishing the values of actuated joint coordinates given the moving platform pose [Mer10]. It is essential for position control of PMs. For a given moving platform pose, the limbs of a PM can have different postures resulting in more than one solution to the inverse kinematics problem. These solutions are called as *working modes* [CW98; BCW07].

**Direct kinematics** involves the determination of the moving platform pose from the actuated joint coordinate values [Mer10]. In general, this problem is computationally expensive to solve compared to inverse kinematics problem for parallel architectures. There are usually many solutions to this problem meaning that there are several ways to assemble the PM. Therefore, they are also called as *assembly modes* [WC98; BCW07].

**Operation modes** *Operation mode analysis* is essentially the task of determining the number and types of operation modes and transitions between them for a reconfigurable manipulator.

Another PM with the same topology as that of the DYMO robot shown in Fig. 1.11 is the

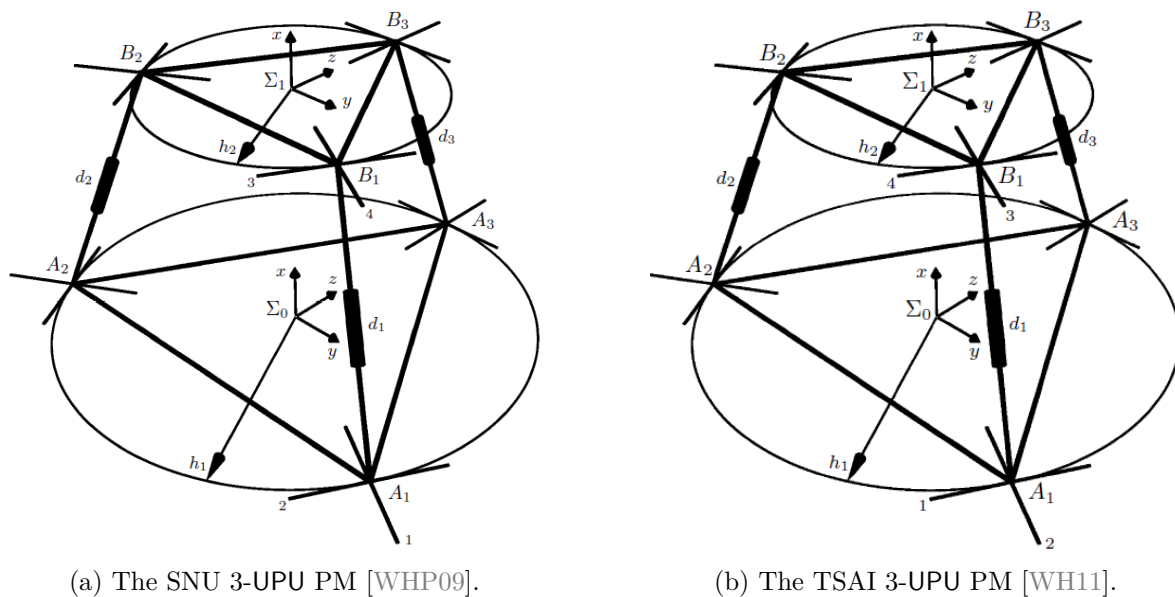


Figure 1.14 – 3-UPU PMs (The numbers at the first limb describe the order of the rotational axes of the U-joints).

SNU 3-UPU from Seoul National University. It is different from the TSAI 3-UPU [Tsa96] as shown in Fig 1.14, where each leg is rotated by  $90^\circ$  about the prismatic joint axis. The former was developed to exhibit *3-dof* pure translations while the latter, *3-dof* pure rotational motions until Husty *et al.* performed a complete operation mode analysis to reveal their other hidden operation modes [WHP09; WH11]. It was found that the SNU 3-UPU has seven *3-dof* operation

modes whereas the TSAI 3-UPU has five 3-*dof* operation modes and yet the latter was found to be more complex.

## Singularities of PMs

**Definition 20.** *The configurations of a manipulator where it loses or gains one or more dof are called singular configurations.*

Depending on the singular configuration, the robot might lose its inherent rigidity resulting in uncontrollable degrees of freedom of the moving platform [Mer10]. Hence, it is necessary to avoid singularities in the workspace.

A PM can mainly fall into two types of singular configurations [Mer10; Tsa99; JT02; CC08]:

1. *Serial singularity* or limb singularity where the platform loses one or several degrees of freedom. This type of singularity is the transition between the working modes and hence defines the boundaries of the workspace.
2. *Parallel singularity* where the platform can perform infinitesimal motions even though the actuators are locked. It corresponds to the transition between the assembly modes or the operation modes. Parallel singularities can be further classified as follows:
  - *Actuation singularities* belong to a single operation mode [WHP09; WH11]. In these configurations, the actuators cannot control the velocity of the moving platform [AMC16].
  - *Constraint singularities* are the transitions between the operation modes. For this reason, they are also known as *transition configurations* [Sch+14; Kon14]. Since operation modes correspond to the partitions of configuration space, these singularities are also called *C-space singularities* [ZBG02a; ZBG02b; AMC16]. Moreover, constraint singularities are inherent to the kinematic linkage and do not depend on the choice of actuation [CC08].
  - *Compound singularities* are parallel singularities when the PM is neither in a constraint singularity nor in an actuation singularity [MNC16; NC15]. They are well understood in a theoretical point of view but their physical interpretation is still a loose end.

Numerous methods exist in the literature to determine the singular configurations of PMs such as using the velocity equation formulation algebraically [ZFB95a; ZFB95b] and numerically [Nad13], theory of reciprocal screws [JT02; BZG03], Grassmann-Cayley algebra [BHS06; BHS09; Kan+09; Ami11; Ami+12a; Ami+12b; AMC16] and using algebraic geometry tools [Sch+14; WHP09; WH11; NCW15a; Nur+16; Hus+07; HS13; HS10; Nay+17b; Sch14; Nur15].

### 1.1.2 Series-parallel manipulators

Both SMs and PMs have earned their places in the robotics world due to their inherent properties such as high stiffness of PMs [Mer10] and large workspace of SMs [Tsa99]. Hence, a marriage between serial and parallel manipulators with a hope to reap the merits of both, has led to hybrid manipulators [Tan00; Che+95; Sha95; WRR89; ZS94; Rom99; ZBL04]. A hybrid manipulator could be mainly of three kinds:

- (i) An SM mounted on a PM [TGK99; Tho88; IW05; SL04b].
- (ii) A PM mounted on a SM [WRR89].
- (iii) serially stacked PMs called as S-PMs [Sha95; Rom99; Tan00; ZBL04].



Figure 1.15 – A 5-*dof* industrial hybrid manipulator [TGK99].



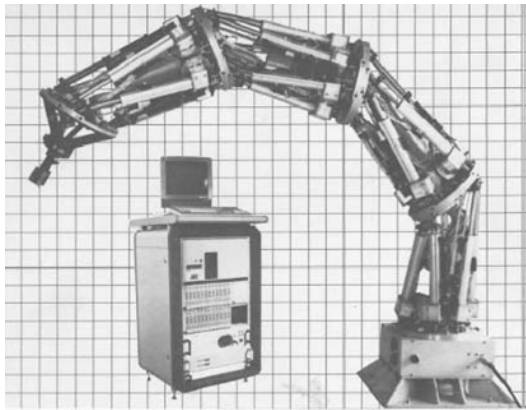
Figure 1.16 – Tricept modular hybrid robot [SL04b].

There are myriad examples of kinds (i) and (ii) compared to kind (iii) hybrid manipulators due to the fact that for an S-PM, the actuators at every module increase the inertia of the system making it bulky and impractical for applications.

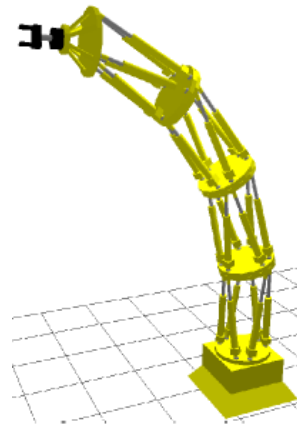
An example for an SM mounted on a PM is the Georg V. [TGK99] robot. Fig. 1.15 shows that it is a tripod (3-RPS PM) with a 2-*dof* wrist joint mounted on it. It is used as a laser cutting machine. 6-*dof* GEC Tetrapod is another example with a spherical wrist mounted on a translational PM [Tho88] used as an assembly robot. The most successful modular hybrid robot is the 5(or 6)-*dof* Tricept robot as shown in 1.16. It has more than 300 units installed worldwide with applications ranging from robotics assembly drilling and milling of hard metals [SL04b]. However, this doctoral thesis focuses mainly on the serial arrangement of two or more PMs, known as S-PMs. To the best of the author's knowledge, the only industrial example of an S-PM is the LX robot built by the company Logabex by piling up hexapods as shown in Fig. 1.17. It weighs 120 kgs [Mer10] and its configuration space is a 25 dimensional variety embedded in a 97-dimensional joint space [CS04] and the control is evidently difficult [Cha90]. Therefore, from a practical view point, S-PMs are not very useful, but theoretically, they are fascinating and pose a lot of interesting problems to be solved in order to understand their behavior.

### Kinematic analysis of S-PMs

As much as they are regarded for their merits, hybrid manipulators also bear the demerits of their constituent manipulators in the sense that their kinematic modeling and singularity analysis are more complicated. Various approaches have been proposed in the literature to analyze S-PMs: Shahinpoor [Sha95] solved the direct and inverse kinematics of modular 3-axis parallel manipulators mounted in series as an  $n$ -axis S-PM. Romdhane [Rom99] performed the forward displacement analysis of a Stewart-like S-PM. Tanev [Tan00] studied a novel 6 degrees of



(a) Industrial prototype [Mer10].



(b) CAD model [CS04].

Figure 1.17 – Logabex LX4 S-PM.

freedom (dof) S-PM and derived the closed-form solutions to its forward and inverse kinematics. Moreover, Zheng *et al.* [ZBL04] obtained closed-form kinematic solutions for the design of a 6-dof S-PM composed of a 3-UPU translational PM and a 3-UPU rotational PM mounted in series. In most of these S-PMs, the constituent modules possess the degrees of freedom that are pure rotations or translations. Hence, each module can be replaced by a set of equivalent lower kinematic pairs that can simplify the understanding of the S-PM behaviour.

There exist other S-PMs in which the constitutive PMs have their degrees of freedom coupled and hence give rise to parasitic motions. Hu, Lu and Alvarado [Hu+12; LHY09; GA+08; Hu14; GA+15] have contributed considerably to the design and analysis of this kind of series-parallel manipulators. Lu and Hu [LHY09] pursued the kinematic analysis of a 2(SP+SPR+SPU) S-PM and plotted its workspace. They also performed the static analysis [Hu+12] of S-PMs with  $k$ -PMs in series. In addition, Hu [Hu14] formulated the Jacobian matrix for S-PMs as a function of Jacobians of the individual parallel modules. Alvarado [GA+08] used screw theory and the principle of virtual work to carry out the kinematic and dynamic analysis of a 2-(3-RPS) S-PM. The 3-RPS-3-SPR S-PM is another example of a S-PM composed of two parallel modules with coupled degrees of freedom [HLYZ12; GA+15; NCW18d]. Though there are well-developed methods for kinematics of S-PMs, the singularity analysis is generally overlooked. Therefore, this doctoral thesis sheds some light into this area considering S-PMs with two or more lower mobility PMs mounted in series.

### 1.1.3 Compliant mechanisms

Although, people have been building machines with rigid links and joints to accomplish a motion, almost every moving thing in nature is flexible with parts that can bend to simulate motion. Examples include bee wings, elephant trunks, eels, human body parts such as heart, muscles along with the man-made designs of ancient bows and mechanisms of Leonardo da Vinci as shown in Fig. 1.18 [HMO13].

**Definition 21.** *Compliant mechanisms consist of flexible elements whose elastic deformation is utilized in order to transmit a force and/or motion [How01].*

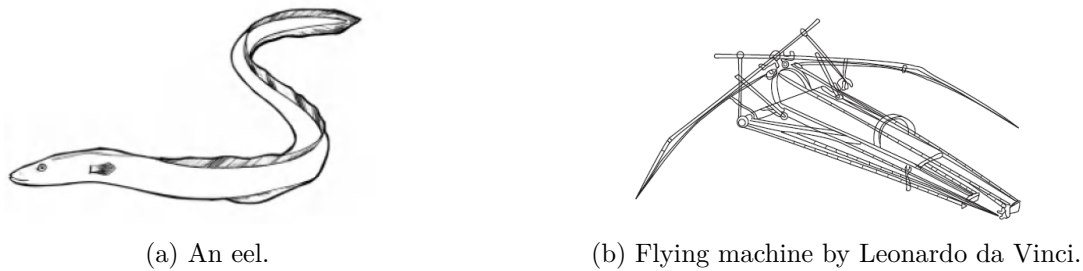


Figure 1.18 – Natural and man-made compliant mechanisms [HMO13].

Compliant mechanisms have many advantages as compared to their rigid counterparts. They are simpler to manufacture (usually monolithic) with lower costs of manufacturing, possess high precision due to reduced wear and backlash, are light weight and can be miniaturized. Nonetheless, they also offer some challenges such as the deflections are often non-linear and require care in defining their motion and are prone to fatigue due to high stresses in the compliant joints [HMO13].

The Handbook of compliant mechanisms lists the following methods to design a compliant mechanism [HMO13]:

1. *Synthesis through Freedom and Constraint Topologies* (FACT) method is a systematic approach that depends on the mathematics of screw theory [HC10a; HC10b; Hop10].
2. *Synthesis through topology optimization*: Initially a design domain is defined as the allowable space for design and then a topology is decided through the distribution of a material and void within this domain [Roz14]. The result is usually the stiffest, least weight mechanism.
3. *Synthesis through rigid body replacement* involves choosing a rigid-body mechanism capable of accomplishing a desired task whose rigid links and movable joints are then replaced with equivalent compliant members and joints to obtain a compliant mechanism. Usually, there are several ways to replace the rigid parts of a mechanism by compliant parts [Ols+10; HL15; How01]. To choose the best design, type synthesis is done using Pseudo-Rigid Body Modeling (PRBM) that provides a simple method for analyzing the non-linear deflections of compliant members in a mechanism by modeling their deflection using rigid-body components that have equivalent force or deflection characteristics [MHM04].
4. *Synthesis through the use of building blocks* mainly relies on the designer's creative capacity to decompose a problem into sub-problems that can be addressed by subsystems or building blocks [KMK08].

### Reconfigurable compliant mechanisms

Though there are abundant reconfigurable rigid-body mechanisms in the literature, the study of reconfigurable compliant mechanisms is limited. Hao studied the mobility and structure reconfiguration of compliant mechanisms [Hao16] while Hao and Li introduced a position-space-based structure reconfiguration (PSR) approach to the reconfiguration of compliant mechanisms and to minimize parasitic motions [HLK16; LH15].

As it will be shown in this doctoral thesis, the constraint singularities of lower-mobility PMs can be exploited to design reconfigurable compliant mechanisms.

## 1.2 Fundamental concepts and tools

### 1.2.1 Line geometry

The set of straight lines in the projective space  $\mathbb{P}^3$  is a four dimensional manifold. Felix Klein (1849-1925) introduced an easier way to study line geometry by mapping every line in  $\mathbb{P}^3$  to a point on a quadric in the projective 5-space  $\mathbb{P}^5$ . This mapping is called the *Klein model* and the quadric on which these points lie is called the *Klein quadric*.

#### Plücker coordinates

Following H.Grassman and J.Plücker, the coordinates of a line  $\mathcal{L}$  spanned by two points  $A$  and  $B$  with homogeneous coordinates  $(a_0, \mathbf{a}) = (a_0, a_1, a_2, a_3)$  and  $(b_0, \mathbf{b}) = (b_0, b_1, b_2, b_3)$ , respectively are given by their exterior product as follows [PW01]:

$$(a_0, a_1, a_2, a_3) \wedge (b_0, b_1, b_2, b_3) = (\mathbf{l}, \bar{\mathbf{l}}) = (p_{01}, p_{02}, p_{03}, p_{23}, p_{31}, p_{12}), \quad p_{ij} = a_i b_j - a_j b_i. \quad (1.1)$$

The six-tuple  $= (p_{01}, p_{02}, p_{03}, p_{23}, p_{31}, p_{12})$  contains the Plücker coordinates of a line and they must satisfy the following *Plücker identity*:

$$p_{01}p_{23} + p_{02}p_{31} + p_{03}p_{12} = 0 \quad (1.2)$$

The vector  $\mathbf{l}$  denotes the direction vector of  $\mathcal{L}$  and the vector  $\bar{\mathbf{l}}$  denotes the moment vector of the line with respect to origin.

Thus, a line  $\mathcal{L}$  carries a pencil of points. By duality it also carries a pencil of planes leading to dual Plücker coordinates. For instance, the line of intersection of two planes  $\mathcal{U}$  and  $\mathcal{W}$  with homogeneous coordinates  $(u_0, \mathbf{u}) = (u_0, u_1, u_2, u_3)$  and  $(v_0, \mathbf{v}) = (v_0, v_1, v_2, v_3)$ , respectively has the following dual Plücker coordinates:

$$(u_0, u_1, u_2, u_3) \wedge (v_0, v_1, v_2, v_3) = (p_{01}^*, p_{02}^*, p_{03}^*, p_{23}^*, p_{31}^*, p_{12}^*), \quad p_{ij}^* = u_i v_j - v_j u_i. \quad (1.3)$$

#### Span and intersection

The line  $\mathcal{L}$  spanned by two points  $(a_0, \mathbf{a})$  and  $(b_0, \mathbf{b})$  can also be expressed as:

$$\mathcal{L} = (\mathbf{l}, \bar{\mathbf{l}}) = (a_0 \mathbf{b} - b_0 \mathbf{a}, \mathbf{a} \times \mathbf{b}) \quad (1.4)$$

where  $\times$  denotes the vector cross product in  $\mathbb{R}^3$ . Every line  $\mathcal{L} = (\mathbf{l}, \bar{\mathbf{l}})$  contains a point at infinity called as the *ideal point* whose homogeneous coordinates are  $(0, \mathbf{l}) = (0, l_{01}, l_{02}, l_{03})$ . Similarly, the line  $\mathcal{L}$  contained in two planes  $(u_0, \mathbf{u})$  and  $(v_0, \mathbf{v})$  is given by:

$$\mathcal{L} = (\mathbf{l}, \bar{\mathbf{l}}) = (\mathbf{u} \times \mathbf{v}, u_0 \mathbf{v} - v_0 \mathbf{u}) \quad (1.5)$$

If a line  $(\mathbf{l}, \bar{\mathbf{l}})$  and a point  $(a_0, \mathbf{a})$  are not incident, the plane  $(u_0, \mathbf{u})$  spanned by them is computed by the formula:

$$(u_0, \mathbf{u}) = (\mathbf{a} \cdot \bar{\mathbf{l}}, -a_0 \bar{\mathbf{l}} + \mathbf{a} \times \mathbf{l}), \quad (1.6)$$

where  $\cdot$  denotes the scalar product in  $\mathbb{R}^3$ . The dual formula to compute the intersection point  $(a_0, \mathbf{a})$  of a plane  $(u_0, \mathbf{u})$  and a line  $(\mathbf{l}, \bar{\mathbf{l}})$  is given by:

$$(a_0, \mathbf{a}) = (\mathbf{u} \cdot \mathbf{l}, -u_0 \mathbf{l} + \mathbf{u} \times \bar{\mathbf{l}}) \quad (1.7)$$

If two lines  $\mathcal{G} = (\mathbf{g}, \bar{\mathbf{g}})$  and  $\mathcal{H} = (\mathbf{h}, \bar{\mathbf{h}})$  intersect in a real point, the plane spanned by them  $\mathcal{G} \vee \mathcal{H} = (u_0, \mathbf{u})$  is computed as follows:

$$(u_0, \mathbf{u}) = (\mathbf{g} \cdot \bar{\mathbf{h}}, \mathbf{g} \times \mathbf{h}). \quad (1.8)$$

The intersection point  $\mathcal{G} \cap \mathcal{H} = (p_0, \mathbf{p})$  of these lines are computed by the following dual formula

$$(p_0, \mathbf{p}) = (\bar{\mathbf{g}} \cdot \mathbf{h}, \bar{\mathbf{g}} \times \bar{\mathbf{h}}). \quad (1.9)$$

### Incidence relations

The point  $(p_0, \mathbf{p})$  is incident with the plane  $(u_0, \mathbf{u})$  if and only if

$$u_0 p_0 + \mathbf{u} \cdot \mathbf{p} = 0 \quad (1.10)$$

A point  $(a_0, \mathbf{a})$  is contained in the line  $(\mathbf{l}, \bar{\mathbf{l}})$  if and only if their exterior product vanishes as follows:

$$\mathbf{a} \cdot \bar{\mathbf{l}} = 0, \quad -a_0 \bar{\mathbf{l}} + \mathbf{a} \times \mathbf{l} = 0 \quad (1.11)$$

Dually, a plane  $(u_0, \mathbf{u})$  and a line  $(\mathbf{l}, \bar{\mathbf{l}})$  if and only if

$$\mathbf{u} \cdot \mathbf{l} = 0, \quad -u_0 \mathbf{l} + \mathbf{u} \times \bar{\mathbf{l}} = 0 \quad (1.12)$$

The following Lemma is stated for the intersection of two lines [PW01]:

**Lemma 1.** *Two lines  $\mathcal{G} = (\mathbf{g}, \bar{\mathbf{g}})$  and  $\mathcal{H} = (\mathbf{h}, \bar{\mathbf{h}})$  intersect if and only if*

$$\mathbf{g} \cdot \bar{\mathbf{h}} + \bar{\mathbf{g}} \cdot \mathbf{h} = 0 \quad (1.13)$$

### 1.2.2 Screw theory

Screw theory has been proven to be a powerful mathematical tool for the analysis of spatial mechanisms. A screw can be used to denote the position and orientation of a spatial vector, the linear and angular velocity of a rigid body, or a force and a moment. Though screw theory approach is local, it provides a quick and efficient methodology to understand the mobility of a moving platform at a given instant. Furthermore, singularities present in the manipulator are easy to determine and visualize using screw theory approach.

Expressing the motion of a rigid body as a combination of a rotation and a translation was first proposed by Chasles (1830) and further developed by Poinsot (1848). Then, Plücker gave the expression for a screw [Plu65]. In 1900, Ball [Bal00] published his classical work, in which he studied the screw theory systematically. He contributed greatly to the formulation of clear ideas about the kinematics and dynamics of a rigid body using screw theory. Hunt [Hun87] further developed screw theory with a geometrical emphasis. Initially he dealt with planar mechanisms and then he analyzed spatial mechanisms. With an introduction to line geometry, the major contribution of Hunt was to classify the screw systems. For instance, he showed that all the screws of the second-order screw system lie on a cylindroid whereas all the screws of the third-order screw system with same pitches lie on a hyperboloid of one sheet. Furthermore, Phillips [Phi84] presented the mechanisms as the geometric essence of machinery. He elaborated on line geometry explaining line complexes and congruences utilizing them to further



describe the classifications of screws as screw systems. Many other researchers, such as Waldron [Wal66], Roth [Rot67], Duffy [Duf82], Angeles [Ang94] have made significant contributions to screw theory. Lately, in 2007, Kong and Gosselin [KG07] have used screw theory to synthesize mechanisms. Recently, Carricato [Car05; CZ14] synthesized numerous type of legs which he classified into invariant, non-invariant and persistent screw systems. The following subsections briefly describe the theoretical concepts behind screw theory.

At any instant the combination of angular velocity and translational velocity of a rigid body along the same line, produces an instantaneous movement. This movement can be expressed as a resultant angular velocity vector  $\omega$  together with a translational velocity vector  $\mathbf{v}$  along the same instantaneous screw axis (ISA), denoted by a *twist*  $\mathbf{t}$ . Similarly, a system of forces,  $\mathbf{f}$  and moments  $\mathbf{m}$  acting on a rigid body can be represented as a *wrench*  $\mathbf{w}$ :

$$\mathbf{t} = \begin{bmatrix} \omega \\ \mathbf{v} \end{bmatrix} ; \quad \mathbf{w} = \begin{bmatrix} \mathbf{f} \\ \mathbf{m} \end{bmatrix} \quad (1.14)$$

Thus, a screw is defined as follows:

**Definition 22.** A *screw* is defined by an axis, the position of a point onto this axis with respect to a reference frame and a pitch.

In general, a screw  $\$$  can be represented as

$$\$ = \begin{bmatrix} \mathbf{s} \\ \mathbf{r} \times \mathbf{s} + h\mathbf{s} \end{bmatrix} \quad (1.15)$$

where  $\mathbf{s}$  is the direction vector of the screw,  $h$  is the pitch of the screw and  $\mathbf{r}$  is the position vector of any point on the screw. Given a twist,  $\mathbf{r}$  and  $h$  can be calculated from the angular and translational velocity vectors in the following way [Bea85]:

$$\mathbf{r} = \frac{\omega \times \mathbf{v}}{\omega \cdot \omega} \quad h = \frac{\omega \cdot \mathbf{v}}{\omega \cdot \omega} \quad s = \frac{\omega}{\|\omega\|} \quad (1.16)$$

Depending on the pitch, three classifications of screws have proved to be useful :

- *Zero-pitch screws*:  $h = 0$ ,  $\$ _0 = \begin{bmatrix} \mathbf{s} \\ \mathbf{r} \times \mathbf{s} \end{bmatrix}$ .
- *Infinite-pitch screws*:  $h = \infty$ ,  $\$ _\infty = \begin{bmatrix} \mathbf{0}_{3 \times 1} \\ \mathbf{s} \end{bmatrix}$ .
- *Finite-pitch screws*:  $h \neq 0$ ,  $h \neq \infty$ . They can be written as a linear combination of  $\$ _0$  and  $\$ _\infty$ .

Furthermore, a *zero-pitch twist* and a *infinite-pitch twist* are represented as  $\xi_0$  and  $\xi_\infty$ , respectively, while a *zero-pitch wrench* and a *infinite-pitch wrench* are represented as  $\zeta_0$  and  $\zeta_\infty$ , respectively.

## Screw systems

**Definition 23.** A *screw system* of order  $n$  ( $0 \leq n \leq 6$ ) comprises of  $n$  linearly independent screws that result in a  $n$  degree-of-freedom system.

Hunt [Hun87] covers all screw systems, the one-system to the five-system, in their general and special forms. The *first-order screw system* or *one-system* consists of a single screw. The

*second-order screw system* or *two-system* comprises of  $\infty^1$  screws and the general ruled surface on which these screws lie is a cylindroid. The *third-order screw system* or *three-system* comprises of  $\infty^2$  screws and the general ruled surface on which these screws lie is a hyperboloid and so on. These screw systems explain the transitory mobility of spatial linkages which can be extended to full-cycle mobility for a great number of linkages.

### Reciprocity conditions

**Definition 24.** Two screws are considered to be **reciprocal** when their contribution to the rate of working is zero. Specifically, if a rigid body is constrained to move about an ISA,  $\xi$  (Figure 1.19) and a wrench  $\zeta$  can contribute nothing to the rate at which work is done by the body, then,  $\xi$  and  $\zeta$  are said to be reciprocal screws [Hun87].

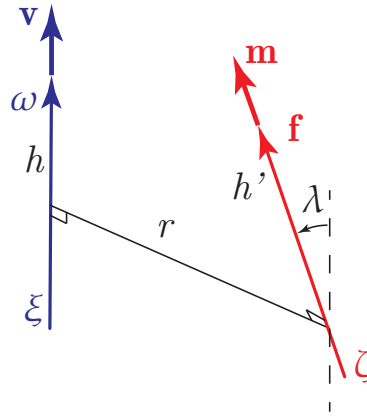


Figure 1.19 – Reciprocal screws

In Figure 1.19, a body is constrained about the ISA  $\xi$  with pitch  $h$ . Its instantaneous angular velocity and translational velocity are  $\omega$  and  $\mathbf{v}$ , respectively. The pitch  $h$  satisfies the relation  $\mathbf{v} = h\omega$ . The screw  $\zeta$  contains a wrench with pitch  $h'$  has its intensity  $\mathbf{f}$  and the moment  $\mathbf{m} = h'\mathbf{f}$ . The shortest distance between  $\xi$  and  $\zeta$  is  $r$  and the angle between them is  $\lambda$ . The work done by the wrench  $\zeta$  on the twist  $\xi$  can be represented as :

$$\begin{aligned} \zeta \circ \xi &= \mathbf{f} \cdot \mathbf{v} + \mathbf{m} \cdot \omega \\ &= \begin{bmatrix} \mathbf{v} & \omega \end{bmatrix} \begin{bmatrix} \mathbf{f} \\ \mathbf{m} \end{bmatrix} \\ &= (\mathbf{\Pi t})^T \mathbf{w}, \quad \text{where } \mathbf{\Pi} = \begin{bmatrix} \mathbf{0}_{3 \times 3} & \mathbf{I}_{3 \times 3} \\ \mathbf{I}_{3 \times 3} & \mathbf{0}_{3 \times 3} \end{bmatrix} \end{aligned} \quad (1.17)$$

where,  $\circ$  is the *reciprocal product* between two screws. For Figure 1.19, when no work is done, the following relationship is obtained:

$$\begin{aligned} \zeta \circ \xi &\implies (\mathbf{f}\mathbf{v} + \mathbf{m}\omega) \cos(\lambda) - \mathbf{f}r\omega \sin(\lambda) = 0 \\ &\implies \mathbf{f}\omega ((h + h') \cos(\lambda) - r \sin(\lambda)) = 0 \end{aligned} \quad (1.18)$$

If the locations and pitches of the screws  $\xi$  and  $\zeta$  are such that

$$(h + h') \cos(\lambda) - r \sin(\lambda) = 0, \quad (1.19)$$

Screw 1	Screw 2	Reciprocity condition
$\$_{10}$	$\$_{2\infty}$	orthogonal axes
$\$_{1\infty}$	$\$_{20}$	orthogonal axes
$\$_{10}$	$\$_{20}$	coplanar axes
$\$_{1\infty}$	$\$_{2\infty}$	always reciprocal

Table 1.1 – Reciprocity conditions

then, irrespective of the applied wrench or the amplitude of the instantaneous twist, the contribution the wrench makes to the instantaneous working rate is zero and the screws are reciprocal. Equation (1.19) is called the *reciprocity condition*. Some important instances of any two reciprocal screws are listed in Table 1.1.

### Twist and wrench systems of parallel manipulators

For a serial kinematic chain with  $n$  joints, there are  $n$  twists associated to the chain and the span of these twists is called the *twist system* of the kinematic chain.

A parallel manipulator consists of a set of  $m$  serial kinematic chains, called as limbs with  $n_i, i = 1, \dots, m$  joints in each limb. If each joint is assigned a twist,  $\xi_{ji}, j = 1, \dots, n_i, i = 1..m$ , there are  $n_i$  twists associated to each limb. Therefore, the twist system  $\mathcal{T}_i$  of each limb is the span of these twists. Additionally, the *wrench system*,  $\mathcal{W}_i$  of the  $i$ -th limb is the span of the wrenches reciprocal to each and every twist  $\xi_{ji}, j = 1, \dots, n_i$ . In other words,  $\mathcal{T}_i$  and  $\mathcal{W}_i$  are orthogonal screw systems and their orders must add up to 6:

$$\mathcal{T}_i = \text{span}\{\xi_{1i}, \xi_{2i}, \dots, \xi_{n_i i}\} \quad ; \quad \mathcal{W}_i = \mathcal{T}_i^\perp, \quad i = 1, \dots, m. \quad (1.20)$$

Moreover, due to the parallel arrangement of the limbs, the global twist system of the parallel kinematic chain  $\mathcal{T}$  is the intersection of the twist systems of each limb,  $\mathcal{T}^i$ . Dually, the wrench system for a parallel kinematic chain is the linear combination of the wrench system from each serial kinematic chain  $\mathcal{W}^i$ :

$$\mathcal{T} = \bigcap_{i=1}^m \mathcal{T}_i \quad ; \quad \mathcal{W} = \bigoplus_{i=1}^m \mathcal{W}_i \quad ; \quad \mathcal{T} = \mathcal{W}^\perp, \quad i = 1, \dots, m. \quad (1.21)$$

Computationally, it is easier to find the linear combination between vector spaces than their intersections. Hence, the twist system of a PM is obtained by first finding its wrench system as a linear combination of the wrench systems of its limbs and then finding the orthogonal screw system.

### Actuation and constraint wrench systems

A parallel manipulator consists of a *total wrench system* of order 6. It can be considered as the linear combination of *actuation wrench system*,  $\mathcal{W}^a$  and *constraint wrench system*,  $\mathcal{W}^c$ .

If the PM has  $m$  number of limbs and each limb has a twist system  $\mathcal{T}_i, (i = 1, \dots, m)$  of order  $t$ , then, the constraint wrench system,  $\mathcal{W}_i^c$  of each leg will be of order  $6 - t$ .

If each leg has  $n(< t)$  unactuated joints, the wrench system reciprocal to unactuated joints is

of order  $6 - n$ . Then, the actuation wrench system of each leg consists of wrenches that do not belong to  $\mathcal{W}^c$ . Therefore, the total wrench system of the PM can be found as

$$\mathcal{W} = \mathcal{W}^a \oplus \mathcal{W}^c \quad (1.22)$$

In a general configuration, the constraint and actuation wrench systems of parallel manipulators form a 6-system. It means that by locking the actuators, the moving platform must be fully constrained, otherwise the manipulator reaches a parallel singularity [KG07]. A parallel singularity can be an actuation singularity, a constraint singularity or a compound singularity [Nur15; Ami11; AMC16; MNC16; NC15].

### Extended Jacobian matrix

Based on the theory of reciprocal screws [Hun87; Phi84], Joshi and Tsai [JT02] developed a methodology to express the  $6 \times 6$  extended Jacobian matrix,  $\mathbf{J}_E$  for lower-mobility PMs that includes constraint and actuation wrenches. It is expressed as the concatenation of actuation and constraint wrenches of the PM:

$$\mathbf{J}_E = \begin{bmatrix} \mathcal{W}^a & \mathcal{W}^c \end{bmatrix} \quad (1.23)$$

### 1.2.3 Algebraic geometry

In algebraic geometry, methods from both algebra and geometry are used to gain understanding of the solution system to a given set of polynomial equations over a field,  $k$ .  $k$  can be a set of  $\mathbb{Q}$  (rational numbers), or  $\mathbb{C}$  (complex numbers), or  $\mathbb{R}$  (real numbers). The set of all polynomials in  $x_1, \dots, x_n$  with coefficients in  $k$  is denoted  $k[x_1, \dots, x_n]$ . Since parallel manipulators are governed by geometric constraints that can be written in terms of polynomial equations, algebraic geometry tools can be used to understand their kinematic behavior.

It should be noted that all the following definitions and examples are chosen from Cox, Little and O'Shea [CLO07], where the reader can find further explanations.

### Ideals and Varieties

**Definition 25.** A subset  $\mathcal{J} \subset k[x_1, \dots, x_n]$  is an **ideal** if it satisfies:

$$\begin{aligned} (i) & \quad 0 \in \mathcal{J} \\ (ii) & \quad \text{If } f, g \in \mathcal{J} \text{ then } f + g \in \mathcal{J} \\ (iii) & \quad \text{If } f \in \mathcal{J} \text{ and } h \in k[x_1, \dots, x_n], \text{ then } hf \in \mathcal{J} \end{aligned} \quad (1.24)$$

The first natural example of an ideal is the ideal generated by a finite number of polynomials.

**Definition 26.** Let  $f_1, \dots, f_s$  be polynomials in  $k[x_1, \dots, x_n]$ , then

$$\langle f_1, \dots, f_s \rangle = \left\{ \sum_{i=1}^s h_i f_i : h_1, \dots, h_s \in k[x_1, \dots, x_n] \right\} \quad (1.25)$$

is an ideal.

**Lemma 2.** If  $f_1, \dots, f_s \in k[x_1, \dots, x_n]$  then  $\langle f_1, \dots, f_s \rangle$  is an ideal of  $k[x_1, \dots, x_n]$  and  $\langle f_1, \dots, f_s \rangle$  is called the ideal generated by  $f_1, \dots, f_s$ .

An ideal  $\mathcal{J}$  is *finitely generated* if there exist  $f_1, \dots, f_s \in k[x_1, \dots, x_n]$  such that  $\mathcal{J} = \langle f_1, \dots, f_s \rangle$ , and  $f_1, \dots, f_s$  are called a *basis* of  $\mathcal{J}$ .

**Definition 27.** If  $f_1, \dots, f_s$  are polynomials in the field  $k[x_1, \dots, x_n]$  and if

$$\mathbf{V}(f_1, \dots, f_s) = \{(a_1, \dots, a_n) \in k^n : f_i(a_1, \dots, a_n) = 0, \text{ for all } 1 \leq i \leq s\} \quad (1.26)$$

then  $\mathbf{V}(f_1, \dots, f_s)$  is called an **affine variety** defined by the polynomials  $f_i$ .

Thus, an affine variety  $\mathbf{V}(f_1, \dots, f_s) \subset k^n$  is the set of all solutions of the system of equations  $f_1(x_1, \dots, x_n) = \dots = f_s(x_1, \dots, x_n) = 0$ .

**Lemma 3.** If  $V \subset k^n$  is an affine variety, then  $\mathbf{I}(V) \subset k[x_1, \dots, x_n]$  defined as

$$\mathbf{I}(V) = \{f \in k[x_1, \dots, x_n] : f(a_1, \dots, a_n) = 0 \text{ for all } (a_1, \dots, a_n) \in V\} \quad (1.27)$$

is called as the *ideal* of  $V$ .

An affine variety can also be defined as the *vanishing set* of an ideal. The following example clarifies the definitions of ideals and varieties [McC86]:

**Example 1.** A circle of center  $(0,0)$  and a line are given as  $x_1^2 + x_2^2 - 1 = 0$  and  $x_1 + x_2 - 1 = 0$  respectively. Then the ideal generated by these two equations is given by  $\mathcal{J} = \langle x_1^2 + x_2^2 - 1, x_1 + x_2 - 1 \rangle$  and the corresponding variety is  $\{(1,0), (0,1)\}$ . Figure 1.20 shows the variety corresponding

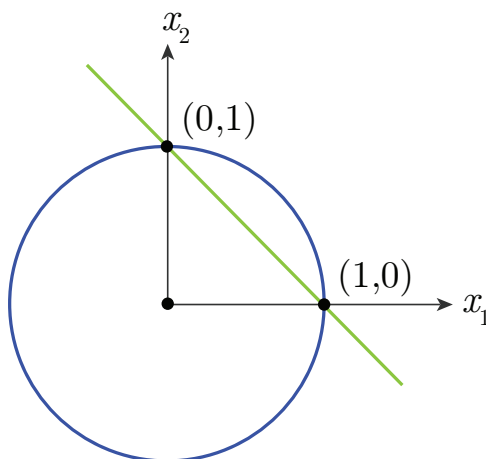


Figure 1.20 – Variety corresponding to the ideal  $\mathcal{J} = \langle x_1^2 + x_2^2 - 1, x_1 + x_2 - 1 \rangle$ .

to the ideal  $\mathcal{J}$ .

### Hilbert Basis Theorem and Gröbner Basis

In the algebra of polynomial ideals and the geometry of affine varieties, the following two problems are of concern:

- The Ideal Description Problem* : Does every ideal  $\mathcal{J} \subset k[x_1, \dots, x_n]$  have a finite generating set? In other words, can we write  $\mathcal{J} = \langle f_1, \dots, f_s \rangle$  for some  $f_i \in k[x_1, \dots, x_n]$ ?
- The Ideal Membership Problem* : Given  $f \in k[x_1, \dots, x_n]$  and an ideal  $\mathcal{J} = \langle f_1, \dots, f_s \rangle$ , determine if  $f \in \mathcal{J}$ . Geometrically, this is closely related to the problem of determining whether  $\mathbf{V}(f_1, \dots, f_s)$  lies on the variety  $\mathbf{V}(f)$ .

The following theorem answers the ideal description problem :

**Theorem 1. (Hilbert Basis Theorem)** : Every ideal  $\mathcal{J} \subset k[x_1, \dots, x_n]$  has a finite generating set. That is,  $\mathcal{J} = \langle g_1, \dots, g_t \rangle$  for some  $g_1, \dots, g_t \in \mathcal{J}$ .

A notion of ordering of terms in polynomials is a key ingredient in algebraic geometry. It helps in division and row-reduction algorithms of the polynomials which are important to solve linear equations. The ordering used in this context is *lexicographic ordering* defined as follows:

**Definition 28. (Lexicographic order)**: Let  $\alpha = (\alpha_1, \dots, \alpha_n)$  and  $\beta = (\beta_1, \dots, \beta_n) \in \mathbb{Z}_{\geq 0}^n$ . It is said that  $\alpha >_{lex} \beta$  if, in the vector difference  $\alpha - \beta \in \mathbb{N}^n$ , the leftmost nonzero entry is positive. The monomials  $x^\alpha >_{lex} x^\beta$  if  $\alpha >_{lex} \beta$ .

Fixing the monomial ordering, the standard basis can be defined as :

**Definition 29.** A finite subset  $G = g_1, \dots, g_t$  of an ideal  $\mathcal{J}$  is said to be a **Gröbner basis** (or **standard basis**) if  $\langle LT(g_1), \dots, LT(g_t) \rangle = \langle LT(\mathcal{J}) \rangle$ .

where  $LT$  is the *Leading Term* of the polynomial. Equivalently, but more informally, a set  $g_1, \dots, g_t \in \mathcal{J}$  is a Gröbner basis of  $\mathcal{J}$  if and only if the leading term of any element of  $\mathcal{J}$  is divisible by one of the  $LT(g_i)$ .

Some applications of Gröbner basis include:

1. Solving the *ideal membership problem* along with the help of division algorithm of polynomials which gives the condition for the existence of a solution.

**Example 2.** Let  $\mathcal{J} = \langle f_1, f_2 \rangle = \langle xz - y^2, x^3 - y^2 \rangle$ . Does the polynomial  $f = -4x^2y^2z^2 + y^6 + 3z^5$  belong to the ideal  $\mathcal{J}$ ?

Using *lex ordering*, the Gröbner basis of ideal  $\mathcal{J}$  can be computed using a computer algebra system:

$$G = \{f_1, f_2, f_3, f_4, f_5\} = \{xz - y^2, x^3 - z^2, x^2y^2 - z^3, xy^4 - z^4, y^6 - z^5\}.$$

Dividing  $f$  by  $G$  gives:

$$f = (-4xy^2z - 4y^4)f_1 - 3f_5,$$

proving that  $f \in \mathcal{J}$ .

2. *Solving polynomial equations*: This is the most relevant application in this context and is explained with the help of a simple example:

**Example 3.** For a set of equations in  $\mathbb{R}^3$ ,

$$x^2 + y + z = 1$$

$$x + y^2 + z = 1$$

$$x + y + z^2 = 1$$

the ideal is determined as  $\mathcal{J} = \langle x^2 + y + z - 1, x + y^2 + z - 1, x + y + z^2 - 1 \rangle \subset \mathbb{R}[x, y, z]$  and all the points in  $\mathbf{V}(\mathcal{J})$  are to be found.

Computing a Gröbner basis on  $\mathcal{J}$  with respect to *lex order* gives

$$g_1 = x + y + z^2 - 1$$

$$g_2 = y^2 - y - z^2 + z$$

$$g_3 = 2yz^2 + z^4 - z^2$$

$$g_4 = z^6 - 4z^4 + 4z^3 - z^2$$

Here the polynomial  $g_4$  depends on  $z$  alone, hence, the possible values of  $z$  are  $0, 1$  and  $-1 \pm \sqrt{2}$ . Substituting these values into  $g_2 = 0$  and  $g_3 = 0$ , determines the  $y$ 's, and then finally  $g_1 = 0$  gives the corresponding  $x$ 's. Thus, the solutions for the three polynomial equations are  $(1, 0, 0)$ ,  $(0, 1, 0)$ ,  $(0, 0, 1)$ ,  $(-1+\sqrt{2}, -1+\sqrt{2}, -1+\sqrt{2})$  and  $(-1-\sqrt{2}, -1-\sqrt{2}, -1-\sqrt{2})$ . The intersection curves of the three pairs of polynomials in the ideal  $\mathcal{J} =$

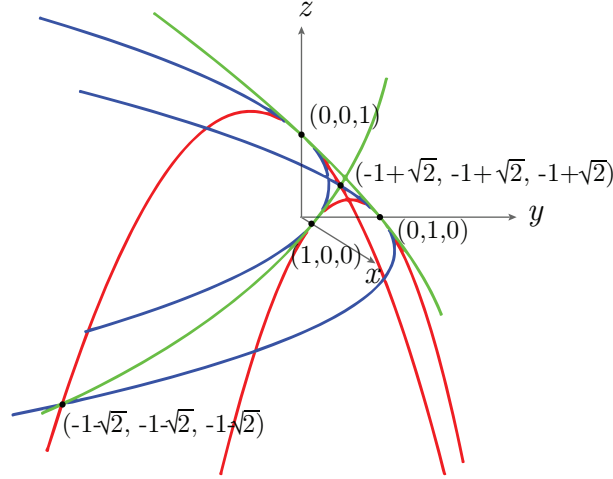


Figure 1.21 – Solution to the system of equations  $\{x^2 + y + z = 1, x + y^2 + z = 1, x + y + z^2 = 1\}$ .

$\langle x^2 + y + z - 1, x + y^2 + z - 1, x + y + z^2 - 1 \rangle$  are shown in Fig. 1.21. Additionally, the solutions to the given set of equations are indicated.

3. The implicitization problem in which a variety  $V \subset k^n$  is given parametrically as  $x_1 = g_1(t_1, \dots, t_m), \dots, x_n = g_n(t_1, \dots, t_m)$  and the task is to find out the system of polynomial equations that defines the variety.

### Primary decomposition

It is sometimes useful to decompose a given ideal into simpler ideals and study them separately. The original ideal can then be expressed as the intersection of these sub-ideals.

**Definition 30.** The intersection  $\mathcal{J} \cap \mathcal{J}$  of two ideals  $\mathcal{J}$  and  $\mathcal{J}$  in  $k[x_1, \dots, x_n]$  is the set of polynomials which belong to both  $\mathcal{J}$  and  $\mathcal{J}$ .

Intersection of ideals is equivalent to the union of corresponding varieties according to the following theorem:

**Theorem 2.** If  $\mathcal{J}$  and  $\mathcal{J}$  are ideals in  $k[x_1, \dots, x_n]$ , then  $\mathbf{V}(\mathcal{J} \cap \mathcal{J}) = \mathbf{V}(\mathcal{J}) \cup \mathbf{V}(\mathcal{J})$

In this light, the following theorem has been stated

**Theorem 3.** Every ideal  $\mathcal{J} \subseteq k[x_1, \dots, x_n]$  can be written as a finite intersection of primary ideals.

A Primary Ideal and a Prime Ideal is defined as follows:

**Definition 31.** An ideal  $\mathcal{J}$  in  $k[x_1, \dots, x_n]$  is **primary** if  $fg \in \mathcal{J}$  implies either  $f \in \mathcal{J}$  or some power  $g^m \in \mathcal{J}$  for some  $m > 0$ .

An ideal  $\mathcal{J}$  in  $k[x_1, \dots, x_n]$  is **prime** if  $fg \in \mathcal{J}$  implies either  $f \in \mathcal{J}$  or  $g \in \mathcal{J}$ .

**Example 4.**  $\langle x^2 \rangle$  is a primary ideal, but not prime.

Eventually, the *Primary Decomposition* of an ideal can be defined in the following way:

**Definition 32.** A **primary decomposition** of a given ideal  $\mathcal{J}$  is an expression of  $\mathcal{J}$  as an intersection of primary ideals, namely  $\mathcal{J} = \bigcap_{i=1}^r Q_i$ . Such a decomposition is called *minimal* if the radicals  $\sqrt{Q_i}$  are all different and  $Q_i \cap_{i \neq j} Q_j$ . Furthermore, if no radical  $\sqrt{Q_i}$  is strictly contained in radical  $\sqrt{Q_j}$ , then the primary components  $Q_i$  are uniquely determined. The radicals  $\sqrt{Q_i} = P_i$  are the corresponding prime ideals.

The radical ideal is defined as :

**Definition 33.** Let  $\mathcal{J} \subset k[x_1, \dots, x_n]$  be an ideal. The **radical** of  $\mathcal{J}$ , denoted  $\sqrt{\mathcal{J}}$ , is the set  $\{f : f^m \in \mathcal{J} \text{ for some integer } m \geq 1\}$ .

**Example 5.** The primary decomposition of the ideal  $\langle x^3 - xy^3 \rangle \subset k[x, y]$  yields two prime ideals  $\langle x \rangle$  and  $\langle x^2 - y^3 \rangle$ . Figure 1.22 depicts the primary decomposition of the ideals as the union of their corresponding varieties.

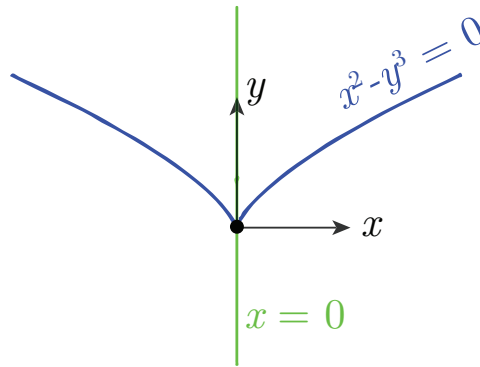


Figure 1.22 –  $\mathbf{V}(\langle x^3 - xy^3 \rangle)$  as the union of varieties  $\mathbf{V}(\langle x \rangle)$  in green and  $\mathbf{V}(\langle x^2 - y^3 \rangle)$  in blue.

**Example 6.** The primary decomposition of an ideal need not be unique. For instance, the ideal  $\langle x^2, xy \rangle \subset k[x, y]$  has two distinct minimal decompositions whose radicals are identical :  $\langle x^2, xy \rangle = \langle x \rangle \cap \langle x^2, xy, y^2 \rangle = \langle x \rangle \cap \langle x^2, y \rangle$ .

## Hilbert dimension

**Theorem 4.** Let  $V = V(\mathcal{J})$  be an affine variety, where  $\mathcal{J} \subset k[x_1, \dots, x_n]$  is an ideal. If  $k$  is algebraically closed, then the dimension of  $V$  is the maximum dimension of a coordinate subspace in  $V(\langle LT(I) \rangle)$

The degree of *Hilbert polynomial* also yields the dimension of  $V$  and is known as the *Hilbert dimension*. If the Hilbert dimension is zero, it means that there are finite number of intersections between the polynomials that constitute the corresponding ideal. It has been proved that the degrees of freedom of a mechanism is the Hilbert dimension of the ideal of its constraint polynomials [HS08].

For radical ideals and algebraically closed fields, Table 1.2 summarizes the mapping between algebra and geometry.



ALGEBRA	GEOMETRY
radical ideals	varieties
addition of ideals	intersection of varieties
product of ideals	union of varieties
intersection of ideals	union of varieties
quotient of ideals	difference of varieties
elimination of variables	projection of varieties
prime ideals	irreducible varieties

Table 1.2 – Mapping between algebra and geometry in algebraic geometry [CLO07]

### Trigonometric identities

Algebraic geometry tools can only be used if the constraint equations are algebraic. But the geometric constraint equations are often trigonometric and the following formulas and substitutions are recalled to perform the simplifications and make them algebraic:

$$\sin^2(\theta) + \cos^2(\theta) = 1 \quad (1.28)$$

where  $\theta$  is arbitrary.

A useful change of variables is the *Weierstrass substitution* named after Karl Weierstrass (1815-1897):

$$t = \tan\left(\frac{\theta}{2}\right). \quad (1.29)$$

With this transformation and the double-angle trigonometric identities, it immediately follows:

$$\sin(\theta) = \frac{2t}{1+t^2}, \quad \cos(\theta) = \frac{1-t^2}{1+t^2}, \quad \tan(\theta) = \frac{2t}{1-t^2}. \quad (1.30)$$

It is commonly known as the *tangent half-angle substitution* and the mapping has a pre-image  $[0, 2\pi]$  and the image  $\mathbb{R} \cup \{\infty\}$ .

#### 1.2.4 Study's kinematic mapping

A *kinematic mapping* converts the variables specifying a displacement into a set of coordinates of a point in a higher dimensional space [McC86]. These variables can be the three orientation angles of a rotation or the three position coordinates along with three orientation angles of a spatial displacement. For parallel manipulators, kinematic mapping is a transformation of their configuration space to another space called the image space in which the geometric study of the constraints typical of mechanical systems is simplified.

Euclidean three space is the three dimensional vector space  $\mathbb{R}^3$  together with the usual scalar product  $\mathbf{x}^T \mathbf{y} = \sum_{i=1}^3 x_i y_i$ . The spatial Euclidean displacement is a mapping of

$$\gamma : \mathbb{R}^3 \rightarrow \mathbb{R}^3, \quad \mathbf{x} = \mathbf{R}\mathbf{x} + \mathbf{d} \quad (1.31)$$

where  $\mathbf{R} \in SO(3)$  is a proper orthogonal three by three matrix and  $\mathbf{d} \in \mathbb{R}^3$  is a displacement vector. The entries of matrix  $\mathbf{R}$  fulfill the well-known orthogonality condition  $\mathbf{R}^T \mathbf{R} = \mathbf{I}$  where,  $\mathbf{I}$  is the identity matrix.

The group of all Euclidean displacements is denoted by  $SE(3)$ . To incorporate homogeneous coordinates, it is convenient to write Equation (1.31) as follows:

$$\begin{bmatrix} 1 \\ \mathbf{x} \end{bmatrix} = \begin{bmatrix} 1 & \mathbf{0}_{3 \times 1}^T \\ \mathbf{d} & \mathbf{R} \end{bmatrix} \cdot \begin{bmatrix} 1 \\ \mathbf{x} \end{bmatrix} \quad (1.32)$$

Study in 1891 introduced a set of 8 parameters to represent a spatial displacement. Hence, *Study's kinematic mapping* maps each spatial Euclidean displacement  $\gamma$  of  $SE(3)$  onto a point in  $\mathbf{p} \in \mathbb{P}^7$ . In this parametrization, a point  $[x, y, z]$  is transformed to  $[x', y', z']$  according to:

$$[1, x', y', z']^T = \mathbf{M}[1, x, y, z]^T \quad (1.33)$$

where, the matrix  $\mathbf{M} \in SE(3)$  is represented as [Hus+07]:

$$\mathbf{M} = \begin{bmatrix} x_0^2 + x_1^2 + x_2^2 + x_3^2 & \mathbf{0}_{3 \times 1}^T \\ \mathbf{M}_T & \mathbf{M}_R \end{bmatrix} \quad (1.34a)$$

$$\mathbf{M}_T = \begin{bmatrix} -2x_0y_1 + 2x_1y_0 - 2x_2y_3 + 2x_3y_2 \\ -2x_0y_2 + 2x_1y_3 + 2x_2y_0 - 2x_3y_1 \\ -2x_0y_3 - 2x_1y_2 + 2x_2y_1 + 2x_3y_0 \end{bmatrix} \quad (1.34b)$$

$$\mathbf{M}_R = \begin{bmatrix} x_0^2 + x_1^2 - x_2^2 - x_3^2 & -2x_0x_3 + 2x_1x_2 & 2x_0x_2 + 2x_1x_3 \\ 2x_0x_3 + 2x_1x_2 & x_0^2 - x_1^2 + x_2^2 - x_3^2 & -2x_0x_1 + 2x_3x_2 \\ -2x_0x_2 + 2x_1x_3 & 2x_0x_1 + 2x_3x_2 & x_0^2 - x_1^2 - x_2^2 + x_3^2 \end{bmatrix} \quad (1.34c)$$

where  $\mathbf{M}_T$  and  $\mathbf{M}_R$  represent the translational and rotational parts of the transformation matrix  $\mathbf{M}$  respectively. The parameters  $x_i, y_i, i \in \{0, \dots, 3\}$  present in the transformation matrix  $\mathbf{M}$  are called the *Study-parameters*. An Euclidean transformation can be represented by a point  $p \in \mathbb{P}^7$  if and only if the following equation and inequality are satisfied:

$$x_0y_0 + x_1y_1 + x_2y_2 + x_3y_3 = 0 \quad (1.35)$$

$$x_0^2 + x_1^2 + x_2^2 + x_3^2 \neq 0 \quad (1.36)$$

All the points that satisfy the Equation (1.35) belong to the 6-dimensional *Study quadric*,  $S_6^2$ . The points that do not satisfy the inequality (1.36) lie on the *exceptional generator*  $x_0 = x_1 = x_2 = x_3 = 0$ .

Study's kinematic mapping is closely related to the algebra of *dual quaternions*, where the eight basis elements of a dual quaternion correspond to Study parameters. The inverse of the transformation matrix  $\mathbf{M}^{-1}$  expressed in the Study-parameters  $(x_0 : x_1 : x_2 : x_3 : y_0 : y_1 : y_2 : y_3)$  is given by  $(x_0 : -x_1 : -x_2 : -x_3 : y_0 : -y_1 : -y_2 : -y_3)$ .

To find this inverse mapping, we need to know how to obtain the Study-parameters from the entries of matrix  $\mathbf{R} = [a_{ij}]_{i,j=1,\dots,3}$  and the displacement vector  $\mathbf{d} = [d_1, d_2, d_3]^T$ . It was shown by Study that the quadruple  $x_0 : x_1 : x_2 : x_3$  can be computed in one of the following ways :

$$\begin{aligned} x_0 : x_1 : x_2 : x_3 &= 1 + a_{11} + a_{22} + a_{33} : a_{32} - a_{23} : a_{13} - a_{31} : a_{21} - a_{12} \\ &= a_{32} - a_{23} : 1 + a_{11} - a_{22} - a_{33} : a_{21} + a_{12} : a_{13} - a_{31} \\ &= a_{13} - a_{31} : a_{21} + a_{12} : 1 - a_{11} + a_{22} - a_{33} : a_{32} + a_{23} \\ &= a_{21} - a_{12} : a_{13} + a_{31} : a_{32} - a_{23} : 1 - a_{11} - a_{22} + a_{33} \end{aligned} \quad (1.37)$$

Some of the ratios can be zero simultaneously, however Study showed that at least one of the ratios is not equal to  $(0 : 0 : 0 : 0)$ . The remaining Study-parameters are computed as:

$$\begin{aligned} 2y_0 &= d_1x_1 + d_2x_2 + d_3x_3 \\ 2y_1 &= -d_1x_0 + d_3x_2 = d_2x_3 \\ 2y_2 &= -d_2x_0 - d_3x_1 + d_1x_3 \\ 2y_3 &= -d_3x_0 + d_2x_1 - d_1x_2 \end{aligned} \quad (1.38)$$

### 1.2.5 Transformation axis

The French geometer Michel Chasles (1793-1880) stated the following theorem:

**Theorem 5.** *Any rigid body displacement can be produced by translation along a line followed by rotation about that line.*

Such a combination of rotation and translation is known as the *Screw displacement* and the line is called as the *Finite Screw Axis (FSA)* [BR79]. It is advantageous to represent the FSA in terms of *Plücker coordinates*,  $\mathcal{L} = (p_{01}, p_{02}, p_{03}, p_{23}, p_{31}, p_{12})$ . The FSA corresponds to the transformation that maps the coordinate frame attached to the fixed base of a PM to the coordinate frame attached to the moving platform of the PM [Nur15]. The Plücker-coordinates of the corresponding FSA in terms of the Study-parameters is given as [Sch+14]:

$$\begin{aligned} p_{01} &= (-x_1^2 - x_2^2 - x_3^2)x_1, & p_{23} &= x_0y_0x_1 - (-x_1^2 - x_2^2 - x_3^2)y_1 \\ p_{02} &= (-x_1^2 - x_2^2 - x_3^2)x_2, & p_{31} &= x_0y_0x_2 - (-x_1^2 - x_2^2 - x_3^2)y_2 \\ p_{03} &= (-x_1^2 - x_2^2 - x_3^2)x_3, & p_{12} &= x_0y_0x_3 - (-x_1^2 - x_2^2 - x_3^2)y_3 \end{aligned} \quad (1.39)$$

where,  $(p_{01}, p_{02}, p_{03})^T$  is the direction vector of the FSA. Furthermore, if the Study-parameters are normalized ( $x_0^2 + x_1^2 + x_2^2 + x_3^2 = 1$ ), the angle  $\phi$  of the rotational part and the distance  $s$  of the translational part of the given transformation can be computed from the Study-parameters directly with

$$\cos\left(\frac{\phi}{2}\right) = x_0 \quad ; \quad s = \frac{2y_0}{\sqrt{x_1^2 + x_2^2 + x_3^2}} \quad (1.40)$$

### 1.2.6 Tilt and Torsion angles

There are several ways to parametrize the orientation of a rigid body. The orientation Study parameters  $x_0, x_1, x_2, x_3$  do this job and are useful to interpret and analyze the motion of a mechanism algebraically. However, they are not intuitive and require some manipulation to clearly understand the orientation capabilities of a mechanism. In this vein, Bonev *et al.* [BR99; BZG02] introduced a set of modified Euler angles that offer a compact and intuitive representation of the orientation workspace of PMs. They are known as *Tilt and Torsion angles (T&T angles)* and are shown in Fig. 1.23.

In case of ZXZ Euler convention, a rotation matrix is decomposed as:

$$\mathbf{R} = \mathbf{R}_z(\phi)\mathbf{R}_x(\theta)\mathbf{R}_z(\psi), \quad (1.41)$$

where  $\phi$ ,  $\theta$  and  $\psi$  represent yaw, pitch and roll angles respectively. However, *T&T angles* use only two rotations:

$$\mathbf{R} = \mathbf{R}_a(\theta)\mathbf{R}_z(\sigma) \quad (1.42)$$

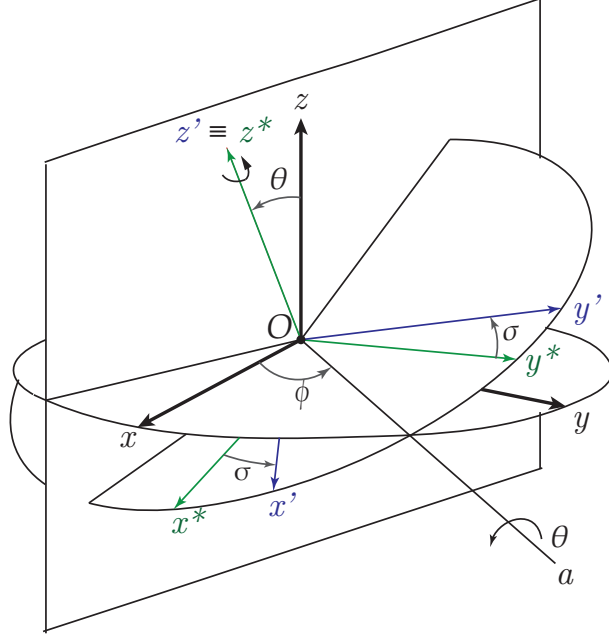


Figure 1.23 – Tilt and Torsion angles [BZG02]

where  $\theta$  is the tilt and  $\sigma$  represents the torsion angle. This is the reason why they are named as Tilt and Torsion angles. However, it should be noted that the azimuth angle locates the axis  $a$ . It is measured as  $\phi$  from the initial position of  $x$ -axis. This simple yet effective change of angles makes the whole analysis much simpler and suitable for the study of a PM. The change of parametrization from the orientation dual quaternions to T&T angles is done as follows:

$$\begin{aligned}
 x_0 &= \cos\left(\frac{\theta}{2}\right) \cos\left(\frac{\sigma}{2}\right) \\
 x_1 &= \sin\left(\frac{\theta}{2}\right) \cos\left(\phi - \frac{\sigma}{2}\right) \\
 x_2 &= \sin\left(\frac{\theta}{2}\right) \sin\left(\phi - \frac{\sigma}{2}\right) \\
 x_3 &= \cos\left(\frac{\theta}{2}\right) \sin\left(\frac{\sigma}{2}\right)
 \end{aligned} \tag{1.43}$$

### 1.3 Conclusions

In this chapter, the existing literature on PMs, S-PMs and compliant mechanisms was reviewed and the mathematical tools necessary to analyze those mechanisms were presented.

This doctoral thesis focuses on reconfigurable lower mobility parallel manipulators and other mechanisms whose architectures are based on them. Therefore, the technological advancements and applications of PMs were discussed. Serial arrangements of these PMs lead to series-parallel manipulators. The theoretical importance of S-PMs was highlighted. Moreover, the origin and growing interest in compliant mechanisms were presented emphasizing their synthesis based on the parallel singularities of lower mobility PMs.

Furthermore, the fundamental concepts and tools necessary to analyze the aforementioned mechanisms were explained starting with the line geometry. Screw theory tools used for local

kinematic analysis and algebraic geometry tools used for global kinematic analysis were presented with examples. Study's kinematic mapping was explained with an aim to derive the algebraic constraint equations. Finally, the transformation axis coordinates were expressed in terms of Study parameters and Tilt and Torsion angles that come in handy for some special PMs.

The operation mode analysis is performed in detail in Chapter 2 for some PMs revealing their reconfigurable behavior.

## Chapter 2

# Operation modes of parallel manipulators

This chapter presents the operation mode analysis of some parallel manipulators (PM) starting with the simplest one, a parallelogram linkage. It is analyzed to determine the constraint singularities that will be later used to design a compliant mechanism in Chapter 5. Furthermore, a family of 3-[PP]S PMs is studied to determine their operation modes with an ultimate goal to compare their performances as will be shown in Chapter 3. It is followed by the analysis of a RUU limb, there by identifying the operation modes of a 3-RUU PM and a 4-rRUU reconfigurable PM whose working prototype will be constructed.

Initially, the manipulator architecture is examined to determine the underlying geometrical constraints. To convert these constraints as equations, it is necessary to express all the vectors in the same coordinate system, usually the one associated with the fixed base. Study's kinematic mapping is exploited for this purpose so that the constraint equations are algebraic. Consequently, algebraic geometry tools can be applied to determine the operation modes. This is done by performing the primary decomposition of the ideal of constraint polynomials in a computer algebra system SINGULAR [Dec+18]. The obtained sub-ideals correspond to the operation modes exhibited by the PM.

### 2.1 Operation mode analysis

#### 2.1.1 An equilateral four-bar linkage

The simplest PM is a four bar linkage. This section presents the operation mode analysis of a four-bar linkage with equal link lengths with an algebraic view point.

A planar equilateral four-bar linkage with equal link lengths,  $l$  is depicted in Fig. 2.1. Link  $AD$  is fixed,  $AB$  and  $CD$  are the cranks and  $BC$  is the coupler. The origin of the fixed frame ( $\Sigma_0$ ),  $O_0$  coincides with the center of link  $AD$  while that of the moving frame ( $\Sigma_1$ )  $O_1$  with the center of  $BC$ . The coordinate axes are oriented in such a way that the position vectors of the intersection points between the revolute joint axes and the  $x_0y_0$  plane can be homogeneously written as follows:

$$\begin{aligned} \mathbf{r}_A^0 &= [1, \frac{-l}{2}, 0]^T & \mathbf{r}_D^0 &= [1, \frac{l}{2}, 0]^T \\ \mathbf{r}_B^1 &= [1, \frac{-l}{2}, 0]^T & \mathbf{r}_C^1 &= [1, \frac{l}{2}, 0]^T \end{aligned} \quad (2.1)$$

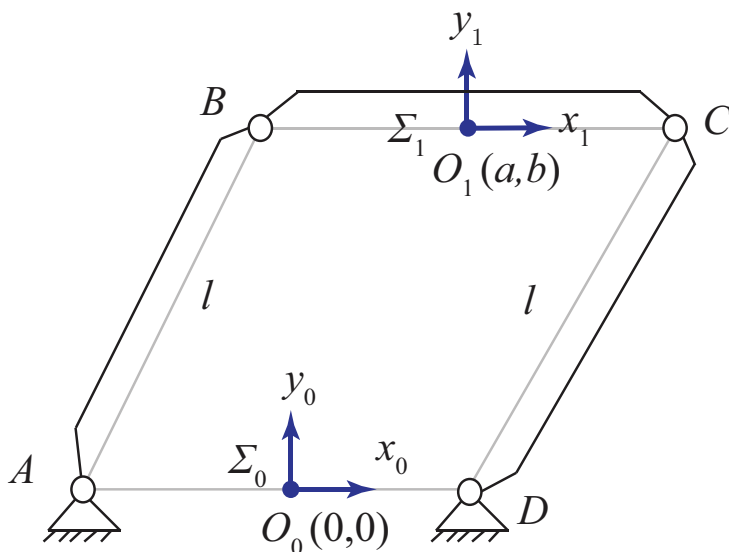


Figure 2.1 – An equilateral four bar linkage.

The displacement of the coupler with respect to the fixed frame can be rendered by  $(a, b, \phi)$ , where  $a$  and  $b$  represent the positional displacement of the coupler (nothing but the coordinates of point  $O_1$  in  $\Sigma_0$ ) and  $\phi$  is the angular displacement about  $z_0$ -axis (angle between  $x_0$  and  $x_1$ ). Thus, the corresponding set of displacements can be mapped onto a three-dimensional projective space,  $\mathbb{P}^3$  with homogeneous coordinates  $x_i$  ( $i = 1, 2, 3, 4$ ) [BR79]. This mapping (also known as Blaschke mapping in the literature [BR79]) is defined by the following matrix  $\mathbf{M}$  :

$$\mathbf{M} = \begin{bmatrix} 1 & 0 & 0 \\ \frac{2x_1x_3 + 2x_2x_4}{x_3^2 + x_4^2} & \frac{-x_3^2 + x_4^2}{x_3^2 + x_4^2} & \frac{-2x_3x_4}{x_3^2 + x_4^2} \\ \frac{-2x_1x_4 + 2x_2x_3}{x_3^2 + x_4^2} & \frac{2x_3x_4}{x_3^2 + x_4^2} & \frac{-x_3^2 + x_4^2}{x_3^2 + x_4^2} \end{bmatrix} \quad (2.2)$$

The planar kinematic mapping can also be derived as a special case of Study's kinematic mapping by setting  $x_1 = x_2 = y_0 = y_3 = 0$  in Eq. 1.34c [Hus+07]. To avoid the rotational part of  $\mathbf{M}$  to be undefined, the following equation is defined:

$$H := x_3^2 + x_4^2 = 1 \quad (2.3)$$

Without loss of generality,  $x_i$  can be expressed in terms of  $(a, b, \phi)$ , as follows [BR79] :

$$x_1 : x_2 : x_3 : x_4 = (au - bv) : (av + bu) : 2u : 2v, \quad u = \sin\left(\frac{\phi}{2}\right), \quad v = \cos\left(\frac{\phi}{2}\right). \quad (2.4)$$

### Constraint Equations

Points  $B$  and  $C$  are constrained to move along circles of centers  $A$  and  $D$ , respectively and with radius  $l$  each. The position vectors of points  $B$  and  $C$  are expressed algebraically in frame  $\Sigma_0$  as follows :

$$\mathbf{r}_B^0 = M \mathbf{r}_B^1 \quad ; \quad \mathbf{r}_C^0 = M \mathbf{r}_C^1 \quad (2.5)$$

Therefore, the algebraic constraint equations take the form :

$$(\mathbf{r}_B^0 - \mathbf{r}_A^0)^T(\mathbf{r}_B^0 - \mathbf{r}_A^0) = l^2 \implies g_1 := 4(x_1^2 + x_2^2) + 4lx_1x_3 - l^2x_4^2 = 0 \quad (2.6)$$

$$(\mathbf{r}_C^0 - \mathbf{r}_D^0)^T(\mathbf{r}_C^0 - \mathbf{r}_D^0) = l^2 \implies g_2 := 4(x_1^2 + x_2^2) - 4lx_1x_3 - l^2x_4^2 = 0 \quad (2.7)$$

Since  $g_1 \pm g_2 = 0$  gives the same variety as (2.6) and (2.7), the final simplified constraint equations are :

$$H_1 := g_1 - g_2 := 4lx_1x_3 = 0 \quad (2.8)$$

$$H_2 := g_1 + g_2 := 4(x_1^2 + x_2^2) - l^2x_4^2 = 0 \quad (2.9)$$

Equation (2.8) degenerates into two planes  $x_1 = x_3 = 0$  into the image space and Eq. (2.9) amounts to a cylinder with a circular cross-section in the image space. Assuming  $x_4 \neq 0$ , these constraint manifolds can be represented in the affine space,  $\mathbb{A}^3$ , as shown in Fig. 2.2.

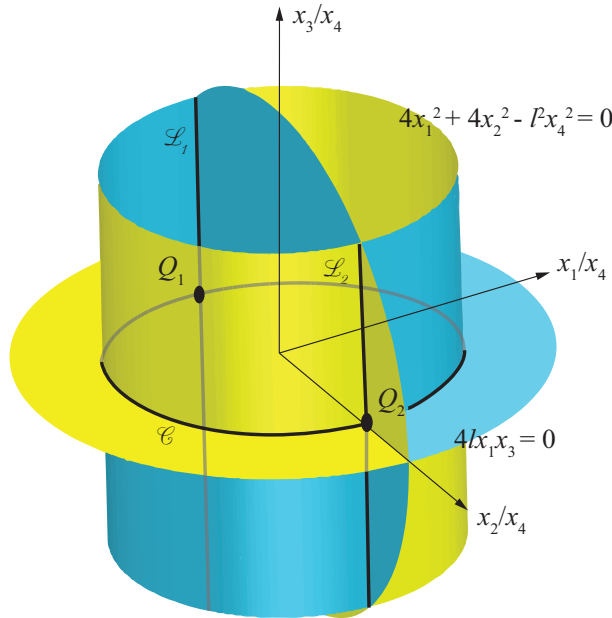


Figure 2.2 – Constraint manifolds of the four-bar linkage in image space.

## Operation Modes

The affine variety of the polynomials  $H_1$  and  $H_2$  amounts to all the possible displacements attainable by the coupler. This variety is nothing but the intersection of these constraint surfaces in the image space [Hus+07]. The intersections can be seen as two lines and a circle in Fig. 2.2. In fact, these curves can be algebraically represented by decomposing the constraint equations (2.8) and (2.9). A primary decomposition of the ideal  $\mathcal{J} = \langle H_1, H_2 \rangle$  onto the field  $\mathbb{K}(x_1, x_2, x_3, x_4)$  results in the following sub-ideals:

$$\mathcal{J}_1 = \langle x_1, 2x_2 - lx_4 \rangle \quad (2.10)$$

$$\mathcal{J}_2 = \langle x_1, 2x_2 + lx_4 \rangle \quad (2.11)$$

$$\mathcal{J}_3 = \langle x_3, 4(x_1^2 + x_2^2) - l^2x_4^2 \rangle \quad (2.12)$$



It shows that this four-bar linkage has three operation modes. The Hilbert dimension of the ideals  $\mathcal{J}_i$  including the polynomial  $H$  from Eq. (2.3) is calculated to be one, indicating that the DOF of the four-bar mechanism is one in each of these three operation modes.  $\mathcal{J}_1$  and  $\mathcal{J}_2$  correspond to  $x_1 = 0$  implying  $u = \frac{b}{a}$  from Eq. (2.4). Furthermore, for  $\mathcal{J}_1$ , eliminating  $u$  from  $2x_2 - lx_4 = 0$  gives

$$a^2 + b^2 - al = 0 \quad (2.13)$$

which is the equation of a circle of center point  $B$  of Cartesian coordinates  $(\frac{l}{2}, 0)$  and radius  $\frac{l}{2}$  as shown in Fig. 2.3.

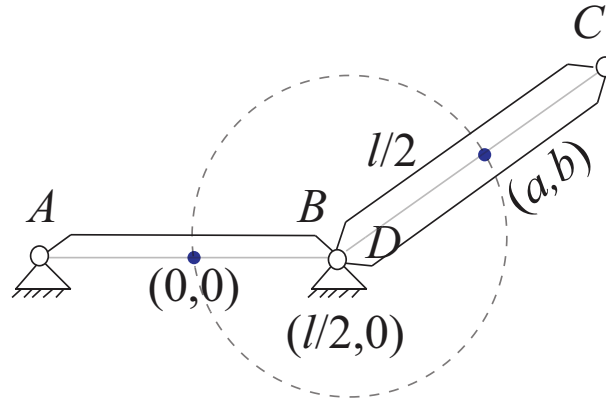


Figure 2.3 – Operation mode 1 :  $a^2 + b^2 - al = 0$

Similarly,  $\mathcal{J}_2$  yields

$$a^2 + b^2 + al = 0 \quad (2.14)$$

which is the equation of a circle of center point  $C$  of Cartesian coordinates  $(-\frac{l}{2}, 0)$  and radius  $\frac{l}{2}$  as shown in Fig. 2.4.

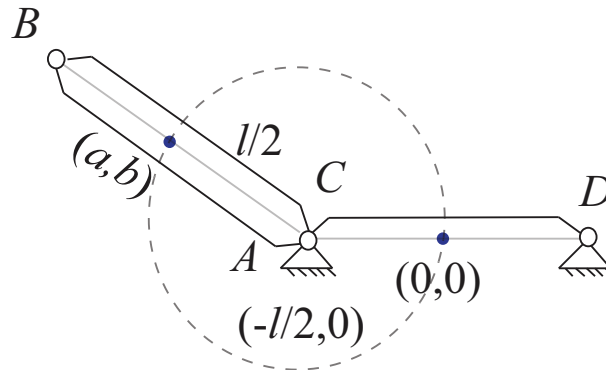


Figure 2.4 – Operation mode 2 :  $a^2 + b^2 + al = 0$ .

The third ideal  $\mathcal{J}_3$  corresponds to  $x_3 = 0$  and hence  $u = 0$  implying  $\phi = 0$ . The second

equation of the same ideal results in

$$a^2 + b^2 - l^2 = 0 \quad (2.15)$$

being the equation of a circle of center  $(0, 0)$  and radius  $l$  as shown in Fig. 2.5. As a result,  $\mathcal{J}_1$  and  $\mathcal{J}_2$  represent rotational modes while  $\mathcal{J}_3$  represents a translational mode.

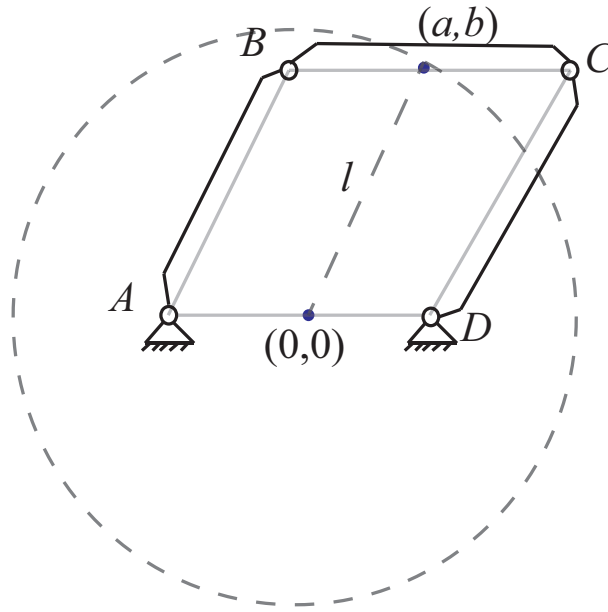


Figure 2.5 – Operation mode 3 :  $a^2 + b^2 - l^2 = 0$ .

Ultimately, in Fig. 2.2, the intersection lines  $\mathcal{L}_1$  and  $\mathcal{L}_2$  of the constraint manifolds portray the rotational motion modes while the circle  $\mathcal{C}$  portrays the translational motion mode. It will be shown in Chapter 5 how the transition between these operation modes can be exploited to design a reconfigurable compliant mechanism.

### 2.1.2 3-[PP]S and 3-S[PP] PMs

A popular category of zero torsion mechanisms is the 3-[PP]S type, for which each leg is confined to move in a plane with the first two joints generating a motion equivalent to two coplanar translations, denoted as [PP]. When these planes are arranged such that they intersect at  $120^\circ$  in a common line, they are henceforth addressed as the 3-[PP]S-Y family. If the arrangement of those planes is based on equilateral pattern, they will be part of the so-called 3-[PP]S- $\Delta$  family. If these planes are arranged orthogonally, they are already known as the 3-[PP]S-cube family. For instance, the 3-RPS-cube manipulator analyzed in [Nur+15] is part of the 3-[PP]S-cube family.

Figure 2.6 represents six manipulators from the 3-[PP]S-Y family. The two coplanar translational motions can be obtained with the following serial kinematic chains: RP, PhR, PvR, RR, PvPh or PhPv with Ph denoting a prismatic joint of horizontal direction and Pv denoting a prismatic joint of vertical direction. It should be noted that these directions are considered following the notation defined in [LB08] and it is assumed that the fixed base is horizontal. Though there are other possible orientations of the prismatic joints [NCW15a], most practical

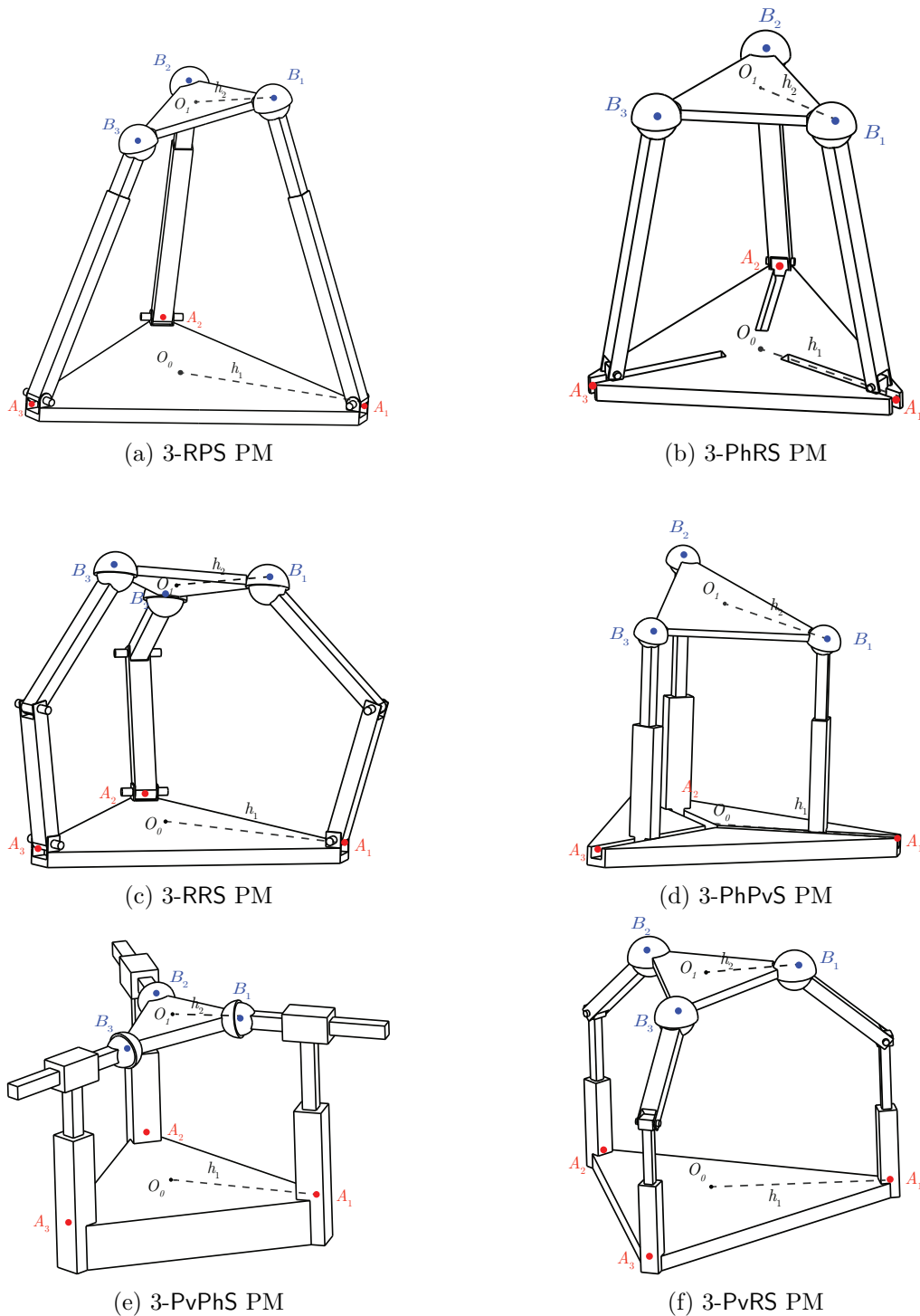


Figure 2.6 – Six parallel manipulators belonging to the 3-[PP]S-Y family

applications include horizontal or vertical prismatic joints. The spherical joint centers are restricted to move along the vertical planes  $\mathcal{P}_1$ ,  $\mathcal{P}_2$  and  $\mathcal{P}_3$  shown in Fig. 2.7. These planes are considered in the fixed coordinate frame such that they pass through points  $A_1$ ,  $A_2$  and  $A_3$ , respectively. They have a common line of intersection,  $\mathcal{L}$  along the  $z_0$  axis where they subtend an angle of  $120^\circ$ . This geometric condition is used to derive the constraint equations for these manipulators. Similarly inverting the arrangement of the joints leads to 3-S[PP]-Y mechanisms. In this case, the spherical joint centers,  $A_1, A_2$  and  $A_3$  are fixed and the planes  $\mathcal{P}_1, \mathcal{P}_2$  and  $\mathcal{P}_3$  considered in moving coordinate frame are restricted to pass through these points, respectively as shown in Fig. 2.7. Table 2.1 gives a list of twelve manipulators belonging to the 3-[PP]S-Y family and a list of twelve manipulators belonging to the 3-S[PP]-Y family, where the underlined joint symbol means that it is actuated.

No.	3-[PP]S-Y family	No.	3-S[PP]-Y family
1a	3-PvRS	1b	3-SRPv
2a	3-PhRS	2b	3-SRPh
3a	3-PvRS	3b	3-SRPv
4a	3-PhRS	4b	3-SRPh
5a	3-RPS	5b	3-SPR
6a	3-RPS	6b	3-SPR
7a	3-RRS	7b	3-SRR
8a	3-RRS	8b	3-SRR
9a	3-PhPvS	9b	3-SPvPh
10a	3-PhPvS	10b	3-SPvPh
11a	3-PvPhS	11b	3-SPhPv
12a	3-PvPhS	12b	3-SPhPv

Table 2.1 – Manipulators belonging to the 3-[PP]S-Y and 3-S[PP]-Y families

Both the base and platform are equilateral triangles with vertices  $A_i$  and  $B_i$ ,  $i = 1, 2, 3$  and with circumradii  $h_1$  and  $h_2$ , respectively. The origin  $O_0$  of the fixed coordinate frame  $\Sigma_0$  coincides with base circumcenter while origin  $O_1$  of frame  $\Sigma_1$  coincides with the platform circumcenter. The  $x_0$ -axis of  $\Sigma_0$  is along line  $(O_0A_1)$  and the  $x_1$ -axis of frame  $\Sigma_1$  is along line  $(O_1B_1)$ . Thus, the axes  $y_i$ ,  $i = 1, 2$  are parallel to lines  $(A_2A_3)$  and  $(B_2B_3)$ , respectively and the axes  $z_i$ ,  $i = 1, 2$  are normal to the base and the moving-platform, respectively.

### Constraint Equations

This section aims to determine the constraint equations of the manipulators under study. Those constraint equations are expressed algebraically based on the motions of the moving-platform that are constrained by the legs.

From Fig. 2.7, the coordinates of points  $A_i$  and  $B_i$  in coordinate frames  $\Sigma_0$  and  $\Sigma_1$ , respectively, are expressed as follows:

$$\begin{aligned}
 {}^0\mathbf{a}_1 &= [h_1, 0, 0]^T, & {}^0\mathbf{a}_2 &= [-\frac{1}{2}h_1, \frac{\sqrt{3}}{2}h_1, 0]^T, & {}^0\mathbf{a}_3 &= [-\frac{1}{2}h_1, -\frac{\sqrt{3}}{2}h_1, 0]^T \\
 {}^1\mathbf{b}_1 &= [h_2, 0, 0]^T, & {}^1\mathbf{b}_2 &= [-\frac{1}{2}h_2, \frac{\sqrt{3}}{2}h_2, 0]^T, & {}^1\mathbf{b}_3 &= [-\frac{1}{2}h_2, -\frac{\sqrt{3}}{2}h_2, 0]^T
 \end{aligned} \tag{2.16}$$

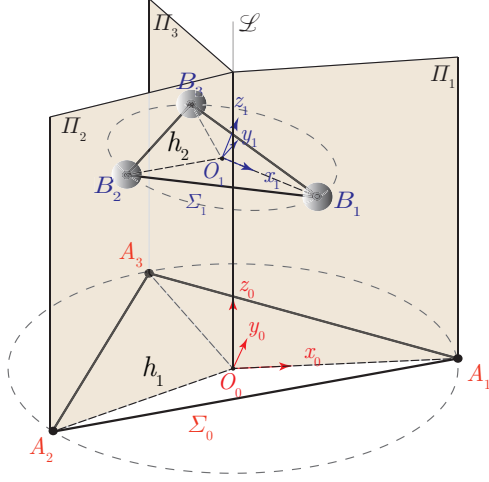


Figure 2.7 – Planes containing the limbs of the 3-[PP]S-Y PMs

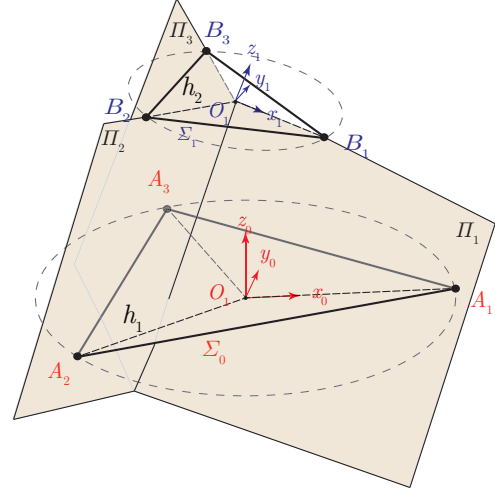


Figure 2.8 – Planes containing the limbs of the 3-S[PP]-Y PMs

The rotation matrix  ${}^0\mathbf{R}_1$  from frame  $\Sigma_0$  to frame  $\Sigma_1$  is expressed as:

$${}^0\mathbf{R}_1 = \begin{bmatrix} x_0^2 + x_1^2 - x_2^2 - x_3^2 & -2x_0x_3 + 2x_1x_2 & 2x_0x_2 + 2x_1x_3 \\ 2x_0x_3 + 2x_1x_2 & x_0^2 - x_1^2 + x_2^2 - x_3^2 & -2x_0x_1 + 2x_3x_2 \\ -2x_0x_2 + 2x_1x_3 & 2x_0x_1 + 2x_3x_2 & x_0^2 - x_1^2 - x_2^2 + x_3^2 \end{bmatrix} \quad (2.17)$$

where  $x_j$ ,  $j = 0, 1, 2, 3$  are the unit orientation quaternions satisfying:  $x_0^2 + x_1^2 + x_2^2 + x_3^2 = 1$  and  ${}^0\mathbf{p}_1$  is the point-displacement vector from the origin  $O_0$  of  $\Sigma_0$  to the origin  $O_1$  of  $\Sigma_1$  expressed in  $\Sigma_0$  as  $[X, Y, Z]^T$ .

From Fig. 2.7, for each leg, the vector connecting points  $A_i$  and  $B_i$  should always lie in the plane  $\mathcal{P}_i$ . This geometrical constraint holds true for all manipulators belonging to the 3-[PP]S-Y family. To derive the constraint equations, we can express the normal vector  $\mathbf{s}_i$  to planes  $\mathcal{P}_i$ ,  $i = 1, 2, 3$ , in frame  $\Sigma_0$  as follows:

$${}^0\mathbf{s}_1 = [0, -1, 0]^T, \quad {}^0\mathbf{s}_2 = \left[\frac{\sqrt{3}}{2}, \frac{1}{2}, 0\right]^T, \quad {}^0\mathbf{s}_3 = \left[-\frac{\sqrt{3}}{2}, \frac{1}{2}, 0\right]^T \quad (2.18)$$

In the fixed coordinate frame  $\Sigma_0$ , the co-ordinates of point  $B_i$  can be expressed as follows:

$${}^0\mathbf{b}_i = {}^0\mathbf{R}_1 {}^1\mathbf{b}_i + {}^0\mathbf{p}_1, \quad i = 1, 2, 3 \quad (2.19)$$

Vector  $\overrightarrow{A_iB_i}$  is perpendicular to  $\mathbf{s}_i$ , which is expressed as  $({}^0\mathbf{b}_i - {}^0\mathbf{a}_i)^T {}^0\mathbf{s}_i = 0$  which after simplification yields the following three equations:

$$g_1 := x_0x_3 = 0 \quad (2.20)$$

$$g_2 := Xx_0^2 + Xx_1^2 + Xx_2^2 + Xx_3^2 - h_2x_1^2 + h_2x_2^2 = 0 \quad (2.21)$$

$$g_3 := Yx_0^2 + Yx_1^2 + Yx_2^2 + Yx_3^2 - 4h_2x_0x_3 + 2h_2x_1x_2 = 0 \quad (2.22)$$

On the other hand, the similar constraints for the 3-S[PP]-Y PMs lead to following equations:

$$g_1 := x_0 x_3 = 0 \quad (2.23)$$

$$g_2 := Xx_0^2 + Xx_1^2 - Xx_2^2 - Xx_3^2 + 2Yx_0x_3 + 2Yx_1x_2 - 2Zx_0x_2 + 2Zx_1x_3 \\ + h_1x_1^2 - h_1x_2^2 = 0 \quad (2.24)$$

$$g_3 := 2Xx_0x_3 - 2Xx_1x_2 - Yx_0^2 + Yx_1^2 - Yx_2^2 + Yx_3^2 - 2Zx_0x_1 - 2Zx_2x_3 \\ + 4h_1x_0x_3 + 2h_1x_1x_2 = 0 \quad (2.25)$$

Depending upon the actuated joints, three other equations,  $g_4 = 0$ ,  $g_5 = 0$  and  $g_6 = 0$  can be derived. For instance, in case of the 3-RPS PM (Figure 2.6a), the Euclidean distance between  $A_i$  and  $B_i$  must be equal to the prismatic joint length,  $r_i$  for the  $i$ -th leg of the manipulator. As a result,  $\|{}^0\mathbf{b}_i - {}^0\mathbf{a}_i\|^2 = r_i^2$  leads to three additional equations [SWH12] :

$$g_4 := (4Xh_2 - 4h_1h_2)x_0^2 - 4Zh_2x_0x_2 + 4Yh_2x_0x_3 + (4Xh_2 - 4h_1h_2)x_1^2 \\ + 4Yh_2x_1x_2 + 4Zh_2x_1x_3 + X^2 - 2Xh_1 - 2Xh_2 + Y^2 + Z^2 + h_1^2 + 2h_1h_2 \\ + h_2^2 - r_1^2 = 0 \quad (2.26)$$

$$g_5 := (-2\sqrt{3}Yh_2 - 2Xh_2 - 4h_1h_2)x_0^2 - 2\sqrt{3}Zh_2x_0x_1 + 2Zh_2x_0x_2 + (2\sqrt{3}Xh_2 \\ - 2Yh_2)x_0x_3 + (-2Xh_2 - h_1h_2)x_1^2 + (-2\sqrt{3}Xh_2 - 2\sqrt{3}h_1h_2 - 2Yh_2)x_1x_2 \\ - 2Zh_2x_1x_3 + (-2\sqrt{3}Yh_2 - 3h_1h_2)x_2^2 - 2\sqrt{3}Zh_2x_2x_3 + \sqrt{3}Yh_1 + \sqrt{3}Yh_2 \\ + X^2 + Xh_1 + Xh_2 + Y^2 + Z^2 + h_1^2 + 2h_1h_2 + h_2^2 - r_2^2 = 0 \quad (2.27)$$

$$g_6 := (2\sqrt{3}Yh_2 - 2Xh_2 - 4h_1h_2)x_0^2 + 2\sqrt{3}Zh_2x_0x_1 + 2Zh_2x_0x_2 + (-2\sqrt{3}Xh_2 \\ - 2Yh_2)x_0x_3 + (-2Xh_2 - h_1h_2)x_1^2 + (2\sqrt{3}Xh_2 + 2\sqrt{3}h_1h_2 - 2Yh_2)x_1x_2 \\ - 2Zh_2x_1x_3 + (2\sqrt{3}Yh_2 - 3h_1h_2)x_2^2 + 2\sqrt{3}Zh_2x_2x_3 - \sqrt{3}Yh_1 - \sqrt{3}Yh_2 \\ + X^2 + Xh_1 + Xh_2 + Y^2 + Z^2 + h_1^2 + 2h_1h_2 + h_2^2 - r_3^2 = 0 \quad (2.28)$$

In addition, the normalization equation of the unit quaternion is to be considered to satisfy the inequality (1.36), namely,

$$S_6^2 := x_0^2 + x_1^2 + x_2^2 + x_3^2 - 1 = 0 \quad (2.29)$$

It is noteworthy that Eq. (2.20) reveals that both 3-[PP]S-Y and 3-S[PP]-Y families of PMs can have at least two operation modes characterized by  $x_0 = 0$  and  $x_3 = 0$ . The following section examines the primary decomposition of the ideal of constraint equations to identify different operation modes of the mechanisms under study.

## Operation Modes

The constraint equations (2.20) to (2.22) describe the configuration space of the manipulators. The first constraint equation is recalled:

$$x_0 x_3 = 0 \quad (2.30)$$

As a result, their configuration space can be split into two parts  $x_0 = 0$  and  $x_3 = 0$ , called the operation modes [NCW15a; Sch+15; MNC16] separated by a constraint or C-space singularity [ZBG02a]. To obtain other equations in each operation mode, a polynomial ideal is

defined consisting of equations  $g_1, g_2, g_3$  and  $S_6^2$  with variables  $\{x_0, x_1, x_2, x_3, X, Y, Z\}$  over the coefficient ring  $\mathbb{C}[h_1, h_2]$  as follows:

$$\mathcal{J} = \langle g_1, g_2, g_3, S_6^2 \rangle \quad (2.31)$$

The *primary decomposition* of ideal  $\mathcal{J}$  results in two ideals  $\mathcal{J}_k$  ( $i = 1, 2$ ) confirming two operation modes for all the PMs in the 3-[PP]S-Y family, no matter their actuation scheme.

$$\begin{aligned} \mathcal{J}_1 : \langle &x_0, x_1y_1 + x_2y_2 + x_3y_3, h_1x_1x_2 + x_1y_3 - x_2y_0 - x_3y_1, h_1x_1^2 - h_1x_2^2 \\ &+ 2x_1y_0 + 2x_2y_3 - 2x_3y_2, h_1x_2^2y_2 + h_1x_2x_3y_3 - x_1y_1y_3 + x_2y_0y_1 \\ &+ x_3y_1^2, h_1x_2^3 + x_1^2y_3 - 3x_1x_2y_0 - x_1x_3y_1 - 2x_2^2y_3 + 2x_2x_3y_2, \\ &h_1x_1x_2y_2 + h_1x_1x_3y_3 + h_1x_2^2y_1 - 2x_1y_0y_1 - 2x_2y_1y_3 + 2x_3y_1y_2, \\ &h_1^2x_2^2y_3 - h_1x_1y_0y_3 + h_1x_2y_1^2 - 3h_1x_2y_2^2 - h_1x_2y_3^2 - h_1x_3y_2y_3 \\ &- 2y_0^2y_3 - 2y_1^2y_3 - 2y_2^2y_3 - 2y_3^3, -h_1^2x_2^2y_0y_3 + h_1^2x_2^2y_1y_2 \\ &+ h_1^2x_2x_3y_1y_3 + h_1x_1y_0^2y_3 - h_1x_1y_1^2y_3 + 3h_1x_2y_0y_2^2 + h_1x_2y_0y_3^2 \\ &+ h_1x_3y_0y_2y_3 + h_1x_3y_1^3 + 2y_0^3y_3 + 2y_0y_1^2y_3 + 2y_0y_2^2y_3 + 2y_0y_3^3 \rangle \end{aligned} \quad (2.32)$$

$$\begin{aligned} \mathcal{J}_2 : \langle &x_3, x_0y_0 + x_1y_1 + x_2y_2, h_1x_1x_2 + x_0y_2 + x_1y_3 - x_2y_0, h_1x_1^2 \\ &- h_1x_2^2 - 2x_0y_1 + 2x_1y_0 + 2x_2y_3, h_1x_2^3 + x_0x_1y_2 + 2x_0x_2y_1 \\ &+ x_1^2y_3 - 3x_1x_2y_0 - 2x_2^2y_3, h_1^2x_2^2y_0 - h_1x_1y_0^2 - h_1x_1y_2^2 \\ &- h_1x_2y_0y_3 - 3h_1x_2y_1y_2 - 2y_0^3 - 2y_0y_1^2 - 2y_0y_2^2 - 2y_0y_3^2 \rangle \end{aligned} \quad (2.33)$$

$$\mathcal{J}_3 : \langle x_0, x_1, x_2, x_3 \rangle \quad (2.34)$$

The intersection of these so called primary ideals returns the ideal  $\mathcal{J}$ . From a geometrical viewpoint, the variety  $V(\mathcal{J})$  can be written as the union of the varieties of the primary ideals  $V(\mathcal{J}_i), i = 1, 2, 3$ .

$$\mathcal{J} = \bigcap_{i=1}^3 \mathcal{J}_i \quad \text{or} \quad V(\mathcal{J}) = \bigcup_{i=1}^3 V(\mathcal{J}_i) \quad (2.35)$$

Nonetheless the third ideal,  $\mathcal{J}_3$  is discarded as the variety  $V(\mathcal{J}_3 \cup g_8)$  is null over the field of interest  $\mathbb{C}$ . In other words, there exists no real or complex set of solutions for  $x_i, i = 0, \dots, 3$  that simultaneously satisfies the Equation (2.29) and the polynomial equations  $x_i = 0$ . As a result, the 3-SPR manipulator ends up with two operation modes, represented by  $x_0 = 0$  and  $x_3 = 0$ , which is noticeable from Equation (2.20).

The analysis is completed by adding the remaining constraint equations  $g_4 = g_5 = g_6 = 0$  to the primary ideals  $\mathcal{J}_1$  and  $\mathcal{J}_2$ , which returns two ideals  $\mathcal{K}_1$  and  $\mathcal{K}_2$ . As a consequence, the ideals  $\mathcal{K}_i$  correspond to the two operation modes and can be studied separately.

$$\mathcal{K}_k = \mathcal{J}_k \cup \langle g_4, g_5, g_6 \rangle \quad k = 1, 2 \quad (2.36)$$

**Ideal  $\mathcal{K}_1$ –Operation mode 1, OM1** ( $x_0 = 0$ ): The moving platform is always found to be displaced about a finite screw axis by 180 degrees from the identity position where  $\Sigma_0$  coincides with  $\Sigma_1$  [Sch+15]. Substituting  $x_0 = 0$  and solving for  $X, Y$  from the ideal  $\mathcal{K}_1$  shows that the translational motions can be parametrized by  $Z$  and the rotational motions by  $x_1, x_2$

and  $x_3$  along with  $x_1^2 + x_2^2 + x_3^2 = 1$  [Sch+15].

**Ideal  $\mathcal{K}_2$ –Operation mode 2, OM2 ( $x_3 = 0$ )** : The moving platform is displaced about a finite screw axis with a rotation angle  $\alpha$  defined as:  $\alpha = \pm 2 \arccos(x_0)$ . The screw axis in this case stays parallel to the xy-plane [Sch+15]. Substituting  $x_3 = 0$  and solving for  $X, Y, Z$  from the ideal  $\mathcal{K}_2$  shows that the translational motions can be parametrized by  $Z$  and the rotational motions by  $x_0, x_1$  and  $x_2$  along with  $x_0^2 + x_1^2 + x_2^2 = 1$  [Sch+15].

Therefore, PMs belonging to the 3-[PP]S-Y and 3-S[PP]-Y family exhibit two operation modes.

### 2.1.3 3-RUU PM

Although the 3-RUU PM is already known in the literature, its complete kinematic analysis is lacking. In this section, two different ways to derive the constraint equations of a 3-RUU PM are compared. Using them, the DKM is solved and it is shown to have a translational operation mode [Sti+19].

#### Manipulator Architecture

The 3-RUU PM is shown in Figure 2.9. Each limb consists of a revolute joint and two universal joints in succession. The moving platform and the fixed base form equilateral triangles with vertices  $C_i$  and  $A_i$ , respectively,  $i = 1, 2, 3$ . The revolute-joint axes vectors in the  $i$ -th limb are marked  $\mathbf{s}_{ij}$ ,  $i = 1, 2, 3$ ;  $j = 1, \dots, 5$ .  $\mathbf{s}_{i5}$  and  $\mathbf{s}_{i1}$  are tangential to the circumcircles (with centers  $P$  and  $O$ ) of the moving platform and the base triangles, respectively. Vectors  $\mathbf{s}_{i1}$  and  $\mathbf{s}_{i2}$  are always parallel, so are vectors  $\mathbf{s}_{i3}$  and  $\mathbf{s}_{i4}$ . The origin of the fixed coordinate frame,  $\mathcal{F}_O$  is at  $O$  and the  $z_O$ -axis lies along the normal to the base plane whereas the origin of the moving coordinate frame  $\mathcal{F}_P$  is at  $P$  and the  $z_P$ -axis lies along the normal to the moving platform plane.  $x_O$  and  $x_P$  axes are directed along  $OA_1$  and  $PC_1$ , respectively.  $r_0$  and  $r_1$  are the circumradii of base and the moving platform, respectively.  $a_1$  and  $a_3$  are the link lengths.  $\theta_{i1}$  is the angle of rotation of the first revolute joint about the axis represented by vector  $\mathbf{s}_{i1}$  measured from the base plane whereas  $\theta_{i2}$  is the angle of rotation of the second revolute joint about the axis represented by vector  $\mathbf{s}_{i2}$  measured from the first link.

#### Derivation of Constraint Equations

The constraint equations of the 3-RUU PM are derived using a geometrical approach and Linear Implicitization Algorithm (LIA) [WH10]. First, canonical constraint equations for a limb of the PM are derived by attaching the fixed and the moving coordinate frames to the two extreme joints of a RUU limb as shown in Fig. 2.10. Each U-joint is characterized by two revolute joints with orthogonally intersecting axes and the DH convention is used to attach coordinate frames at each joint. Thus,  $\mathcal{F}_0$  and  $\mathcal{F}_1$  are the fixed and the moving coordinate frames with their corresponding  $z$ -axes along the first and the last revolute joint axes, respectively. Later on, general constraint equations are derived for the whole manipulator.



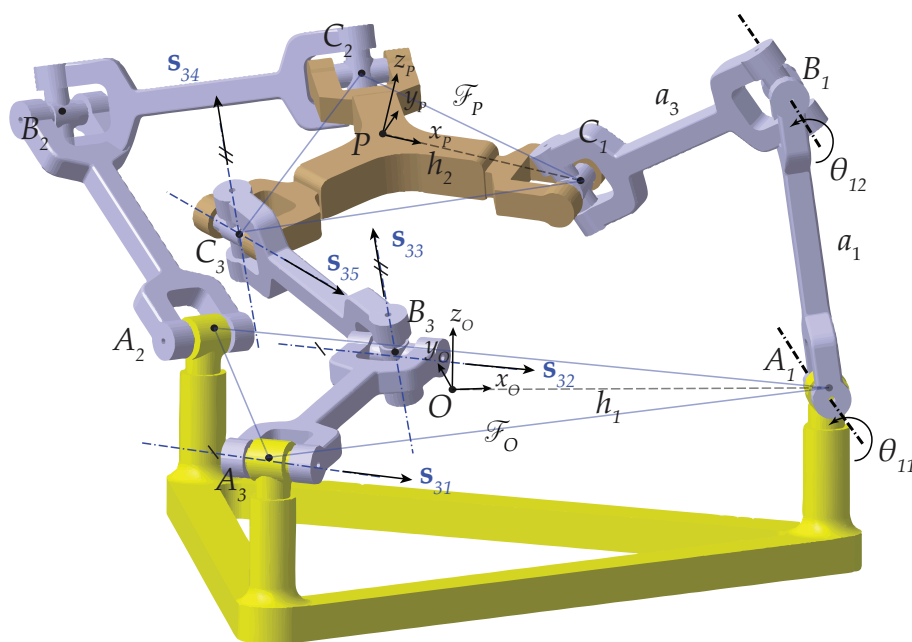


Figure 2.9 – The 3-RUU- $\Delta$  parallel manipulator in a general configuration

### Geometrical Approach

**Canonical Constraints** In order to derive the geometric constraints for a RUU limb, Fig. 2.10 is referred to write down the homogeneous coordinates<sup>1</sup> of points  $A, B, C$  ( $\mathbf{a}, \mathbf{b}, \mathbf{c}$ , respectively) and vectors  $\mathbf{s}_j$ ,  $j = 1, \dots, 5$ .

$$\begin{aligned} {}^0\mathbf{a} &= [1, 0, 0, 0]^T & {}^0\mathbf{b} &= [1, a_1 \cos(\theta_1), a_1 \sin(\theta_1), 0]^T & {}^1\mathbf{c} &= [1, 0, 0, 0]^T \\ {}^0\mathbf{s}_1 &= [0, 0, 0, 1]^T & {}^0\mathbf{s}_2 &= [0, 0, 0, 1]^T & {}^0\mathbf{s}_3 &= [0, \cos(\theta_1 + \theta_2), \sin(\theta_1 + \theta_2), 0]^T \\ {}^0\mathbf{s}_4 &= [0, \cos(\theta_1 + \theta_2), \sin(\theta_1 + \theta_2), 0]^T & {}^1\mathbf{s}_5 &= [0, 0, 0, 1]^T \end{aligned} \quad (2.37)$$

where  $\theta_1$  and  $\theta_2$  are the angles of rotation of the first and the second revolute joints, respectively.

Study's kinematic mapping described in Sec. 1.2.4 is used to express the vectors  $\mathbf{c}$  and  $\mathbf{s}_5$  in the fixed coordinate frame  $\mathcal{F}_0$ , using the transformation matrix  $M$  shown in Eq. (1.34a) consisting of Study parameters  $x_i$  and  $y_i$ ,  $i = 0, 1, 2, 3$ :

$${}^0\mathbf{c} = \mathbf{M} {}^1\mathbf{c} \quad ; \quad {}^0\mathbf{s}_5 = \mathbf{M} {}^1\mathbf{s}_5 \quad (2.38)$$

All the vectors are now expressed in the base coordinate frame and hence the geometric constraints can be derived. Due to the choice of homogeneous coordinates, the following constraints are already satisfied:

1. First and the second revolute joint axes are parallel:  $\mathbf{s}_1 = \mathbf{s}_2$
2. Third and the fourth revolute joint axes are parallel:  $\mathbf{s}_3 = \mathbf{s}_4$
3.  $\overrightarrow{AB}$  is perpendicular to the first or the second revolute joint axis:  $(\mathbf{b} - \mathbf{a})^T \mathbf{s}_1 = 0$
4. Second revolute joint axis is perpendicular to the third revolute joint axis:  $\mathbf{s}_2^T \mathbf{s}_3 = 0$
5. Length of the link  $AB$  is  $a_1$ :  $\|\mathbf{b} - \mathbf{a}\| = a_1$

1. left superscript  $k$  denotes the vector in coordinate frame  $\mathcal{F}_k$ ,  $k \in \{0, 1\}$

The remaining geometric constraints are derived as algebraic equations using tangent half angle substitution:

1. The second revolute joint axis, the fifth revolute joint axis and the link  $BC$  lie in the same plane. In other words, the scalar triple product of the corresponding vectors is zero:

$$\begin{aligned}
g_1 : (\mathbf{b} - \mathbf{c})^T (\mathbf{s}_2 \times \mathbf{s}_5) &= 0 \\
\implies & \left( -2t_1^2 a_1 + 2a_1 \right) x_0^3 x_1 + 4t_1 a_1 x_0^3 x_2 + 4t_1 a_1 x_0^2 x_1 x_3 + \left( 4t_1^2 + 4 \right) x_0^2 x_1 y_1 \\
& + \left( 2t_1^2 a_1 - 2a_1 \right) x_0^2 x_2 x_3 + \left( 4t_1^2 + 4 \right) x_0^2 x_2 y_2 + \left( -2t_1^2 a_1 + 2a_1 \right) x_0 x_1^3 \\
& + 4t_1 a_1 x_0 x_1^2 x_2 + \left( -4t_1^2 - 4 \right) x_0 x_1^2 y_0 + \left( -2t_1^2 a_1 + 2a_1 \right) x_0 x_1 x_2^2 \\
& + \left( -2t_1^2 a_1 + 2a_1 \right) x_0 x_1 x_3^2 + 4t_1 a_1 x_0 x_2^3 + \left( -4t_1^2 - 4 \right) x_0 x_2^2 y_0 \\
& + 4t_1 a_1 x_0 x_2 x_3^2 + 4t_1 a_1 x_1^3 x_3 + \left( 2t_1^2 a_1 - 2a_1 \right) x_1^2 x_2 x_3 \left( -4t_1^2 - 4 \right) x_1^2 x_3 y_3 \\
& + 4t_1 a_1 x_1 x_2^2 x_3 + 4t_1 a_1 x_1 x_3^3 + \left( 4t_1^2 + 4 \right) x_1 x_3^2 y_1 + \left( 2t_1^2 a_1 - 2a_1 \right) x_2^3 x_3 \\
& + \left( -4t_1^2 - 4 \right) x_2^2 x_3 y_3 + \left( 2t_1^2 a_1 - 2a_1 \right) x_2 x_3^3 + \left( 4t_1^2 + 4 \right) x_2 x_3^2 y_2 = 0 \quad (2.39)
\end{aligned}$$

2. Vector  $\overrightarrow{BC}$  is perpendicular to the third or the fourth revolute joint axis:

$$\begin{aligned}
g_2 : (\mathbf{b} - \mathbf{c})^T \mathbf{s}_4 &= 0 \\
\implies & \left( t_1^2 t_2^2 a_1 - t_1^2 a_1 + t_2^2 a_1 - a_1 \right) x_0^2 + \left( -2t_1^2 t_2^2 + 2t_1^2 + 8t_1 t_2 + 2t_2^2 \right. \\
& \left. - 2 \right) x_0 y_1 + \left( 4t_1^2 t_2 + 4t_1 t_2^2 - 4t_1 - 4t_2 \right) x_0 y_2 + \left( t_1^2 t_2^2 a_1 - t_1^2 a_1 + t_2^2 a_1 \right. \\
& \left. - a_1 \right) x_1^2 + \left( 2t_1^2 t_2^2 - 2t_1^2 - 8t_1 t_2 - 2t_2^2 + 2 \right) x_1 y_0 + \left( -4t_1^2 t_2 - 4t_1 t_2^2 \right. \\
& \left. + 4t_1 + 4t_2 \right) x_1 y_3 + \left( t_1^2 t_2^2 a_1 - t_1^2 a_1 + t_2^2 a_1 - a_1 \right) x_2^2 + \left( -4t_1^2 t_2 - 4t_1 t_2^2 \right. \\
& \left. + 4t_1 + 4t_2 \right) x_2 y_0 + \left( -2t_1^2 t_2^2 + 2t_1^2 + 8t_1 t_2 + 2t_2^2 - 2 \right) x_2 y_3 + \left( t_1^2 t_2^2 a_1 \right. \\
& \left. - t_1^2 a_1 + t_2^2 a_1 - a_1 \right) x_3^2 + \left( 4t_1^2 t_2 + 4t_1 t_2^2 - 4t_1 - 4t_2 \right) x_3 y_1 + \left( 2t_1^2 t_2^2 \right. \\
& \left. - 2t_1^2 - 8t_1 t_2 - 2t_2^2 + 2 \right) x_3 y_2 = 0 \quad (2.40)
\end{aligned}$$

3. The fourth and the fifth revolute joint axis are perpendicular:

$$\begin{aligned}
g_3 : \mathbf{s}_4^T \mathbf{s}_5 &= 0 \\
\implies & \left( 2t_1^2 t_2 + 2t_1 t_2^2 - 2t_1 - 2t_2 \right) x_0 x_1 + \left( t_1^2 t_2^2 - t_1^2 - 4t_1 t_2 - t_2^2 + 1 \right) x_0 x_2 \\
& + \left( t_1^2 t_2^2 - t_1^2 - 4t_1 t_2 - t_2^2 + 1 \right) x_1 x_3 + \left( -2t_1^2 t_2 - 2t_1 t_2^2 + 2t_1 \right. \\
& \left. + 2t_2 \right) x_2 x_3 = 0 \quad (2.41)
\end{aligned}$$

4. Length of the link  $BC$  is  $a_3$ :

$$\begin{aligned}
g_4 : & \|\mathbf{b} - \mathbf{c}\| - a_3 = 0 \\
\implies & (t_1^2 a_1^2 - t_1^2 a_3^2 + a_1^2 - a_3^2) x_0^2 + (-4 t_1^2 a_1 + 4 a_1) x_0 y_1 + 8 t_1 a_1 x_0 y_2 \\
& + (t_1^2 a_1^2 - t_1^2 a_3^2 + a_1^2 - a_3^2) x_1^2 + (4 t_1^2 a_1 - 4 a_1) x_1 y_0 - 8 t_1 a_1 x_1 y_3 \\
& + (t_1^2 a_1^2 - t_1^2 a_3^2 + a_1^2 - a_3^2) x_2^2 - 8 t_1 a_1 x_2 y_0 + (-4 t_1^2 a_1 + 4 a_1) x_2 y_3 \\
& + (t_1^2 a_1^2 - t_1^2 a_3^2 + a_1^2 - a_3^2) x_3^2 + 8 t_1 a_1 x_3 y_1 + (4 t_1^2 a_1 - 4 a_1) x_3 y_2 \\
& + (4 t_1^2 + 4) y_0^2 + (4 t_1^2 + 4) y_1^2 + (4 t_1^2 + 4) y_2^2 + (4 t_1^2 + 4) y_3^2 = 0 \quad (2.42)
\end{aligned}$$

Furthermore, Study's quadric,  $S_6^2$  in Eq. (1.35) is considered for every Euclidean transformation mapped to a point in  $\mathbb{P}_7$  lies in it.

The five geometric relations  $g_1 = g_2 = g_3 = g_4 = \mathcal{S} = 0$  describe a RUU limb. In fact, when the first revolute joint is actuated, each limb must have only two constraints. Equations (2.21) and (2.22) contain the passive joint variable  $t_2$  along with the active joint variable  $t_1$ . Eliminating  $t_2$  from  $g_2 = 0$  and  $g_3 = 0$  results in an equation which is identical to  $g_1 = 0$ . Therefore, the two constraint equations (excluding the Study's quadric) describing a RUU limb are  $g_1 = 0$  and  $g_4 = 0$  shown in Eqs. (2.20) and (2.26). The polynomials  $g_1, g_4$  and  $\mathcal{S}$  are enclosed in an ideal defined over the field of Study parameters:

$$J_1 = \langle g_1, g_4, S_6^2 \rangle \subseteq k[x_0, x_1, x_2, x_3, y_0, y_1, y_2, y_3], \quad (2.43)$$

where

$$\begin{aligned}
g_1 := & ((x_0 x_1 - x_2 x_3) (t_1^2 - 1) + (-2 x_0 x_2 - 2 x_1 x_3) t_1) (x_0^2 + x_1^2 + x_2^2 + x_3^2) a_1 \\
& - 2((x_0^2 + x_3^2)(x_1 y_1 + x_2 y_2) + 2(x_1^2 + x_2^2)(x_0 y_0 + x_3 y_3))(t_1^2 - 1) = 0, \quad (2.44)
\end{aligned}$$

$$\begin{aligned}
g_4 := & -(x_0^2 + x_1^2 + x_2^2 + x_3^2) (t_1^2 + 1) a_1^2 + (4(y_1 x_0 - y_0 x_1 + y_3 x_2 - y_2 x_3) t_1^2 \\
& + 8(-x_0 y_2 + x_1 y_3 + x_2 y_0 - x_3 y_1) t_1 + 4(y_2 x_3 - y_3 x_2 - y_1 x_0 + y_0 x_1)) a_1 \\
& + ((x_0^2 + x_1^2 + x_2^2 + x_3^2) a_3^2 - 4(y_2^2 + y_3^2 + y_0^2 + y_1^2)) (t_1^2 + 1) = 0. \quad (2.45)
\end{aligned}$$

**General Constraints** To derive the general constraints that do not contain the passive joint variable  $\theta_{i2}, i = 1, 2, 3$ , only the constraints in Eqs. (2.39) and (2.42) must be satisfied. From Fig. 2.9, the homogeneous coordinates of the necessary vectors are listed below:

$$\begin{aligned}
{}^0 \mathbf{b}_i &= \mathbf{R}_z(\beta_i) [1, r_0 + a_1 \cos(\theta_{i1}), 0, a_1 \sin(\theta_{i1})]^T \\
{}^0 \mathbf{c}_i &= \mathbf{R}_z(\beta_i) \mathbf{M} [1, r_1, 0, 0]^T, \\
{}^0 \mathbf{s}_{i2} &= \mathbf{R}_z(\beta_i) [0, 0, 1, 0]^T, \\
{}^0 \mathbf{s}_{i5} &= \mathbf{R}_z(\beta_i) \mathbf{M} [0, 0, 1, 0]^T, \quad i = 1, 2, 3,
\end{aligned} \quad (2.46)$$

where  $\mathbf{R}_z(\beta_i)$  is the homogeneous rotation matrix about the  $z$ -axis by an angle  $\beta_i$ ,  $\beta_1 = 0$ ,  $\beta_2 = \frac{2\pi}{3}$  and  $\beta_3 = \frac{4\pi}{3}$ . Therefore, the two geometric constraints  $g_1 = g_4 = 0$  for each limb,  $g_{i1} = g_{i4} = 0, i = 1, 2, 3$ , the Study quadric,  $S_6^2 = 0$  and the normalization condition  $\mathcal{N} : x_0^2 + x_1^2 + x_2^2 + x_3^2 - 1 = 0$  constitute the eight geometric constraint equations of the 3-RUU PM:

$$J = \langle g_{11}, g_{14}, g_{21}, g_{24}, g_{31}, g_{34}, \mathcal{S}, \mathcal{N} \rangle \subseteq k[x_0, x_1, x_2, x_3, y_0, y_1, y_2, y_3] \quad (2.47)$$

Joint	1	2	3	4	5
$\alpha$	0	$\frac{\pi}{2}$	0	$-\frac{\pi}{2}$	0
$a$	$a_1$	0	$a_3$	0	0
$d$	0	0	0	0	0

Table 2.2 – DH parameters of a RUU limb shown in Fig. 2.10

### Linear Implicitization Algorithm

**Canonical Constraints** The same general pose of a RUU limb is chosen as shown in Fig.2.10 to derive the canonical constraint equations using LIA [WH10]. To describe the RUU kinematic chain using DH parameters, the following  $4 \times 4$  matrices are defined:

$$\mathbf{T} = \mathbf{M}_1 \cdot \mathbf{G}_1 \cdot \mathbf{M}_2 \cdot \mathbf{G}_2 \cdot \mathbf{M}_3 \cdot \mathbf{G}_3 \cdot \mathbf{M}_4 \cdot \mathbf{G}_4 \cdot \mathbf{M}_5 \quad (2.48)$$

where the  $\mathbf{M}_i$ -matrices describe a rotation about the  $z$ -axis with  $u_i$  as the rotation angle. The  $\mathbf{G}_i$ -matrices describe the relative pose of one joint to the next.

$$\mathbf{M}_i = \begin{bmatrix} 1 & 0 & 0 & 0 \\ 0 & \cos(u_i) & -\sin(u_i) & 0 \\ 0 & \sin(u_i) & \cos(u_i) & 0 \\ 0 & 0 & 0 & 1 \end{bmatrix}, \quad \mathbf{G}_i = \begin{bmatrix} 1 & 0 & 0 & 0 \\ a_i & 1 & 0 & 0 \\ 0 & 0 & \cos(\alpha_i) & -\sin(\alpha_i) \\ d_i & 0 & \sin(\alpha_i) & \cos(\alpha_i) \end{bmatrix}. \quad (2.49)$$

As shown in Fig. 2.11, parameters in  $\mathbf{G}_i$  are the distance along  $x$ -axis  $a_i$ , the offset along  $z$ -axis  $d_i$  and the twist angle between the axes  $\alpha_i$ . For the RUU limb shown in Fig. 2.10, the DH

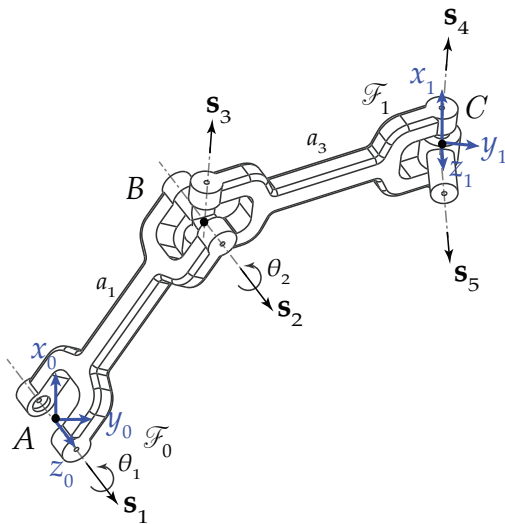


Figure 2.10 – A RUU limb

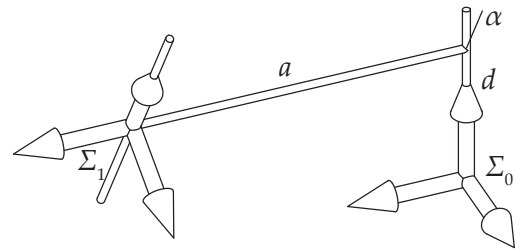


Figure 2.11 – Relative position of two lines in space

parameters are listed in Table 2.2.

Computing the Study-Parameters based on the transformation matrix  $\mathbf{T}$  yields the parametric representation of the limb [Hus+07]. Applying LIA yields the quadratic canonical constraint equations. To start with the LIA, a degree for the Ansatz polynomial has to be defined. The degree refers to the expected degree of the solution. Since we would like to have the lowest

possible degree of the solution we also have to start with the lowest possible degree for the Ansatz. The RUU leg consists of 5 joints, therefore we skipped the linear Ansatz and started with degree 2.

One also has to specify which motion-parameters should be eliminated. To keep only the active joint variable  $t_1$  in the constraint equations, we chose  $t_2, t_3, t_4$  and  $t_5$  to be eliminated.

In the next step the Study parameters, which represent  $x_0, x_1 \dots y_3$  are substituted in the Ansatz polynomial and the motion-parameters  $t$  are collected. Since the equation has to be fulfilled for all motion-parameters  $t$ , the coefficient equations have to be solved. Therefore a coefficient matrix is useful. The solutions for all coefficients are again substituted in the Ansatz polynomial. The new introduced parameters are collected. To ensure, that the equation is fulfilled again all coefficients have to vanish. Therefore each coefficient equation has to be fulfilled. Every single equation is a constraint equation of the mechanism.

$f_1$  and  $f_2$ :

$$\mathcal{J}_1 = \langle f_1, f_2, \mathbb{S}_6^2 \rangle \subseteq k[x_0, x_1, x_2, x_3, y_0, y_1, y_2, y_3], \quad (2.50)$$

where

$$\begin{aligned} f_1 := & \left( (x_0 x_1 - x_2 x_3) (t_1^2 - 1) + (-2x_0 x_2 - 2x_1 x_3) t_1 \right) a_1 \\ & + 2 (t_1^2 + 1) (x_0 y_0 + x_3 y_3) = 0 \end{aligned} \quad (2.51)$$

$$\begin{aligned} f_2 := & - \left( x_0^2 + x_1^2 + x_2^2 + x_3^2 \right) (t_1^2 + 1) a_1^2 + \left( 4(y_1 x_0 - y_0 x_1 + y_3 x_2 - y_2 x_3) t_1^2 \right. \\ & + 8(-x_0 y_2 + x_1 y_3 + x_2 y_0 - x_3 y_1) t_1 + 4(y_2 x_3 - y_3 x_2 - y_1 x_0 + y_0 x_1) \left. \right) a_1 \\ & + \left( (x_0^2 + x_1^2 + x_2^2 + x_3^2) a_3^2 - 4(y_2^2 + y_3^2 + y_0^2 + y_1^2) \right) (t_1^2 + 1) = 0 \end{aligned} \quad (2.52)$$

**General Constraints** To obtain the constraint equations of the whole mechanism from the canonical constraint equations, coordinate transformations are applied in the base and moving platform. To facilitate the comparison of the constraint equations derived by two different approaches, the coordinate transformations should be consistent with the global frames  $\mathcal{F}_O$  and  $\mathcal{F}_P$  as shown in Fig. 2.9. This can be done directly in the image space  $\mathbb{P}^7$  [Pfu06] by the mapping

$$\begin{bmatrix} x_0 \\ x_1 \\ x_2 \\ x_3 \\ y_0 \\ y_1 \\ y_2 \\ y_3 \end{bmatrix} \mapsto \begin{bmatrix} 2(v_0^2 + 1)x_0 \\ -2v_0^2 x_1 + 4v_0 x_2 + 2x_1 \\ 2(v_0^2 + 1)x_3 \\ 2v_0^2 x_2 + 4v_0 x_1 - 2x_2 \\ ((r_0 - r_1)x_1 + 2y_0)v_0^2 - 2x_2(r_0 - r_1)v_0 + (-r_0 + r_1)x_1 + 2y_0 \\ ((r_0 - r_1)x_0 - 2y_1)v_0^2 + 4v_0 y_2 + (r_0 - r_1)x_0 + 2y_1 \\ ((-r_0 - r_1)x_2 + 2y_3)v_0^2 - 2(r_0 + r_1)x_1 v_0 + (r_0 + r_1)x_2 + 2y_3 \\ ((r_0 + r_1)x_3 + 2y_2)v_0^2 + 4v_0 y_1 + (r_0 + r_1)x_3 - 2y_2 \end{bmatrix}, \quad (2.53)$$

where  $v_0 = \tan(\beta_i), i = 1, 2, 3, \beta_1 = 0, \beta_2 = \frac{2\pi}{3}$  and  $\beta_3 = \frac{4\pi}{3}$ . The resulting general constraint equations are the transformed equations from  $f_1=f_2 = 0$ , i.e.,  $f_{i1} = f_{i2} = 0, i = 1, 2, 3, \mathcal{S} = 0$  and  $\mathcal{N} = 0$ :

$$\mathcal{J} = \langle f_{11}, f_{12}, f_{21}, f_{22}, f_{31}, f_{32}, \mathbb{S}_6^2, \mathcal{N} \rangle \subseteq k[x_0, x_1, x_2, x_3, y_0, y_1, y_2, y_3] \quad (2.54)$$

### Ideal Comparison

A careful observation of the ideals  $\mathcal{J}_1$  and  $\mathcal{J}_1$  spanned by the canonical constraint polynomials reveals that  $g_4 = f_2$  and  $g_1 = f_1(x_0^2 + x_1^2 + x_2^2 + x_3^2) - 2(x_0^2 + x_2^2)(t_1^2 + 1)\mathbb{S}_6^2$ . Since,  $x_0^2 + x_1^2 + x_2^2 + x_3^2$

cannot be null, these ideals are the same. Thus, it follows that the ideals  $\mathcal{J}$  and  $\mathcal{J}$  spanned by the constraint equations of the whole manipulator are also contained in each other.

$$\mathcal{J} \subseteq \mathcal{J} \subseteq \mathcal{J}. \quad (2.55)$$

Since  $\mathcal{J}$  and  $\mathcal{J}$  are the basis of the same ideal, the variety of the constraint polynomials must be the same [CLO07]. Therefore, the set of constraint equations derived in Section 2.1.3 is used for further computations since it only contains quadratic equations. Although these equations are simpler, the set of equations derived by the geometrical approach in Section 2.1.3 have the advantage that they have a physical interpretation.

### Direct Kinematics: Numerical Examples

Because of the complexity of the algebra involved in the constraint equations of the manipulator, it is not possible to compute the direct kinematics without the use of numerical examples. In the following subsections, the design parameters of the manipulator are given the following arbitrary values:

$$a_1 = 3, a_3 = 5, r_0 = 11, r_1 = 7$$

**Identical Inputs** Assuming the input joint angles are equal,  $\theta_{i1} = \frac{\pi}{2}, i = 1, 2, 3$  for simplicity, the system of constraint equations in Eq. (2.54) yields the following real solutions and the corresponding manipulator poses are shown in Fig. 2.12.

$$\begin{aligned} (a) & \left\{ x_0 = \frac{\sqrt{23023}}{154}, y_3 = -\frac{3}{2}x_0, x_3 = -\frac{3\sqrt{77}}{154}, y_0 = \frac{3}{2}x_3, x_1 = x_2 = y_1 = y_2 = 0 \right\}, \\ (b) & \left\{ x_0 = \frac{\sqrt{23023}}{154}, y_3 = -\frac{3}{2}x_0, x_3 = \frac{3\sqrt{77}}{154}, y_0 = \frac{3}{2}x_3, x_1 = x_2 = y_1 = y_2 = 0 \right\}, \\ (c) & \{x_0 = 1, x_1 = x_2 = x_3 = y_0 = y_1 = y_2 = y_3 = 0\}, \\ (d) & \{x_0 = 1, x_1 = x_2 = x_3 = y_0 = y_1 = y_2 = 0, y_3 = -3\}. \end{aligned} \quad (2.56)$$

**Different Inputs** Substituting distinct arbitrary inputs and computing a Groebner basis over the field of Study parameters with pure lexicographic ordering yields a univariate polynomial

$$y_0 \cdot P(y_0) = 0 \quad (2.57)$$

where  $\text{degree}(P(y_0)) = 80$ .

### Translational Operation Mode

The univariate polynomial in Eq. (2.57) shows that this manipulator exhibits at least two operation modes. The one corresponding to  $y_0 = 0$  yields pure translational motion of the moving platform with the identity as the orientation. In this case the set of constraint equations

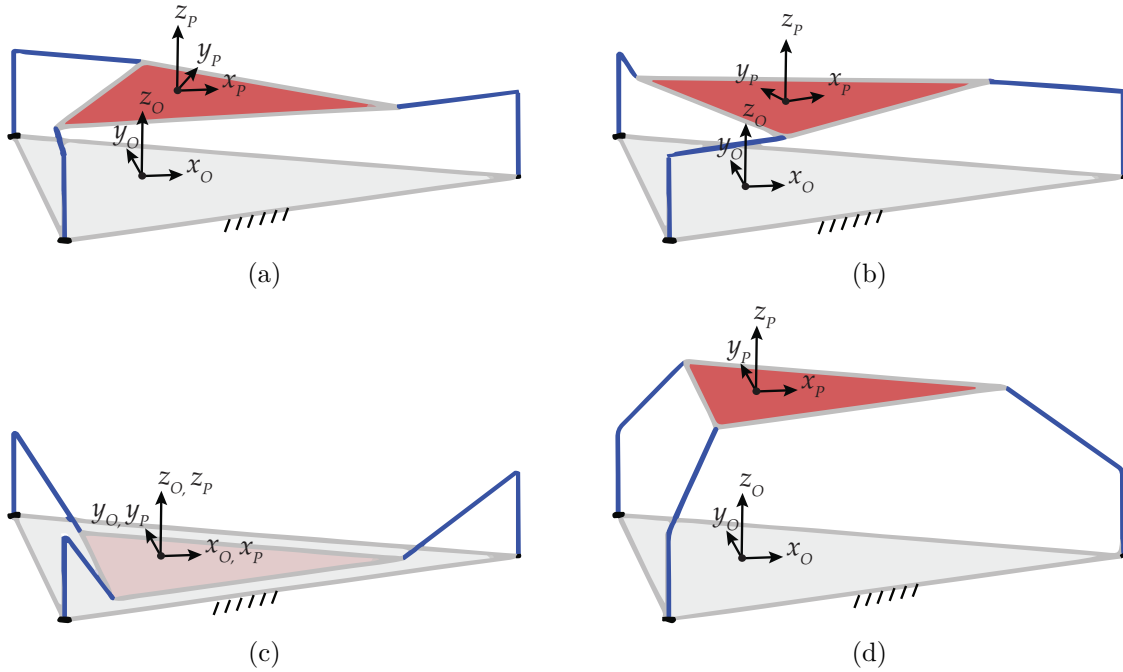


Figure 2.12 – A numerical example: solutions to direct kinematics corresponding to Eq. (2.56).

reduce to

$$\begin{aligned}
 & [(3y_3 - y_1^2 - y_2^2 - y_3^2 - 4y_1) t_1^2 - 6(y_1 + 2) t_1 - y_1^2 - y_2^2 - y_3^2 - 4y_1 - 3y_3, \\
 & - (2t_2^2 + 3t_2 + 2) y_2 \sqrt{3} + (-y_1^2 - y_2^2 - y_3^2 + 2y_1 + 3y_3) t_2^2 + (3y_1 - 12) t_2 - y_1^2 \\
 & - y_2^2 - y_3^2 + 2y_1 - 3y_3, (2t_3^2 + 3t_3 + 2) y_2 \sqrt{3} + (-y_1^2 - y_2^2 - y_3^2 + 2y_1 + 3y_3) t_3^2 \\
 & + (3y_1 - 12) t_3 - y_1^2 - y_2^2 - y_3^2 + 2y_1 - 3y_3] \quad (2.58)
 \end{aligned}$$

This system of equations yields a quadratic univariate in one of the  $y_i$ , which gives a parametrization of the motion dependent on the input variables  $v_{i1} = \tan(\theta_{i1}/2)$ ,  $i = 1, 2, 3$ .

#### 2.1.4 4-rRUU dual reconfigurable PM

This section presents a novel dual reconfigurable 4-rRUU PM proposed under the framework of this thesis in [NCW18a]. By allowing the base R-joint of a 4-RUU PM to have any orientation, an architectural reconfigurability is imparted to the existing mechanism. Finally, the design and construction of a 4-rRUU prototype is detailed.

##### Manipulator Architecture

The architecture of the dual reconfigurable 4-rRUU PM with a square base and a platform is shown in Fig. 2.13 and its constituent double-Hooke's joint linkage is shown in Fig. 2.14.

A reconfigurable revolute joint (rR) and two universal joints (UU) mounted in series constitute each limb of the 4-rRUU PM. Point  $L_i$ ,  $i = 1, 2, 3, 4$  lies on the pivotal axis of the double-Hooke's joint linkage as shown in Fig. 2.14. Point  $A_i$  lies on the first revolute joint axis of the 4-rRUU PM and it can be obtained from point  $L_i$  by traversing a horizontal distance of  $l_i$

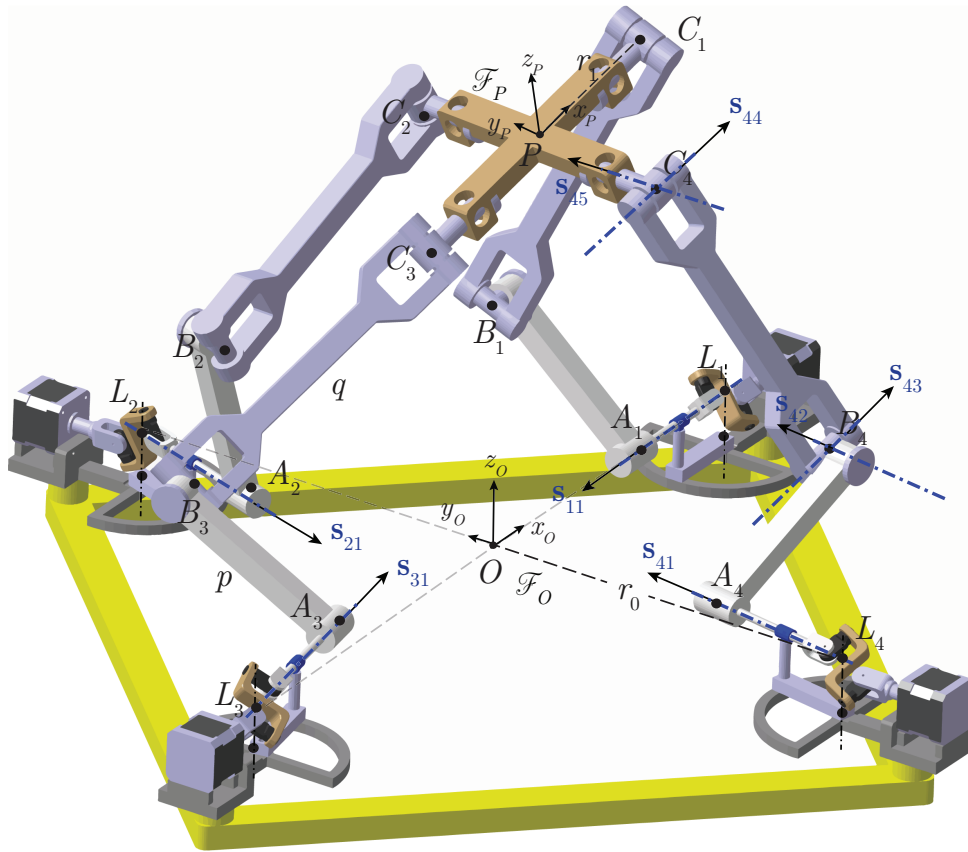


Figure 2.13 – A 4-rRUU parallel manipulator

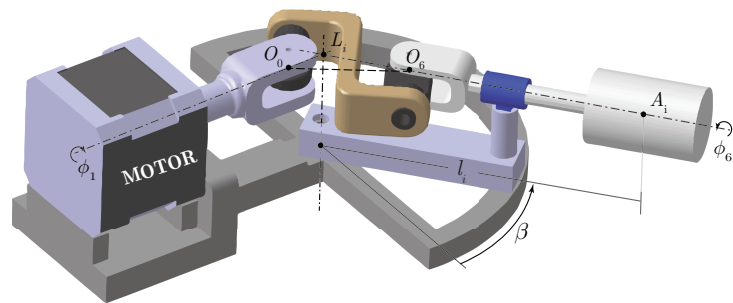


Figure 2.14 – Double Hooke's joint



Table 2.3 – DH parameters of the double-Hooke's joint

Joint	1	2	3	4	5	6
$\alpha$	$\frac{\pi}{2}$	$\frac{\pi}{2}$	0	$\frac{\pi}{2}$	$\frac{\pi}{2}$	0
$a$	0	0	$a_3$	0	0	0
$d$	0	0	0	0	0	0

along the first revolute joint axis. Points  $B_i$  and  $C_i$  are the geometric centers of the first and the second universal joints, respectively. Points  $L_i$  and  $C_i$  form the corners of the square base and the platform, respectively.  $\mathcal{F}_O$  and  $\mathcal{F}_P$  are the coordinate frames attached to the fixed base and the moving platform such that their origins  $O$  and  $P$  lie at the centers of the respective squares. The revolute-joint axes vectors in  $i$ -th limb are marked  $\mathbf{s}_{ij}$ ,  $i = 1, 2, 3, 4$ ;  $j = 1, \dots, 5$ . Vectors  $\mathbf{s}_{i1}$  and  $\mathbf{s}_{i2}$  are always parallel, so are vectors  $\mathbf{s}_{i3}$  and  $\mathbf{s}_{i4}$ . For simplicity, it is assumed that the orientation of vector  $\mathbf{s}_{i1}$  expressed in coordinate frame  $\mathcal{F}_O$  is the same as that of  $\mathbf{s}_{i5}$  expressed in coordinate frame  $\mathcal{F}_P$ . The position vectors of points  $L_i, A_i, B_i$  and  $C_i$  expressed in frame  $\mathcal{F}_k, k \in O, P$  are denoted as  ${}^k\mathbf{l}_i, {}^k\mathbf{a}_i, {}^k\mathbf{b}_i$  and  ${}^k\mathbf{c}_i$ , respectively.  $r_0$  and  $r_1$  are half the diagonals of the base and the moving platform squares, respectively.  $p$  and  $q$  are the link lengths.

### Double-Hooke's joint linkage

The double Hooke's joint linkage is shown in Fig. 2.14. The first three and the last three revolute joint axes intersect at points  $O_0$  and  $O_6$ , respectively. The first revolute joint is driven by a motor with an input angle of  $\phi_1$  and the last revolute joint rotates with an output angle of  $\phi_6$  and their axes intersect at point  $L_i, i = 1, 2, 3, 4$ . It is noteworthy that for a constant-velocity transmission, the triangle  $\triangle O_0 O_6 L_i$  must be isosceles with  $O_0 L_i = O_6 L_i$ . The angle between the input and the output shafts is denoted as  $\beta \in [0, \pi]$ . Double-Hooke's joint is known to be a constant-velocity transmitter [Bak02; Die95; MR95]. To derive the input-output relations, the Denavit-Hartenber (DH) convention is adopted where the coordinate frames are attached to each joint. To describe the over-constrained 6R-mechanism using DH parameters, the following  $4 \times 4$  matrices are defined:

$${}^0\mathbf{T}_6 = \mathbf{M}_1 \cdot \mathbf{G}_1 \cdot \mathbf{M}_2 \cdot \mathbf{G}_2 \cdot \mathbf{M}_3 \cdot \mathbf{G}_3 \cdot \mathbf{M}_4 \cdot \mathbf{G}_4 \cdot \mathbf{M}_5 \cdot \mathbf{G}_5 \cdot \mathbf{M}_6 \quad (2.59)$$

$\mathbf{M}_i$ - and  $\mathbf{G}_i$ -matrices are described in Eq. (2.49). For the double Hooke's joint linkage shown in Fig. 2.14, the DH parameters are listed in Table 2.3. By cosine rule,  $a_3 = 2b^2(1 - \cos(\beta)) = 2b^2(1 + \cos(\delta))$ , where  $\delta = \pi - \beta$ . By extracting the dual quaternions from the transformation matrix  ${}^0\mathbf{T}_6$  and by tangent half angle substitution  $v_i = \tan(\frac{\phi_i}{2}), i = 1, \dots, 6$  yields parametric representation of the constraint manifold of the double Hooke's joint linkage as a function of  $v_i, i = 1, \dots, 6$ .

From Fig. 2.14,  ${}^0\mathbf{T}_6$  can also be determined by traversing the loop in the other way and it leads to the following transformation matrix:

$${}^0\mathbf{T}_6 = \begin{bmatrix} 1 & 0 & 0 & 0 \\ -b \sin(\delta) & \cos(\delta) & 0 & -\sin(\delta) \\ 0 & 0 & 1 & 0 \\ b + b \cos(\delta) & \sin(\delta) & 0 & \cos(\delta) \end{bmatrix} \quad (2.60)$$

Substituting  $t = \tan(\frac{\delta}{2})$  in Eq. (2.60) yields the dual quaternion  $[4, 0, -4t, 0, 0, 0, -4b]^T$ . Equating it with the dual quaternion obtained by DH parametrization and solving for  $v_i$  results in

$$v_6 = -v_1 \quad (2.61)$$

Equation (2.61) is consistent with the linear input-output relation derived in Eq. (5.11) by Baker [Bak02], considering the property of parallel clevis-pins on the connecting rod for an industrial application such as the one in this paper. Equation (2.61) implies that the double Hooke's joint linkage is indeed a constant velocity transmitter independent of the angle  $\beta$ . In fact, the input-output relations can be derived between any two joint variables and are as follows for  $\beta = \frac{\pi}{2}$ :

$$v_2 = \frac{-v_1^2 + \sqrt{2v_1^4 + 2} + 1}{v_1^2 + 1}, \quad (2.62a)$$

$$v_3 = -1/2 \frac{v_1^2 \sqrt{2} + \sqrt{2} - \sqrt{2v_1^4 + 2}}{v_1}, \quad (2.62b)$$

$$v_4 = -1/2 \frac{v_1^2 \sqrt{2} + \sqrt{2} - \sqrt{2v_1^4 + 2}}{v_1}, \quad (2.62c)$$

$$v_5 = \frac{v_1^2 + \sqrt{2v_1^4 + 2} - 1}{v_1^2 + 1}, \quad (2.62d)$$

$$v_6 = -v_1 \quad (2.62e)$$

Figure 2.15 shows the top view of the 4-rRUU PM without the links. For architectural reconfigurability, the reconfigurable revolute joint axis in the base is allowed to have a horizontal orientation  $\beta_i, i = 1, 2, 3, 4$ . It is noteworthy that  $\beta_i$  will be changed manually in the prototype under construction.

### Constraint Equations

From the previous section, since the reconfigurable revolute joint is actuated, a RUU limb must satisfy the following two constraints:

1. The second revolute joint axis, the fifth revolute joint axis and link  $BC$  must lie in the same plane. In other words, the scalar triple product of the corresponding vectors must be null:

$$g_i : (\mathbf{b}_i - \mathbf{c}_i)^T (\mathbf{s}_{i2} \times \mathbf{s}_{i5}) = 0, \quad i = 1, 2, 3, 4 \quad (2.63)$$

2. The length of link  $BC$  must be  $q$ :

$$g_{i+4} : \|\mathbf{b}_i - \mathbf{c}_i\| - q = 0, \quad i = 1, 2, 3, 4 \quad (2.64)$$

Since the length of link  $BC$  does not affect the operation modes of the 4-rRUU PM, only the principal geometric constraint from Eq. (2.63) is considered. To express it algebraically, the



$$\begin{aligned}
& + 8pt_1v_1)x_1^2 + (-4pt_1v_1^4 + 24pt_1v_1^2 - 4pt_1)x_1x_2 + (4pt_1^2v_1^3 \\
& + 4r_0t_1^2v_1^3 + 4r_1t_1^2v_1^3 + 4pt_1^2v_1 - 4pv_1^3 - 4r_0t_1^2v_1 + 4r_0v_1^3 \\
& - 4r_1t_1^2v_1 + 4r_1v_1^3 - 4pv_1 - 4r_0v_1 - 4r_1v_1)x_1x_3 + (4t_1^2v_1^4 - 8t_1^2v_1^2 \\
& + 4v_1^4 + 4t_1^2 - 8v_1^2 + 4)y_1x_1 + (-8t_1^2v_1^3 + 8t_1^2v_1 - 8v_1^3 + 8v_1)x_1y_2 \\
& + (8pt_1v_1^3 - 8pt_1v_1)x_2^2 + (2pt_1^2v_1^4 + 2r_0t_1^2v_1^4 + 2r_1t_1^2v_1^4 - 2pv_1^4 \\
& - 4r_0t_1^2v_1^2 + 2r_0v_1^4 - 4r_1t_1^2v_1^2 + 2r_1v_1^4 - 2pt_1^2 + 2r_0t_1^2 - 4r_0v_1^2 \\
& + 2r_1t_1^2 - 4r_1v_1^2 + 2p + 2r_0 + 2r_1)x_2x_3 + (-8t_1^2v_1^3 + 8t_1^2v_1 - 8v_1^3 \\
& + 8v_1)x_2y_1 + (16t_1^2v_1^2 + 16v_1^2)x_2y_2 + (4t_1^2v_1^4 + 8t_1^2v_1^2 + 4v_1^4 \\
& + 4t_1^2 + 8v_1^2 + 4)y_3x_3 = 0
\end{aligned} \tag{2.66a}$$

$$\begin{aligned}
g_2 := & (4pt_2^2v_2^3 + 4r_0t_2^2v_2^3 - 4r_1t_2^2v_2^3 + 4pt_2^2v_2 - 4pv_2^3 - 4r_0t_2^2v_2 \\
& + 4r_0v_2^3 + 4r_1t_2^2v_2 - 4r_1v_2^3 - 4pv_2 - 4r_0v_2 + 4r_1v_2)x_0x_1 + (2pt_2^2v_2^4 \\
& + 2r_0t_2^2v_2^4 - 2r_1t_2^2v_2^4 - 2pv_2^4 - 4r_0t_2^2v_2^2 + 2r_0v_2^4 + 4r_1t_2^2v_2^2 \\
& - 2r_1v_2^4 - 2pt_2^2 + 2r_0t_2^2 - 4r_0v_2^2 - 2r_1t_2^2 + 4r_1v_2^2 + 2p + 2r_0 \\
& - 2r_1)x_0x_2 + (4pt_2v_2^4 + 8pt_2v_2^2 + 4pt_2)x_0x_3 + (8pt_2v_2^3 - 8pt_2v_2)x_1^2 \\
& + (4pt_2v_2^4 - 24pt_2v_2^2 + 4pt_2)x_1x_2 + (-2pt_2^2v_2^4 - 2r_0t_2^2v_2^4 - 2r_1t_2^2v_2^4 \\
& + 2pv_2^4 + 4r_0t_2^2v_2^2 - 2r_0v_2^4 + 4r_1t_2^2v_2^2 - 2r_1v_2^4 + 2pt_2^2 - 2r_0t_2^2 \\
& + 4r_0v_2^2 - 2r_1t_2^2 + 4r_1v_2^2 - 2p - 2r_0 - 2r_1)x_1x_3 + (16t_2^2v_2^2 \\
& + 16v_2^2)y_1x_1 + (8t_2^2v_2^3 - 8t_2^2v_2 + 8v_2^3 - 8v_2)x_1y_2 + (-8pt_2v_2^3 \\
& + 8pt_2v_2)x_2^2 + (4pt_2^2v_2^3 + 4r_0t_2^2v_2^3 + 4r_1t_2^2v_2^3 + 4pt_2^2v_2 - 4pv_2^3 \\
& - 4r_0t_2^2v_2 + 4r_0v_2^3 - 4r_1t_2^2v_2 + 4r_1v_2^3 - 4pv_2 - 4r_0v_2 - 4r_1v_2)x_2x_3 \\
& + (8t_2^2v_2^3 - 8t_2^2v_2 + 8v_2^3 - 8v_2)x_2y_1 + (4t_2^2v_2^4 - 8t_2^2v_2^2 + 4v_2^4 \\
& + 4t_2^2 - 8v_2^2 + 4)x_2y_2 + (4t_2^2v_2^4 + 8t_2^2v_2^2 + 4v_2^4 + 4t_2^2 + 8v_2^2 \\
& + 4)y_3x_3 = 0
\end{aligned} \tag{2.66b}$$

$$\begin{aligned}
g_3 := & (-2pt_3^2v_3^4 - 2r_0t_3^2v_3^4 + 2r_1t_3^2v_3^4 + 2pv_3^4 + 4r_0t_3^2v_3^2 - 2r_0v_3^4 \\
& - 4r_1t_3^2v_3^2 + 2r_1v_3^4 + 2pt_3^2 - 2r_0t_3^2 + 4r_0v_3^2 + 2r_1t_3^2 - 4r_1v_3^2 \\
& - 2p - 2r_0 + 2r_1)x_0x_1 + (4pt_3^2v_3^3 + 4r_0t_3^2v_3^3 - 4r_1t_3^2v_3^3 + 4pt_3^2v_3 \\
& - 4pv_3^3 - 4r_0t_3^2v_3 + 4r_0v_3^3 + 4r_1t_3^2v_3 - 4r_1v_3^3 - 4pv_3 - 4r_0v_3 \\
& + 4r_1v_3)x_0x_2 + (4pt_3v_3^4 + 8pt_3v_3^2 + 4pt_3)x_0x_3 + (-8pt_3v_3^3 \\
& + 8pt_3v_3)x_1^2 + (-4pt_3v_3^4 + 24pt_3v_3^2 - 4pt_3)x_1x_2 + (-4pt_3^2v_3^3 \\
& - 4r_0t_3^2v_3^3 - 4r_1t_3^2v_3^3 - 4pt_3^2v_3 + 4pv_3^3 + 4r_0t_3^2v_3 - 4r_0v_3^3 \\
& + 4r_1t_3^2v_3 - 4r_1v_3^3 + 4pv_3 + 4r_0v_3 + 4r_1v_3)x_1x_3 + (4t_3^2v_3^4 - 8t_3^2v_3^2 \\
& + 4v_3^4 + 4t_3^2 - 8v_3^2 + 4)y_1x_1 + (-8t_3^2v_3^3 + 8t_3^2v_3 - 8v_3^3 + 8v_3)x_1y_2 \\
& + (8pt_3v_3^3 - 8pt_3v_3)x_2^2 + (-2pt_3^2v_3^4 - 2r_0t_3^2v_3^4 - 2r_1t_3^2v_3^4 + 2pv_3^4 \\
& + 4r_0t_3^2v_3^2 - 2r_0v_3^4 + 4r_1t_3^2v_3^2 - 2r_1v_3^4 + 2pt_3^2 - 2r_0t_3^2 + 4r_0v_3^2 \\
& - 2r_1t_3^2 + 4r_1v_3^2 - 2p - 2r_0 - 2r_1)x_2x_3 + (-8t_3^2v_3^3 + 8t_3^2v_3 - 8v_3^3 \\
& + 8v_3)x_2y_1 + (16t_3^2v_3^2 + 16v_3^2)x_2y_2 + (4t_3^2v_3^4 + 8t_3^2v_3^2 + 4v_3^4
\end{aligned}$$

$$\begin{aligned}
& + 4t_3^2 + 8v_3^2 + 4)y_3x_3 = 0 \\
g_4 := & (-4pt_4^2v_4^3 - 4r_0t_4^2v_4^3 + 4r_1t_4^2v_4^3 - 4pt_4^2v_4 + 4pv_4^3 + 4r_0t_4^2v_4 \\
& - 4r_0v_4^3 - 4r_1t_4^2v_4 + 4r_1v_4^3 + 4pv_4 + 4r_0v_4 - 4r_1v_4)x_0x_1 + (-2pt_4^2v_4^4 \\
& - 2r_0t_4^2v_4^4 + 2r_1t_4^2v_4^4 + 2pv_4^4 + 4r_0t_4^2v_4^2 - 2r_0v_4^4 - 4r_1t_4^2v_4^2 \\
& + 2r_1v_4^4 + 2pt_4^2 - 2r_0t_4^2 + 4r_0v_4^2 + 2r_1t_4^2 - 4r_1v_4^2 - 2p - 2r_0 \\
& + 2r_1)x_0x_2 + (4pt_4v_4^4 + 8pt_4v_4^2 + 4pt_4)x_0x_3 + (8pt_4v_4^3 - 8pt_4v_4)x_1^2 \\
& + (4pt_4v_4^4 - 24pt_4v_4^2 + 4pt_4)x_1x_2 + (2pt_4^2v_4^4 + 2r_0t_4^2v_4^4 + 2r_1t_4^2v_4^4 \\
& - 2pv_4^4 - 4r_0t_4^2v_4^2 + 2r_0v_4^4 - 4r_1t_4^2v_4^2 + 2r_1v_4^4 - 2pt_4^2 + 2r_0t_4^2 \\
& - 4r_0v_4^2 + 2r_1t_4^2 - 4r_1v_4^2 + 2p + 2r_0 + 2r_1)x_1x_3 + (16t_4^2v_4^2 \\
& + 16v_4^2)y_1x_1 + (8t_4^2v_4^3 - 8t_4^2v_4 + 8v_4^3 - 8v_4)x_1y_2 + (-8pt_4v_4^3 \\
& + 8pt_4v_4)x_2^2 + (-4pt_4^2v_4^3 - 4r_0t_4^2v_4^3 - 4r_1t_4^2v_4^3 - 4pt_4^2v_4 + 4pv_4^3 \\
& + 4r_0t_4^2v_4 - 4r_0v_4^3 + 4r_1t_4^2v_4 - 4r_1v_4^3 + 4pv_4 + 4r_0v_4 + 4r_1v_4)x_2x_3 \\
& + (8t_4^2v_4^3 - 8t_4^2v_4 + 8v_4^3 - 8v_4)x_2y_1 + (4t_4^2v_4^4 - 8t_4^2v_4^2 + 4v_4^4 \\
& + 4t_4^2 - 8v_4^2 + 4)x_2y_2 + (4t_4^2v_4^4 + 8t_4^2v_4^2 + 4v_4^4 + 4t_4^2 + 8v_4^2 \\
& + 4)y_3x_3 = 0
\end{aligned} \tag{2.66c}$$

The constraint polynomials  $g_i, i = 1, 2, 3, 4$  form the following ideal:

$$\mathcal{J} = \langle g_1, g_2, g_3, g_4 \rangle \subseteq k[x_0, x_1, x_2, x_3, y_0, y_1, y_2, y_3] \tag{2.67}$$

To simplify the determination of the operation modes, the 4-rRUU PM is split into two 2-rRUU PMs [Nur+16] by considering two ideals:

$$\mathcal{J}_{(I)} = \langle g_1, g_3, S_6^2 \rangle \tag{2.68a}$$

$$\mathcal{J}_{(II)} = \langle g_2, g_4, S_6^2 \rangle \tag{2.68b}$$

Furthermore,  $\mathcal{J}_{(I)}$  and  $\mathcal{J}_{(II)}$  can be decomposed into simpler ideals using primary decomposition to understand the operation modes of the 2-rRUU PMs. Thus, the union of the corresponding prime ideals characterize the operation modes of the whole 4-rRUU PM. Two cases can be considered:

*Case 1: When the revolute joint axes are arbitrarily oriented,* the primary decomposition of  $\mathcal{J}_{(I)}$  and  $\mathcal{J}_{(II)}$  for leads to one sub-ideal each. These sub-ideals depend on the design parameters and are mixed motion modes which are not of interest in the context of this paper.

*Case 2: When the opposite revolute joint axes have the same orientation* i.e.  $v_1 = v_3$  and  $v_2 = v_4$ , the operation modes can be determined as follows:

All planar orientations of the rR-joint axes are covered by varying  $\beta_i \in [-90^\circ, 90^\circ]$  and hence  $v_i \in [-1, 1]$ . Design parameters were substituted as  $r_0 = 2, r_1 = 3, p = 5, q = 7$  to simplify the primary decomposition of ideals  $\mathcal{J}_{(I)}$  and  $\mathcal{J}_{(II)}$  in Eq. (2.68). The operation modes could be determined only when arbitrary rational values are substituted for  $v_1 = v_3 = v_{13}$  and  $v_2 = v_4 = v_{24}$ . The primary decomposition is performed in a computer algebra system SINGULAR and it leads to three sub-ideals each. The first two are independent of the design parameters

and actuated variables. They are of the following form:

$$\begin{aligned} \mathcal{J}_{(I)} &= \mathcal{J}_{1(I)} \cap \mathcal{J}_{2(I)} \cap \mathcal{J}_{3(I)}, \\ \text{where } \mathcal{J}_{1(I)} &= \langle x_0, h_1x_1 + h_2x_2, x_1y_1 + x_2y_2 + x_3y_3 \rangle \\ \text{and } \mathcal{J}_{2(I)} &= \langle x_3, -h_2x_1 + h_1x_2, x_0y_0 + x_1y_1 + x_2y_2 \rangle \end{aligned} \quad (2.69a)$$

$$\begin{aligned} \mathcal{J}_{(II)} &= \mathcal{J}_{1(II)} \cap \mathcal{J}_{2(II)} \cap \mathcal{J}_{3(II)}, \\ \text{where } \mathcal{J}_{1(II)} &= \langle x_0, -h_2x_1 + h_1x_2, x_1y_1 + x_2y_2 + x_3y_3 \rangle \\ \text{and } \mathcal{J}_{2(II)} &= \langle x_3, h_1x_1 + h_2x_2, x_0y_0 + x_1y_1 + x_2y_2 \rangle \end{aligned} \quad (2.69b)$$

where  $h_1$  and  $h_2$  are functions of  $v_{13}$  and  $v_{24}$ . For instance,  $\mathcal{J}_{1(I)}$  consists of  $x_0$  and  $S_6^2|_{x_0=0}$

$v_{13}$	-1	$-\frac{1}{2}$	$-\frac{1}{4}$	0	$\frac{1}{4}$	$\frac{1}{2}$	1	$w$
$h_1$	-1	-4	-8	0	8	4	1	$\frac{2}{w}, w \neq 0$
$h_2$	0	-3	-15	0	-15	-3	0	$1 - \frac{1}{w^2}, w \neq 0$

Table 2.4 –  $h_1$  and  $h_2$  as functions of  $v_{13}$  such that  $\langle h_1x_1 + h_2x_2 \rangle \in \mathcal{J}_{1(I)}$

irrespective of the value of  $v_{13}$ . The remaining polynomial has coefficients  $h_1$  and  $h_2$ , whose values are listed in Table 3.3 for arbitrarily chosen  $v_{13}$  along with their interpolated values for a general  $v_{13} = w$ . Thus, Eq. (2.69) can be further simplified as follows:

$$\begin{aligned} \mathcal{J}_{1(I)} &= \langle x_0, 2v_{13}x_1 + (v_{13}^2 - 1)x_2, x_1y_1 + x_2y_2 + x_3y_3 \rangle \\ \mathcal{J}_{2(I)} &= \langle x_3, (1 - v_{13}^2)x_1 + 2v_{13}x_2, x_0y_0 + x_1y_1 + x_2y_2 \rangle \end{aligned} \quad (2.70a)$$

$$\begin{aligned} \mathcal{J}_{1(II)} &= \langle x_0, (1 - v_{24}^2)x_1 + 2v_{24}x_2, x_1y_1 + x_2y_2 + x_3y_3 \rangle \\ \mathcal{J}_{2(II)} &= \langle x_3, 2v_{24}x_1 + (v_{24}^2 - 1)x_2, x_0y_0 + x_1y_1 + x_2y_2 \rangle \end{aligned} \quad (2.70b)$$

As a result, the first two operation modes of the 4-rRUU PM are:

$$\begin{aligned} \mathcal{J}_1 &= \mathcal{J}_{1(I)} \cup \mathcal{J}_{1(II)} \\ &= \langle x_0, 2v_{13}x_1 + (v_{13}^2 - 1)x_2, (1 - v_{24}^2)x_1 + 2v_{24}x_2, x_1y_1 + x_2y_2 + x_3y_3 \rangle \end{aligned} \quad (2.71a)$$

$$\begin{aligned} \mathcal{J}_2 &= \mathcal{J}_{2(I)} \cup \mathcal{J}_{2(II)} \\ &= \langle x_3, (1 - v_{13}^2)x_1 + 2v_{13}x_2, 2v_{24}x_1 + (v_{24}^2 - 1)x_2, x_0y_0 + x_1y_1 + x_2y_2 \rangle \end{aligned} \quad (2.71b)$$

In general,  $\mathcal{J}_1 = \langle x_0, x_1, x_2, y_3 \rangle$  and  $\mathcal{J}_2 = \langle x_3, x_1, x_2, y_0 \rangle$ . The former corresponds to a 3-*dof* pure translational mode, where the platform is upside down with the  $z_P$ -axis pointing downwards whose transformation matrix is as follows:

$$\mathbf{M}_1 = \begin{bmatrix} 1 & 0 & 0 & 0 \\ \frac{2y_2}{x_3} & -1 & 0 & 0 \\ -\frac{2y_1}{x_3} & 0 & -1 & 0 \\ \frac{2y_0}{x_3} & 0 & 0 & 1 \end{bmatrix} \quad (2.72)$$

The latter is also a 3-*dof* translational mode, but the platform is in upright position with  $z_P$ -axis pointing upwards whose transformation matrix is as follows:

$$\mathbf{M}_2 = \begin{bmatrix} 1 & 0 & 0 & 0 \\ -\frac{2y_1}{x_0} & 1 & 0 & 0 \\ -\frac{2y_2}{x_0} & 0 & 1 & 0 \\ -\frac{2y_3}{x_0} & 0 & 0 & 1 \end{bmatrix} \quad (2.73)$$

An example with these operation modes is shown in Fig. 2.16 with  $\beta_i = 90^\circ, i = 1, 2, 3, 4$  [NCW18d].

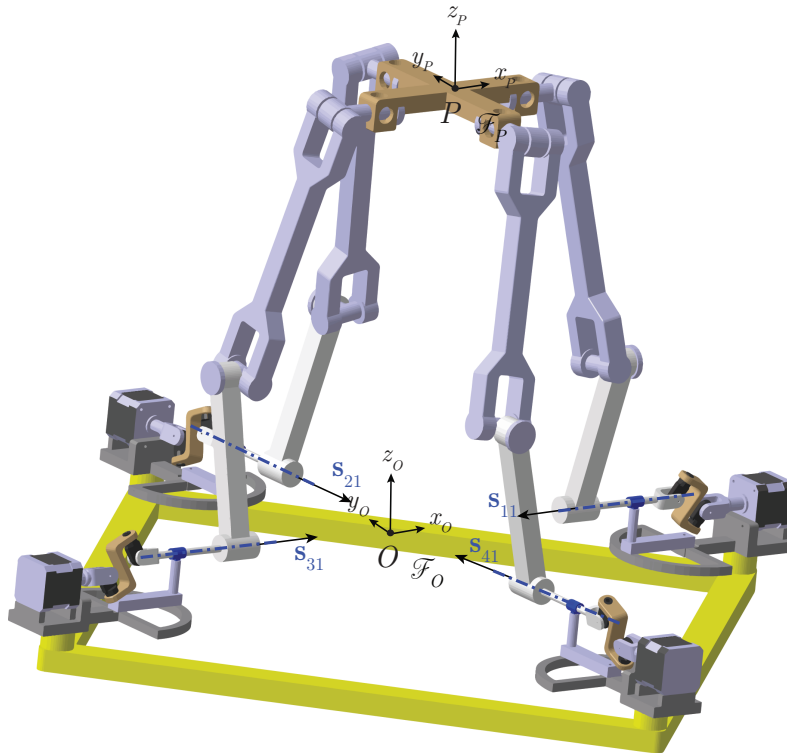


Figure 2.16 – A 4-rRUU PM with horizontal and intersecting base revolute joint axes

However, the set of binomial equations  $2v_{13}x_1 + (v_{13}^2 - 1)x_2 = 0$  and  $(1 - v_{24}^2)x_1 + 2v_{24}x_2 = 0$  can have non-trivial values for  $x_1$  and  $x_2$  if the following conditions are satisfied:

$$\begin{aligned} \frac{2v_{13}}{v_{13}^2 - 1} = \frac{1 - v_{24}^2}{2v_{24}} &\implies \tan(\beta_1) = \tan(\beta_3) = -\cot(\beta_2) = -\cot(\beta_4) \\ &\implies \beta_1 = \beta_3 = \beta_2 - 90^\circ = \beta_4 - 90^\circ \end{aligned} \quad (2.74)$$

In that case, the first two operation modes are

$$\begin{aligned} \mathcal{J}_1 &= \mathcal{J}_{1(I)} \cup \mathcal{J}_{1(II)} \\ &= \langle x_0, 2v_{13}x_1 + (v_{13}^2 - 1)x_2, x_1y_1 + x_2y_2 + x_3y_3 \rangle \end{aligned} \quad (2.75a)$$

$$\begin{aligned} \mathcal{J}_2 &= \mathcal{J}_{2(I)} \cup \mathcal{J}_{2(II)} \\ &= \langle x_3, (1 - v_{13}^2)x_1 + 2v_{13}x_2, x_0y_0 + x_1y_1 + x_2y_2 \rangle. \end{aligned} \quad (2.75b)$$

With  $x_3 = 1$ , the Study parameters corresponding to the first operation mode,  $\mathcal{J}_1$  are  $\{0, x_1, x_2, 1, y_0, y_1, y_2, -x_1y_1 - x_2y_2\}$ . The corresponding transformation matrix in Eq. (1.34a) yields:

$$\mathbf{M}_2 = \begin{bmatrix} 1 & 0 & 0 & 0 \\ -\frac{2y_1}{x_0} & 1 & 0 & 0 \\ -2(x_0y_2 - x_1y_3) & 0 & x_0^2 - x_1^2 & -2x_0x_1 \\ -2(x_0y_3 + 2x_1y_2) & 0 & 2x_0x_1 & x_0^2 - x_1^2 \end{bmatrix} \quad (2.76)$$

Thus, only four independent parameters are sufficient to characterize this operation mode and it corresponds to a 4-*dof* Schönflies mode in which the translational motions are parametrized by  $y_0, y_1$  and  $y_2$  and the rotational motion is parametrized by  $x_1, x_2$  along with  $2v_{13}x_1 + (v_{13}^2 - 1)x_2 = (1 - v_{24}^2)x_1 + 2v_{24}x_2 = 0$ . In this operation mode, the platform is upside down with the  $z_P$ -axis pointing in a direction opposite to the  $z_O$ -axis. The rotational motion is about an axis located at an angle of  $\beta_1 - 90^\circ = \beta_3 - 90^\circ = \beta_2 = \beta_4$  from the  $x_O$ -axis.

Similarly, with  $x_0 = 1$ , the Study parameters corresponding to the first operation mode,  $\mathcal{J}_2$  are  $\{1, x_1, x_2, 0, -x_1y_1 - x_2y_2, y_1, y_2, y_3\}$ . The transformation matrix in Eq. (1.34a) yields:

$$\mathbf{M}_1 = \begin{bmatrix} 1 & 0 & 0 & 0 \\ -\frac{2y_3}{x_2} & -1 & 0 & 0 \\ 2(x_2y_0 - x_3y_1) & 0 & x_2^2 - x_3^2 & 2x_2x_3 \\ 2(x_2y_1 + x_3y_0) & 0 & 2x_2x_3 & -x_2^2 + x_3^2 \end{bmatrix} \quad (2.77)$$

Thus, only four independent parameters are sufficient to characterize this operation mode and it is a 4-*dof* Schönflies mode in which the translational motions are parametrized by  $y_1, y_2$  and  $y_3$  and the rotational motion is parametrized by  $x_1, x_2$  along with  $(1 - v_{13}^2)x_1 + 2v_{13}x_2 = 2v_{24}x_1 + (v_{24}^2 - 1)x_2 = 0$ . In this operation mode, the platform is in upright position with rotational motion about an axis located at an angle of  $\beta_1 - 90^\circ = \beta_3 - 90^\circ = \beta_2 = \beta_4$  from the  $x_O$ -axis.

Hence, it can be concluded from Eqs. (2.74) and (2.75) that when all the base R-joint axes of the 4-rRUU PM have the same horizontal orientations, it exhibits a Schönflies motion mode with the rotational *dof* about a horizontal axis with the same orientation as those R-joint axes. An example is the configuration shown in Fig. 2.17, where  $\beta_1 = \beta_3 = 90^\circ$ ,  $\beta_2 = \beta_4 = 0^\circ$  and the orientation *dof* of the moving platform is about the  $x_O$ -axis [NCW18d].

The double-Hooke's joint allows a planar transmission and hence the 4-rRUU PM can have any orientation of the base revolute joints such that  $\beta_i \in [0, \pi]$ . Additionally, with the help of a L-fixture, it is possible to have a vertical orientation of the base revolute joint axes as shown in Fig. 2.18.



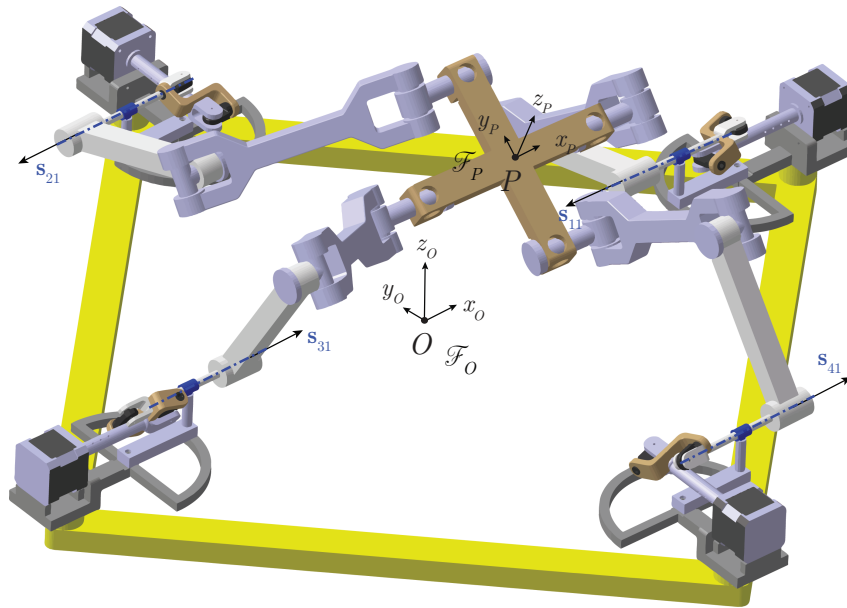


Figure 2.17 – A 4-RUU PM with horizontal and parallel base revolute joint axes

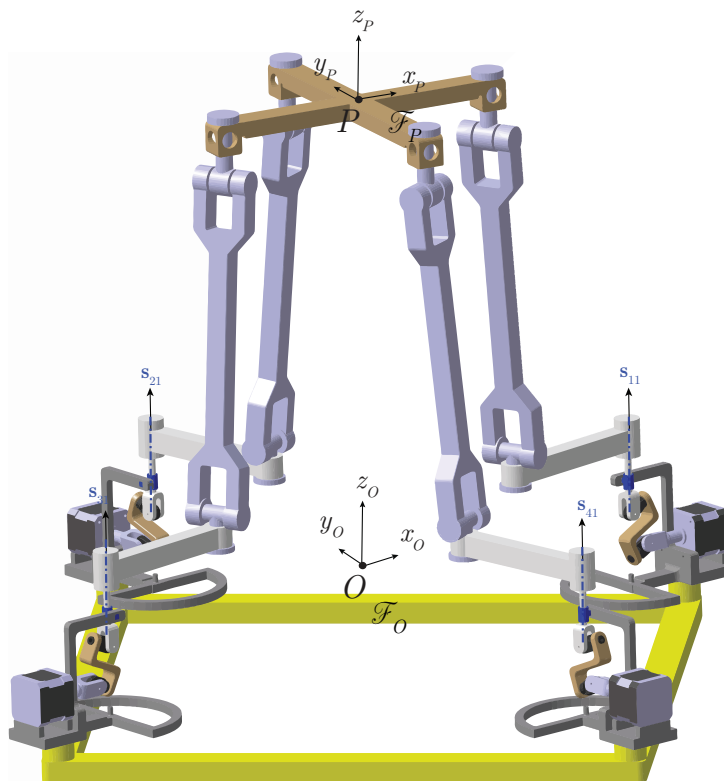


Figure 2.18 – A dual reconfigurable 4-rRUU PM with vertical base revolute joint axes

Reconfiguration analysis of this mechanism already exists in the literature [Nur+16], where it was shown to have three operation modes. The first operation mode is a 4-*dof* Schönflies mode in which the platform is upside down and the rotational axis is parallel to  $z_O$ -axis. The second operation mode is a 4-*dof* Schönflies mode with the rotational axis parallel to  $z_O$ -axis, but in this case, the posture of the platform is upright. The third operation mode is a 2-*dof* coupled motion mode and is less relevant from a practical view point.

### Workspace for the same orientations of base R-joint axes

The moving platform center of the 4-rRUU PM lies on the boundary of the translational workspace only when at least one of its limbs is in a fully extended or a folded configuration. In this case, the limb is said to be in a limb or serial or input singularity [GA90]. It can happen when the  $8 \times 4$  input Jacobian matrix  $\mathbf{J}_I = \frac{\partial \mathbf{g}}{\partial \mathbf{t}_i}$  with  $i = 1, 2, 3, 4$  and  $\mathbf{g} = [g_1, g_2, \dots, g_8]$  is not full-rank. One approach to deal with the non-square matrix is to search for conditions such that all its  $4 \times 4$  minors vanish as shown for a 3-RUU PM in [SPH19]. However, the first three equations of the 3-RUU PM do not depend on the variable  $t_i$  which is the half tangent of the actuated joint variable  $\theta_i$ . Likewise, here,  $g_i$  does not depend on  $t_i$ ,  $i = 1, 2, 3, 4$ . Therefore, the input singularities corresponding to limb  $i$  can be simply calculated as  $f_i : \frac{\partial g_{i+4}}{\partial t_i} = 0, i = 1, 2, 3, 4$ . Eliminating  $t_i$  from  $f_i$  and  $g_{i+4}$  leads to four polynomials,  $S_i$  solely in terms of Study parameters. The singularity surfaces (tori shaped) are nothing but the varieties of these polynomials and the workspace boundary is given by their intersection. By considering the 4-rRUU PMs in Schönflies motion mode, it is possible to visualize the translational workspace boundaries for different fixed orientations of the moving platform. For instance, the singularity surfaces of a 4-rRUU PM with base R-joint axes parallel to  $x_O$ -axis and with design parameters  $r_0 = 2, r_1 = 1, p = 2, q = 3$  have the following implicit representations:

$$S_1 : x^4 + 2x^2y^2 + 2x^2z^2 + y^4 + 2y^2z^2 + z^4 - 4x^3 - 4xy^2 - 4xz^2 - 4x^2 - 24y^2 - 24z^2 + 16x + 16 = 0 \quad (2.78a)$$

$$S_2 : x^4 + 2x^2y^2 + 2x^2z^2 + y^4 + 2y^2z^2 + z^4 - 4x^2y - 4y^3 - 4yz^2 - 8x^2 - 20y^2 - 24z^2 + 48y = 0 \quad (2.78b)$$

$$S_3 : x^4 + 2x^2y^2 + 2x^2z^2 + y^4 + 2y^2z^2 + z^4 + 4x^3 + 4xy^2 + 4xz^2 - 4x^2 - 24y^2 - 24z^2 - 16x + 16 = 0 \quad (2.78c)$$

$$S_4 : x^4 + 2x^2y^2 + 2x^2z^2 + y^4 + 2y^2z^2 + z^4 + 4x^2y + 4y^3 + 4yz^2 - 8x^2 - 20y^2 - 24z^2 - 48y = 0 \quad (2.78d)$$

where the orientation of moving platform,  $\phi = 0^\circ$  and  $(x, y, z)$  are the coordinates of point  $P$ . The workspace boundary for this PM is shown in Fig. 2.19c. Additionally, Fig. 2.19 shows the workspaces for three configurations of the PM with their base R-joint axes parallel to  $x_O, y_O$  and  $z_O$ -axes, henceforth named as 4-R<sub>x</sub>UU, 4-R<sub>y</sub>UU and 4-R<sub>z</sub>UU PMs, respectively. The workspaces are plotted for different orientations of the moving platform including their cross-sections about a symmetric axis  $\mathbf{a}$  for the 4-R<sub>a</sub>UU PM, where  $\mathbf{a}$  can be  $x, y$  or  $z$ .

### Design optimization

With an ultimate goal to build a working prototype of the 4-rRUU PM, the design parameters are determined using a Pareto optimization procedure shown in Algorithm 1. Although

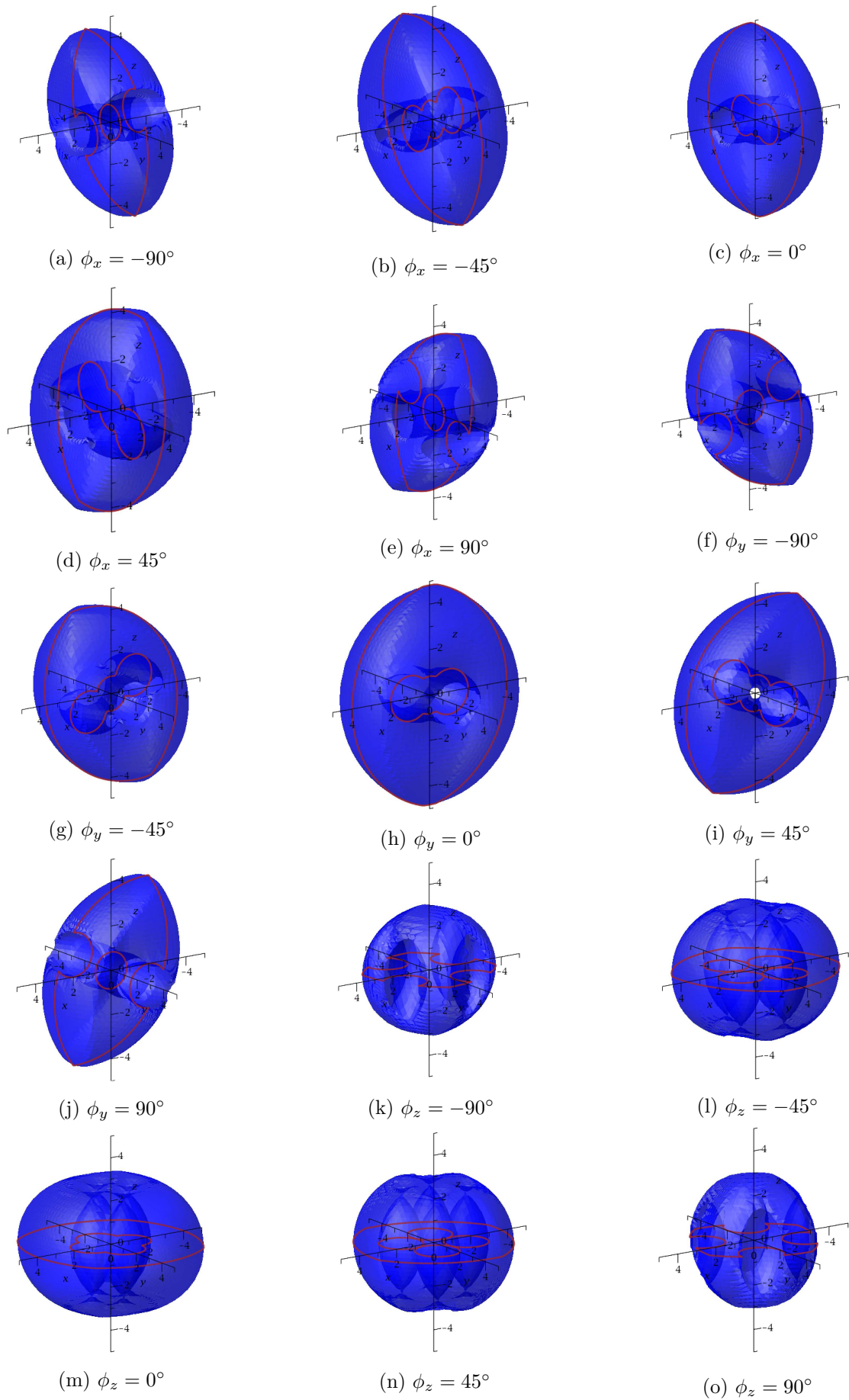


Figure 2.19 – Workspaces of 4- $R_x$ UU(a-e), 4- $R_y$ UU(f-j) and 4- $R_z$ UU(k-o) PMs

there are infinitely many possible orientations of the base R-joint axes, the optimization problem is simplified by only considering 4-R<sub>x</sub>UU, 4-R<sub>y</sub>UU and 4-R<sub>z</sub>UU PMs. Moreover, these PMs are examined with zero orientations of their moving platform since it is the only pose shared by them.

---

**Algorithm 1** Design optimization of a 4-rRUU PM
 

---

```

1: procedure
2:    $ax \leftarrow$  Orientation of base R-joints ▷ 1,2,3 for Rx, Ry and Rz, respectively
3:    $\kappa \leftarrow$  Inverse condition number of the homogenized forward Jacobian matrix
4:    $\kappa_{th} \leftarrow$  Threshold value of  $\kappa$ 
5:    $r_0 \leftarrow$  Base circum-radius
6:    $r_1 \leftarrow$  Platform circum-radius
7:    $p \leftarrow$  Proximal link length
8:    $q \leftarrow$  Distal link length
9:    $\nu := 1$ 
10:   $r_0 := 1$ ;
11:  for  $r_1 \leftarrow l$  by  $d$  to  $u$  do
12:    for  $p \leftarrow l$  by  $d$  to  $u$  do
13:      for  $q \leftarrow l$  by  $d$  to  $u$  do
14:         $\text{ObjS}(\nu) := \frac{r_1 + p + q}{6}$ ; ▷ Objective function: Size
15:         $x, y, z \leftarrow -val : res : val$ ;
16:         $n := 2 \frac{val}{res} + 1$ ;
17:        for  $i \leftarrow 1$  to  $n$  do
18:          for  $j \leftarrow 1$  to  $n$  do
19:            for  $k \leftarrow 1$  to  $n$  do
20:              if  $(x(i), y(j), z(k))$  is in the workspace and there
                exists at least one real solution to IKM without
                internal collisions with  $\kappa > \kappa_{th}$  then
21:                 $\mathbf{W}_{ax}(i, j, k) := 1$ 
22:              else
23:                 $\mathbf{W}_{ax}(i, j, k) := 0$ 
24:              end if
25:            end for
26:          end for
27:        end for
28:         $W_{ax} := \frac{\sum_i \sum_j \sum_k \mathbf{W}_{ax}(i, j, k)}{n^3}$ 
29:
30:         $\text{ObjW}(\nu) := 1 - \min_{ax=1}^3 W_{ax}$  ▷ Objective function: Workspace density
31:      end for
32:    end for
33:  end for
34:   $\nu := \nu + 1$ 
35: end procedure

```

---

The design parameters are  $r_0, r_1, p$  and  $q$ . They must be homogenized to facilitate scaling of the final design, which is done by setting the circum-radius of the base,  $r_0$  to unity. It also

reduces the number of parameters and hence the computation time. Their arithmetic mean is the first objective function  $\mathbf{ObjS} \in [0, 1]$  which gives the overall size of the PM. Eventually, design parameters are varied from  $l = \frac{r_0}{5}$  to  $u = 2r_0$  with an increment of  $d = \frac{r_0}{5}$ . For a given set of  $\{r_1, p, q\}$ , a cube of side length  $2val = 6r_0$  is discretized into  $n^3 = 61^3$  points. At each of these points, the following conditions are checked in the prescribed order:

I. *Does it belong to the workspace of the PM?*

Thanks to the polynomials  $S_i(x, y, z)$  in Eq. (4.26) corresponding to serial singularities, a point  $(x, y, z)$  lies in the workspace when  $S_i(x, y, z) < 0 \forall i \in \{1, 2, 3, 4\}$ .

II. *Does there exist at least one working mode?*

A working mode implies a real solution to the Inverse Kinematics Model (IKM). Given  $(x, y, z)$ , a solution to IKM involves finding the actuated joint variables. This could be done by first obtaining the coordinates of point  $B_i$ , which is the intersection of a circle with center  $A_i$ , radius  $p$  and a sphere with center  $C_i$ , radius  $q$ . In  $\mathbb{C}^3$ , a circle and a sphere always intersect at two points. Hence, in  $\mathbb{R}^3$ , there are at most  $2^4 = 16$  IKM solutions. Thus, a real solution to IKM exists if coordinates of  $B_i$  turn out to be real.

III. *Aren't there any internal collisions?*

The links are approximated as capsules to determine their interferences. A capsule is a

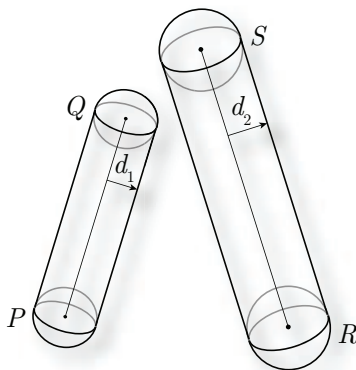


Figure 2.20 – Link interferences as collision between two capsules

cylinder between two hemispheres as shown in Fig. 2.20. They are defined by line segments and a radius. Two capsules  $PQ$  and  $RS$  with radii  $d_1$  and  $d_2$  intersect if and only if the distance between line segments  $\overline{PQ}$  and  $\overline{RS}$  is less than  $d_1 + d_2$ . There are umpteen ways to calculate the distance between two line segments. The algorithm used here is based on the approach by Eberly [Ebe07].

Couples of eight line segments  $\overline{A_i B_i}$  of length  $p$ , capsule radius  $0.1p$  and  $\overline{B_i C_i}$  of length  $q$ , capsule radius  $0.1q$ ,  $i = 1, 2, 3, 4$  are checked for collision. Out of these  $\binom{8}{2} = 28$  combinations, there is a definite intersection between four of them sharing the point  $B_i$ . Thus, if there is an intersection between at least one of the remaining 24 couples, the PM is deemed to have internal collisions.

IV. *Is the inverse conditioning number of the forward Jacobian matrix  $\kappa > \kappa_{th}$ ?*

Based on the theory of reciprocal screws, the reduced kinematic modeling of the 4-rRUU

PM can be expressed as

$$\mathbf{A}_r {}^0\mathbf{t}_r = \mathbf{B}_r \dot{\theta} \implies \begin{bmatrix} ({}^0\overrightarrow{PC}_1 \times {}^0\mathbf{u}_1)^T & {}^0\mathbf{u}_1^T \\ ({}^0\overrightarrow{PC}_2 \times {}^0\mathbf{u}_2)^T & {}^0\mathbf{u}_2^T \\ ({}^0\overrightarrow{PC}_3 \times {}^0\mathbf{u}_3)^T & {}^0\mathbf{u}_3^T \\ ({}^0\overrightarrow{PC}_4 \times {}^0\mathbf{u}_4)^T & {}^0\mathbf{u}_4^T \end{bmatrix} \begin{bmatrix} {}^0\omega \\ {}^0\mathbf{v}_P \end{bmatrix} = \mathbf{B}_r \begin{bmatrix} \dot{\theta}_1 \\ \dot{\theta}_2 \\ \dot{\theta}_3 \\ \dot{\theta}_4 \end{bmatrix} \quad (2.79)$$

where  $\dot{\theta}$  is the set of actuated joint rates and  ${}^0\mathbf{t}_r$  is the reduced twist of the moving platform with respect to the fixed base i.e., it contains the angular velocity vector of the moving platform and the linear velocity vector of its circum-center. Since 4-rRUU PM in its Schönflies operation mode has only one component of its angular velocity,  ${}^0\mathbf{t}_r$  is essentially a  $4 \times 1$  vector.  $\mathbf{A}_r$  is the  $4 \times 4$  reduced forward Jacobian matrix and it incorporates the actuation wrenches of the PM such that its columns correspond to non-zero values of  ${}^0\mathbf{t}$  with  ${}^0\mathbf{u}_i = \frac{\overrightarrow{B_iC_i}}{|\overrightarrow{B_iC_i}|}$ .  $\mathbf{B}_r$  is the reduced inverse Jacobian matrix. It is diagonal with its elements being the scalar product of actuation wrenches and the actuated joint twists.

$\mathbf{A}_r$  is homogenized by dividing its elements in the first column by  $r_1$  since  $r_1$  is the norm of vectors  $\overrightarrow{PC_i}$ . Thus, the inverse condition number,  $\kappa$  is calculated.  $\kappa$  gives a measure of how close the manipulator is to a parallel singularity. If it is small, the matrix is said to be ill-conditioned and is almost singular while if it is close to 1, the matrix is far from singularities. A threshold of  $\kappa_{th} = 0.3$  is set and it is checked if  $\kappa > \kappa_{th}$ .

Consequently, the number of points satisfying conditions I-IV are counted and are divided by the total number of points considered, to obtain  $W_{ax} \in [0, 1]$ , where  $ax = 1, 2, 3$  for 4-R<sub>x</sub>UU, 4-R<sub>y</sub>UU and 4-R<sub>z</sub>UU PMs, respectively. Considering the  $\min(W_1, W_2, W_3)$  leads to design parameters with larger workspaces for all three orientations of the base R-joint axes. This value is subtracted by 1 to ensure the preference of smaller values compared to larger ones in both objective functions.

Fig. 2.21 shows the feasible solutions, highlighting those that lie on the Pareto front. Some Pareto-optimal designs are also depicted. The Pareto-optimal design with  $r_0 = 1, r_1 = 0.4, p = 1, q = 1.4$  is selected as a potential candidate for the prototype.

The goal of constructing a prototype of the 4-rRUU PM is to use it for milling operations. A milling cutter will be mounted on the moving platform, whose axis will be normal to the latter as roughly represented in Fig. 2.22 (not drawn to scale). The workpiece is assumed to be a cuboid of dimension  $0.12 \text{ m} \times 0.05 \text{ m} \times 0.05 \text{ m}$ . To place the workpiece, it is necessary choose a location in the workspace that is free of internal collisions and far from singularities and is done as follows:

The minimum condition number among 4-R<sub>x</sub>UU, 4-R<sub>y</sub>UU and 4-R<sub>z</sub>UU PMs is calculated for each of their working modes. The maximum of these values is plotted in Fig. 2.23 throughout the translational workspace. A point  $F$  with  $x = 0.2, y = 0.1, z = 0.6$  is chosen as the midpoint of the cuboidal workpiece. Accordingly, the necessary actuated joint torques and velocities can be calculated as follows:

$$\tau = \mathbf{J}^T \mathbf{F}, \quad \dot{\theta} = (\mathbf{J}^{-1}) {}^0\mathbf{t}_r \quad (2.80)$$

$$\text{with } \mathbf{J} = \mathbf{A}_r^{-1} \mathbf{B}_r \quad \mathbf{J}^{-1} = \mathbf{B}_r^{-1} \mathbf{A}_r, \quad (2.81)$$

where  $\tau = [\tau_1, \tau_2, \tau_3, \tau_4]$  and  $\dot{\theta} = [\dot{\theta}_1, \dot{\theta}_2, \dot{\theta}_3, \dot{\theta}_4]$  are sets of actuated joint torques and velocities, respectively.  $\mathbf{F} = [M, F_x, F_y, F_z]$  and  ${}^0\mathbf{t}_r = [\omega, v_x, v_y, v_z]$  are the external forces and velocities

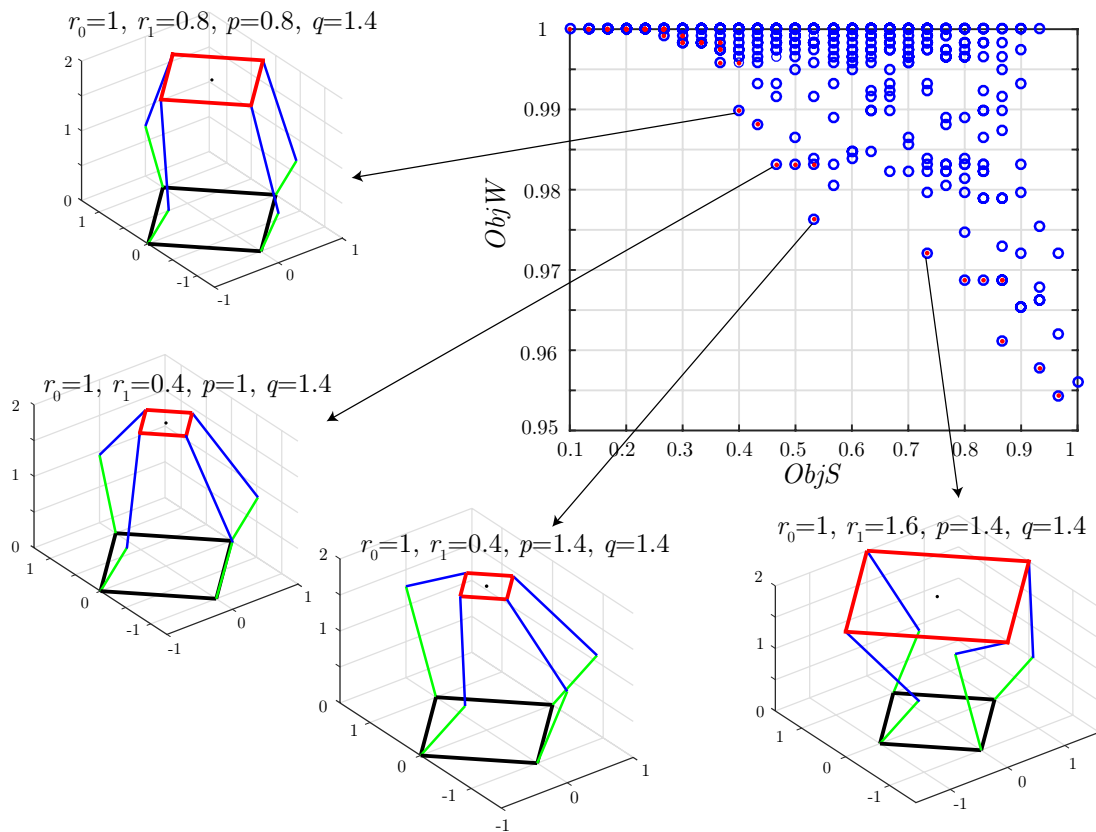


Figure 2.21 – Pareto-optimal solutions to the design optimization of the 4-rRUU PM.

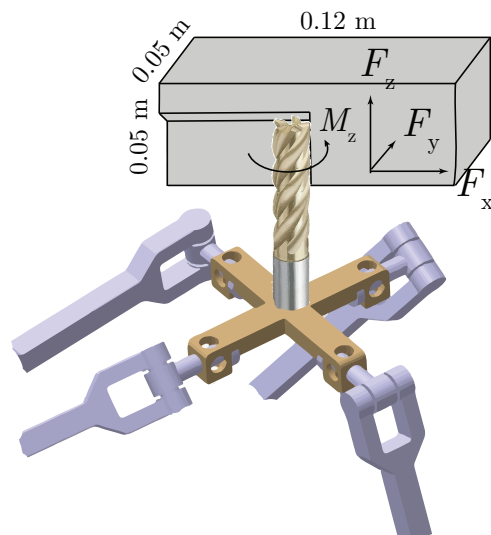


Figure 2.22 – Milling as a tentative application of the 4-rRUU PM prototype.

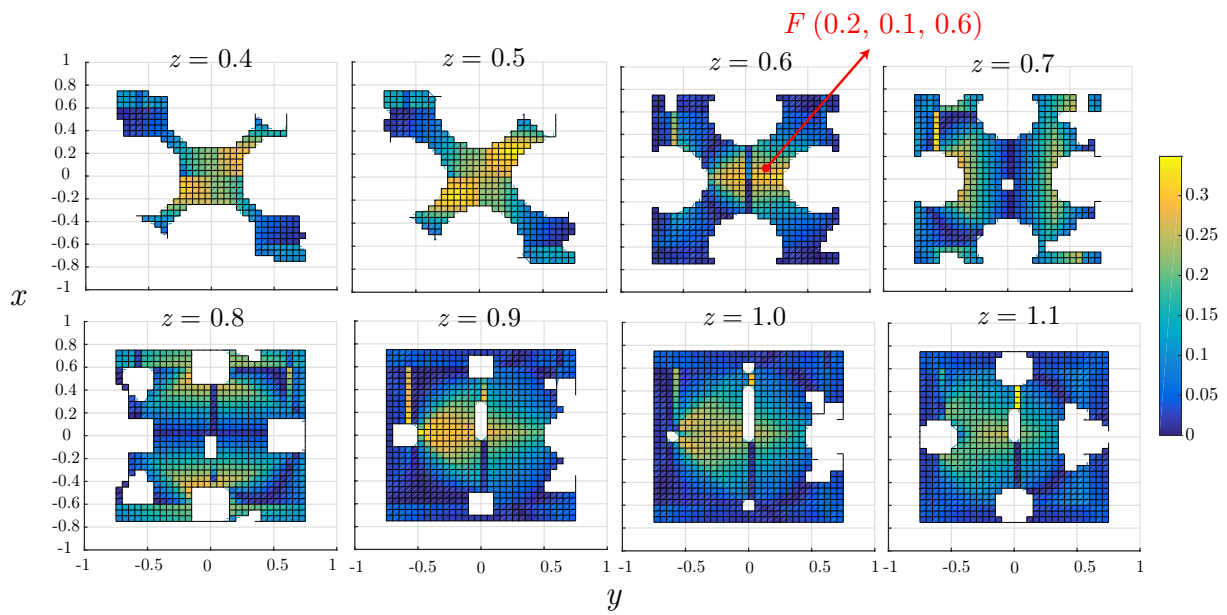


Figure 2.23 – Variation of condition number,  $\kappa_m = \max_{ikm=1}^{16}(\min_{ax=1}^3(\kappa))$

applied on the moving platform, respectively. The direction of angular velocity  $\omega$  and moment  $M$  depend on the orientation of base R-joint axes.  $M_x = M_y = 0$ ,  $M_z = F_x r_t$ , where  $r_t$  is the tool radius. The algorithm to plot  $\kappa_m$  in Fig. 2.23 and the choice of point  $F$  ensure that there exists at least one IKM solution for each orientation of the base R-joint axes where the actuated torques and velocities are smooth.

Figure 2.24 shows the variation of actuated joint torques and velocities for the IKM solution

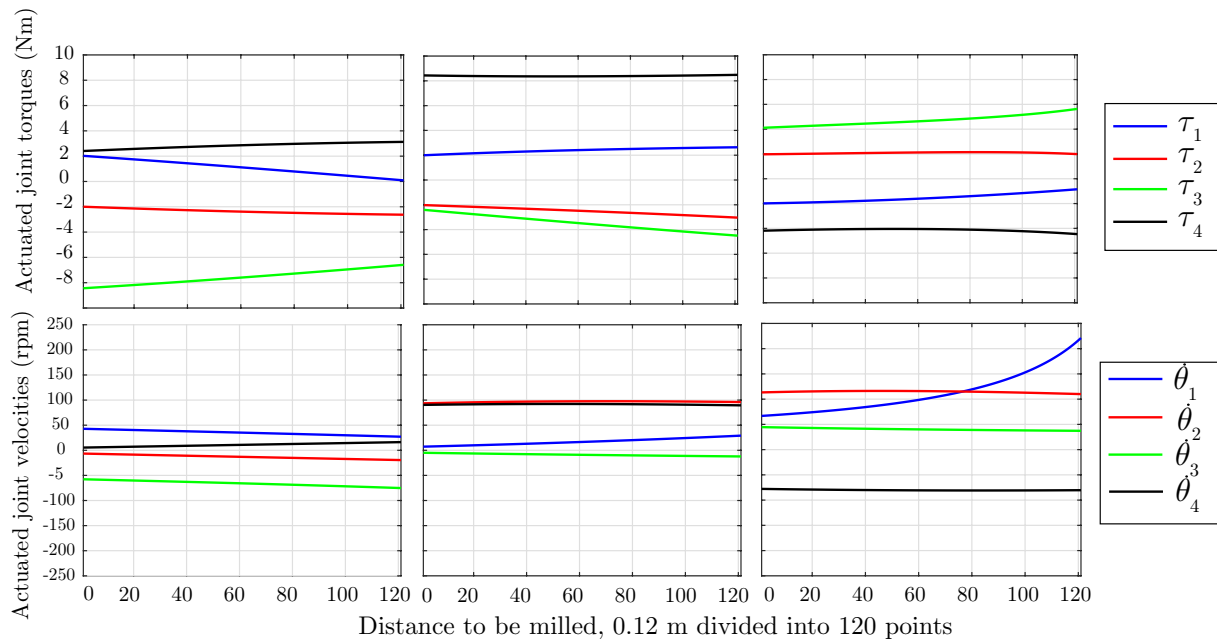


Figure 2.24 – Variation of actuated joint torques and velocities through 120 points divided along the distance to be milled



Design parameters (in m)	$r_0$	$r_1$	$p$	$q$
	0.6	0.24	0.6	0.84
External forces, $\mathbf{F}$	$M_z(\text{Nm})$	$F_x(\text{N})$	$F_y(\text{N})$	$F_z(\text{N})$
	0.06	20	20	20
Moving platform velocities ${}^0\mathbf{t}_r$	$\omega(\text{rads}^{-1})$	$v_x(\text{ms}^{-1})$	$v_y(\text{ms}^{-1})$	$v_z(\text{ms}^{-1})$
	0	0.5	0	0

Table 2.5 – Inputs to calculate actuated joint torques and velocities

with the largest  $\kappa$  that corresponds to Fig. 2.23. In this figure, the design parameters are scaled so that the fixed base of the PM is confined within a square of side 1 m. The tool radius is assumed to be 0.003 m and the remaining assigned values are listed in Table 2.5.

From Fig. 2.24, the nominal absolute torque and velocity are observed to be 10 Nm and 250 rpm, respectively. Based on these specifications, motors are bought out. The CAD model of the 4-R<sub>x</sub>UU prototype is shown in Appendix-A along with the manufacturing drawings.

## 2.2 Influence of design parameters on operation modes

The 3-RPS PM is a three degree-of-freedom (DOF) spatial mechanism, initially proposed by Hunt [Hun83]. This manipulator allows one pure vertical translation and two rotations about axes parallel to the horizontal plane, but since those axes do not remain fixed when the manipulator moves, the two rotations generate two parasitic horizontal translations. The mechanism is composed of three identical limbs connecting its base to its moving platform. Each limb consists of a revolute joint, a prismatic joint and a spherical joint mounted in series.

Several arrangements of the joints are possible, e.g. the R-joint axes in the base frame can be tangential to a circle, parallel or intersect at a common point.

Several research works have dealt with the kinematic analysis of the 3-RPS PM. Huang and Fang described the constraints of the manipulator [HF95] using screw theory. The number of solutions to the direct kinematics was first published by Tsai [Tsa99]. Self-motions [Sch+13] were investigated by Schadlbauer *et al.* in which a spatial 3-RPS Manipulator was considered with R-joints tangential to the base circum-circle. Workspace and joint space analysis [Cha+14] using quaternions was done by Chablat *et al.*, and more special configurations of the 3-RPS manipulator [Nur+14] like the 3-RPS cube manipulator as well as the synthesis of design parameters with respect to specific operation modes [NCW15b] were both investigated by Nurahmi *et al.* Moreover, a complete algebraic analysis of the 3-RPS PM was published, using Study's kinematic mapping in [Sch+14] and in [SWH12]. Gallardo *et al.* analyzed the kinematics of the 3-RPS PM by using screw theory [GOR08].

The motion capabilities of the 3-RPS PM were exploited in telescope applications studied by Carretero *et al.* [Car+97] and in machine tool heads, investigated by Hernandez *et al.* [Her+08]. The application for medical purposes like human machine interactions were investigated in [Ver+09], including the control of the manipulator with PID controllers.

Apparently, the 3-RPS PM is one of the celebrated PMs with only two operation modes which makes it the right candidate to commence the study on how the architecture of a PM influences its number of operation modes. Therefore, the subject of this section is about the determination

of some conditions on the design parameters of 3-RPS manipulators with coplanar revolute joint axes for those manipulators to have two operation modes [Nay+18].

### 2.2.1 Manipulator Architectures

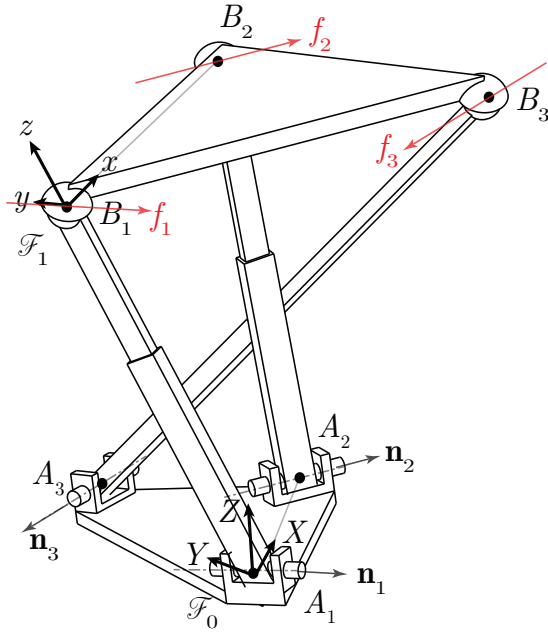


Figure 2.25 – Architecture of a 3-RPS parallel manipulator with coplanar revolute joints

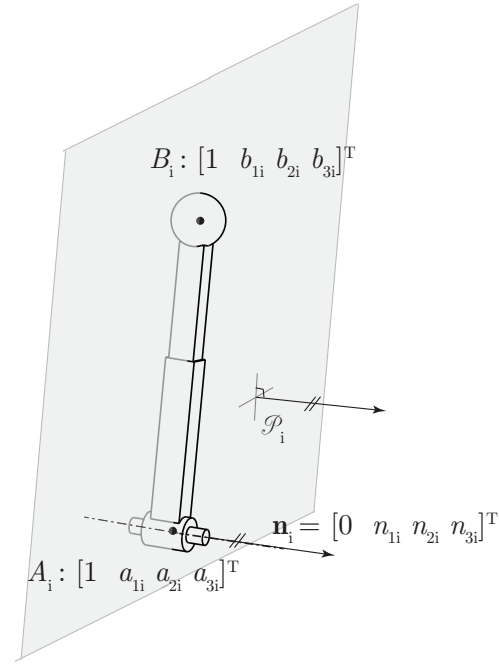


Figure 2.26 – A RPS limb

The investigated spatial PM shown in Fig. 2.25 consists of a moving platform connected to a fixed base with three limbs. Each limb is composed of a revolute joint, a prismatic joint and a spherical joint mounted in series. The three prismatic joints are actuated. Figure 2.26 represents a RPS limb. The base of the 3-RPS manipulator is specified by 3 base-points  $A_1, A_2$  and  $A_3$  in the fixed frame  $\mathcal{F}_0$ . The fixed frame is defined such that  $A_1$  is the origin of the coordinate frame,  $A_2$  is along the  $x$ -axis and  $A_3$  is an arbitrary point in the  $XY$ -plane.  $B_1, B_2$  and  $B_3$  are the vertices of the triangular moving-platform,  $B_1$  is the origin of the moving-platform frame  $\mathcal{F}_1$ ,  $B_2$  is along the  $x$ -axis of  $\mathcal{F}_1$  and  $B_3$  lies in the  $xy$ -plane.

The  $i$ th revolute joint axis of direction  $\mathbf{n}_i$  is perpendicular to the direction of the  $i$ th prismatic joint, namely,

$$\mathbf{n}_i \cdot \overrightarrow{A_i B_i} = 0, \quad i = 1, 2, 3 \quad (2.82)$$

### 2.2.2 Kinematic Modeling

To derive the constraint equations of the 3-RPS PMs with coplanar revolute joint axes, the homogeneous coordinates of point  $A_i$  and vector  $\mathbf{n}_i$  are firstly expressed in frame  $\mathcal{F}_0$  while that

of the point  $B_i$  are expressed in frame  $\mathcal{F}_1$ :

$${}^0\mathbf{a}_1 = (1, 0, 0, 0), \quad {}^0\mathbf{a}_2 = (1, a_{12}, 0, 0), \quad {}^0\mathbf{a}_3 = (1, a_{13}, a_{23}, 0), \quad (2.83)$$

$${}^1\mathbf{b}_1 = (1, 0, 0, 0), \quad {}^1\mathbf{b}_2 = (1, b_{12}, 0, 0), \quad {}^1\mathbf{b}_3 = (1, b_{13}, b_{23}, 0), \quad (2.84)$$

$${}^0\mathbf{n}_1 = (0, n_{11}, n_{21}, n_{31}), \quad {}^0\mathbf{n}_2 = (0, n_{12}, n_{22}, n_{32}), \quad {}^0\mathbf{n}_3 = (0, n_{13}, n_{23}, n_{33}), \quad (2.85)$$

with the first entry of each vector being the homogenizing coordinate<sup>2</sup>. Since points  $B_i$  are given in the moving frame, a transformation is applied to obtain it in  $\mathcal{F}_0$  frame. *Study's kinematic mapping* can be used for this purpose. The transformation to obtain  ${}^0\mathbf{b}_i$  from  ${}^1\mathbf{b}_i$  is given in Eq. (1.34a).

The geometric constraints of the PM can be derived as follows. As the prismatic joints are actuated, the distance between points  $A_i$  and  $B_i$  is equal to the prismatic joint length  $r_i$ . Therefore, the following first three distance constraints arise:

$$g_i : ({}^0\mathbf{a}_i - {}^0\mathbf{b}_i)^T ({}^0\mathbf{a}_i - {}^0\mathbf{b}_i) - r_i^2 = 0, \quad i = 1, 2, 3. \quad (2.86)$$

The next three geometric constraints of the manipulator are derived from the perpendicularity between the revolute joint and the prismatic joint direction within each limb, namely, from Eq. (2.82):

$$g_{i+3} : {}^0\mathbf{n}_i^T ({}^0\mathbf{a}_i - {}^0\mathbf{b}_i) = 0, \quad i = 1, 2, 3. \quad (2.87)$$

As a result, the six constraint equations are expressed as follows after some mathematical simplifications:

$$g_1 := (x_0^2 + x_1^2 + x_2^2 + x_3^2)r_1^2 - 4y_0^2 - 4y_1^2 - 4y_2^2 - 4y_3^2 = 0 \quad (2.88a)$$

$$\begin{aligned} g_2 := & (x_0^2 + x_1^2 + x_2^2 + x_3^2)(r_2^2 - b_{12}^2 - a_{12}^2) + (2x_0^2 + 2x_1^2 - 2x_2^2 - 2x_3^2)a_{12}b_{12} \\ & + (-4x_0y_1 + 4x_1y_0 - 4x_2y_3 + 4x_3y_2)a_{12} + (4x_0y_1 - 4x_1y_0 - 4x_2y_3 + 4x_3y_2)b_{12} \\ & - 4y_0^2 - 4y_1^2 - 4y_2^2 - 4y_3^2 = 0 \end{aligned} \quad (2.88b)$$

$$\begin{aligned} g_3 := & (x_0^2 + x_1^2 + x_2^2 + x_3^2)(r_3^2 - a_{13}^2 - a_{23}^2 - b_{13}^2 - b_{23}^2) + (2x_0^2 + 2x_1^2 - 2x_2^2 \\ & - 2x_3^2)a_{13}b_{13} + (-4x_0x_3 + 4x_1x_2)a_{13}b_{23} + (-4x_0y_1 + 4x_1y_0 - 4x_2y_3 + 4x_3y_2)a_{13} \\ & + (4x_0x_3 + 4x_1x_2)a_{23}b_{13} + (2x_0^2 - 2x_1^2 + 2x_2^2 - 2x_3^2)a_{23}b_{23} + (-4x_0y_2 + 4x_1y_3 \\ & + 4x_2y_0 - 4x_3y_1)a_{23} + (4x_0y_1 - 4x_1y_0 - 4x_2y_3 + 4x_3y_2)b_{13} + (4x_0y_2 + 4x_1y_3 \\ & - 4x_2y_0 - 4x_3y_1)b_{23} - 4y_0^2 - 4y_1^2 - 4y_2^2 - 4y_3^2 = 0 \end{aligned} \quad (2.88c)$$

$$g_4 := (2x_0y_1 - 2x_1y_0 + 2x_2y_3 - 2x_3y_2)n_{11} + (2x_0y_2 - 2x_1y_3 - 2x_2y_0 + 2x_3y_1)n_{21} = 0 \quad (2.88d)$$

$$\begin{aligned} g_5 := & (2x_0y_1 - 2x_1y_0 + 2x_2y_3 - 2x_3y_2)n_{12} + (2x_0y_2 - 2x_1y_3 - 2x_2y_0 + 2x_3y_1)n_{22} \\ & + a_{12}n_{12}(x_0^2 + x_1^2 + x_2^2 + x_3^2) + (-x_0^2 - x_1^2 + x_2^2 + x_3^2)b_{12}n_{12} \\ & + (-2x_0x_3 - 2x_1x_2)b_{12}n_{22} = 0 \end{aligned} \quad (2.88e)$$

$$\begin{aligned} g_6 := & (2x_0y_1 - 2x_1y_0 + 2x_2y_3 - 2x_3y_2)n_{13} + (2x_0y_2 - 2x_1y_3 - 2x_2y_0 + 2x_3y_1)n_{23} \\ & - (a_{13}n_{13} + a_{23}n_{23})(x_0^2 + x_1^2 + x_2^2 + x_3^2) + (-x_0^2 - x_1^2 + x_2^2 + x_3^2)b_{13}n_{13} \\ & + (-x_0^2 + x_1^2 - x_2^2 + x_3^2)b_{23}n_{23} + (-2x_0x_3 - 2x_1x_2)b_{13}n_{23} + (2x_0x_3 \\ & - 2x_1x_2)b_{23}n_{13} = 0 \end{aligned} \quad (2.88f)$$

---

2. A vector expressed in  $\mathcal{F}_0$  is denoted as  ${}^0\{\cdot\}$  whereas a vector expressed in  $\mathcal{F}_1$  is indicated as  ${}^1\{\cdot\}$ .

It should be noted that those six equations are a function of fifteen design parameters  $a_{12}, a_{13}, a_{23}, b_{12}, b_{13}, b_{23}, n_{ij}$  ( $i, j \in \{1, 2, 3\}$ ), three actuated prismatic joint variables  $r_1, r_2, r_3$  and the Study parameters.

### 2.2.3 Operation modes

This section aims to find the conditions on the fifteen design parameters such that the 3-RPS manipulator with coplanar revolute joints can exhibit more than one operation mode. Since the R-joint axes are assumed coplanar,  $n_{31} = n_{32} = n_{33} = 0$ .

From the standpoint of algebraic geometry, it is known that the existence of more than one operation mode requires the factorization of a polynomial belonging to the ideal of constraint polynomials (preferably the ones independent of actuated joint variables) [Sch+14]. In this context, an ideal  $\mathcal{J}$  is considered such that it is a subset of the field of Study parameters:

$$\mathcal{J} = \langle g_4, g_5, g_6 \rangle \mid \mathcal{J} \subseteq K[x_0, x_1, x_2, x_3, y_0, y_1, y_2, y_3] \quad (2.89)$$

From the definition of an ideal, if a polynomial  $g \in \mathcal{J}$  and  $h \in K$ ,  $K$  being the field over which the ideal  $\mathcal{J}$  is defined, then  $hg \in \mathcal{J}$  [CLO07]. From Eqs. (2.88) and (2.89), a polynomial  $g$  is defined such that

$$g = h_1g_4 + h_2g_5 + h_3g_6 \in \mathcal{J}, \text{ where } h_i \neq 0 \in K[x_0, x_1, x_2, x_3, y_0, y_1, y_2, y_3], i = 1, 2, 3 \quad (2.90)$$

For simplicity,  $h_i$  is only allowed to be a function of design parameters. This assumption forces the polynomial  $g$  to be quadratic. To this end, the problem boils down to find the coefficients  $h_i$  such that  $g$  can be factorized. In search of linear factors, two general linear equations are introduced in Eq. (2.91) and are multiplied to obtain a general quadratic polynomial  $s_{12}$  in the kinematic image space,  $\mathbb{P}^7$ .

$$\begin{aligned} s_1 &: m_1x_0 + m_2x_1 + m_3x_2 + m_4x_3 + m_5y_0 + m_6y_1 + m_7y_2 + m_8y_3 = 0 \\ s_2 &: n_1x_0 + n_2x_1 + n_3x_2 + n_4x_3 + n_5y_0 + n_6y_1 + n_7y_2 + n_8y_3 = 0 \\ s_{12} &= s_1 \cdot s_2 \end{aligned} \quad (2.91)$$

where  $m_k$  and  $n_k$ ,  $k = 1, \dots, 8$  are constants. If  $m_k$  and  $n_k$  can be determined as functions of design variables, the ideal  $\mathcal{J}$  can be decomposed into two ideals  $\mathcal{J}_1 = \langle g_4, g_5, g_6, s_1 \rangle$  and  $\mathcal{J}_2 = \langle g_4, g_5, g_6, s_2 \rangle$ . If  $\mathcal{J}_1$  and  $\mathcal{J}_2$  are not contained in each other, or if they do not share the same radical ideal, the manipulator at hand must have two operation modes characterized by those sub-ideals.

Equating the respective coefficients of  $g$  and  $s_{12}$  leads to a system of 36 linear equations in 31 unknowns. Solving for all the parameters  $b_{12}, b_{13}, b_{23}, a_{12}, a_{13}, a_{23}, h_1, h_2, h_3, m_k, n_k, k = 1, \dots, 8$ , yields 36 solutions. It is noteworthy that some equations are dependent and the system is underdetermined. Nonetheless, the *solve* function in Maple parametrizes the solutions in terms of one or more unknowns. Investigating the solution set reveals that there are some trivial solutions (complex ones and the ones with  $h_i = 0, a_{12} = 0, a_{13} = 0, a_{23} = 0, b_{12} = 0, b_{13} = 0$  or  $b_{23} = 0$ ) and some are special cases of the general one ( $n_{ij} = 0, i = 1, 2, j = 1, 2, 3$ ). The focus is on the two general solutions:

Solution 1

$$m_1 = \frac{(n_{13} \pm \sqrt{n_{13}^2 + n_{23}^2}) m_4}{n_{23}}, \quad m_2 = m_3 = 0, \quad m_4 = m_4, \quad m_5 = m_6 = m_7 = m_8 = 0, \quad (2.92a)$$

$$n_1 = \frac{2(n_{13} \pm \sqrt{n_{13}^2 + n_{23}^2}) b_{23} h_3}{m_4}, \quad n_2 = n_3 = 0, \quad n_4 = 2 \frac{b_{23} h_3 n_{23}}{m_4}, \quad n_5 = n_6 = n_7 = n_8 = 0, \quad (2.92b)$$

$$a_{12} = \frac{(n_{11} n_{22} - n_{12} n_{21})(a_{13} n_{13} + a_{23} n_{23})}{(n_{11} n_{23} - n_{13} n_{21}) n_{12}}, \quad a_{13} = a_{13}, \quad a_{23} = a_{23} \quad (2.92c)$$

$$b_{12} = -\frac{b_{23}(n_{13}^2 + n_{23}^2)(n_{11} n_{22} - n_{12} n_{21})}{(n_{12} n_{23} - n_{13} n_{22})(n_{11} n_{23} - n_{13} n_{21})}, \quad b_{13} = -\frac{b_{23}(n_{12} n_{13} + n_{22} n_{23})}{n_{12} n_{23} - n_{13} n_{22}}, \quad b_{23} = b_{23} \quad (2.92d)$$

$$h_1 = \frac{h_3(n_{12} n_{23} - n_{13} n_{22})}{n_{11} n_{22} - n_{12} n_{21}}, \quad h_2 = -\frac{h_3(n_{11} n_{23} - n_{13} n_{21})}{n_{11} n_{22} - n_{12} n_{21}}, \quad h_3 = h_3 \quad (2.92e)$$

Solution 2

$$m_1 = 0, \quad m_2 = \frac{(n_{13} \pm \sqrt{n_{13}^2 + n_{23}^2}) m_3}{n_{23}}, \quad m_3 = m_3, \quad m_4 = m_5 = m_6 = m_7 = m_8 = 0, \quad (2.93a)$$

$$n_1 = 0, \quad n_2 = \frac{2b_{23} h_3 n_{23}^2}{(n_{13} \pm \sqrt{n_{13}^2 + n_{23}^2}) m_3}, \quad n_3 = -2 \frac{b_{23} h_3 n_{23}}{m_3}, \quad n_4 = n_5 = n_6 = n_7 = n_8 = 0, \quad (2.93b)$$

$$a_{12} = \frac{(n_{11} n_{22} - n_{12} n_{21})(a_{13} n_{13} + a_{23} n_{23})}{(n_{11} n_{23} - n_{13} n_{21}) n_{12}}, \quad a_{13} = a_{13}, \quad a_{23} = a_{23} \quad (2.93c)$$

$$b_{12} = \frac{b_{23}(n_{13}^2 + n_{23}^2)(n_{11} n_{22} - n_{12} n_{21})}{(n_{12} n_{23} - n_{13} n_{22})(n_{11} n_{23} - n_{13} n_{21})}, \quad b_{13} = \frac{b_{23}(n_{12} n_{13} + n_{22} n_{23})}{n_{12} n_{23} - n_{13} n_{22}}, \quad b_{23} = b_{23} \quad (2.93d)$$

$$h_1 = \frac{h_3(n_{12} n_{23} - n_{13} n_{22})}{n_{11} n_{22} - n_{12} n_{21}}, \quad h_2 = -\frac{h_3(n_{11} n_{23} - n_{13} n_{21})}{n_{11} n_{22} - n_{12} n_{21}}, \quad h_3 = h_3 \quad (2.93e)$$

Upon substitution of Solution 1 into Eq. (2.90) or Eq. (2.91) that describe the general quadric, the following conic comes out:

$$s_{12} = g = 2 b_{23} h_3 (2 n_{13} x_0 x_3 - n_{23} x_0^2 + n_{23} x_3^2) \quad (2.94)$$

The conic is degenerate and can be factorized as follows:

$$s_{12} = g = 2 \frac{b_{23} h_3}{n_{23}} (x_3 \sqrt{n_{13}^2 + n_{23}^2} + n_{13} x_3 - n_{23} x_0) (x_3 \sqrt{n_{13}^2 + n_{23}^2} - n_{13} x_3 + n_{23} x_0), \quad (2.95)$$

$$= -2 b_{23} h_3 n_{23} (x_0 - x_3 (\sqrt{\hat{n}^2 + 1} + \hat{n})) (x_0 + x_3 (\sqrt{\hat{n}^2 + 1} - \hat{n})), \quad \hat{n} = \frac{n_{13}}{n_{23}}, \quad n_{23} \neq 0. \quad (2.96)$$

bringing to light two operation modes characterized by:

$$\begin{aligned} \text{Operation mode 1 : } & x_0 - x_3 (\sqrt{\hat{n}^2 + 1} + \hat{n}) = 0 \\ \text{Operation mode 2 : } & x_0 + x_3 (\sqrt{\hat{n}^2 + 1} - \hat{n}) = 0, \quad \hat{n} = \frac{n_{13}}{n_{23}}, \quad n_{23} \neq 0. \end{aligned} \quad (2.97)$$

In the same vein, upon substituting Solution 2 into Eq. (2.90) or Eq. (2.91) results in the general quadric

$$s_{12} = g = -2 \left( 2 n_{13} x_1 x_2 - n_{23} x_1^2 + n_{23} x_2^2 \right) b_{23} h_3, \quad (2.98)$$

which splits into two polynomials characterizing the following two operation modes:

$$\begin{aligned} \text{Operation mode 1 : } & x_1 - x_2 \left( \sqrt{\hat{n}^2 + 1} + \hat{n} \right) = 0 \\ \text{Operation mode 2 : } & x_1 + x_2 \left( \sqrt{\hat{n}^2 + 1} - \hat{n} \right) = 0, \quad \hat{n} = \frac{n_{13}}{n_{23}}, \quad n_{23} \neq 0 \end{aligned} \quad (2.99)$$

As a result, when the design parameters  $b_{12}, b_{13}$  and  $b_{23}$  follow the ratio

$$\begin{aligned} b_{12} : b_{13} : b_{23} &= (n_{11} n_{22} - n_{12} n_{21}) \left( n_{13}^2 + n_{23}^2 \right) \\ &: (n_{12} n_{13} + n_{22} n_{23}) (-n_{13} n_{21} + n_{11} n_{23}) \\ &: \pm (-n_{13} n_{22} + n_{12} n_{23}) (-n_{13} n_{21} + n_{11} n_{23}), \end{aligned} \quad (2.100)$$

and parameters  $a_{12}, a_{13}$  and  $a_{23}$  satisfy the relation

$$(n_{11} n_{23} - n_{13} n_{21}) a_{12} n_{12} + (n_{12} n_{21} - n_{11} n_{22}) (+a_{13} n_{13} + a_{23} n_{23}) = 0, \quad (2.101)$$

then, the 3-RPS PM with coplanar revolute joint axes has two operation modes characterized by Eqs. (2.97) or (2.99). To derive these characteristic polynomials starting from the plane constraints, the scalar coefficients of their linear combination must follow the ratio

$$h_1 : h_2 : h_3 = n_{12} n_{23} - n_{13} n_{22} : n_{11} n_{23} - n_{13} n_{21} : n_{11} n_{22} - n_{12} n_{21}. \quad (2.102)$$

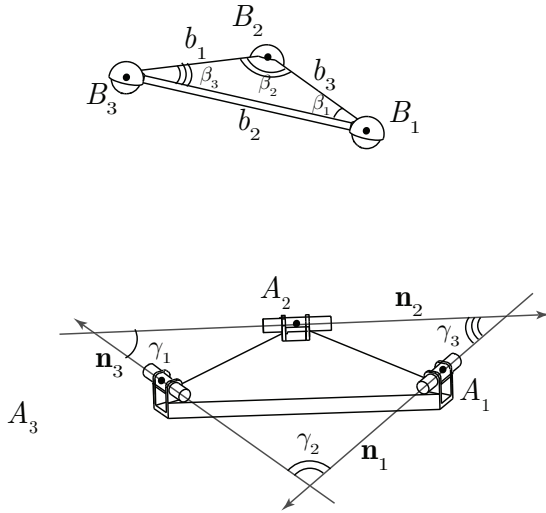


Figure 2.27 – Similarity condition between the moving platform triangle and the triangle enclosed by the R-joint axes.

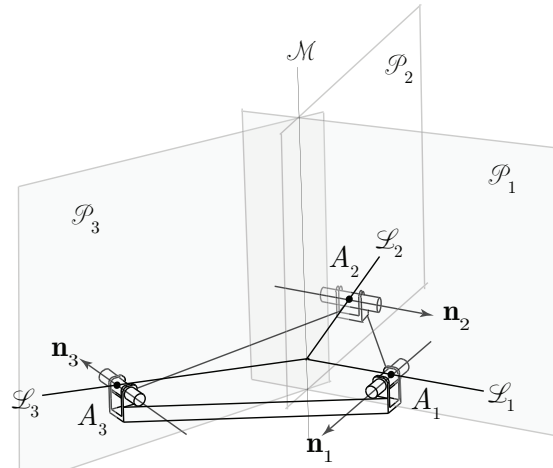


Figure 2.28 – The planes normal to R-joint axes must have a common line of intersection.

The condition in Eq. (2.100) can be geometrically interpreted as the similarity (also called as homothety) between the moving platform triangle and the triangle enclosed by the three R-joint axes. This claim is proven as follows. Figure 2.27 shows the moving platform triangle

and the triangle enclosed by the revolute joints. The sides of the moving platform triangle are  $b_1 = \sqrt{(b_{13} - b_{12})^2 + b_{23}^2}$ ,  $b_2 = |b_{13} - b_{12}|$  and  $b_3 = |b_{12}|$ . Knowing the sides, the cosine of the angles  $\beta_1$ ,  $\beta_2$  and  $\beta_3$  can be determined using the cosine rule. Similarly, the cosine of the angles  $\gamma_1$ ,  $\gamma_2$  and  $\gamma_3$  between the R-joint axes  $\mathbf{n}_1$ ,  $\mathbf{n}_2$  and  $\mathbf{n}_3$ , can be determined. Equating the cosine of respective angles results in three equations<sup>3</sup>.

$$\cos(\beta_i) = \cos(\gamma_i) \implies \frac{b_j^2 + b_k^2 - b_i^2}{2b_j b_k} = \frac{\mathbf{n}_j \mathbf{n}_k}{\|\mathbf{n}_j\| \|\mathbf{n}_k\|} \quad i, j, k = (123) \quad (2.103)$$

Solving the equations for  $b_{12}$ ,  $b_{13}$  and  $b_{23}$  yields the conditions in Eq. (2.100) proving that the considered triangles are similar (or homothetic).

Besides, Eq. (2.101) has a geometrical meaning too. It can be written as the determinant of a matrix,  $\mathbf{P}$ :

$$|\mathbf{P}| = \begin{vmatrix} n_{11} & n_{21} & 0 \\ n_{12} & n_{22} & -n_{12}a_{12} \\ n_{13} & n_{23} & -n_{13}a_{13} - n_{23}a_{23} \end{vmatrix} = 0 \quad (2.104)$$

$|\mathbf{P}|$  is the Grassmannian of three lines  $\mathcal{L}_1$ ,  $\mathcal{L}_2$  and  $\mathcal{L}_3$  which are the projections of planes  $\mathcal{P}_1$ ,  $\mathcal{P}_2$  and  $\mathcal{P}_3$  onto the  $XY$ -plane as shown in Fig. 2.28. The equation of a line  $\mathcal{L}_i$ ,  $i = 1, 2, 3$ , orthogonal to R-joint axis  $\mathbf{n}_i$  and passing through a point  $A_i$  is  $n_{1i}x_0 + n_{2i}y_0 - \mathbf{n}_i^T \mathbf{a}_i$ ,  $i = 1, 2, 3$ . Therefore,  $|\mathbf{P}| = 0$  implies that lines  $\mathcal{L}_i$  are concurrent, namely, planes  $\mathcal{P}_1$ ,  $\mathcal{P}_2$  and  $\mathcal{P}_3$  intersect at line  $\mathcal{M}$ .

Thus, a 3-RPS PM with coplanar revolute joint axes will have two operation modes if the following geometric conditions are satisfied:

- i. The moving platform triangle is homothetic to the triangle enclosed by the revolute joint axes.
- ii. The three planes normal to the three revolute joint axes, respectively, have a common line of intersection.

It can be shown that the above conditions are also necessary for the existence of two operation modes as explained thereafter.

Equations (2.97) and (2.99) are the polynomials characterizing the two operation modes. The transition between them is when both polynomials vanish at the same time, i.e., when  $x_0 = x_3 = 0$  for Solution 1 and when  $x_1 = x_2 = 0$  for Solution 2. Transition pose is known to be a constraint singularity and in case of Solution 1, it corresponds to configurations in which the moving platform is upside down as explained in [Sch+14; Sch+13]. For Solution 2, the transition pose corresponds to configurations in which the moving platform is in an upright position parallel to the fixed base. The existence of two operation modes definitely implies a constraint singularity that separates those operation modes but the reciprocity is not necessarily true as explained in subsection 2.2.4. This fact is exploited to prove the necessary conditions for a 3-RPS PM to have two operation modes.

A PM reaches a constraint singularity when its constraint wrench system is rank deficient [ZBG02a; ZBG02b; AMC16]. At this instant, the PM gains at least one dof. The constraint wrench system of a 3-RPS PM shown in Fig. 2.25 is spanned by three forces  $f_1$ ,  $f_2$  and  $f_3$  that are parallel to

3. The notation (1,2,3) represents a cyclic permutation. It means that  $i, j, k$  are initially assigned to values 1,2,3, respectively, 2,3,1, subsequently and 3,1,2, finally.

the revolute joint axes  $\mathbf{n}_1, \mathbf{n}_2$  and  $\mathbf{n}_3$  and pass through points  $B_1, B_2$  and  $B_3$ , respectively. A constraint singularity implies that the variety spanned by these three lines has a rank lower than 3. This can happen only when these lines reduce to a planar pencil of lines, i.e., when they are coplanar and concurrent. The Plücker coordinates of the force lines can be written as follows:

$$\mathbf{f}_1 = [{}^0\mathbf{n}_1, {}^0\mathbf{b}_1 \times {}^0\mathbf{n}_1] \quad (2.105a)$$

$$\mathbf{f}_2 = [{}^0\mathbf{n}_2, {}^0\mathbf{b}_2 \times {}^0\mathbf{n}_2] \quad (2.105b)$$

$$\mathbf{f}_3 = [{}^0\mathbf{n}_3, {}^0\mathbf{b}_3 \times {}^0\mathbf{n}_3] \quad (2.105c)$$

### Coplanarity condition

Any two lines intersect when the reciprocal product of their Plücker coordinates vanishes. Therefore, the coplanarity condition can be formulated as the mutual vanishing of the reciprocal product between the force lines yielding the following three equations:

$$E_1 := 2 \frac{b_{12}(x_0x_2 - x_1x_3)(n_{11}n_{22} - n_{12}n_{21})}{x_0^2 + x_1^2 + x_2^2 + x_3^2} = 0 \quad (2.106a)$$

$$E_2 := 2 \frac{(n_{11}n_{23} - n_{13}n_{21})(b_{13}x_0x_2 - b_{13}x_1x_3 - b_{23}x_0x_1 - b_{23}x_2x_3)}{x_0^2 + x_1^2 + x_2^2 + x_3^2} = 0 \quad (2.106b)$$

$$E_3 := -2 \frac{(n_{12}n_{23} - n_{13}n_{22})(b_{12}x_0x_2 - b_{12}x_1x_3 - b_{13}x_0x_2 + b_{13}x_1x_3 + b_{23}x_0x_1 + b_{23}x_2x_3)}{x_0^2 + x_1^2 + x_2^2 + x_3^2} = 0 \quad (2.106c)$$

Solving the previous system of equations in Eq. (2.106) for Study parameters  $x_0, x_1, x_2, x_3$  gives two solutions:

$$x_0 = x_3 = 0, \quad (2.107)$$

$$x_1 = x_2 = 0. \quad (2.108)$$

Calculating  ${}^0\mathbf{b}_i$ ,  $i = 1, 2, 3$  with solutions (2.107) or (2.108) shows that the  $z$ -coordinates of the resulting points are the same proving that they indeed lie in a plane parallel onto the  $XY$ -plane.

### Concurrency condition

**Case 1:**  $x_0 = x_3 = 0$

The  $z$ -coordinate of points  $B_i$  is expressed  $\frac{-2(x_1y_2 - x_2y_1)}{x_1^2 + x_2^2}$ . Without loss of generality, these lines can now be projected to the  $XY$ -plane to simplify the concurrency condition. Their projections have the equations:

$$L_i := -n_{2i}X + n_{1i}Y - (-n_{2i}{}^0b_{ix} + n_{1i}{}^0b_{iy}) = 0, \quad i = 1, 2, 3, \quad (2.109)$$

where  ${}^0b_{ix}$  and  ${}^0b_{iy}$  are the  $x$ - and  $y$ -coordinates of point  $B_i$ , respectively. Therefore, the condition for concurrency of the three lines defined by equations  $L_i = 0$  is

$$\begin{aligned} & \begin{vmatrix} -n_{21} & n_{11} & n_{21}{}^0b_{1x} - n_{11}{}^0b_{1y} \\ -n_{22} & n_{12} & n_{22}{}^0b_{2x} - n_{12}{}^0b_{2y} \\ -n_{23} & n_{13} & n_{23}{}^0b_{3x} - n_{13}{}^0b_{3y} \end{vmatrix} \\ &= (b_{12}n_{11}n_{22}n_{23} - b_{12}n_{13}n_{21}n_{22} - b_{13}n_{11}n_{22}n_{23} + b_{13}n_{12}n_{21}n_{23} - b_{23}n_{11}n_{13}n_{22} + b_{23}n_{12}n_{13}n_{21})(x_2^2 - x_1^2) \\ & \quad + 2(b_{12}n_{11}n_{12}n_{23} - b_{12}n_{12}n_{13}n_{21} - b_{13}n_{11}n_{13}n_{22} + b_{13}n_{12}n_{13}n_{21} + b_{23}n_{11}n_{22}n_{23} - b_{23}n_{12}n_{21}n_{23})x_1x_2 \\ &= 0 \end{aligned} \quad (2.110)$$



Equating the coefficients to zero leads to the following relations between the design parameters:

$$b_{12} = -\frac{(n_{11}n_{22} - n_{12}n_{21})b_{23}(n_{13}^2 + n_{23}^2)}{(-n_{13}n_{22} + n_{12}n_{23})(-n_{13}n_{21} + n_{11}n_{23})}, \quad b_{13} = -\frac{(n_{12}n_{13} + n_{22}n_{23})b_{23}}{n_{12}n_{23} - n_{13}n_{22}}, \quad b_{23} = b_{23} \quad (2.111)$$

which are exactly those defined by Eq. (2.92d).

Furthermore, upon substitution of the values of  $b_{12}$  and  $b_{13}$  and  $x_0 = x_3 = 0$  in constraint equations  $g_1 = g_2 = g_3 = 0$  defined by Eqs. (2.88d)-(2.88f) and eliminating  $b_{23}$ , results in the following equation:

$$(n_{11}n_{23} - n_{13}n_{21})a_{12}n_{12} + (n_{12}n_{21} - n_{11}n_{22})(+a_{13}n_{13} + a_{23}n_{23}) = 0, \quad (2.112)$$

which is the relation derived in Eq. (2.101).

**Case 2:**  $x_1 = x_2 = 0$

In this case, we obtain the following symmetric relations between the design parameters:

$$b_{12} = \frac{(n_{11}n_{22} - n_{12}n_{21})b_{23}(n_{13}^2 + n_{23}^2)}{(-n_{13}n_{22} + n_{12}n_{23})(-n_{13}n_{21} + n_{11}n_{23})}, \quad b_{13} = \frac{(n_{12}n_{13} + n_{22}n_{23})b_{23}}{n_{12}n_{23} - n_{13}n_{22}}, \quad b_{23} = b_{23}, \quad (2.113)$$

$$(n_{11}n_{23} - n_{13}n_{21})a_{12}n_{12} + (n_{12}n_{21} - n_{11}n_{22})(+a_{13}n_{13} + a_{23}n_{23}) = 0, \quad (2.114)$$

that corresponds to the relations derived in Eqs. (2.93d) and (2.101), respectively.

As a conclusion, the following theorem can be stated:

**Theorem 6.** *A 3-RPS PM with coplanar revolute joint axes will have two operation modes if and only if the following geometric conditions are satisfied*

- i. *Moving platform triangle is homothetic to the triangle enclosed by the revolute joint axes.*
- ii. *The three planes normal to the three revolute joint axes, respectively, have a common line of intersection.*

Since the relationship between the number of operation modes and architecture is established, the design parameters can be chosen in such a way that a constraint singularity is avoided.

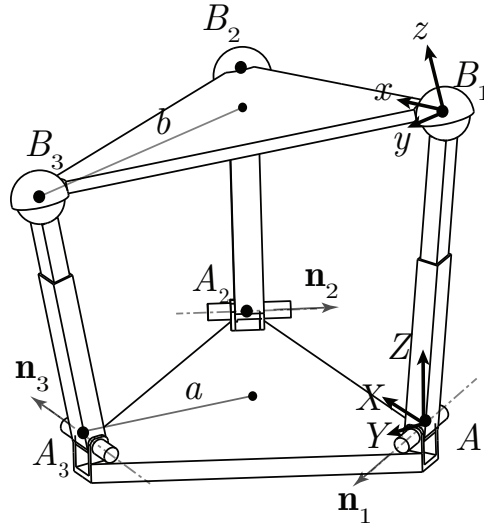
In case the revolute joint axes are no longer coplanar, equating a general quadric in  $\mathbb{P}^7$  defined in Eq. (2.91) with the linear combination of the plane constraint polynomials  $g_4, g_5$  and  $g_6$  shown in Eqs. (2.88d)-(2.88f), does not yield any solution. The problem of finding the influence of design parameters on the operation modes of a general 3-RPS PM is left for future work.

## 2.2.4 Examples

In this section, some example 3-RPS manipulators are considered to verify the proposed conditions.

### Example 1: 3-RPS PM with $n_{23} = 0$

The well-known 3-RPS PM introduced by Hunt [Hun83] has been the spotlight of numerous research topics and applications [HF95; Sch+13; Cha+14; Nur+14; Sch+14; SWH12; GOR08; Ver+09]. Its architecture is shown in Fig. 2.29. The moving platform and the base are equilateral triangles with circum-radius  $b$  and  $a$ , respectively. The R-joint axes are coplanar and tangential

Figure 2.29 – A 3-RPS parallel manipulator with  $n_{23} = 0$ 

to the base circum-circle. The P-joint in each leg is normal to its corresponding R-joint axis. The design parameters are listed below:

$$\begin{aligned}
 a_{12} &= \sqrt{3}a, & a_{13} &= \frac{\sqrt{3}}{2}a, & a_{23} &= \frac{3}{2}a, \\
 b_{12} &= \sqrt{3}b, & b_{13} &= \frac{\sqrt{3}}{2}b, & b_{23} &= \frac{3}{2}b, \\
 n_{11} &= \frac{1}{2}, & n_{21} &= -\frac{\sqrt{3}}{2}, & n_{31} &= 0, & n_{12} &= \frac{1}{2}, & n_{22} &= \frac{\sqrt{3}}{2}, & n_{32} &= 0, & n_{13} &= -1, & n_{23} &= 0, & n_{33} &= 0.
 \end{aligned} \tag{2.115}$$

Calculating the right hand side of Eq. (2.100) gives  $b_{12} : b_{13} : b_{23} = \frac{\sqrt{3}}{2} : \frac{\sqrt{3}}{4} : \pm \frac{3}{4}$ , which is consistent with the design parameters listed in Eq. (2.115). It is also straightforward to see that the design parameters satisfy Eq. (2.101). Thus, according to Theorem 6, the manipulator must exhibit two operation modes. To determine the characteristic equations of the operation modes, the plane constraint equations corresponding to Eq. (2.87) are considered:

$$g_4 := -\sqrt{3}x_0y_2 + \sqrt{3}x_1y_3 + \sqrt{3}x_2y_0 - \sqrt{3}x_3y_1 + x_0y_1 - x_1y_0 + x_2y_3 - x_3y_2 = 0 \tag{2.116}$$

$$\begin{aligned}
 g_5 := & \sqrt{3}x_0y_2 - \sqrt{3}x_1y_3 - \sqrt{3}x_2y_0 + \sqrt{3}x_3y_1 + x_0y_1 - x_1y_0 + x_2y_3 - x_3y_2 + \frac{\sqrt{3}}{2}(x_0^2 + x_1^2 + x_2^2 \\
 & + x_3^2)a - \frac{\sqrt{3}}{2}(2\sqrt{3}x_0x_3 + 2\sqrt{3}x_1x_2 + x_0^2 + x_1^2 - x_2^2 - x_3^2)b = 0
 \end{aligned} \tag{2.117}$$

$$\begin{aligned}
 g_6 := & -2x_0y_1 + 2x_1y_0 - 2x_2y_3 + 2x_3y_2 - \frac{\sqrt{3}}{2}(x_0^2 + x_1^2 + x_2^2 + x_3^2)a - \frac{\sqrt{3}}{2}(2\sqrt{3}x_0x_3 - 2\sqrt{3}x_1x_2 \\
 & - x_0^2 - x_1^2 + x_2^2 + x_3^2)b = 0.
 \end{aligned} \tag{2.118}$$

Equation (2.102) can be used to find the constants  $h_1, h_2$  in terms of  $h_3$  to be multiplied to the constraint polynomials  $g_4, g_5$  and  $g_6$ , respectively to obtain a factorable polynomial  $g$ . For this manipulator, the design parameters yield  $h_1 = h_3$  and  $h_2 = h_3$ . Thus from Eqs. (2.90)

and (2.116)

$$g = h_1g_4 + h_2g_5 + h_3g_6 = h_3(g_4 + g_5 + g_6) = -6h_3bx_0x_3 \quad (2.119)$$

showing that the manipulator at hand can have two operation modes characterized by  $x_0 = 0$  and  $x_3 = 0$  as already presented in [Sch+14; SWH12]. In fact, substituting  $n_{23} = 0$  in Eq. (2.94) results in the factorable polynomial  $x_0x_3$ .

**Example 2: 3-RPS PM with  $n_{13} = 0$**

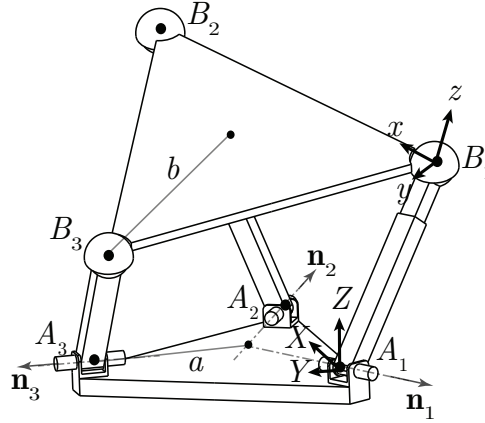


Figure 2.30 – A 3-RPS parallel manipulator with  $n_{13} = 0$

Another special case of the 3-RPS PM is when the R-joint axes are intersecting as shown in Fig. 2.30. The base and the platform are still equilateral triangles with circum-radius  $a$  and  $b$ , respectively. Also, the P-joints are orthogonal to their corresponding R-joint axes in each leg. The design parameters for this manipulator are listed below:

$$\begin{aligned} a_{12} &= \sqrt{3}a, & a_{13} &= \frac{\sqrt{3}}{2}a, & a_{23} &= \frac{3}{2}a, \\ b_{12} &= \sqrt{3}b, & b_{13} &= \frac{\sqrt{3}}{2}b, & b_{23} &= \frac{3}{2}b, \\ n_{11} &= \frac{\sqrt{3}}{2}, & n_{21} &= \frac{1}{2}, & n_{31} &= 0, & n_{12} &= \frac{\sqrt{3}}{2}, & n_{22} &= -\frac{1}{2}, & n_{32} &= 0, & n_{13} &= 0, & n_{23} &= 1, & n_{33} &= 0 \end{aligned} \quad (2.120)$$

The ratio between  $b_{12}, b_{13}$  and  $b_{23}$  calculated using Eq. (2.100) gives  $b_{12} : b_{13} : b_{23} = -\frac{\sqrt{3}}{2} : -\frac{\sqrt{3}}{4} : \pm\frac{3}{4}$ , which is consistent with the design parameters listed in Eq. (2.120). Thus, the condition i. of Theorem 6 is satisfied. It can also be verified by the fact that the R-joint axes intersect in a point, which is homothetic with the moving platform equilateral triangle. On the other hand, the left hand side of Eq. (2.101) gives  $\frac{-3\sqrt{3}a}{2} \neq 0$  proving that this manipulator can have only one operation mode. As a matter of fact, inspecting Fig. 2.30 reveals that the planes normal to  $\mathbf{n}_i$  and passing through  $A_i$  do not have a common line of intersection and hence this manipulator cannot exhibit more than one operation mode since condition ii. of Theorem 6 is

not satisfied. It is noteworthy that when  $a = b$ , the manipulator at hand has only one degree of freedom, where the moving platform can only translate along the  $Z$ -axis. Figure 2.31a shows

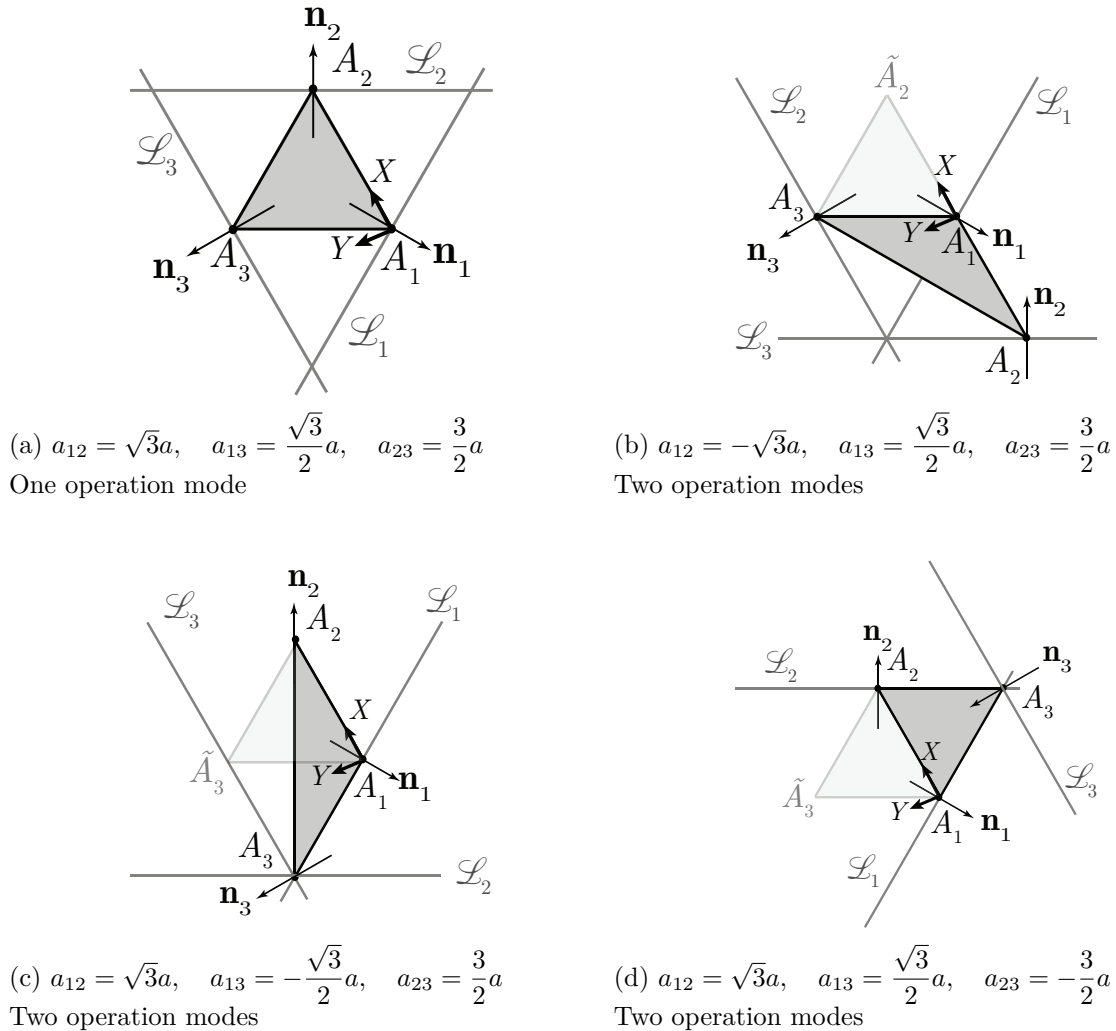


Figure 2.31 – Slight modification of design parameters can influence the number of operation modes

the projections of planes  $\mathcal{P}_i$  as lines  $\mathcal{L}_i$  onto the  $XY$ -plane.

Nonetheless, the design parameters can be altered so that the condition ii. is satisfied. Changing  $n_{ij}, i = 1, 2, j = 1, 2, 3$  might alter condition i. of Theorem 6, hence  $a_{12}, a_{13}$  or  $a_{23}$  can be changed so that condition i. is kept intact. From Eq. (2.101), writing  $a_{12}$  as a function of other design parameters and substituting the values from Eq. (2.120) yields  $a_{12} = -\sqrt{3}a$ . The design with  $a_{12} = -\sqrt{3}a$  is shown in Fig. 2.31b and it exhibits two operation modes.  $\tilde{A}_2$  represents the initial position of point  $A_2$ . In fact,  $a_{13}$  or  $a_{23}$  can also be changed similarly to obtain the designs shown in Figs. 2.31c and 2.31d, respectively. In these figures,  $\tilde{A}_3$  represents the initial position of point  $A_3$ . Calculating  $h_i, i = 1, 2, 3$  from Eq. (2.102) and substituting in the general quadric of Eq.(2.90) gives the characteristic polynomial of each operation mode as  $x_0 - x_3$  and  $x_0 + x_3$ .

Consequently, it provides an interesting example of how architecture of a manipulator influences

its number of operation modes. The procedure explained can be used to design 3-RPS PMs to have the necessary number of operation modes. Moreover, for a 3-RPS PM with two operation modes, the constraint singularity between the operation modes can be escaped by slightly modifying the design parameters such that one of the conditions in Theorem 6 is not fulfilled.

### 2.2.5 Example 3: Arbitrary design parameters

Finally, a numerical example is studied with the following arbitrary design parameters:

$$\begin{aligned} a_{13} = 2, \quad a_{23} = 2, \quad b_{23} = 3, \quad n_{11} = -3, \quad n_{21} = 5, \quad n_{31} = 0, \\ n_{12} = -3, \quad n_{22} = 2, \quad n_{32} = 0, \quad n_{13} = 2, \quad n_{23} = 1, \quad n_{33} = 0 \end{aligned}$$

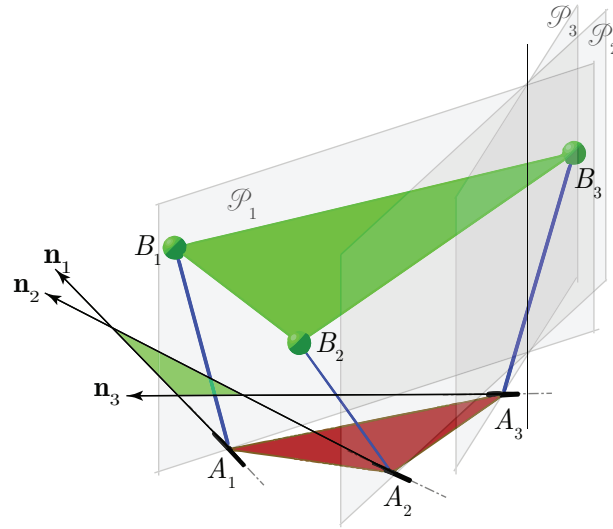


Figure 2.32 – A 3-RPS parallel manipulator with two operation modes characterized by  $x_0 - x_3(2 + \sqrt{5}) = 0$  and  $x_0 - x_3(2 - \sqrt{5}) = 0$

The remaining design parameters  $a_{12}$ ,  $b_{12}$  and  $b_{13}$  are calculated from the relations in Eqs. (2.101) and (2.100) so that the manipulator has two operation modes. Thus,  $a_{12} = \frac{18}{13}$ ,  $b_{12} = \pm \frac{135}{91}$  and  $b_{13} = \pm \frac{12}{7}$ . Fig. 2.32 shows the architecture of the manipulator at hand, where it can be pointed out that condition i. and ii. of Theorem 6 are satisfied. Substituting the design parameters with  $b_{12} = -\frac{135}{91}$  and  $b_{13} = -\frac{12}{7}$  in Eq. (2.95) gives

$$g := (x_0 - x_3(2 + \sqrt{5}))(x_0 - x_3(2 - \sqrt{5})) = 0 \quad (2.121)$$

whereas, substituting the design parameters with  $b_{12} = \frac{135}{91}$  and  $b_{13} = \frac{12}{7}$  in Eq. (2.95) gives

$$g := (x_1 - x_2(2 + \sqrt{5}))(x_1 - x_2(2 - \sqrt{5})) = 0 \quad (2.122)$$

The two polynomials  $x_0 - x_3(2 + \sqrt{5})$  and  $x_0 - x_3(2 - \sqrt{5})$  or  $x_1 - x_2(2 + \sqrt{5})$  and  $x_1 - x_2(2 - \sqrt{5})$  represent the two operation modes of the mechanism<sup>4</sup>.

Assuming the prismatic joints are actuated, the direct kinematics of the manipulator can be solved by substituting arbitrary values to joint parameters  $r_1 = 2, r_2 = 2$  and  $r_3 = 3$ . The constraint equations  $g_1 = 0$  to  $g_6 = 0$  and  $S_6^2 = 0$  can be written from Eqs. (4.48) and (2.88). Adding a normalization equation  $x_0^2 + x_1^2 + x_2^2 + x_3^2 = 1$  yields a set of eight equations to be solved for eight Study parameters. Finding the Groebner basis of the ideal of constraint polynomials with a pure lexicographic monomial ordering  $x_0 <_{lex} x_1 <_{lex} x_2 <_{lex} x_3 <_{lex} y_0 <_{lex} y_1 <_{lex} y_2 <_{lex} y_3$  results in a 16-degree univariate polynomial in variable  $y_3$ . As anticipated, the polynomial can be factorized into two polynomials of degree 8, each corresponding to the two operation modes. It shows that a 3-RPS PM can have at most eight solutions to its direct kinematics in each operation mode. When the joint parameters are fixed, the direct kinematics of a 3-RPS PM amounts to locating three points on three fixed circles with centers  $A_i$  and radii  $r_i$ . To this end, a corollary follows as a consequence of Theorem 6:

**Corollary 1.** *For the 3-points on 3-circles problem, if the geometry satisfies the following conditions*

- i normals to the planes containing the circles and passing through their centers are coplanar,*
- ii planes containing the circles have a common line of intersection and*
- iii the triangle formed by the three points is homothetic to the triangle enclosed by three normals to the planes passing through the centers of the circles,*

*then the 16-degree univariate characteristic polynomial factorizes into two 8-degree polynomials.*

For the above-mentioned example, eight real solutions to its direct kinematics problem are found. The solutions form four pairs of manipulator postures, one being the mirror image of another about the  $XY$ -plane. Four of these solutions are displayed in Fig. 2.12.

The first two solutions satisfy  $\frac{x_0}{x_3} = 2 - \sqrt{5}$  or  $\frac{x_1}{x_2} = 2 + \sqrt{5}$  and hence belong to the operation mode corresponding to  $x_0 - x_3(2 - \sqrt{5}) = 0$  or  $x_1 - x_2(2 + \sqrt{5}) = 0$ , respectively while the last two satisfy  $\frac{x_0}{x_3} = 2 + \sqrt{5}$  or  $\frac{x_1}{x_2} = 2 - \sqrt{5}$  and hence belong to the operation mode characterized by  $x_0 - x_3(2 + \sqrt{5}) = 0$  or  $x_1 - x_2(2 - \sqrt{5}) = 0$ .

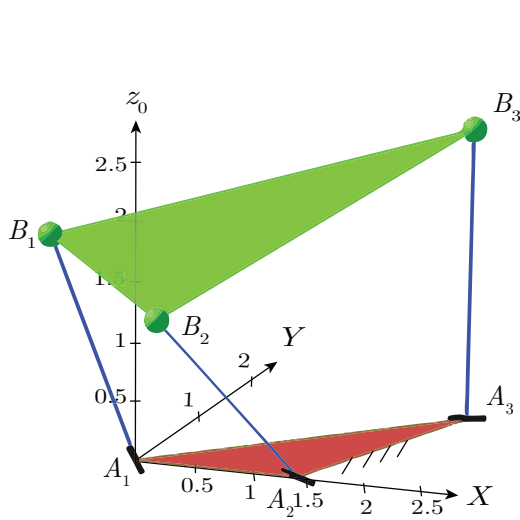
## 2.3 Conclusions

This chapter dealt with the operation mode analysis of some PMs. The operation modes were determined using the Study kinematic mapping and the primary decomposition of the ideal of constraint polynomials. A parallelogram linkage was shown to have three operation modes. The constraint manifolds were depicted to exhibit its two operation modes with rotational motion and the third one with a translational motion.

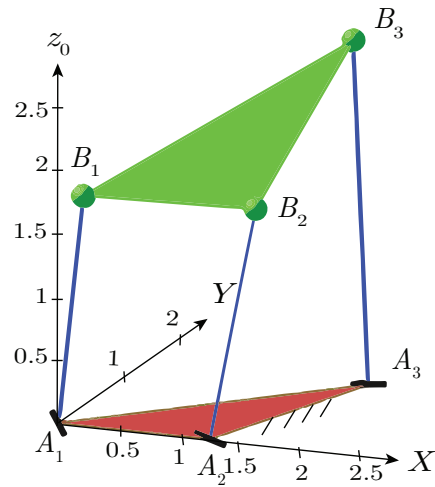
It was also shown that the zero torsion PMs belonging to the 3-[PP]S-Y and 3-S[PP]-Y family exhibit two operation modes whose physical interpretation is still an open problem.

In the same vein, the constraint equations of a 3-RUU PM were derived by two different approaches: geometrical approach, where all possible constraints were listed based on the geometry of the manipulator and Linear Implimentation Algorithm (LIA) in which it was enough to specify

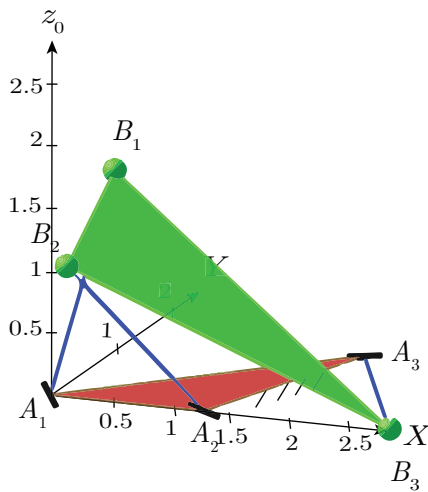
4. To be able to factorize the polynomial  $g$ , the field of rational numbers must be extended to include  $\sqrt{n_{23}^2 + n_{13}^2}$  i.e.  $\sqrt{5}$  for this example



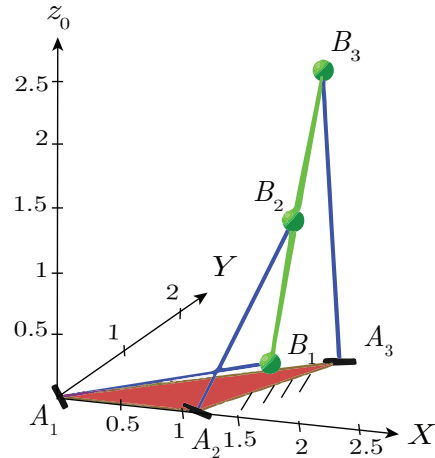
(a)  $x_0 = 0.0593, x_1 = -0.2925, x_2 = -0.9206, x_3 = -0.2515, y_0 = 0.0001, y_1 = -0.8954, y_2 = 0.3571, y_3 = -0.2658$  OR  
 $x_0 = .9206, x_1 = .2515, x_2 = 0.0593, x_3 = -0.2925, y_0 = -0.3571, y_1 = .2658, y_2 = 0.0001, y_3 = -0.8954.$



(b)  $x_0 = 0.0264, x_1 = 0.0940, x_2 = -0.9889, x_3 = -0.1119, y_0 = -0.1607, y_1 = -0.9782, y_2 = -0.1060, y_3 = 0.0775$  OR  
 $x_0 = -0.9889, x_1 = -0.1119, x_2 = -0.0264, x_3 = -0.0940, y_0 = -0.1060, y_1 = 0.0775, y_2 = .1607, y_3 = .9782.$



(c)  $x_0 = 0.2482, x_1 = -0.6214, x_2 = -0.7407, x_3 = 0.0586, y_0 = -0.2019, y_1 = -0.7792, y_2 = 0.5742, y_3 = -0.1490$  OR  
 $x_0 = .7407, x_1 = -0.0586, x_2 = .2482, x_3 = -0.6214, y_0 = -0.5742, y_1 = .1490, y_2 = -0.2019, y_3 = -0.7792.$



(d)  $x_0 = -0.6304, x_1 = 0.0743, x_2 = -0.7582, x_3 = -0.1488, y_0 = -0.3408, y_1 = 0.5290, y_2 = 0.1872, y_3 = 0.7541$  OR  
 $x_0 = .7582, x_1 = .1488, x_2 = -0.6304, x_3 = 0.0743, y_0 = -0.1872, y_1 = -0.7541, y_2 = -0.3408, y_3 = .5290.$

Figure 2.33 – Solutions to direct kinematics of a 3-RPS manipulator with arbitrary design parameters

the degree of equations and the algorithm did its job. Both approaches have a boon and a bane such that it is possible to miss a constraint by merely observing the manipulator geometry while it is hard to interpret the physical meaning of the equations derived through LIA. However, it turned out that the ideals spanned by the constraint polynomials in both approaches were the same let alone their varieties. As a result, the simplest set of equations was chosen for further analysis. Due to the complexity of the mechanism, a primary decomposition of these ideals was impossible in order to characterize the operation modes. Nonetheless, the direct kinematics problem was solved and a factor of the resulting univariate polynomial implied a pure translational operation mode of the PM.

Similarly, knowing the geometric constraints of a RUU limb, the constraint equations were derived for a dual reconfigurable 4-rRUU PM consisting of a reconfigurable revolute joint based on the double-Hooke's joint linkage. It was shown how a double-Hooke's joint linkage can be exploited to impact an architectural reconfigurability to a 4-RUU PM. The resulting dual reconfigurable 4-rRUU PM was shown to exhibit at least the following operation modes: a pure translational operation mode and Schönflies motion modes with different axes of rotation depending on the orientation of base revolute joint axes.

Furthermore, the influence of design parameters on the number of operation modes of a 3-RPS PM with coplanar revolute joints was studied.

The constraint equations of a general 3-RPS PM were derived. The linear combination of plane constraint polynomials were equated to a general quadric in  $\mathbb{P}^7$  and the coefficients were solved to obtain two solutions with some relations between design parameters. These relations were substituted back into the general quadric and it factorized into two polynomials characterizing two operation modes. The conditions on the design parameters for the existence of two operation modes in 3-RPS manipulator with coplanar revolute joints was summarized as a theorem with proof. The first condition is the homothety between the moving platform triangle and the triangle enclosed by revolute joint axes, while the second condition is when three planes on which the spherical joints are confined to move have a common line of intersection. Two special cases were considered: one that has two operation modes and the other one with one operation mode. For the latter manipulator, it was shown that one can modify the design parameters to be able to have two operation modes. Finally, a numerical example was considered following the proposed theorem. Its characteristic 16-degree univariate polynomial was derived to show that it splits into two polynomials of degree 8 each, representing two operation modes. The direct kinematic solutions lying in each operation mode were shown.



## Chapter 3

# Comparison between parallel manipulators

### 3.1 Introduction

The PMs of type 3-[PP]S-Y were studied in Chapter 2 and it was shown that they exhibit two operation modes. Since their number of dof and motion types are the same, they can be used for similar applications although their parasitic motions (horizontal displacements due to horizontal axes rotations) may differ.

This chapter aims at finding a common ground to compare the mechanisms belonging to the 3-[PP]S-Y family. Several techniques have already been introduced in the literature to compare PMs. A comparison study of four 3-dof translational PMs was performed by Tsai and Joshi based on their well conditioned workspace, stiffness and inertia properties [TJ01]. Pong and Carretero compared the 3-PRS, 3-RPS and the Tricept PMs by formulating their dimensionally homogeneous square Jacobian matrices and then calculating the condition number and singular values of the Jacobian [PC07]. Li *et al.* compared 3-PRS PMs with different limb arrangements with respect to their parasitic motions [Li+11] and listed 1T2R PMs without parasitic motions [LH10]. In this chapter, the comparison of mechanisms belonging to the 3-[PP]S-Y family is performed [NCW18b] with respect to their singularity free orientation workspace and their parasitic motions. An index, named Maximum Inscribed Circle Radius (MICR), introduced in [Nay+17b] is used to quantify the singularity free orientation workspace of the manipulators. The maximum parasitic motion, denoted as  $\mu$  within the Maximum Inscribed Circle is used as a second performance index. Furthermore, the manipulators are compared based on their design parameters and actuation scheme. The kinematic and singularity analysis problems are tackled locally using screw theory and globally using algebraic geometry tools [SWH12]. Finally, the Pareto optimal (the set of non-dominated) solutions obtained with respect to the two objective functions MICR and  $\mu$  are ranked based on their kinematic complexities using the complexity indices defined in [Kha+07; Car+10b]. It should be noted that joint limits and internal collisions are not entirely considered in this chapter.

The 3-[PP]S PMs are shown in Fig. 2.6 and their different actuation schemes are listed in Table 2.1. It is recalled here that they all exhibit two operation modes characterized by  $x_0 = 0$  and  $x_3 = 0$ .

## 3.2 Singularity Analysis and Parasitic Motions

For each operation mode, the motion of the moving platform can be parametrized by  $Z$  and any two of the orientation parameters  $x_i$  [NCW15a]. It simplifies the singularity analysis and the singular surfaces can be visualized in the three dimensional Euclidean space,  $\mathbb{E}^3$ . However, the rotations of the moving-platform are not pure. Indeed some undesired translational motions, called parasitic motions, arise. This section is dedicated to the evaluation of the singularity-free orientation workspace and the parasitic motions of PMs belonging to the 3-[PP]S-Y family. The forward kinematic Jacobian matrix is derived in two ways: (i) differentiating the constraint equations with respect to the output variables (ii) using screw theory. It is shown how screw theory methods simplify the determination of the Jacobian matrix for different actuation schemes. An index is defined to assess the maximum singularity-free orientation workspace of the mechanisms under study. Additionally, their parasitic motions are also assessed.

### 3.2.1 Kinematic Jacobian Matrix obtained by differentiating the constraint equations

The kinematic Jacobian matrix is defined for each operation mode as a matrix composed of the first order partial derivatives of the constraint equations with respect to the parameters  $x_0, x_1, x_2, x_3, X, Y$  and  $Z$  [Hus+07; HS10], i.e.,

$$\mathbf{J}_k = \left( \frac{\partial g_m}{\partial x_i}, \frac{\partial g_m}{\partial X}, \frac{\partial g_m}{\partial Y}, \frac{\partial g_m}{\partial Z} \right) \text{ where } k = 1, 2; \quad m = 1, \dots, 7; \quad i = 0, \dots, 3 \quad (3.1)$$

where,  $g_m, m = 1, \dots, 7$  are the constraint equations for the manipulator at hand. Thus, the manipulator reaches a kinematic singularity when  $\det(\mathbf{J}_k) = 0$ . The vanishing condition of  $\det(\mathbf{J}_k)$  results in a hyper-variety for each operation mode:

$$S_1: x_3 \cdot f_1(x_1, x_2, x_3, X, Y, Z) = 0 \quad \text{and} \quad S_2: x_0 \cdot f_2(x_0, x_1, x_2, X, Y, Z) = 0 \quad (3.2)$$

The polynomials  $f_1$  and  $f_2$ , whose degree depends on the PM at hand describe the singularities in each operation mode, which depend on the actuation scheme.  $x_0 = x_3 = 0$  describes the constraint singularity that exhibits the transition between  $\mathcal{K}_1$  and  $\mathcal{K}_2$ .

It is noteworthy that this method is not always convenient to use as equations  $g_4, g_5$  and  $g_6$  depend on the manipulator actuation scheme. For instance, the equations for the 3-RPS manipulator expressed in Sec. 2.1.2 depend on the actuated prismatic joint lengths. Besides, it should be noted that the derivation of equations  $g_4, g_5$  and  $g_6$  as a function of the actuated revolute joint angles is usually tedious. To overcome this problem, screw theory techniques are adopted to derive the kinematic Jacobian matrices of the PMs.

### 3.2.2 Kinematic Jacobian Matrix obtained based on Screw Theory

Based on the theory of reciprocal screws, the velocity model of a parallel manipulator can be expressed as

$$\mathbf{A}\mathbf{t} = \mathbf{B}\dot{\boldsymbol{\rho}} \quad (3.3)$$

where  $\dot{\boldsymbol{\rho}}$  is the actuated joint rate vector.  $\mathbf{t}$  is the moving platform twist with respect to the fixed base i.e., it contains the angular velocity vector of the moving platform and the linear velocity vector of the MP geometric center.  $\mathbf{A}$  is called the forward Jacobian matrix and it incorporates the actuation and constraint wrenches of the PM while  $\mathbf{B}$  is named the inverse

Jacobian matrix [JT02]. For a non redundantly actuated and non overconstraint PM,  $\mathbf{A}$  is a  $6 \times 6$  square matrix whereas  $\mathbf{B}$  is a  $6 \times n$  matrix where  $n$  is the number of actuated joints. To compare the manipulators of the 3-[PP]S-Y family, only the parallel singularities are considered such that  $\mathbf{A}$  is rank deficient. Since  $\mathbf{A}$  is square, configurations satisfying  $\det(\mathbf{A}) = 0$  are singular. Moreover, the manipulators belonging to the 3-[PP]S family cannot meet any serial singularity corresponding to the rank deficiency of  $\mathbf{B}$  except the 3-RRS PM.

For instance, the kinematic modeling of the 3-RPS and 3-RPS PMs following Eq. 3.3 can be expressed as

$$\mathbf{A}_{3-\underline{\text{RPS}}} \mathbf{}^0\mathbf{t} = \mathbf{B}_{3-\underline{\text{RPS}}} \dot{\boldsymbol{\rho}} \implies \begin{bmatrix} ({}^0\mathbf{R}_1^1 \mathbf{b}_1 \times {}^0\mathbf{u}_1)^T & {}^0\mathbf{u}_1^T \\ ({}^0\mathbf{R}_1^1 \mathbf{b}_2 \times {}^0\mathbf{u}_2)^T & {}^0\mathbf{u}_2^T \\ ({}^0\mathbf{R}_1^1 \mathbf{b}_3 \times {}^0\mathbf{u}_3)^T & {}^0\mathbf{u}_3^T \\ ({}^0\mathbf{R}_1^1 \mathbf{b}_1 \times {}^0\mathbf{s}_1)^T & {}^0\mathbf{s}_1^T \\ ({}^0\mathbf{R}_1^1 \mathbf{b}_2 \times {}^0\mathbf{s}_2)^T & {}^0\mathbf{s}_2^T \\ ({}^0\mathbf{R}_1^1 \mathbf{b}_3 \times {}^0\mathbf{s}_3)^T & {}^0\mathbf{s}_3^T \end{bmatrix} \mathbf{}^0\mathbf{t} = \begin{bmatrix} \mathbf{I}_{3 \times 3} \\ \mathbf{0}_{3 \times 3} \end{bmatrix} \begin{bmatrix} \dot{\rho}_1 \\ \dot{\rho}_2 \\ \dot{\rho}_3 \end{bmatrix} \quad (3.4)$$

$$\mathbf{A}_{3-\underline{\text{RPS}}} \mathbf{}^0\mathbf{t} = \mathbf{B}_{3-\underline{\text{RPS}}} \dot{\boldsymbol{\theta}} \implies \begin{bmatrix} ({}^0\mathbf{R}_1^1 \mathbf{b}_1 \times {}^0\mathbf{v}_1)^T & {}^0\mathbf{v}_1^T \\ ({}^0\mathbf{R}_1^1 \mathbf{b}_2 \times {}^0\mathbf{v}_2)^T & {}^0\mathbf{v}_2^T \\ ({}^0\mathbf{R}_1^1 \mathbf{b}_3 \times {}^0\mathbf{v}_3)^T & {}^0\mathbf{v}_3^T \\ ({}^0\mathbf{R}_1^1 \mathbf{b}_1 \times {}^0\mathbf{s}_1)^T & {}^0\mathbf{s}_1^T \\ ({}^0\mathbf{R}_1^1 \mathbf{b}_2 \times {}^0\mathbf{s}_2)^T & {}^0\mathbf{s}_2^T \\ ({}^0\mathbf{R}_1^1 \mathbf{b}_3 \times {}^0\mathbf{s}_3)^T & {}^0\mathbf{s}_3^T \end{bmatrix} \mathbf{}^0\mathbf{t} = \begin{bmatrix} \mathbf{I}_{3 \times 3} \\ \mathbf{0}_{3 \times 3} \end{bmatrix} \begin{bmatrix} \dot{\theta}_1 \\ \dot{\theta}_2 \\ \dot{\theta}_3 \end{bmatrix} \quad (3.5)$$

$$(3.6)$$

where,  ${}^0\mathbf{u}_i$  is a unit vector along the prismatic joint direction and expressed in  $\Sigma_0$ ,  ${}^0\mathbf{s}_i$  is the unit vector along the  $i$ th revolute joint axis,  ${}^0\mathbf{v}_i$  is a vector normal to both  ${}^0\mathbf{u}_i$  and  ${}^0\mathbf{s}_i$ . Matrices  $\mathbf{A}_{3-\underline{\text{RPS}}}$  and  $\mathbf{A}_{3-\underline{\text{RPS}}}$  incorporate the actuation and constraint wrenches of the 3-RPS and 3-RPS PMs, respectively [JT02]. For the  $i$ -th leg of these manipulators, the constraint wrench,  ${}^0\hat{\zeta}_{0i}^c$  and the actuation wrench,  ${}^0\hat{\zeta}_{0i}^a$  are represented in Figs. 3.1 and 3.2 and are expressed in frame  $\Sigma_0$  as follows:

$$3-\underline{\text{RPS}} \text{ PM} : {}^0\hat{\zeta}_{0i}^c = \begin{bmatrix} {}^0\mathbf{s}_i \\ {}^0\mathbf{R}_1^1 \mathbf{b}_i \times {}^0\mathbf{s}_i \end{bmatrix} \quad {}^0\hat{\zeta}_{0i}^a = \begin{bmatrix} {}^0\mathbf{u}_i \\ {}^0\mathbf{R}_1^1 \mathbf{b}_i \times {}^0\mathbf{u}_i \end{bmatrix} \quad (3.7)$$

$$3-\underline{\text{RPS}} \text{ PM} : {}^0\hat{\zeta}_{0i}^c = \begin{bmatrix} {}^0\mathbf{s}_i \\ {}^0\mathbf{R}_1^1 \mathbf{b}_i \times {}^0\mathbf{s}_i \end{bmatrix} \quad {}^0\hat{\zeta}_{0i}^a = \begin{bmatrix} {}^0\mathbf{v}_i \\ {}^0\mathbf{R}_1^1 \mathbf{b}_i \times {}^0\mathbf{v}_i \end{bmatrix} \quad (3.8)$$

Thus, from Eqs. (2.16), (2.18) and (2.19), the determinant of the forward Jacobian matrix  $\mathbf{A}_{3-\underline{\text{RPS}}}$  and  $\mathbf{A}_{3-\underline{\text{RPS}}}$  in Eqs. (3.4) and (3.5) can be calculated in terms of  $x_0, x_1, x_2, x_3, X, Y, Z$  and of the design parameters. The derivation of the forward Jacobian matrix by differentiating the constraint equations is tedious when a revolute joint is actuated whereas using screw theory, it is straightforward regardless of the actuation scheme. Therefore, the forward singularities for different actuation schemes of 3-[PP]S PMs are determined using screw theory when the determinant of matrix  $\mathbf{A}$  in Eq. (3.3) vanishes.

### 3.2.3 Singularity loci in the orientation workspace

The singularities can be expressed in the orientation workspace by parametrizing the orientation of the platform in terms of *Tilt-and-Torsion* ( $T\mathcal{E}T$ ) angles,  $\phi$  (azimuth),  $\theta$  (tilt) and  $\sigma$

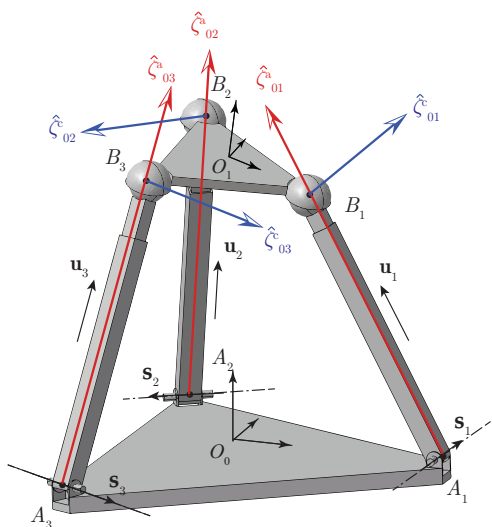


Figure 3.1 – Actuation and constraint wrenches for the 3-RPS PM

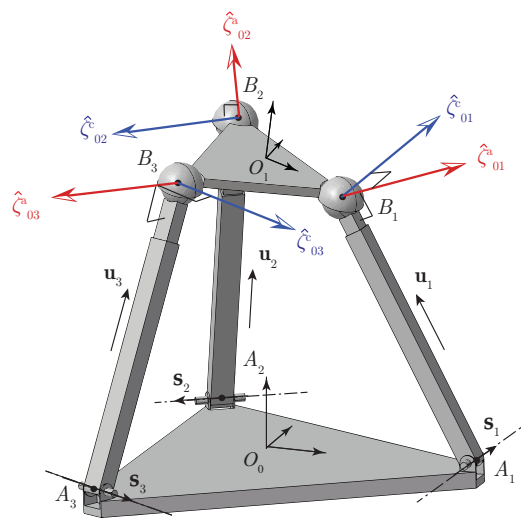


Figure 3.2 – Actuation and constraint wrenches for the 3-RPS PM

(torsion) [BZG02; BR99] as recalled in Fig. 1.23. As shown in [BZG02], those angles are more suitable for 3-[PP]S manipulators, which are known to be zero torsion mechanisms ( $\sigma$  is always equal to 0 or  $\pi$  depending on the operation mode). The orientation quaternions can be expressed in terms of the  $T\mathcal{E}T$  angles as shown in Eq. (1.43).

Quaternions are used to obtain algebraic constraint equations so that the algebraic geometry techniques can be used to analyze those equations. For instance, primary decomposition of the ideal of the constraint polynomials described in Eq. (2.31) yields the exact number of operation modes and their characterization. However, the parametrization is changed to  $T\mathcal{E}T$  angles to be able to visualize the singularities and maximum parasitic displacements in the orientation workspace. Moreover, they offer a more intuitive approach to deal with zero-torsion mechanisms that are compared in this chapter. This is why the change of parameters from quaternions to  $T\mathcal{E}T$  angles is done.

The change of parametrization results in only three parameters expressing the orientation of the moving-platform. Furthermore, for operation mode  $\mathcal{K}_1$ , characterized by  $x_0 = 0$ , Eq. (1.43) gives  $\sigma = \pi$ . Similarly, for operation mode  $\mathcal{K}_2$ , characterized by  $x_3 = 0$ , Eq. (1.43) gives  $\sigma = 0$ . Substituting the values of  $\sigma$  in the remaining equations, leads to  $x_i$  expressed as functions of  $\phi$  and  $\theta$  angles, only.

In order to plot the singularity loci of the manipulator into the orientation workspace, the determinant of the forward Jacobian matrix of the manipulator should be expressed as a function  $\phi$  and  $\theta$  angles, only. All remaining variables should be eliminated from the determinant of the forward Jacobian matrix.  $X$  and  $Y$  can be eliminated using Eqs. (2.21) and (2.22) for the 3-[PP]S-Y PMs as follows:

$$X = h_2 (x_1^2 - x_2^2) \quad Y = -2h_2x_1x_2 \quad (3.9)$$

To this end, the determinant of the forward Jacobian matrix is a function of  $Z$ ,  $x_i$ ,  $i = 0, 1, 2, 3$  and of the actuated joint variables. The actuated joint variables can be eliminated using equations  $g_4 = g_5 = g_6 = 0$  as shown in Sec. 2.1.2. Additionally, from Eq. (1.43),  $x_i$  can be expressed as functions of  $\phi$  and  $\theta$  angles leading to the final expression of the determinant of the forward

Jacobian matrix in terms of  $Z$ ,  $\theta$  and  $\phi$ .

### 3.2.4 Maximum Inscribed Circle Radius (MICR)

From a practical point of view, it is desirable to use a PM in its singularity free region. A performance index, named Maximum Inscribed Circle Radius (MICR) and defined in [Nay+17b], is used in this section to quantify the capability of the Parallel Manipulator (PM) in terms of orientation motions. For a given altitude  $Z$ , this index gives the maximum tilt angle  $\theta$  that the moving-platform can reach for any azimuth angle  $\phi$  without reaching any parallel singularity:

$$MICR = \max_{0 \leq \theta \leq \pi} \{\theta, \forall \phi \in [0, \pi], \det(\mathbf{A}) \neq 0\} \quad (3.10)$$

MICR values are calculated for all the mechanisms at hand in their operation modes for three ratios for  $\frac{h_2}{h_1} = \{\frac{1}{2}, 1, 2\}$  and two ratios for  $\frac{Z}{h_1} = 1, 2$ . The ratios  $\frac{Z}{h_1}$  and  $\frac{h_2}{h_1}$  make sure that the MICR values can be used to compare the mechanisms and their operation modes no matter the platform and base sizes. Thus, MICR is used to compare the PMS belonging to the 3-[PP]S-Y family.

### 3.2.5 Parasitic Motions

For the 3-[PP]S-Y family of PMs, the workspace is expressed in terms of  $Z$ ,  $\phi$  and  $\theta$ . Since the torsion angle  $\sigma$  can only attain the values 0 or  $\pi$  depending on the operation mode, the constrained motions are along the  $x$  and  $y$  axes. The parasitic displacements along the  $x$  and  $y$  coordinates of the moving platform are expressed in terms of  $Z$  and  $x_i$  in Equations (3.9).

To compare the parasitic motions of PMs belonging to the 3-[PP]S-Y family, the maximum displacement within the Maximum Inscribed Circle (MIC) [Nay+17b] is considered. Here, the following index is defined to quantify the parasitic motions of the moving-platform along  $x_0$  and  $y_0$  axes. A parameter with units of length is defined such that

$$\mu = \max \left( \sqrt{X^2 + Y^2} \right) \quad \text{when } 0 \leq \theta \leq MICR; \quad -\pi \leq \phi \leq \pi \quad (3.11)$$

$\mu$  can be expressed in terms of  $h_2$ ,  $\theta$  and  $\phi$  for these manipulators.

### 3.2.6 Internal collisions

A drawback of using parallel manipulators for potential applications is the existence of internal collisions, which do exist in PMs belonging to the 3-[PP]S-Y family listed in Table 2.1. For these manipulators, three kinds of internal collisions should be considered:

1. Collisions between limbs.
2. Collisions between limbs and the moving or fixed platform triangles.
3. Collision between the fixed and moving-platform triangles.

An accurate collision analysis requires the shape and thickness of the limbs as well as the range of motion of the spherical joints. Although collisions are plotted for an example in the subsequent section, they are not exclusively considered for comparing the PMs at hand.

However, it can be observed that most applications of the 3-[PP]S-Y PMs [Car+99; Wah02; Tet+16; Yan+11] require them to be in the second operation mode (characterized by  $x_3 = 0$ ), due to the existence of internal collisions in their first operation mode ( $x_0 = 0$ ). This is partially accounted for a new complexity index introduced on the next section.

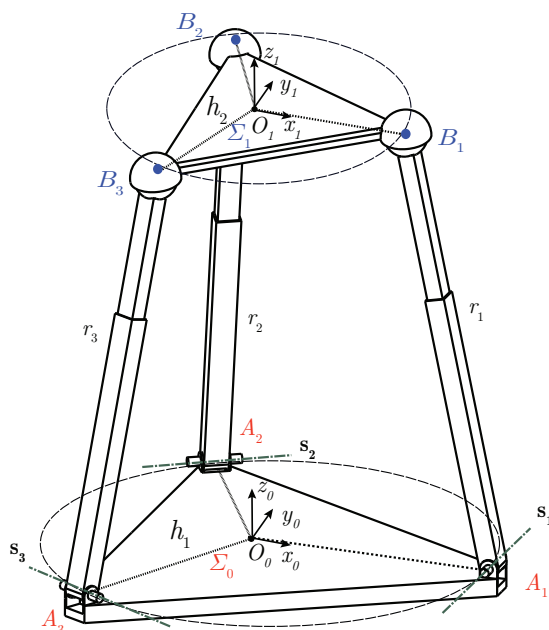


Figure 3.3 – 3-RPS PM architecture

### 3.3 Example: The 3-RPS PM

In this section, the 3-RPS PM is considered and the forward Jacobian matrix is formulated, leading to the determination of MICR for different sizes of its fixed base and moving platforms. Furthermore, the parasitic motions are visualized within the Maximum Inscribed Circle (MIC) by plotting  $\mu$  vs.  $\phi$  and  $\theta$ <sup>1</sup>.

The architecture of the 3-RPS PM belonging to the family of 3-[PP]S-Y of PMs is shown in Figure 3.3.

The determinant of  $\mathbf{A}_{3\text{-RPS}}$  calculated from Eq. (3.4) turns out to be a function of  $x_0$ ,  $x_1$ ,  $x_2$ ,  $x_3$ ,  $X$ ,  $Y$ ,  $Z$ ,  $h_1$  and  $h_2$ .  $X$  and  $Y$  are substituted from Eq. (3.9) and then  $T\mathcal{E}T$  angle substitutions are done (Eq. (1.43)) resulting in the determinant of the forward Jacobian matrix to be a function of  $Z$ ,  $h_1$ ,  $h_2$ ,  $\theta$ ,  $\phi$  and  $\sigma$ . For operation mode 1, after substituting  $\sigma = \pi$  and assigning  $h_1 = 1$  and  $h_2 = 2$ , the implicit plot of the Jacobian can be drawn by varying  $Z$ ,  $\phi$  and  $\theta$  as shown in Fig. 3.4a. For operation mode 2 with  $\sigma = 0$ , the implicit plot is shown in Fig. 3.4b.

A slice of these surfaces at  $Z = h_1 = 1$  gives the singularity loci as shown in Fig. 3.5.

Along with the singularity loci, the so called intersection loci, depicting the collision between each pair of limbs  $A_1B_1$ ,  $A_2B_2$  and  $A_3B_3$  are also plotted. To simplify the problem, they are calculated as follows.

The limbs are assumed to have no thickness and the spherical joints are assumed to have full range of motion. Thus, the problem is reduced to find all possible intersections between three pairs of line segments. For instance, to find the intersection loci of line segments  $A_1B_1$  and

1. Radian is used as the angular unit throughout the text but degree is used in figures for better clarity.

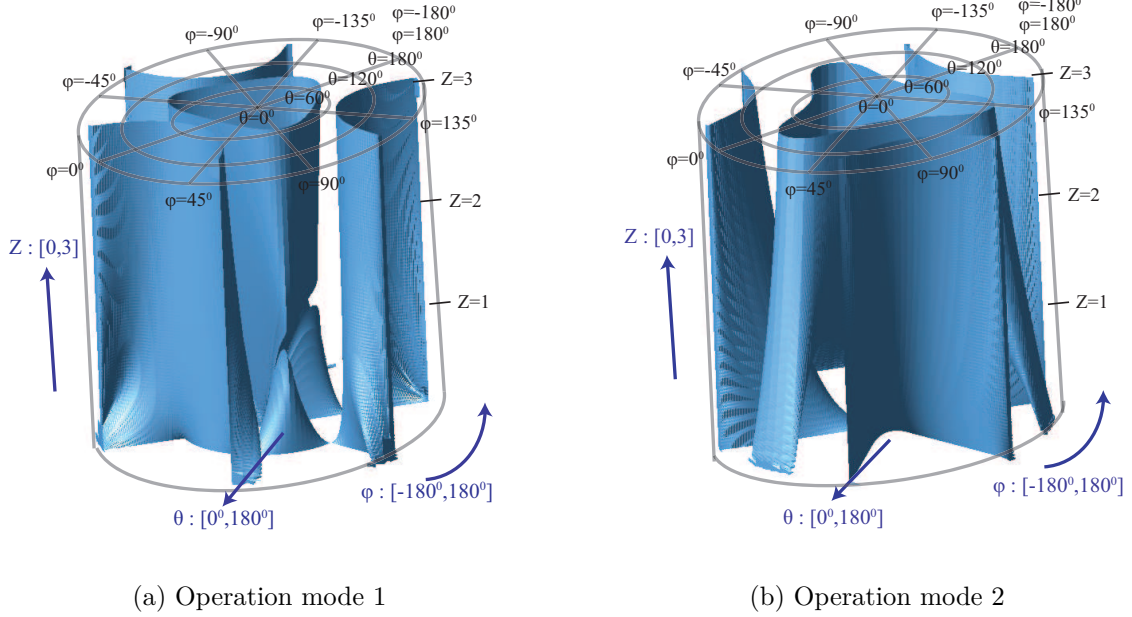


Figure 3.4 – 3-RPS singularity surfaces for  $\frac{h_2}{h_1} = 2$

$A_2B_2$ , their vector equations are written as follows:

$$\mathbf{r}_1 = \mathbf{a}_1 + (\mathbf{b}_1 - \mathbf{a}_1)t_1 \quad t_1 \in [0, 1] \quad (3.12)$$

$$\mathbf{r}_2 = \mathbf{a}_2 + (\mathbf{b}_2 - \mathbf{a}_1)t_2 \quad t_2 \in [0, 1] \quad (3.13)$$

where  $\mathbf{r}_1$  and  $\mathbf{r}_2$  are position vectors of a point on line segments  $A_1B_1$  and  $A_2B_2$ , respectively. An intersection occurs when  $\mathbf{r}_1 = \mathbf{r}_2$ . Eliminating  $t_1$  and  $t_2$  from this equation gives an implicit curve in terms of  $\theta$  and  $\phi$  where the considered line segments intersect under the condition  $t_1, t_2 \in [0, 1]$ . The intersection between the other two pairs of limbs are determined in a similar manner, resulting in the intersection loci as plotted in blue in Fig. 3.5. It is apparent that the internal collisions dominate in operation mode 1 leading the MICR values without practical use. Nonetheless, it is possible to establish a singularity and collision-free workspace by releasing the constraint associated to MIC center lying at  $\theta = \phi = 0$  deg. However, this is left for future work.

MICR, defined in Eq. (3.10). is also marked in these figures. For different ratios of  $h_2$  to  $h_1$ , the variations in MICR values are plotted in Figs. 3.6 and 3.7.

From Eqs. (1.43) and (3.9), the maximum displacement within the Maximum Inscribed Circle (MIC) is written as

$$\mu = \max\left(\sqrt{X^2 + Y^2}\right) = \max\left(h_2^2 \sin\left(\frac{\theta}{2}\right)^4\right) \quad \text{when } 0 \leq \theta \leq MICR; \quad -\pi \leq \phi \leq \pi \quad (3.14)$$

By varying  $Z$  from 0 to 4,  $\theta$  from 0 to MICR and  $\phi$  from  $-\pi$  to  $\pi$ ,  $\mu$  is plotted for the 3-RPS PM as shown in Figs. 3.8 and 3.9. It is observed that the parasitic motion increases as the ratio  $\frac{h_2}{h_1}$  increases. But, the larger the  $\frac{h_2}{h_1}$  ratio, the smaller the MICR and hence, the smaller the singularity free workspace.

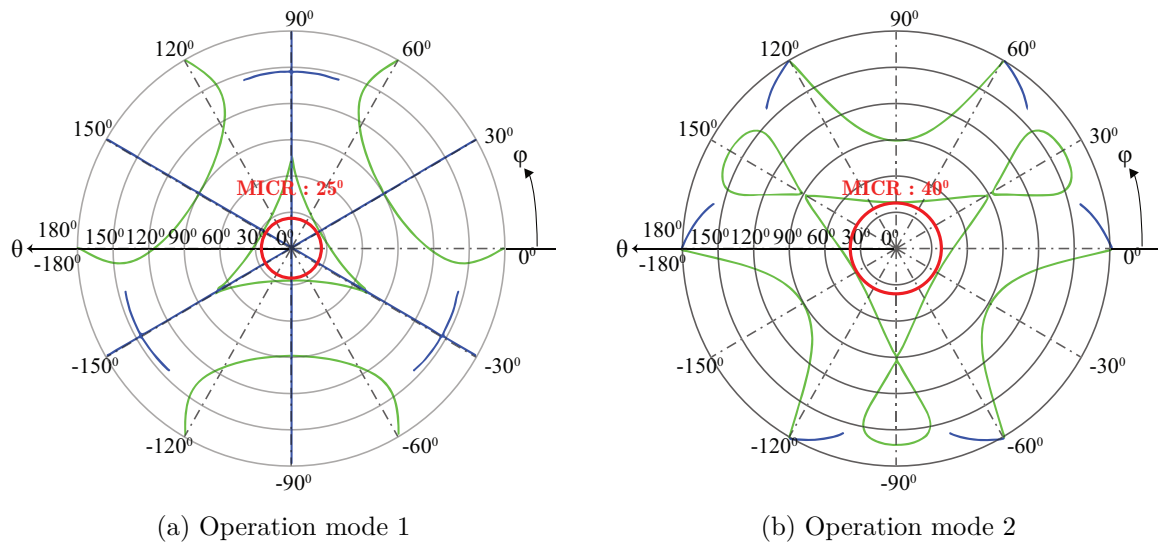


Figure 3.5 – 3-RPS singularity loci (green), link interference loci (blue) and the maximum inscribed singularity-free circle (red),  $\frac{h_2}{h_1} = 2$ ,  $\frac{Z}{h_1} = 1$

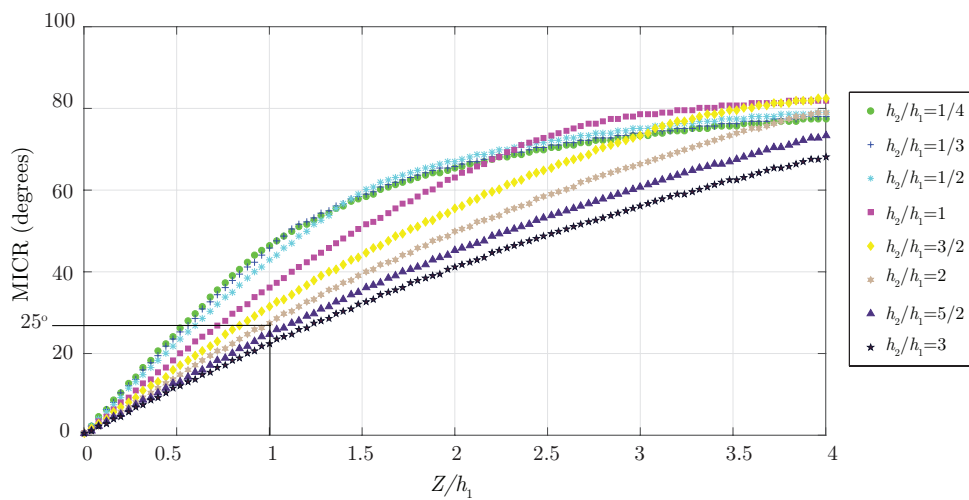


Figure 3.6 – 3-RPS OM1: MICR vs.  $\frac{Z}{h_1}$  as a function of  $\frac{h_2}{h_1}$



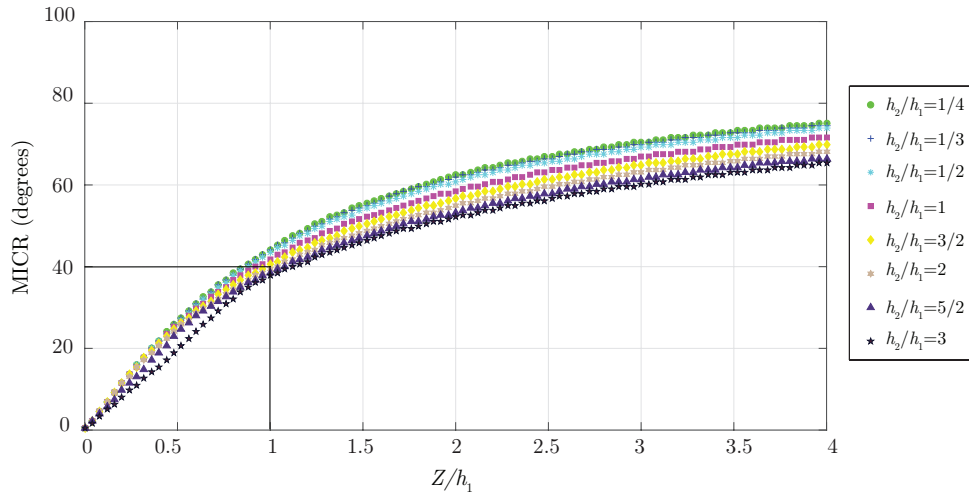


Figure 3.7 – 3-RPS OM2: MICR vs.  $\frac{Z}{h_1}$  as a function of  $\frac{h_2}{h_1}$

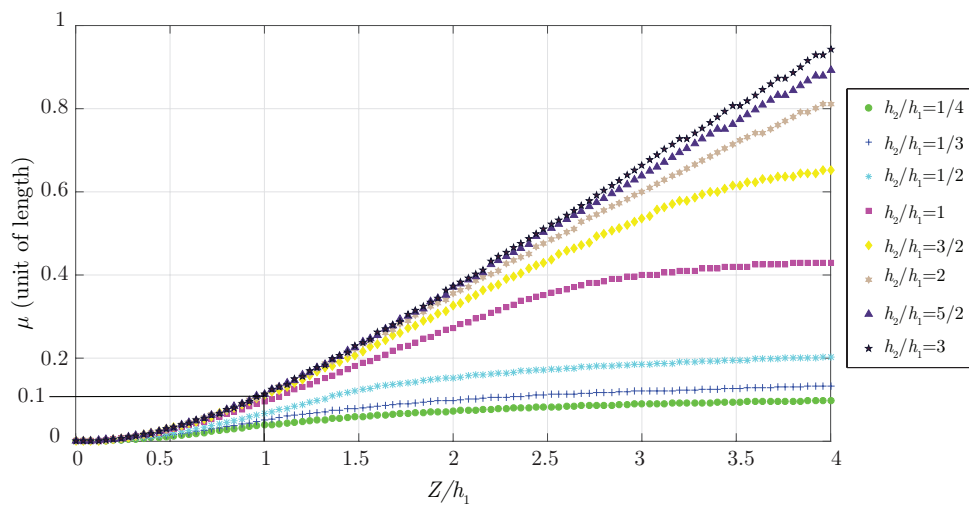


Figure 3.8 – 3-RPS OM1:  $\mu$  vs.  $\frac{Z}{h_1}$  as a function of  $\frac{h_2}{h_1}$

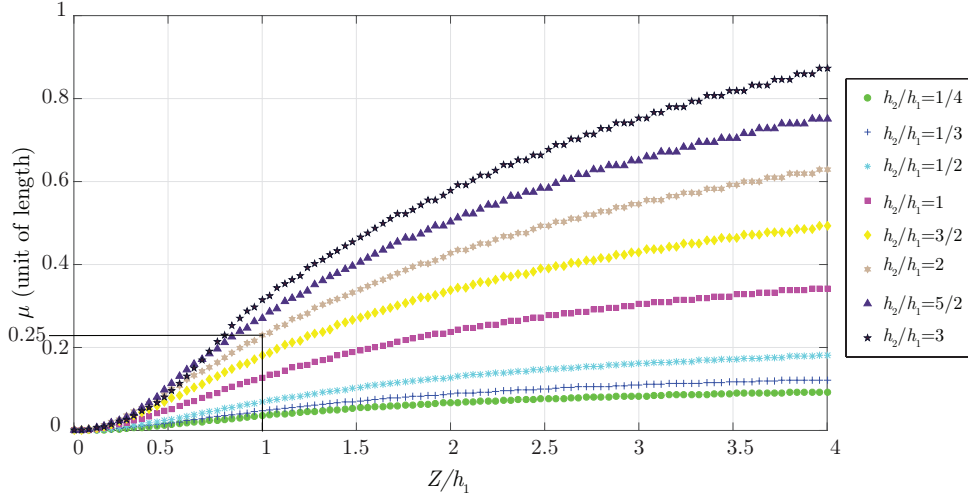


Figure 3.9 – 3-RPS OM2:  $\mu$  vs.  $\frac{Z}{h_1}$  as a function of  $\frac{h_2}{h_1}$

### 3.4 Comparison of 3-[PP]S-Y PMs based on their MICR and parasitic motions

For most applications, it is better to have a large singularity-free orientation workspace with small parasitic motions. To find out the most suitable manipulator for this purpose, MICR vs.  $\mu$  is plotted for all the mechanisms listed in Table 2.1 in their two operation modes, each for three ratios of  $\frac{h_2}{h_1} = \{\frac{1}{2}, 1, 2\}$  and two ratios of  $\frac{Z}{h_1} = \{1, 2\}$ . These points are plotted for the aforementioned ratios in Figures 3.10 to 3.15. From Eq. (3.9), it is noticed that parasitic motions are higher for larger singularity free regions. The abscissa is chosen to be  $\pi$ -MICR since the minimum of this function is preferred and the ordinate is chosen to be  $\mu$ . For a PM from the 3-[PP]S-Y family,  $\pi$ -MICR and  $\mu$  values are preferred to be smaller. Thus, plotting  $\pi$ -MICR vs.  $\mu$  results in a Pareto front as shown in Figs. 3.10 to 3.15.

Among the manipulators listed in Table 2.1, it is noticed that the 3-PhPvS PM behaves exactly like the 3-PvPhS PM and the 3-PhPvS PM like the 3-PvPhS PM. Hence, only the 3-PhPvS PM is considered for analysis. Due to the arrangement of prismatic joints, 3-PvRS and 3-PhPvS are inherently singular at any configuration and hence they are not considered here. Indeed, for these manipulators, the three actuation forces are coplanar and intersect at a point resulting in only two independent forces. In addition, the PMs 3-RPS and 3-RRS; 3-PhRS and 3-PhPvS; behave alike due to identical arrangement of their passive joints. It should be noted that the leg links of the 3-RRS PM are considered to be of length  $h_1$  so that the moving platform can reach the maximum value of  $Z (= 2h_1)$  considered to compare the manipulators at hand.

In Fig. 3.12, the MICR and  $\mu$  values are marked for the 3-RPS PM when  $\frac{h_2}{h_1} = 2$  and  $\frac{Z}{h_1} = 1$ . These points correspond to the MICR and  $\mu$  values spotted in the MICR and  $\mu$  vs.  $\frac{Z}{h_1}$  plots in Sec. 3.3.

To compare the 3-[PP]S-Y family of PMs, their MICR vs.  $\mu$  values are plotted for different ratios of  $\frac{h_2}{h_1}$  and  $\frac{Z}{h_1}$  in Figs. 3.16 and 3.17. The former figure shows the Pareto optimal solutions

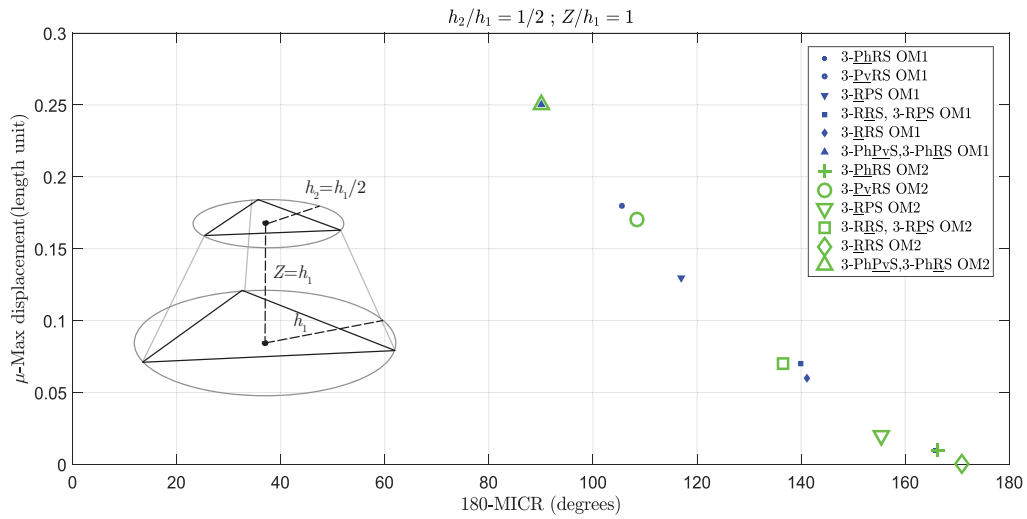


Figure 3.10 – MICR vs. maximum displacement  $\frac{h_2}{h_1} = \frac{1}{2}, \frac{Z}{h_1} = 1$

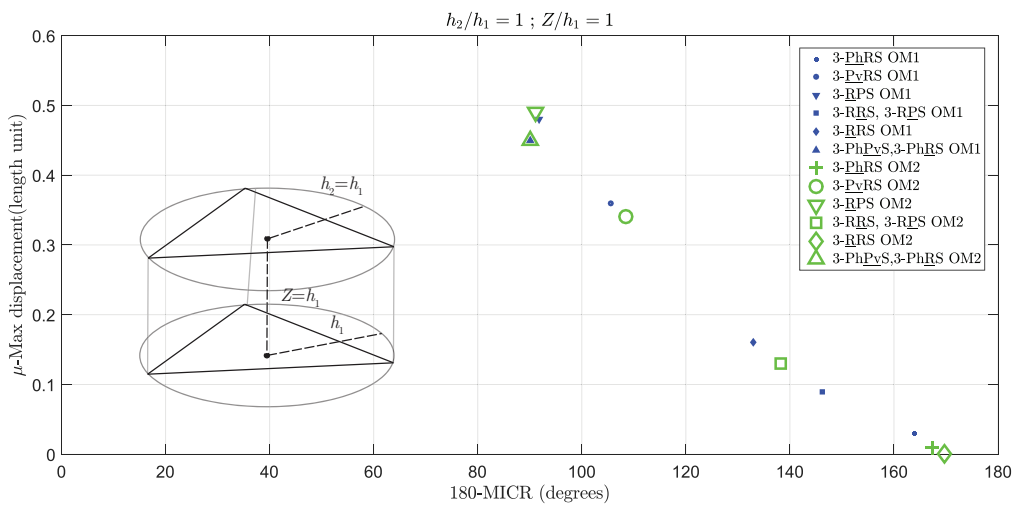


Figure 3.11 – MICR vs. maximum displacement  $\frac{h_2}{h_1} = 1, \frac{Z}{h_1} = 1$

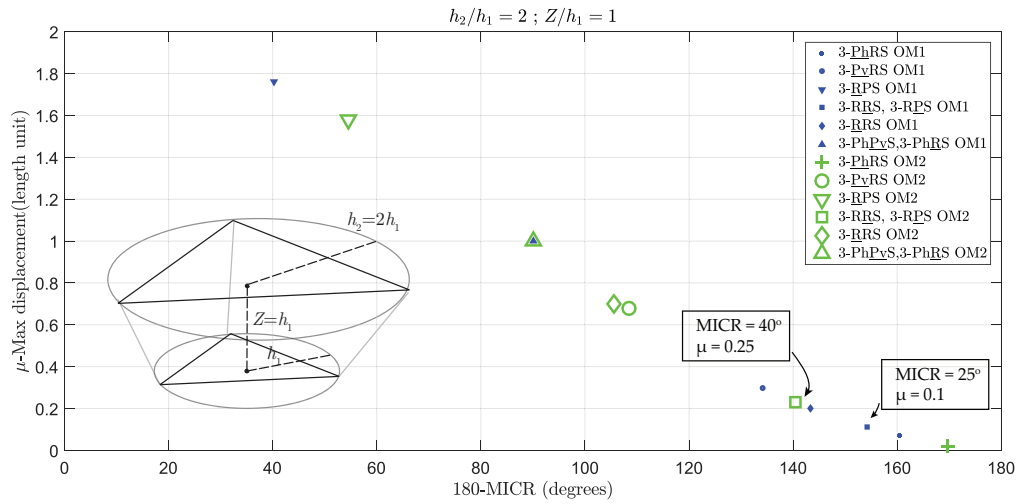


Figure 3.12 – MICR vs. maximum displacement  $\frac{h_2}{h_1} = 2, \frac{Z}{h_1} = 1$

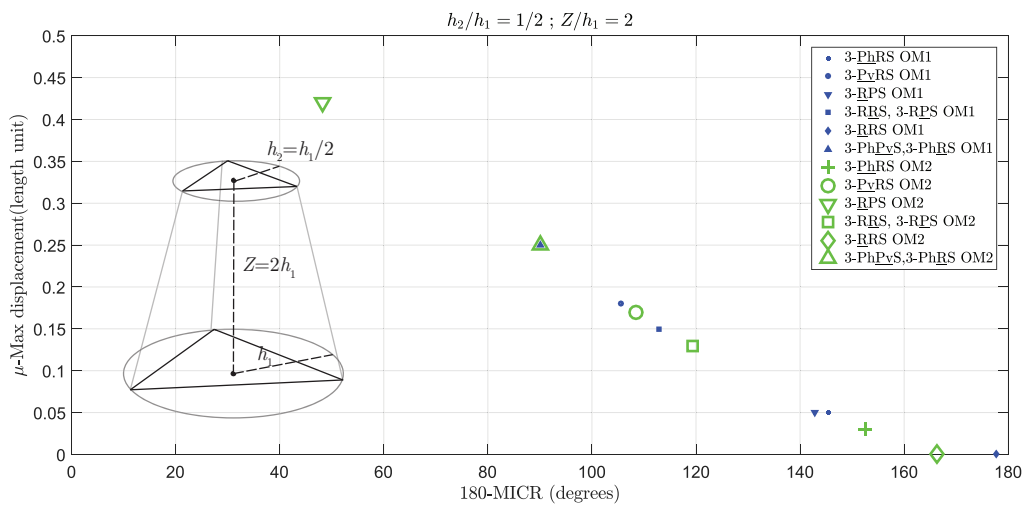


Figure 3.13 – MICR vs. maximum displacement  $\frac{h_2}{h_1} = \frac{1}{2}, \frac{Z}{h_1} = 2$

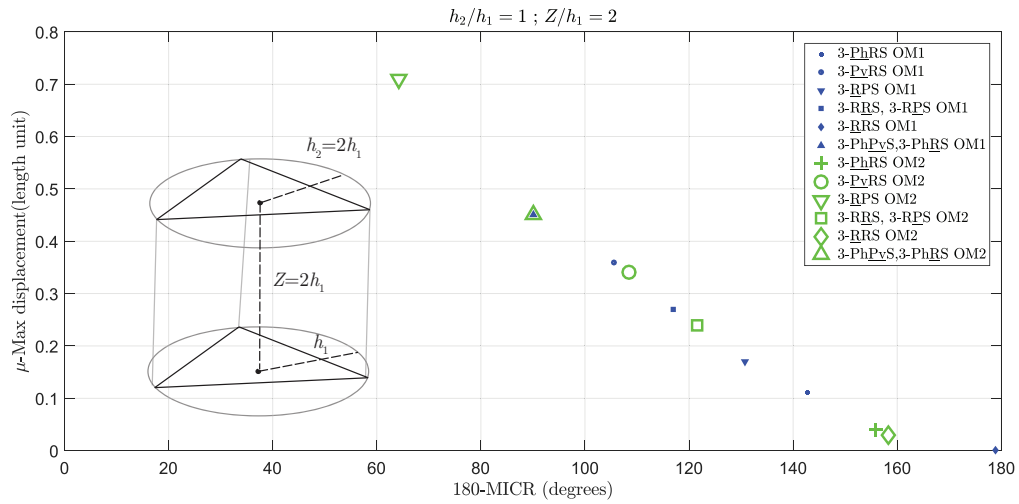


Figure 3.14 – MICR vs. maximum displacement  $\frac{h_2}{h_1} = 1, \frac{Z}{h_1} = 2$

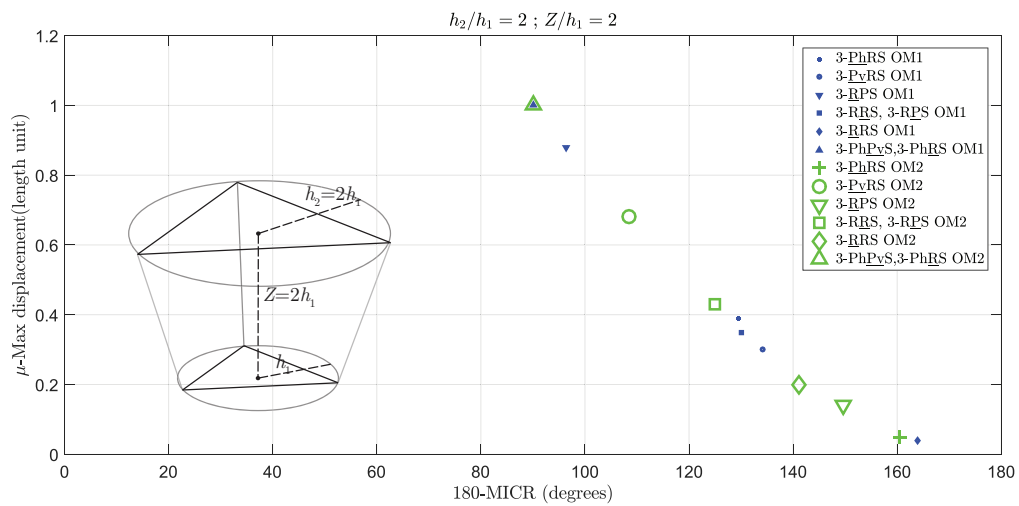


Figure 3.15 – MICR vs. maximum displacement  $\frac{h_2}{h_1} = 2, \frac{Z}{h_1} = 2$

3-[PP]S PM	$\frac{h_2}{h_1}$	$\frac{Z}{h_1}$
3- <u>RPS</u> OM2	1/2	1,2
3- <u>PhPvS</u> OM1	1/2	2
3- <u>PhRS</u> OM1	1/2	2
3- <u>PhPvS</u> OM2	1/2	2
3- <u>PhRS</u> OM2	1/2	2
3- <u>PvRS</u> OM1	1/2	2
3- <u>PvRS</u> OM2	1/2	2
3- <u>RPS</u> OM1	1/2	1,2
3- <u>RRS</u> OM1	1/2	1,2
3- <u>RPS</u> OM1	1/2	1,2
3- <u>RPS</u> OM2	1/2	1,2
3- <u>RRS</u> OM2	1/2	1,2
3- <u>RRS</u> OM1	1/2	1
3- <u>PhRS</u> OM1	1/2	1,2
3- <u>PhRS</u> OM2	1/2	2

Table 3.1 – Pareto-optimal solutions (Fig. 3.16)

3-[PP]S PM	$\frac{h_2}{h_1}$	$\frac{Z}{h_1}$
3- <u>RPS</u> OM1	2	1,2
3- <u>RPS</u> OM2	2	1,2
3- <u>PhPvS</u> OM1	2	2
3- <u>PhRS</u> OM1	2	2
3- <u>PhPvS</u> OM2	2	2
3- <u>PhRS</u> OM2	2	2
3- <u>RRS</u> OM2	2	1,2
3- <u>PvPS</u> OM2	2	2
3- <u>RPS</u> OM2	2	1,2
3- <u>RRS</u> OM2	2	1,2
3- <u>PhRS</u> OM1	2	1,2
3- <u>RPS</u> OM1	2	1,2
3- <u>RRS</u> OM1	2	1,2
3- <u>PvRS</u> OM1	2	2
3- <u>RRS</u> OM1	2	1

Table 3.2 – Solutions that do not dominate any other solutions (Fig. 3.17)

listed in Table 3.1 while the latter shows the solutions that do not dominate any other solutions listed in Table 3.2. Their respective configurations are also displayed in these figures. Operation mode 1 is represented with crossed legs or upside down moving platform. But, this need not always be the case. In fact, the generic pose of the 3-[PP]S family of PMs in each of their operation modes is still an open problem. It is noteworthy that the ordinate is chosen to be  $\log \mu$  so that small and large values of  $\mu$  are clearly visible in the same graph.

Some observations that can be drawn from these curves are that all the Pareto optimal solutions consist of 3-[PP]S-Y type PMs with  $\frac{h_2}{h_1} = \frac{1}{2}$  meaning that the circum-radius of the base is double that of the platform. The solutions that do not dominate any other solution include only 3-[PP]S-Y type PMs with  $\frac{h_2}{h_1} = 2$  implying that the height of the platform is double the circum-radius of the base. Furthermore, the 3-PhRS PM in operation mode 1 with  $\frac{h_2}{h_1} = \frac{1}{2}$ ,  $\frac{Z}{h_1} = 1$  and the 3-PhRS PM in operation mode 2 with  $\frac{h_2}{h_1} = \{\frac{1}{2}, 1\}$ ,  $\frac{Z}{h_1} = 1$  have the least  $\mu$  of all the PMs under study. On the contrary, the 3-RPS PM in its first operation mode with  $\frac{h_2}{h_1} = 2$ ,  $\frac{Z}{h_1} = 1$  has the largest  $\mu$ .







### 3.5 Ranking the Pareto optimal solutions based on complexity indices

Some complexity indices were introduced in [Car+10b; Kha+07] to evaluate the complexity of serial and parallel manipulators at their conceptual design stage. Those indices can be used to rank the parallel manipulators at hand. The complexity is not considered as a separate objective function along with MICR and  $\mu$ . It is given a lesser priority to compare the PMs belonging to the 3-[PP]S-Y family due to the fact that the complexity indices are independent of  $\frac{h_2}{h_1}$  and  $\frac{Z}{h_1}$ . Moreover, due to little differences between architectures of the 3-[PP]S-Y PMs, most of the indices defined in [Kha+07] yield the same complexity. In order to avoid this problem and to rank the Pareto optimal solutions listed in Table 3.1 in order of complexity, two more indices are introduced in this chapter. In total, the following six complexity indices are used to compare the Pareto-optimal solutions listed in Table 3.1:

#### 3.5.1 Joint-number complexity $K_N$

The joint-number complexity  $K_N$  is defined as

$$K_N = 1 - \exp(-q_N N), \quad (3.15)$$

where  $N$  is the number of joints in the PM and  $q_N$  is the resolution parameter defined by

$$q_N = \begin{cases} -\ln(0.1)/N_{max}, & \text{for } N_{max} > 0; \\ 0, & \text{for } N_{max} = 0. \end{cases} \quad (3.16)$$

For all the 3-[PP]S-Y PMs considered here,  $N = N_{max} = 9$  and hence  $k_N = 0.9$ .

#### 3.5.2 Joint-type complexity $K_J$

As the name suggests, the joint-type complexity  $K_J$  is associated with the type of joints in the PM. The 3-[PP]S-Y PMs consist of only revolute, prismatic and spherical joints and it leads to the definition of  $K_J$  as follows:

$$K_J = \frac{n_R K_{G|R} + n_P K_{G|P} + n_S K_{G|S}}{n}, \quad (3.17)$$

where  $n_R, n_P$  and  $n_S$  are the numbers of revolute, prismatic and spherical joints, respectively with  $n = n_R + n_P + n_S$ .  $K_{G|x}$  is the geometric complexity of the pair  $x$  as introduced in [Kha+07]:  $K_{G|R} = 0.5234$ ,  $K_{G|P} = 1$  and  $K_{G|S} = 0$ . The values of  $K_J$  for the Pareto optimal solutions are listed in Table 3.3.

#### 3.5.3 Loop complexity $K_L$

The loop complexity of a PM is defined as:

$$K_L = 1 - \exp(-q_L L), \quad L = l - l_m, \quad (3.18)$$

where  $l$  is the number of kinematic loops and  $l_m$  is the minimum number of loops required to produce a special displacement group or subgroup. Since each PM belonging to the 3-[PP]S-Y

family has non-pure rotations about two horizontal axes and a vertical translation, the three degrees of freedom can be realized using a single kinematic chain. Hence, for all the 3-[PP]S-Y PMs,  $l = 2$  and  $l_m = 0$ .  $q_L$  is defined the same way as in Eq. (3.16):

$$q_L = \begin{cases} -\ln(0.1)/L_{max}, & \text{for } L_{max} > 0; \\ 0, & \text{for } L_{max} = 0. \end{cases} \quad (3.19)$$

where,  $L_{max} = L = 2$  for all the Pareto optimal solutions resulting in  $K_L = 0.9$ .

### 3.5.4 Link diversity $K_B$

Link diversity  $K_B$  is defined to quantify the geometric constraints between neighboring joints. For a revolute joint, its axis of rotation is considered whereas for a prismatic joint, its direction. Five possible joint-constraint types between the neighboring joint axes/directions were reported in [Kha+07]:

1. *Type B<sub>1</sub>*: Orthogonal intersection.
2. *Type B<sub>2</sub>*: Nonorthogonal intersection.
3. *Type B<sub>3</sub>*: Parallelism.
4. *Type B<sub>4</sub>*: Orthogonal but not intersecting.
5. *Type B<sub>5</sub>*: Skew.

Thus, the geometric-constraint diversity was defined as:

$$K_B = \frac{B}{B_{max}}, \quad B = -\sum_{i=1}^c b_i \log_2(b_i), \quad b_i = \frac{M_i}{\sum_{i=1}^c M_i}, \quad (3.20)$$

where  $B$  is the entropy of the joint-constraint types and  $B_{max} = 2.32$  [Kha+07].  $c$  is the number of distinct joint-constraint types and  $M_i$  is the number of instances of each type of joint-constraints.

For 3-[PP]S-Y PMs, the joint-constraint between the first two joints in each limb is of type  $B_1$  except for the 3-RRS PM where the revolute joint axes are parallel and is of type  $B_3$ . The constraint type is always  $B_5$  between the second and the spherical joint while it is either  $B_2$  or  $B_3$  between different limbs. There are three instances of each type due to three limbs and hence for any 3-[PP]S-Y PM,  $b_i = \frac{3}{9}$ ,  $i = 1, 2, 3$ . This leads to  $B = \log_2(3)$  and  $K_B = 0.6832$ .

Two more complexity indices are introduced in [NCW18b] to facilitate the ranking of the Pareto optimal 3-[PP]S-Y PMs:

### 3.5.5 Actuator-position complexity $K_P$

Actuator-position complexity  $K_P$  is defined as:

$$\frac{1}{m} \sum_{i=1}^m \frac{p_i - 1}{n_i}, \quad (3.21)$$

where  $m$  is the number of limbs,  $n_i$  is the total number of joints in the  $i$ -th limb and  $p_i$  is the location of the actuated joint i.e.  $p_i = k$  if  $k$ -th joint is actuated. For 3-[PP]S-Y PMs,  $K_P = 0$  if the first joint is actuated and  $K_P = 1/3$  if the second joint is actuated. It is noteworthy that the actuator position index can be applied to any other SM or a PM even if the position of the actuator differs from one limb to another.

### 3.5.6 Operation mode complexity $K_{OM}$

Operation mode complexity  $K_{OM}$  is defined specifically for 3-[PP]S-Y PMs. As seen in Sec. 2.1.2, a 3-[PP]S-Y PM has two different operation modes. In the first operation mode, the moving platform is rotated upside down by 180 degrees with respect to the fixed base. As a result of this complexity analysis, it is prone to have internal collisions as compared to operation mode 2, as shown for a 3-RPS PM in Sec. 3.3. Although a detailed collision analysis is necessary to overcome this issue, it is partially overcome by introducing a new complexity index as follows:

$$K_{OM} = 1 \text{ for OM1} \quad (3.22)$$

$$K_{OM} = 0 \text{ for OM2} \quad (3.23)$$

### 3.5.7 Total complexity

Total complexity  $K \in [0, 1]$  of a kinematic chain was defined as a convex combination of the different complexity indices [Kha+07]. In the context of 3-[PP]S-Y PMs, it is redefined as

$$K = w_N K_N + w_J K_J + w_L K_L + w_B K_B + w_P K_P + w_{OM} K_{OM} \quad (3.24)$$

where  $w_N, w_J, w_L, w_B, w_P$  and  $w_{OM}$  denote their corresponding weights, such that

$$w_N + w_J + w_L + w_B + w_P + w_{OM} = 1$$

Assigning equal weights to all complexity indices implies

$$K = \frac{1}{6}(K_N + K_J + K_L + K_B + K_P + K_{OM}) \quad (3.25)$$

The Pareto optimal solutions listed in Table 3.1 are ranked in ascending order of complexity in Table 3.3. It is apparent that the 3-RPS, 3-PvRS and 3-PhRS PMs in OM2 dominate their counterparts with higher singularity-free orientation workspaces, lower parasitic motions and are the simplest ones, their complexity being equal to 0.4985. The 3-PhPvS PM in OM1 is the most complex Pareto optimal solution with a complexity equal to 0.7472. Since  $K_N, K_L$  and  $K_B$  are the same for all the 3-[PP]S-Y PMs, the weights  $w_N, w_L$  and  $w_B$  do not affect the complexity ranking. However, when  $w_L = \frac{1}{3}$  and  $w_P = \frac{1}{12}$ , 3-RRS PM in OM2 becomes the simplest PM belonging to the 3-[PP]S-Y family. Eventually, the weights can be chosen according to the application.

Rank	Pareto optimal solutions	$K_N$	$K_J$	$K_L$	$K_B$	$K_P$	$K_{OM}$	$K$
1	3-RPS OM2	0.9	0.5078	0.9	0.6832	0	0	0.4985
	3-PvRS OM2	0.9	0.5078	0.9	0.6832	0	0	0.4985
	3-PhRS OM2	0.9	0.5078	0.9	0.6832	0	0	0.4985
2	3-RRS OM2	0.9	0.3489	0.9	0.6832	0.3333	0	0.5276
3	3-PhRS OM2	0.9	0.5078	0.9	0.6832	0.3333	0	0.5541
	3-RPS OM2	0.9	0.5078	0.9	0.6832	0.3333	0	0.5541
4	3-PhPvS OM2	0.9	0.6667	0.9	0.6832	0.3333	0	0.5805
5	3-RR OM1	0.9	0.3489	0.9	0.6832	0	1	0.6387
6	3-PvRS OM1	0.9	0.5078	0.9	0.6832	0	1	0.6552
	3-PhRS OM1	0.9	0.5078	0.9	0.6832	0	1	0.6552
7	3-RRS OM1	0.9	0.3489	0.9	0.6832	0.3333	1	0.6942
8	3-PhRS OM1	0.9	0.5078	0.9	0.6832	0.3333	1	0.7207
	3-RPS OM1	0.9	0.5078	0.9	0.6832	0.3333	1	0.7207
9	3-PhPvS OM1	0.9	0.6667	0.9	0.6832	0.3333	1	0.7472

Table 3.3 – Complexity indices of Pareto optimal 3-[PP]S-Y PMs in ascending order

### 3.6 Conclusions

In this chapter, different operation and actuation modes of the 3-[PP]S-Y zero torsion parallel manipulators were compared based on their singularity free orientation workspace and parasitic motions. The manipulators belonging to the 3-[PP]S-Y family of PMs were considered and kinematic constraint equations were derived for their general architectures. A primary decomposition of the ideal of the constraint polynomials showed that they have two operation modes. Furthermore, their forward kinematic Jacobian matrices were derived for the mechanisms at hand. The determinant of the Jacobian matrix was expressed as a function of the orientation workspace parameters tilt, azimuth and height of the moving-platform,  $Z$ . The vanishing condition of the determinant was used to visualize the singularity loci in the orientation workspace. An index, named Maximum Inscribed Circle Radius (MICR), was used to quantify the singularity free orientation workspace of the manipulators. The maximum parasitic motion within the Maximum Inscribed Circle denoted as  $\mu$  was used as a second performance index. For  $\frac{h_2}{h_1} = \frac{1}{2}, 1, 2$  and  $\frac{Z}{h_1} = 1, 2$ , MICR vs.  $\mu$  values were plotted for all the mechanisms in Table 2.1. The 3-RPS PM was taken as an example to illustrate the methodology to find the MICR and  $\mu$  values. For all manipulators belonging to the 3-[PP]S-Y family, the plots of  $(180\text{-MICR})$  vs.  $\mu$  were drawn such that a minimum of these objective functions is the preferred solution. Different plots were drawn for different ratios of the circumference of the moving-platform to the circumference of the fixed base. Ultimately,  $(180\text{-MICR})$  vs.  $\log_{10}(\mu)$  points were plotted in the same graph for all the mechanisms for easier comparison. A Pareto front was observed in the plot and manipulator configurations were represented for the Pareto-optimal solutions and the solutions that do not dominate any other solution. It was concluded that the Pareto optimal solutions only include the PMs from the 3-[PP]S-Y family with the circum-radius of the base twice as that of the platform. The solutions that do not dominate any other solutions include the PMs from the 3-[PP]S-Y family with the circum-radius of the platform twice as that of the base. Therefore, the MICR vs.  $\mu$  plots could be used to compare the 3-[PP]S family of PMs

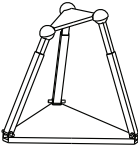
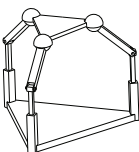
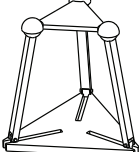
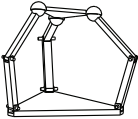
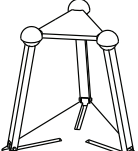
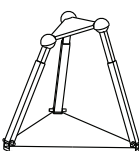
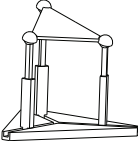

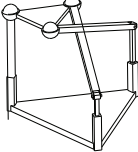
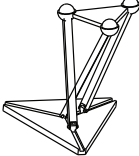
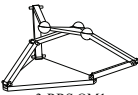
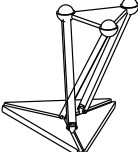
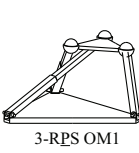
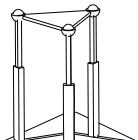
$K$	Pareto optimal 3-[PP]S-Y parallel manipulators		
0.4985	 3-RPS OM2	 3-PvRS OM2	 3-PhRS OM2
0.5276	 3-RRS OM2		
0.5541	 3-PhRS OM2	 3-RPS OM2	
0.5805	 3-PhPvS OM2		
0.6387	 3-RRS OM1		
0.6552	 3-PvRS OM1	 3-PhRS OM1	
0.6942	 3-RRS OM1		
0.7207	 3-PhRS OM1	 3-RPS OM1	
0.7472	 3-PhPvS OM1		

Table 3.4 – Pareto optimal 3-[PP]S-Y parallel manipulators configurations in ascending order of complexity

---

especially while choosing them for a particular application. Furthermore, the complexity indices of the Pareto optimal solutions were calculated. For equal weights of all complexity indices, it was shown that the  $\underline{3}$ -RPS,  $\underline{3}$ -PvRS and  $\underline{3}$ -PhRS PMs in their second operation mode are the simplest ones amongst  $\underline{3}$ -[PP]S-Y PMs.

## Chapter 4

# Kinematics and singularity analyses of series-parallel manipulators

Series-parallel manipulators (S-PMs) are the descendants of PMs which constitute the latter in a serial arrangement. To study the kinematic and singularity analysis of S-PMs knowing the properties of their modules, an S-PM with two lower mobility PMs in series is considered. The 3-RPS-3-SPR S-PM is an S-PM composed of two parallel modules with coupled degrees of freedom. The proximal module is the 3-RPS parallel mechanism which performs a translation and two non pure rotations about non fixed axes, which induce two translational parasitic motions [Hun87] while the distal module is the 3-SPR PM that has the same type of *dof* [Nay+17b]. Hu *et al.* [HLYZ12] analyzed the workspace of this manipulator. Alvarado *et al.* [GA+15] erroneously claimed that this S-PM has 5 *dof*. The reader is referred to Nayak *et al.* [NCW18d] for a better understanding of the mobility of this S-PM. Nayak *et al.* [NCW18d] proved that the full-cycle mobility of this manipulator is equal to six. Nonetheless, there is very little research on the singularities of S-PMs. It is known that if any of the parallel modules are in a singular configuration, the S-PM is also singular [Tan00] but the singularities that arise due to the serial arrangement of the PMs are generally left out. This chapter focuses on the enumeration of those serial singularities in the 3-RPS-3-SPR S-PM [NCW18c]. It is shown that six independent parameters can be used to describe the kinematics of this manipulator. Furthermore, direct and inverse kinematics problems for the 3-RPS-3-SPR S-PM are solved using Study parametrization.

### 4.1 Architecture of the 3-RPS-3-SPR series parallel manipulator

The architecture of the 3-RPS-3-SPR S-PM under study is shown in Fig. 4.1. It consists of a proximal 3-RPS PM module and a distal 3-SPR PM module. The 3-RPS PM is composed of three legs each containing a revolute, a prismatic and a spherical joint mounted in series, while the legs of the 3-SPR PM have these lower pairs in reverse order. Thus, the three equilateral triangular shaped platforms are the fixed base, the coupler and the end effector, coloured brown, green and gray, respectively. The vertices of these platforms are named  $A_i$ ,  $B_i$  and  $C_i$ ,  $i = 1, 2, 3$ , respectively. Hereafter, the subscript 0 corresponds to the fixed base, 1 to the coupler platform and 2 to the end-effector. A coordinate frame  $\mathcal{F}_i$  is attached to each platform such that its origin  $O_i$  lies at its circumcenter. The coordinate axes,  $x_i$  points towards the vertex  $P_1$ ,  $P = A, B, C$   $y_i$  is parallel to the opposite side  $P_3P_2$  and by the right hand rule,  $z_i$  is normal to platform plane. Besides, the circum-radius of the  $i$ -th platform is denoted as  $h_i$ .  $\mathbf{p}_i$  and  $\mathbf{q}_i$ ,  $i = 1, \dots, 6$  are unit vectors along the prismatic joints while  $\mathbf{u}_i$  and  $\mathbf{v}_i$ ,  $i = 1, \dots, 6$  are unit vectors along the revolute

joint axes.  $\alpha_i$  is the plane passing through  $A_i$  with its normal along  $\mathbf{u}_i$ . Similarly,  $\beta_i$  is the plane passing through  $C_i$  with its normal along  $\mathbf{v}_i$ . The spherical joint center  $B_i$  is constrained to lie in planes  $\alpha_i$  and  $\beta_i$  simultaneously.

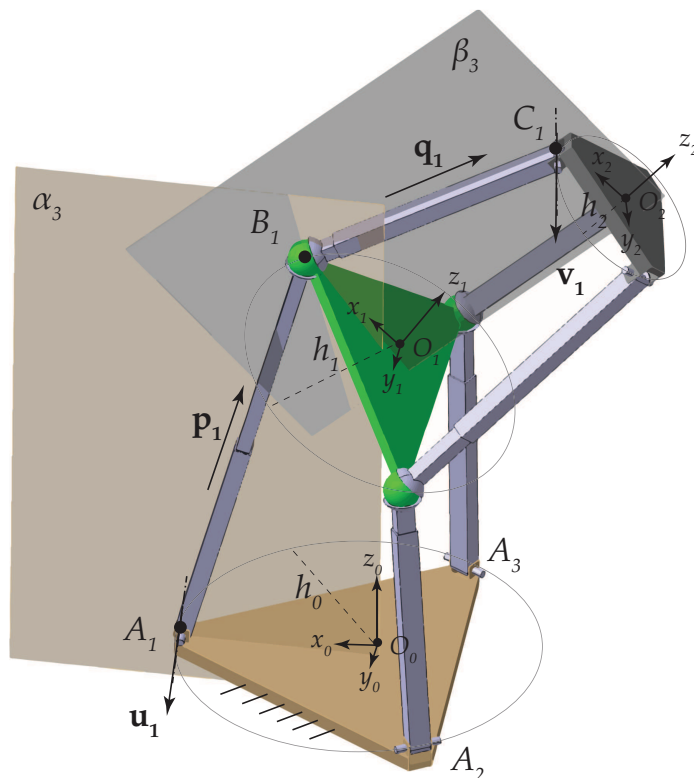


Figure 4.1 – A 3-RPS-3-SPR series-parallel manipulator

## 4.2 Parametric representation of the 3-RPS-3-SPR series-parallel manipulator

This section describes the parametrization of the 3-RPS-3-SPR series-parallel manipulator shown in Fig. 4.1. It will be proved that six independent parameters are sufficient to describe the position and orientation of the moving platform. These parameters are obtained by individually parametrizing the proximal and the distal modules.

To recall, *Study's kinematic mapping* [Hus+07] maps each spatial Euclidean displacement of  $SE(3)$  onto a point in the 7-dimensional projective space,  $\mathbb{P}^7$ . In this parametrization, a point  $[x, y, z]$  is transformed to  $[x', y', z']$  according to:

$$[1, x', y', z']^T = \mathbf{M}[1, x, y, z]^T \quad (4.1)$$

where  $\mathbf{M}$  is the transformation matrix (see Eq. (1.34a)). The parameters  $x_i, y_i, i \in \{0, \dots, 3\}$  present in the transformation matrix  $\mathbf{M}$  are called the *Study-parameters*. A Euclidean transformation can be represented by a point  $\mathbf{p} \in \mathbb{P}^7$  if and only if Eq. (1.35) and the inequality (1.36) are satisfied:

A geometric constraint for each leg of the 3-RPS parallel manipulator is that the spherical joint center is restricted to move in the plane whose normal is directed along the revolute



joint axis. Let  $f_0, f_1, f_2, f_3, g_0, g_1, g_2, g_3$  be the Study parameters. Using Study's kinematic mapping [Hus+07; HS13], three plane constraint equations  $E_i = 0$ ,  $i = 1, 2, 3$  can be written as functions of the Study parameters  $f_i, g_i$ ,  $i = 0, 1, 2, 3$ . Along with the Study's quadric  $E_4$ , there are four constraint equations irrespective of the actuation scheme:

$$E_1 := f_0 f_3 = 0 \quad (4.2)$$

$$E_2 := f_1^2 h_1 - h_1 f_2^2 + 2 f_0 g_1 - 2 f_1 g_0 - 2 f_3 g_2 + 2 g_3 f_2 = 0 \quad (4.3)$$

$$E_3 := -2 f_0 f_3 h_1 + f_1 f_2 h_1 - f_0 g_2 + f_1 g_3 + f_2 g_0 - f_3 g_1 = 0 \quad (4.4)$$

$$E_4 := f_0 g_0 + f_1 g_1 + f_2 g_2 + f_3 g_3 = 0 \quad (4.5)$$

where  $h_1$  is the circum-radius of the coupler platform. A different set of Study parameters,  $[c_0, c_1, c_2, c_3, d_0, d_1, d_2, d_3]$  are considered to parameterize the distal module to distinguish the two modules. The constraint equations for the 3-SPR PM can be obtained by considering the conjugate of the dual quaternion of the 3-RPS PM [SH18]. In other words, assigning

$$f_0 = c_0, f_1 = -c_1, f_2 = -c_2, f_3 = -c_3, g_0 = d_0, g_1 = -d_1, g_2 = -d_2, g_3 = -d_3 \quad (4.6)$$

in Eq. (4.2) to (4.5) yields the necessary equations.

Each module is a three *dof* parallel manipulator and to express these mobilities in terms of three parameters, the mechanism should be considered in one of its operation modes. For example, for the 3-RPS module,  $f_3 = 0$  represents one of its two operation modes [Sch+14]. In this operation mode,  $f_0$  can never be zero. This fact can be exploited to avoid any point  $[f_0, f_1, f_2, f_3, g_0, g_1, g_2, g_3]$  of  $\mathbb{P}^7$  to lie on the exceptional generator  $f_0 = f_1 = f_2 = f_3 = 0$ . This is done by using the normalizing condition,  $f_0 = 1$ . By substituting  $f_3 = 0$  and  $f_0 = 1$  in Eqs. (4.3) to (4.5),  $g_0, g_2$  and  $g_3$  can be linearly solved as follows:

$$g_0 = 1/2 \frac{f_1 h_1 (f_1^2 - 3 f_2^2)}{f_1^2 + f_2^2 + 1} \quad (4.7)$$

$$g_2 = -1/2 \frac{f_1 (2 f_1^2 g_1 + f_1^2 h_1 + 2 f_2^2 g_1 - 3 f_2^2 h_1 + 2 g_1)}{f_2 (f_1^2 + f_2^2 + 1)} \quad (4.8)$$

$$g_3 = -1/2 \frac{3 f_1^2 f_2^2 h_1 - f_2^4 h_1 + 2 f_1^2 g_1 + f_1^2 h_1 + 2 f_2^2 g_1 - f_2^2 h_1 + 2 g_1}{f_2 (f_1^2 + f_2^2 + 1)} \quad (4.9)$$

Thus, the Euclidean transformation matrix for the proximal module in its operation mode  $f_3 = 0$  can be written as a function of only three parameters  $f_1, f_2$  and  $g_1$ :

$$\mathbf{T}_1 = \begin{bmatrix} 1 & 0 & 0 & 0 \\ \frac{h_1 (f_1^2 - f_2^2)}{f_1^2 + f_2^2 + 1} & \frac{f_1^2 - f_2^2 + 1}{f_1^2 + f_2^2 + 1} & \frac{2 f_1 f_2}{f_1^2 + f_2^2 + 1} & \frac{2 f_2}{f_1^2 + f_2^2 + 1} \\ -\frac{2 h_1 f_2 f_1}{f_1^2 + f_2^2 + 1} & \frac{2 f_1 f_2}{f_1^2 + f_2^2 + 1} & \frac{f_1^2 - f_2^2 - 1}{f_1^2 + f_2^2 + 1} & \frac{2 f_1}{f_1^2 + f_2^2 + 1} \\ \frac{2 f_1^2 g_1 + f_1^2 h_1 + 2 f_2^2 g_1 - f_2^2 h_1 + 2 g_1}{f_2 (f_1^2 + f_2^2 + 1)} & -\frac{2 f_2}{f_1^2 + f_2^2 + 1} & \frac{2 f_1}{f_1^2 + f_2^2 + 1} & \frac{f_1^2 + f_2^2 - 1}{f_1^2 + f_2^2 + 1} \end{bmatrix} \quad (4.10)$$

Similarly for the distal 3-SPR module in its operation mode corresponding to  $c_3 = 0$ , normalizing

$c_0 = 1$  and eliminating  $d_0, d_2$  and  $d_3$ , the transformation matrix can be derived as follows:

$$\mathbf{T}_2 = \begin{bmatrix} 1 & 0 & 0 & 0 \\ \frac{c_1^4 h_1 - 6c_1^2 c_2^2 h_1 + c_2^4 h_1 + 4c_1^2 d_1}{(c_1^2 + c_2^2 + 1)^2} & \frac{c_1^2 - c_2^2 + 1}{c_1^2 + c_2^2 + 1} & \frac{2c_1 c_2}{c_1^2 + c_2^2 + 1} & \frac{2c_2}{c_1^2 + c_2^2 + 1} \\ \frac{2c_1(2c_1^2 c_2^2 h_1 - 2c_2^4 h_1 - 2c_1^2 d_1 + c_1^2 h_1 - 2c_2^2 d_1 - 2c_2^2 h_1 - 2d_1)}{(c_1^2 + c_2^2 + 1)^2 c_2} & \frac{2c_1 c_2}{c_1^2 + c_2^2 + 1} & \frac{c_1^2 - c_2^2 - 1}{c_1^2 + c_2^2 + 1} & \frac{2c_1}{c_1^2 + c_2^2 + 1} \\ \frac{2c_1^4 d_1 - c_1^4 h_1 + 4c_1^2 c_2^2 d_1 + 6c_1^2 c_2^2 h_1 + 2c_2^4 d_1 - c_2^4 h_1 + c_1^2 h_1 - c_2^2 h_1 - 2d_1}{(c_1^2 + c_2^2 + 1)^2 c_2} & \frac{2c_2}{c_1^2 + c_2^2 + 1} & \frac{2c_1}{c_1^2 + c_2^2 + 1} & \frac{c_1^2 + c_2^2 - 1}{c_1^2 + c_2^2 + 1} \end{bmatrix} \quad (4.11)$$

Therefore, a transformation matrix between the base frame  $\mathcal{F}_0$  and the moving frame  $\mathcal{F}_2$  can be expressed as  $\mathbf{T} = \mathbf{T}_1 \mathbf{T}_2$  and is a function of six independent parameters. For instance, when both modules are in the operation mode represented by  $f_3 = 0$  and  $c_3 = 0$ ,  $\mathbf{T}$  is a function of  $f_1, f_2, g_1, c_1, c_2$  and  $d_1$  and as a result, indicates that it is indeed a six *dof* mechanism. All possible configurations of the S-PM with its individual modules in different operation modes, include the following cases:

$$\begin{aligned} \text{Case a. } & c_3 = f_3 = 0 \\ \text{Case b. } & c_0 = f_0 = 0 \\ \text{Case c. } & c_0 = f_3 = 0 \\ \text{Case d. } & c_3 = f_0 = 0 \end{aligned} \quad (4.12)$$

It will be shown in the subsequent sections how simple it is to adapt the results of *Case a.* to the remaining three cases.

Consequently, matrices  $\mathbf{T}_1, \mathbf{T}_2$  and  $\mathbf{T}$  can be used to express the co-ordinates of all the vectors in one frame, preferably the fixed co-ordinate frame  $\mathcal{F}_0$  as follows:

$$\begin{aligned} {}^0\mathbf{r}_{A_1} &= [1, h_0, 0, 0]^T; & {}^0\mathbf{r}_{A_2} &= [1, -\frac{h_0}{2}, \frac{\sqrt{3}h_0}{2}, 0]^T; & {}^0\mathbf{r}_{A_3} &= [1, -\frac{h_0}{2}, -\frac{\sqrt{3}h_0}{2}, 0]^T \\ {}^1\mathbf{r}_{B_1} &= [1, h_1, 0, 0]^T; & {}^1\mathbf{r}_{B_2} &= [1, -\frac{h_1}{2}, \frac{\sqrt{3}h_1}{2}, 0]^T; & {}^1\mathbf{r}_{B_3} &= [1, -\frac{h_1}{2}, -\frac{\sqrt{3}h_1}{2}, 0]^T \\ {}^2\mathbf{r}_{C_1} &= [1, h_2, 0, 0]^T; & {}^2\mathbf{r}_{C_2} &= [1, -\frac{h_2}{2}, \frac{\sqrt{3}h_2}{2}, 0]^T; & {}^2\mathbf{r}_{C_3} &= [1, -\frac{h_2}{2}, -\frac{\sqrt{3}h_2}{2}, 0]^T \\ {}^0\mathbf{u}_1 &= [0, 0, 1, 0]^T; & {}^0\mathbf{u}_2 &= [1, -\frac{\sqrt{3}}{2}, -\frac{1}{2}, 0]^T; & {}^0\mathbf{u}_3 &= [1, \frac{\sqrt{3}}{2}, -\frac{1}{2}, 0]^T \\ {}^2\mathbf{v}_1 &= [0, 0, 1, 0]^T; & {}^2\mathbf{v}_2 &= [1, -\frac{\sqrt{3}}{2}, -\frac{1}{2}, 0]^T; & {}^2\mathbf{v}_3 &= [1, \frac{\sqrt{3}}{2}, -\frac{1}{2}, 0]^T \\ {}^0\mathbf{r}_{B_i} &= \mathbf{T}_1 {}^1\mathbf{r}_{B_i}; & {}^0\mathbf{r}_{C_i} &= \mathbf{T}^2 \mathbf{r}_{C_i}; & {}^0\mathbf{v}_i &= \mathbf{T}^2 \mathbf{v}_i, \quad i = 1, 2, 3. \end{aligned} \quad (4.13)$$

### 4.3 Singularities of the 3-RPS-3-SPR S-PM

It is noticed that the 3-RPS-3-SPR series-parallel manipulator can reach two kinds of singularities: a parallel singularity in which at least one of its modules is in a parallel singularity or a serial singularity<sup>1</sup> which occurs due to the serial arrangement of the two modules. This section

1. A serial singularity is defined here as a configuration in which the S-PM experiences a loss of degree(s) of freedom or, equivalently, a drop in the order of the twist system

briefs the derivation of the forward and inverse kinematic Jacobian matrices with a hope to find out if a given configuration is singular, at least numerically. It also explains a geometrical approach to determine the singularities in which the characteristic tetrahedron [EULL02] of the S-PM under study can be expressed algebraically. The bijective mapping between the degeneracy of the tetrahedron and serial singularities can then be exploited to enlist all the serial singularities.

### 4.3.1 Forward and inverse kinematic Jacobian matrices

If the proximal ( $P$ ) and distal ( $D$ ) modules are considered individually, the twist i.e., angular velocity vector of a body and linear velocity vector of a point on the body, of their respective moving platform with respect to their fixed base can be expressed as a function of the actuated joint rates [JT02] as follows:

$$\mathbf{A}_P {}^0\mathbf{t}_{1/0}^P = \mathbf{B}_P \dot{p}_{13} \implies \begin{bmatrix} ({}^0\mathbf{r}_{O_1A_1} \times {}^0\mathbf{p}_1)^T & {}^0\mathbf{p}_1^T \\ ({}^0\mathbf{r}_{O_1B_1} \times {}^0\mathbf{p}_2)^T & {}^0\mathbf{p}_2^T \\ ({}^0\mathbf{r}_{O_1C_1} \times {}^0\mathbf{p}_3)^T & {}^0\mathbf{p}_3^T \\ ({}^0\mathbf{r}_{O_1A_1} \times {}^0\mathbf{u}_1)^T & {}^0\mathbf{u}_1^T \\ ({}^0\mathbf{r}_{O_1B_1} \times {}^0\mathbf{u}_2)^T & {}^0\mathbf{u}_2^T \\ ({}^0\mathbf{r}_{O_1C_1} \times {}^0\mathbf{u}_3)^T & {}^0\mathbf{u}_3^T \end{bmatrix} \begin{bmatrix} {}^0\omega_{1/0}^P \\ {}^0\mathbf{v}_{O_1/0}^P \end{bmatrix} = \begin{bmatrix} \mathbf{I}_{3 \times 3} \\ \mathbf{0}_{3 \times 3} \end{bmatrix} \begin{bmatrix} \dot{p}_1 \\ \dot{p}_2 \\ \dot{p}_3 \end{bmatrix} \quad (4.14)$$

$$\mathbf{A}_D {}^1\mathbf{t}_{2/1}^D = \mathbf{B}_D \dot{q}_{13} \implies \begin{bmatrix} ({}^1\mathbf{r}_{O_2A_1} \times {}^1\mathbf{q}_1)^T & {}^1\mathbf{q}_1^T \\ ({}^1\mathbf{r}_{O_2B_1} \times {}^1\mathbf{q}_2)^T & {}^1\mathbf{q}_2^T \\ ({}^1\mathbf{r}_{O_2C_1} \times {}^1\mathbf{q}_3)^T & {}^1\mathbf{q}_3^T \\ ({}^1\mathbf{r}_{O_2A_1} \times {}^1\mathbf{v}_1)^T & {}^1\mathbf{v}_1^T \\ ({}^1\mathbf{r}_{O_2B_1} \times {}^1\mathbf{v}_2)^T & {}^1\mathbf{v}_2^T \\ ({}^1\mathbf{r}_{O_2C_1} \times {}^1\mathbf{v}_3)^T & {}^1\mathbf{v}_3^T \end{bmatrix} \begin{bmatrix} {}^1\omega_{2/1}^D \\ {}^1\mathbf{v}_{O_2/1}^D \end{bmatrix} = \begin{bmatrix} \mathbf{I}_{3 \times 3} \\ \mathbf{0}_{3 \times 3} \end{bmatrix} \begin{bmatrix} \dot{q}_1 \\ \dot{q}_2 \\ \dot{q}_3 \end{bmatrix} \quad (4.15)$$

where  ${}^0\mathbf{t}_{1/0}^P$  is the twist of the coupler with respect to the base expressed in  $\mathcal{F}_0$  and  ${}^1\mathbf{t}_{2/1}^D$  is the twist of the end effector with respect to the coupler expressed in  $\mathcal{F}_1$ .  $\mathbf{A}_P$  and  $\mathbf{A}_D$  are called forward Jacobian matrices and they incorporate the actuation and constraint wrenches of the 3-RPS and 3-SPR PMs, respectively [JT02].  $\mathbf{B}_P$  and  $\mathbf{B}_D$  are called inverse Jacobian matrices and they are the result of the reciprocal product between wrenches of the mechanism and twists of the joints for the 3-RPS and 3-SPR PMs, respectively.  $\dot{p}_{13} = [\dot{p}_1, \dot{p}_2, \dot{p}_3]^T$  and  $\dot{q}_{13} = [\dot{q}_1, \dot{q}_2, \dot{q}_3]^T$  are the prismatic joint rates of the proximal and distal modules, respectively.  ${}^k\mathbf{r}_{PQ}$  denotes the vector pointing from a point  $P$  to point  $Q$  expressed in frame  $\mathcal{F}_k$ .

It is noteworthy that if matrix  $\mathbf{A}_P$  (resp.  $\mathbf{A}_D$ ) is singular, then the proximal (resp. distal) module will be in a parallel singular configuration. The entries of matrices  $\mathbf{A}_P$  and  $\mathbf{A}_D$  represent the Plücker coordinates of six independent lines in  $\mathbb{P}^3$ . When any two or more of these lines are dependent, the configuration corresponds to a parallel singularity. Many scientific papers deal with this singularity type of both modules [Sch+14; Nay+17b; Kal+15; Sch+13; AMC16; Ami+12a; Ami+12b; MNC16]. It is noteworthy that the 3-RPS-3-SPR S-PM is in a parallel singularity if and only if any of its modules is in a parallel singularity as proved in the following subsection.

On the other hand, due to the serial stacking of the 3-RPS and 3-SPR PMs, the S-PM can also have some serial singular configurations even if the individual modules are non-singular<sup>2</sup>. Hence, a kinematic Jacobian matrix of the S-PM is necessary to explore the serial singularities.

2. The 3-RPS and the 3-SPR PMs do not have any serial singularities as long as the prismatic link lengths  $p_i$  and  $q_i$ ,  $i = 1, 2, 3$  do not vanish

If both  $\mathbf{A}_P$  and  $\mathbf{A}_D$  are nonsingular, the so called serial Jacobian matrix of the S-PM can be expressed as follows [NCW18d]:

$$\mathbf{J}_{S-PM} = \begin{bmatrix} {}^2\mathbf{Ad}_1 \mathbf{A}_P^{-1} \mathbf{B}_P & {}^0\overline{\mathbf{R}}_1 \mathbf{A}_D^{-1} \mathbf{B}_D \end{bmatrix} \quad (4.16)$$

with  ${}^2\mathbf{Ad}_1 = \begin{bmatrix} \mathbf{I}_{3 \times 3} & \mathbf{0}_{3 \times 3} \\ -{}^0\hat{\mathbf{r}}_{O_1O_2} & \mathbf{I}_{3 \times 3} \end{bmatrix}$ ,  ${}^0\hat{\mathbf{r}}_{O_1O_2} = \begin{bmatrix} 0 & -{}^0z_{O_1O_2} & {}^0y_{O_1O_2} \\ {}^0z_{O_1O_2} & 0 & -{}^0x_{O_1O_2} \\ -{}^0y_{O_1O_2} & {}^0x_{O_1O_2} & 0 \end{bmatrix}$

and  ${}^0\overline{\mathbf{R}}_1 = \begin{bmatrix} {}^0\mathbf{R}_1 & \mathbf{I}_{3 \times 3} \\ \mathbf{I}_{3 \times 3} & {}^0\mathbf{R}_1 \end{bmatrix}$

where  ${}^2\mathbf{Ad}_1$  is called the adjoint matrix.  ${}^0\hat{\mathbf{r}}_{O_1O_2}$  is the cross product matrix of vector  ${}^0\mathbf{r}_{O_1O_2} = [{}^0x_{O_1O_2}, {}^0y_{O_1O_2}, {}^0z_{O_1O_2}]$ , pointing from point  $O_1$  to point  $O_2$  expressed in frame  $\mathcal{F}_0$ .  ${}^0\overline{\mathbf{R}}_1$  is called the augmented rotation matrix between frames  $\mathcal{F}_0$  and  $\mathcal{F}_1$  and it contains the rotation matrix  ${}^0\mathbf{R}_1$  from frame  $\mathcal{F}_0$  to frame  $\mathcal{F}_1$ .  $\mathbf{J}_{S-PM}$  fits into the kinematic model of the S-PM in the following way:

$${}^0\mathbf{t}_{2/0} = \mathbf{J}_{S-PM} \begin{bmatrix} \dot{\mathbf{p}} \\ \dot{\mathbf{q}} \end{bmatrix} \quad (4.17)$$

where  ${}^0\mathbf{t}_{2/0}$  is the twist of the moving platform with respect to the fixed base expressed in  $\mathcal{F}_0$  and  $\dot{\mathbf{p}} = [\dot{p}_1, \dot{p}_2, \dot{p}_3]^T$  and  $\dot{\mathbf{q}} = [\dot{q}_1, \dot{q}_2, \dot{q}_3]^T$  are the joint rates of the proximal and the distal modules, respectively. The rank of this matrix provides the local mobility of the S-PM [NCW18d]. Moreover, when  $\mathbf{J}_{S-PM}$  is singular, the series-parallel manipulator at hand is in a serial singularity. When a manipulator configuration is given, it is straightforward to calculate numerically the serial kinematic Jacobian matrix from Eq. (4.16) and to deduce if it is a serial singular configuration. However, it is tedious to derive a symbolic or an implicit equation that could be used to enlist all serial singularities. Therefore, a geometric approach is adopted.

Equations (4.16) and (4.17) can be extended to a series-parallel manipulator with  $n$  modules in series as shown in Fig. 4.2. Thus, the moving platform twist with respect to the fixed base expressed in coordinate frame  $\mathcal{F}_0$  is as follows :

$${}^0\mathbf{t}_{n/0} = \sum_{i=1}^n {}^0\overline{\mathbf{R}}_{(i-1)} {}^n\mathbf{Ad}_i {}^{(i-1)}\mathbf{t}_{i/(i-1)}^{M_i} = \mathbf{J}_{6 \times 3n} \begin{bmatrix} \dot{\rho}_{M_1} \\ \dot{\rho}_{M_2} \\ \vdots \\ \dot{\rho}_{M_n} \end{bmatrix} \quad (4.18)$$

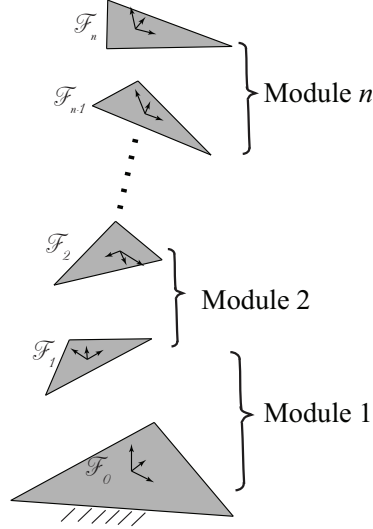
with  ${}^0\overline{\mathbf{R}}_i = \begin{bmatrix} {}^0\mathbf{R}_i & \mathbf{I}_{3 \times 3} \\ \mathbf{I}_{3 \times 3} & {}^0\mathbf{R}_i \end{bmatrix}$ ,  ${}^n\mathbf{Ad}_i = \begin{bmatrix} \mathbf{I}_{3 \times 3} & \mathbf{0}_{3 \times 3} \\ -{}^{(i-1)}\hat{\mathbf{r}}_{O_iO_n} & \mathbf{I}_{3 \times 3} \end{bmatrix}$  and

$$\mathbf{J}_{6 \times 3n} = \begin{bmatrix} {}^n\mathbf{Ad}_1 \mathbf{A}_{M_0}^{-1} \mathbf{B}_{M_0} & {}^0\overline{\mathbf{R}}_1 {}^n\mathbf{Ad}_2 \mathbf{A}_{M_1}^{-1} \mathbf{B}_{M_1} & \dots & {}^0\overline{\mathbf{R}}_n \mathbf{A}_{M_n}^{-1} \mathbf{B}_{M_n} \end{bmatrix}$$

where  $\mathbf{J}_{6 \times 3n}$  is the  $6 \times 3n$  kinematic Jacobian matrix of the  $n$ -module S-PM manipulator.  $M_i$  stands for the  $i$ -th module,  $\mathbf{A}_{M_i}$  and  $\mathbf{B}_{M_i}$  are the forward and inverse Jacobian matrices of  $M_i$ , respectively.  $\dot{\rho}_{M_i}$  is the vector of the actuated prismatic joint rates for the  $i$ -th module.

### 4.3.2 Twist and wrench systems of the 3-RPS-3-SPR PM

Each leg of the 3-RPS and 3-SPR parallel manipulators is composed of three joints, but the order of the limb twist system is equal to five and hence there exist five twists associated to each

Figure 4.2 –  $n$  parallel mechanisms (named modules) arranged in series

leg. Thus, the constraint wrench system of the  $i$ -th leg of the 3-RPS and 3-SPR parallel modules is spanned by a pure force  $\mathcal{W}_P^i$  and  $\mathcal{W}_D^i$  shown as the black and red vectors, respectively in Fig. 4.4. These forces are reciprocal to all the joint twists in each leg, in the respective modules. The three forces in each module span its wrench system  $\mathcal{W}_P$  or  $\mathcal{W}_D$  which is the *third special three-system* of screws [Hun87]:

$$\begin{aligned}
 {}^0\mathcal{W}_P &= \bigoplus_{i=1}^3 {}^0\mathcal{W}_P^i = \text{span} \left\{ \begin{bmatrix} {}^0\mathbf{u}_1 \\ {}^0\mathbf{r}_{O_2B_1} \times {}^0\mathbf{u}_1 \end{bmatrix}, \begin{bmatrix} {}^0\mathbf{u}_2 \\ {}^0\mathbf{r}_{O_2B_2} \times {}^0\mathbf{u}_2 \end{bmatrix}, \begin{bmatrix} {}^0\mathbf{u}_3 \\ {}^0\mathbf{r}_{O_2B_3} \times {}^0\mathbf{u}_3 \end{bmatrix} \right\} \\
 {}^0\mathcal{W}_D &= \bigoplus_{i=1}^3 {}^0\mathcal{W}_D^i = \text{span} \left\{ \begin{bmatrix} {}^0\mathbf{v}_1 \\ {}^0\mathbf{r}_{O_2B_1} \times {}^0\mathbf{v}_1 \end{bmatrix}, \begin{bmatrix} {}^0\mathbf{v}_2 \\ {}^0\mathbf{r}_{O_2B_2} \times {}^0\mathbf{v}_2 \end{bmatrix}, \begin{bmatrix} {}^0\mathbf{v}_3 \\ {}^0\mathbf{r}_{O_2B_3} \times {}^0\mathbf{v}_3 \end{bmatrix} \right\} \\
 {}^0\mathcal{W}_{S-PM} &= {}^0\mathcal{W}_P \cap {}^0\mathcal{W}_D \\
 \dim({}^0\mathcal{W}_P) &= \dim({}^0\mathcal{W}_D) = 3
 \end{aligned} \tag{4.19}$$

Alternatively, the twist system of the 3-RPS-3-SPR S-PM is the union of the twist systems of two modules. The twist systems of each module are the orthogonal vector subspaces of the respective wrench systems and are also the *third special three-system* of screws [Hun87]:

$$\begin{aligned}
 {}^0\mathcal{T}_P &= {}^0\mathcal{W}_P^\perp \\
 {}^0\mathcal{T}_D &= {}^0\mathcal{W}_D^\perp \\
 {}^0\mathcal{T}_{S-PM} &= {}^0\mathcal{T}_P \cup {}^0\mathcal{T}_D \\
 \dim({}^0\mathcal{T}_P) &= \dim({}^0\mathcal{T}_D) = 3
 \end{aligned} \tag{4.20}$$

The mobility of the 3-RPS-3-SPR S-PM is equal to the dimension of the overall twist system,

$\dim({}^0\mathcal{T}_{S-PM})$ . For a general configuration, when the twist systems of each module are independent i.e.,  $\dim({}^0\mathcal{T}_P \cap {}^0\mathcal{T}_D) = 0$ , the mobility was established to be six in [NCW18d]:

$$\begin{aligned} \dim({}^0\mathcal{T}_{S-PM}) &= \dim({}^0\mathcal{T}_P \cup {}^0\mathcal{T}_D) = \dim({}^0\mathcal{T}_P) + \dim({}^0\mathcal{T}_D) - \dim({}^0\mathcal{T}_P \cap {}^0\mathcal{T}_D) \\ &= \dim({}^0\mathcal{T}_P) + \dim({}^0\mathcal{T}_D) \\ &= 3 + 3 = 6 \end{aligned} \quad (4.21)$$

As a conclusion, the following Theorem is stated.

**Theorem 7.** *A parallel singularity of an S-PM arises if and only if at least one of its modules reaches a parallel singularity.*

*Proof:* When the actuators are blocked, the twist system of any module in a parallel singularity is of order more than zero or, equivalently, the wrench system is of order less than six. The sufficient condition is that if at least one module is in a parallel singularity, then the S-PM is in a parallel singularity. In this case, from Eq. (4.21), if the order of the twist system is more than zero for any module, it is reflected in the order of the twist system of the whole S-PM. The necessary condition can be proved as follows. If none of the modules is in a parallel singularity, the wrench system of each module is of order six when the actuated joints are blocked. Thus, the order of the wrench system of the full S-PM is also of order six and thus the S-PM is not in a parallel singularity.

### 4.3.3 Enumeration of serial singularities

A serial singularity is encountered

- when there exists a wrench common to both modules of the S-PM or, equivalently, if the dimension of the intersection of the two wrench systems is more than zero:

$$\dim({}^0\mathcal{W}_P \cap {}^0\mathcal{W}_D) > 0 \quad (4.22)$$

- if the union of the two wrench systems is of dimension lower than six. Indeed,

$$\begin{aligned} \dim({}^0\mathcal{W}_P \cup {}^0\mathcal{W}_D) &= \dim({}^0\mathcal{W}_P) + \dim({}^0\mathcal{W}_D) - \dim({}^0\mathcal{W}_P \cap {}^0\mathcal{W}_D) \\ &= 3 + 3 - \dim({}^0\mathcal{W}_P \cap {}^0\mathcal{W}_D) \end{aligned} \quad (4.23)$$

From Eqs. (4.22) and (4.23),  $\dim({}^0\mathcal{W}_P \cup {}^0\mathcal{W}_D) < 6$

A straightforward sufficient condition for Eq. (4.22) or (4.23) to hold is that at least one revolute joint axis in the base is parallel to the corresponding revolute joint axis in the moving platform. In other words,  ${}^0\mathbf{u}_i \parallel {}^0\mathbf{v}_i$  for any  $i = 1, 2, 3$ . For the  $i$ -th leg, by equating the coordinates of vectors  ${}^0\mathbf{u}_i$  and  ${}^0\mathbf{v}_i$ , three systems of equations are obtained from Eq. (4.13) in parameters  $c_1, c_2, f_1$  and  $f_2$ . Solving the system of equations for three of the four parameters, say,  $c_1, f_1$  and  $c_2$  leads to the following algebraic expressions corresponding to the serial singular configurations:

$$\begin{aligned} {}^0\mathbf{u}_1 \parallel {}^0\mathbf{v}_1 &\implies c_1 = 0, f_1 = 0 \\ {}^0\mathbf{u}_2 \parallel {}^0\mathbf{v}_2 &\implies c_1 = -\sqrt{3}c_2, f_1 = -\sqrt{3}f_2 \\ {}^0\mathbf{u}_3 \parallel {}^0\mathbf{v}_3 &\implies c_1 = \sqrt{3}c_2, f_1 = \sqrt{3}f_2 \\ {}^0\mathbf{u}_i \parallel {}^0\mathbf{v}_i \quad \forall i = 1, 2, 3 &\implies c_1 = -f_1, c_2 = -f_2 \end{aligned} \quad (4.24)$$

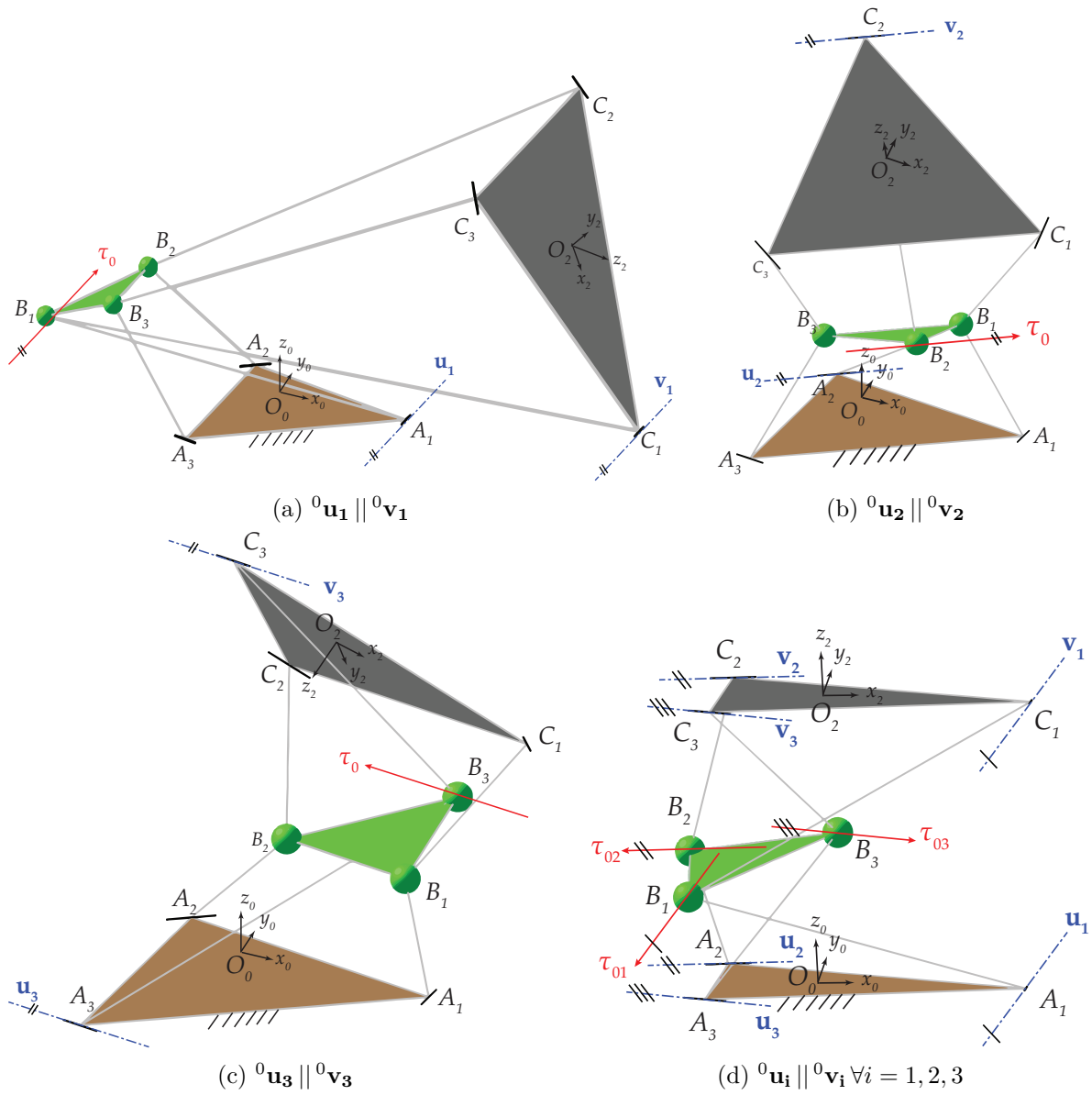


Figure 4.3 – Serial singular configurations with parallel revolute joint axes

When all the base revolute joint axes are parallel to their corresponding platform revolute joint axes, the fixed base and the moving platform are parallel to each other. In this case, the transformation matrix  $\mathbf{T}$  is the Identity matrix resulting in  $\mathbf{T}_1 = \mathbf{T}_2^{-1}$ . Figure 4.3 shows the four cases for arbitrary design parameters. In the first three cases, the constraint wrench  $\tau_0$  prevents the moving-platform from rotating about its axis. Thus, the manipulator has only 5 *dof*. When the base is parallel to the moving platform, the constraint wrench system of the whole manipulator is spanned by three forces  $\tau_{01}, \tau_{02}$  and  $\tau_{03}$  leading to an instantaneous three *dof* S-PM. The degrees of freedom include a pure vertical translation and two non-pure horizontal rotations. In this case, the last condition shown in (4.24) can be substituted in the expression of  $\mathbf{T}$  to find the coordinates of the platform circumcenter  $O_2$  to be  $[0, 0, \frac{2(d_1 + g_1)}{f_2}]$ , where only a  $z$ -translation is allowed. There can be other similar configurations in which the base and the platform are parallel with translations along all three coordinate axes. It is noteworthy that the algebraic relations governing the serial singular configurations described so far are independent of the parameters  $h_0, h_1, h_2, g_1$  and  $d_1$ .

There exist other serial singular configurations in which the constraint wrenches at each spherical joint are not coincident and hence form the *first special two system* of screws [Hun87]. The following section describes a methodology to determine these singularities.

#### 4.3.4 Characteristic tetrahedron of serial singularities

At each spherical joint, if the constraint forces are not coincident, they form a force *pencil*. A *characteristic tetrahedron* is defined combining the planes of the three pencils along with the coupler platform plane passing through the spherical joints as shown in Fig. 4.4.

A Theorem proposed by Uphoff et al.. in [EULL02] is used to identify the remaining serial singularities.

**Theorem 8** ((ref. [EULL02])). *A platform manipulator is in a wrench singularity if and only if the characteristic tetrahedron is singular*

In this context, the wrench singularities correspond to the serial singularities of the S-PM. The method was initially designed to determine the parallel singularities of a parallel manipulator and the same method is used here to enumerate serial singularities of a S-PM [NCW18c]. The homogeneous co-ordinates of the planes (the normal vector to the plane,  $\mathbf{w}_i$  and a point on the plane are known) representing the faces of the tetrahedron are expressed as follows:

$$\begin{aligned}
\Pi_1 & : \mathbf{a} = [w_{01}, \mathbf{w}_1] = [-\mathbf{r}_{B_1}^T(\mathbf{u}_1 \times \mathbf{v}_1), (\mathbf{u}_1 \times \mathbf{v}_1)^T] \\
\Pi_2 & : \mathbf{b} = [w_{02}, \mathbf{w}_2] = [-\mathbf{r}_{B_2}^T(\mathbf{u}_2 \times \mathbf{v}_2), (\mathbf{u}_2 \times \mathbf{v}_2)^T] \\
\Pi_3 & : \mathbf{c} = [w_{03}, \mathbf{w}_3] = [-\mathbf{r}_{B_3}^T(\mathbf{u}_3 \times \mathbf{v}_3), (\mathbf{u}_3 \times \mathbf{v}_3)^T] \\
\Pi_4 & : \mathbf{d} = [w_{04}, \mathbf{w}_4] \\
& = [-\mathbf{r}_{B_1}^T((\mathbf{r}_{B_1} - \mathbf{r}_{B_2}) \times (\mathbf{r}_{B_1} - \mathbf{r}_{B_3})), ((\mathbf{r}_{B_1} - \mathbf{r}_{B_2}) \times (\mathbf{r}_{B_1} - \mathbf{r}_{B_3}))^T] \quad (4.25)
\end{aligned}$$

All the vectors are expressed in frame  $\mathcal{F}_0$ . Hence, a serial singularity occurs when the determinant of the matrix of plane coordinates  $[\mathbf{a} \ \mathbf{b} \ \mathbf{c} \ \mathbf{d}]$  vanishes. A similar approach using Grassman-Cayley algebra was used to find singularities of a six-dof manipulator, 3-PPPS in [Car+10a]. From



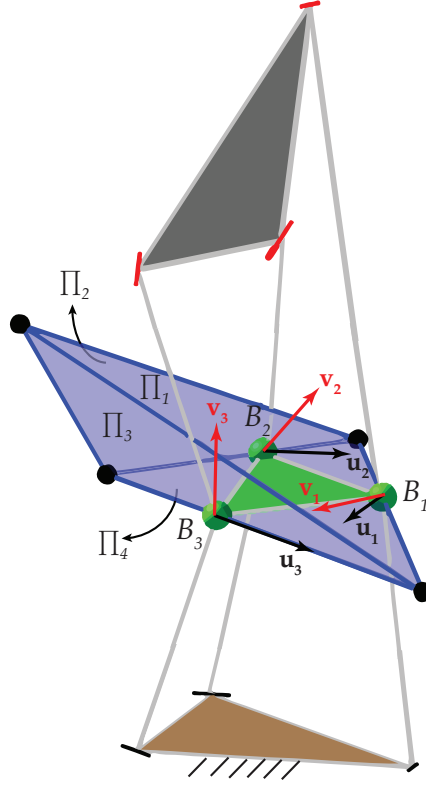


Figure 4.4 – The characteristic tetrahedron of the 3-RPS-3-SPR S-PM

Eqs. (4.13) and (4.25),

$$\begin{aligned}
 |\mathbf{abcd}| = & -\frac{27(c_1 f_1 + c_2 f_2 - 1) h_1^3}{2(c_1^2 + c_2^2 + 1)^3 (f_1^2 + f_2^2 + 1)^3} (4c_1^4 f_1 f_2^2 - 8c_1^3 c_2 f_1^2 f_2 - 8c_1^3 c_2 f_2^3 \\
 & + 4c_1^3 f_1^2 f_2^2 - 4c_1^3 f_2^4 + 4c_1^2 c_2^2 f_1^3 + 12c_1^2 c_2^2 f_1 f_2^2 - 8c_1^2 c_2 f_1^3 f_2 \\
 & + 4c_1 c_2^2 f_1^4 + 12c_1 c_2^2 f_1^2 f_2^2 - 4c_2^4 f_1^3 - 8c_2^3 f_1^3 f_2 + c_1^4 f_1 - 8c_1^3 c_2 f_2 \\
 & + 3c_1^3 f_1^2 - 3c_1^3 f_2^2 + 6c_1^2 c_2^2 f_1 - 6c_1^2 c_2 f_1 f_2 + 3c_1^2 f_1^3 + 3c_1^2 f_1 f_2^2 \\
 & + 3c_1 c_2^2 f_1^2 - 3c_1 c_2^2 f_2^2 - 6c_1 c_2 f_1^2 f_2 - 6c_1 c_2 f_2^3 + c_1 f_1^4 + 6c_1 f_1^2 f_2^2 \\
 & - 3c_1 f_2^4 - 3c_2^4 f_1 - 6c_2^3 f_1 f_2 - 3c_2^2 f_1^3 - 3c_2^2 f_1 f_2^2 - 8c_2 f_1^3 f_2 + c_1^3 \\
 & + 3c_1^2 f_1 - 3c_1 c_2^2 - 6c_1 c_2 f_2 + 3c_1 f_1^2 - 3c_1 f_2^2 - 3c_2^2 f_1 - 6c_2 f_1 f_2 \\
 & + f_1^3 - 3f_1 f_2^2)
 \end{aligned} \tag{4.26}$$

Thus, the points on the surface  $|\mathbf{abcd}| = 0$  correspond to serial singular configurations for the 3-RPS-3-SPR S-PM. From Eq. (4.26), the manipulator is in a serial singular configuration when either  $c_1 f_1 + c_2 f_2 - 1 = 0$  or the second factor, a 7-degree polynomial,  $p^7(c_1, f_1, c_2, f_2) = 0^3$ . In order to enumerate different serial singularities, the conditions for rank deficiency of the matrix  $[\mathbf{abcd}]$  listed in Table 1 of [EULL02] are studied.

3. A 3D animation of the singular surface by varying  $c_1, c_2, f_1$  and  $f_2$  from -3 to 3 is uploaded in <https://www.dropbox.com/s/dzif65bhx59nxd6/sing1.mp4?dl=0> for the first factor of Eq. (4.26) and in <https://www.dropbox.com/s/koezrl6xom3pmmr/singp7.mp4?dl=0> for the second factor of Eq. (4.26).

**Case 1: 4 faces meet in a point** Two subcases must be considered depending on whether the point of intersection is real or lies at infinity. In both cases, the variety spanned by the 6 constraint wrench lines is a *general linear complex* [Mer89] and the 3-RPS-3-SPR S-PM instantaneously behaves as a 5 *dof* mechanism.

**a. A real point:** Considering the second factor of Eq. (4.26)  $p^7(c_1, c_2, f_1, f_2)$ , substituting arbitrary values for any three of the four parameters and finding the fourth one shows that the faces of the characteristic tetrahedron intersect in a point. One such configuration is shown in Fig. 4.5a. Point  $P$  is the intersection point of the four planes  $\Pi_j$ ,  $j = 1, 2, 3, 4$ .

**b. A point at infinity:** This happens when the intersection lines of the planes are parallel. In other words, it is sufficient to check if the ideal point (nothing but the point at infinity of a line) of one of these lines lies in the other three planes. Let the ideal point of line of intersection  $L_{12}$  of planes  $\Pi_1$  and  $\Pi_2$  be  $P_{12}^\infty$ . It is sufficient to check if this point lies on the line of intersection  $L_{34}$  of planes  $\Pi_3$  and  $\Pi_4$ . However, this approach is computationally expensive and yields no results. Therefore, it is first checked whether point  $P_{12}^\infty$  lies on the line of intersection  $L_{13}$  of planes  $\Pi_1$  and  $\Pi_3$  as follows:

$$\mathbf{r}_{P_{12}^\infty} : (0, \mathbf{l}_{12}) = (0, \mathbf{w}_1 \times \mathbf{w}_2) \quad (4.27)$$

$$L_{13} : (\mathbf{l}_{13}, \bar{\mathbf{l}}_{13}) = (\mathbf{w}_1 \times \mathbf{w}_3, w_{01}\mathbf{w}_3 - w_{03}\mathbf{w}_1) \quad (4.28)$$

$$\mathbf{r}_{P_{12}^\infty} \wedge L_{12} = 0 : \mathbf{w}_3 \cdot \mathbf{l}_{12} = 0, \quad -w_{03}\mathbf{l}_{12} + \mathbf{w}_3 \times \bar{\mathbf{l}}_{12} = 0 \quad (4.29)$$

Solving Eq. (4.29) for  $c_1, f_1, c_2$  and  $f_2$  yields the relationship  $c_1 f_1 + c_2 f_2 - 1 = 0$  or  $c_1 f_2 - c_2 f_1 = 0$ . The former relationship corresponds to the intersection of the planes in a real line. It will be discussed in the following paragraph. The latter corresponds to the configuration where the planes  $\Pi_1, \Pi_2$  and  $\Pi_3$  share the same ideal point. It can also mean that they have a common line of intersection at infinity, which will be dealt with in the next paragraph. In other words, their lines of intersection are parallel. Formulating another equation such that the point  $P_{12}^\infty$  lies in the plane  $\Pi_4$  and solving the two equations results in the following relationships:

$$\left. \begin{array}{l} c_1 f_2 - c_2 f_1 = 0 \\ \mathbf{r}_{P_{12}^\infty} \cdot ([w_{04}, \mathbf{w}_4]) = 0 \end{array} \right\} \implies \quad \text{OR} \quad (4.30)$$

$$c_1 = -\frac{f_1}{f_1^2 + f_2^2}, \quad c_2 = -\frac{f_2}{f_1^2 + f_2^2}$$

If the parameters  $c_1, c_2, f_1$  and  $f_2$  satisfy the foregoing conditions, the S-PM is in a serial singularity with the planes of its characteristic tetrahedron intersecting in a point at infinity. One such configuration is depicted in Fig. 4.5b.

**Case 2: 3 sides meet in a line** : The first factor of Eq. (4.26),  $c_1 f_1 + c_2 f_2 - 1 = 0$  corresponds to the serial singularity in which the variety spanned by the 6 constraint wrench lines is a *special linear complex* [Mer89] and the mechanism has 5 *dof*. To prove that  $c_1 f_1 + c_2 f_2 = 1$  corresponds to the singularity when 3 sides of the characteristic tetrahedron meet in a line, two sub cases are considered when the line of intersection of the three sides is

**a. Real line:** The condition  $c_1 f_1 + c_2 f_2 - 1 = 0$  is derived using line geometry. For a line intersection of the three planes, it is sufficient to prove the incidence of the intersection line of first two sides with the third one. The Plücker coordinates of the line of intersection,  $L_{12}$  of

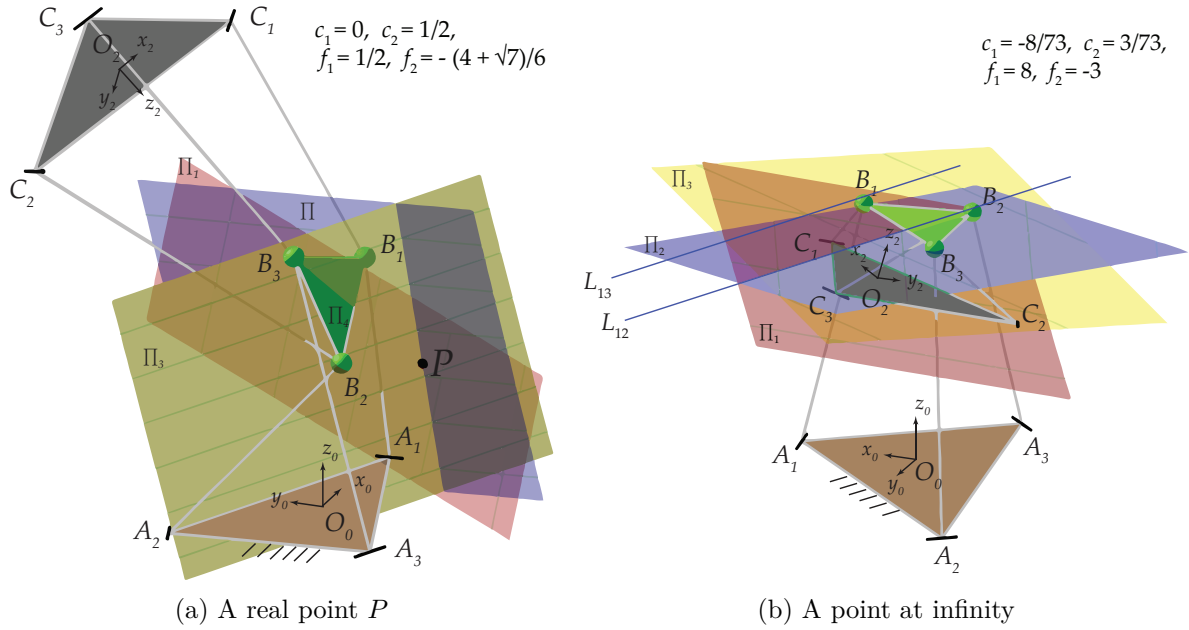


Figure 4.5 – Serial singularity when all faces of the characteristic tetrahedron meet in a point

planes  $\Pi_1$  and  $\Pi_2$  are calculated. The line  $L_{12}$  and the plane  $\Pi_3$  are incident if and only if the following conditions are satisfied [PW01].

$$L_{12} : (\mathbf{l}_{12}, \bar{\mathbf{l}}_{12}) = (\mathbf{w}_1 \times \mathbf{w}_2, w_{01}\mathbf{w}_2 - w_{02}\mathbf{w}_1) \quad (4.31)$$

$$\Pi_3 \wedge L_{12} = 0 : \mathbf{w}_3 \cdot \mathbf{l}_{12} = 0, \quad -w_{03}\mathbf{l}_{12} + \mathbf{w}_3 \times \bar{\mathbf{l}}_{12} = 0 \quad (4.32)$$

The four equations in Eq. (4.32) are solved for parameters  $c_1, c_2, f_1$  and  $f_2$  to obtain the solution  $f_2 = -\frac{c_1 f_1 - 1}{c_2}$  with arbitrary values for  $c_1, c_2$  and  $f_1$ . It means that if the choice of these parameters are bound by the relation  $c_1 f_1 + c_2 f_2 - 1 = 0$ , the three sides intersect in a line and is consistent with the first factor of Eq. (4.26). Figure 4.6a shows one of the serial singular configurations in which the three sides meet in a line  $L$ . It implies that six constraint forces intersect the line  $L$  and hence belong to a singular linear complex.

**b. Line at infinity:** In this case, the side planes are all parallel to each other which is possible only when the fixed base and the moving platform planes are parallel to each other. Since the 3-RPS-3-SPR PM has 6 dof, the only possibilities for the platform and the base to remain parallel is when the moving platform has pure translational motions or has a rotation about the  $z_0$ -axis along with translational motions. The former case is studied in Subsec. 4.3.3 where corresponding revolute joint axes are parallel to each other leading to a 3 dof freedom mechanism. The latter case is investigated by considering the transformation matrix  $\mathbf{T}$ , and forcing the rotation matrix to be of pure rotation about  $z_0$ -axis. This is done by equating  $\mathbf{T}(2, 4)$

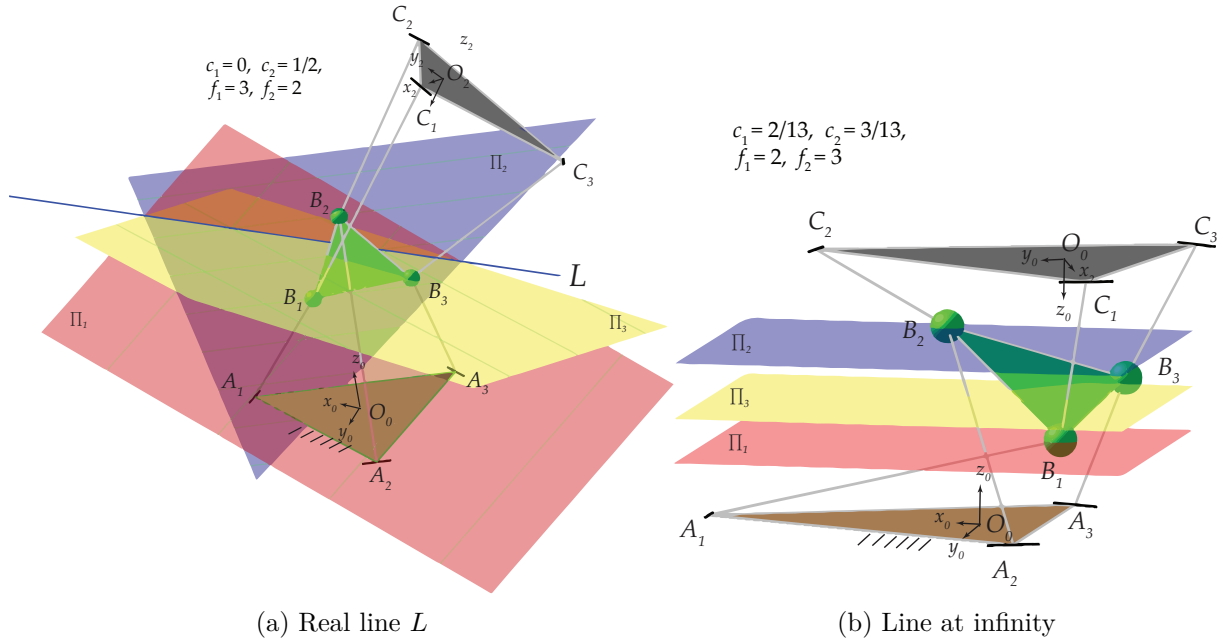


Figure 4.6 – Serial singular configurations when three sides of the characteristic tetrahedron meet in a line

and  $\mathbf{T}(3, 4)$  to zero and solving for two of the four parameters  $c_1, c_2, f_1$  and  $f_2$ :

$$\begin{aligned}
 & f_1 = \frac{c_1}{c_1^2 + c_2^2}, \quad f_2 = \frac{c_2}{c_1^2 + c_2^2} \\
 & \left. \begin{aligned} \mathbf{T}(2, 4) = -\mathbf{T}(4, 2) = 0 \\ \mathbf{T}(3, 4) = -\mathbf{T}(4, 3) = 0 \end{aligned} \right\} \Rightarrow \quad OR \quad (4.33) \\
 & c_1 = \frac{f_1}{f_1^2 + f_2^2}, \quad c_2 = \frac{f_2}{f_1^2 + f_2^2}
 \end{aligned}$$

The relations in Eq. (4.33) satisfy the equation  $c_1 f_1 + c_2 f_2 - 1 = 0$ . Hence, this equation is a necessary and a sufficient condition for three sides to have a common line of intersection and it instantaneously reduces the degree of freedom of the S-PM at hand by 1. Furthermore, by substituting Eq. (4.33) in  $\mathbf{T}$ , the magnitude of rotation about the  $z_0$ -axis is given by  $\sigma = \tan^{-1}\left(\frac{2c_1 c_2}{c_2^2 - c_1^2}\right) = \tan^{-1}\left(\frac{2f_1 f_2}{f_2^2 - f_1^2}\right)$ . A serial singular configuration in which  $\sigma = 67^\circ$  is shown in Fig. 4.6b. Note that in theory the platform can have an upright position or an upside down position and yet stay parallel to the base.

**Case 3: 2 sides and base meet in a line** Considering a side plane  $\Pi_i$ ,  $i = 1, 2, 3$  and the base plane  $\Pi_4$ , their line of intersection must pass through  $B_i$ . To prove if  $\Pi_i, \Pi_j$  and  $\Pi_4$ ,  $i, j = 1, 2, 3$  have a common line of intersection, it is sufficient to prove that the points  $B_i$  and  $B_j$  simultaneously lie on the planes  $\Pi_j$  and  $\Pi_i$ , respectively. If there exists a line common to all the three planes, it should be along  $B_i B_j$  as shown in Fig. 4.7. For instance, if planes  $\Pi_1, \Pi_2$  and  $\Pi_4$  are considered, simultaneous incidence of point  $B_1$  on  $\Pi_2$  and that of point  $B_2$  on  $\Pi_1$

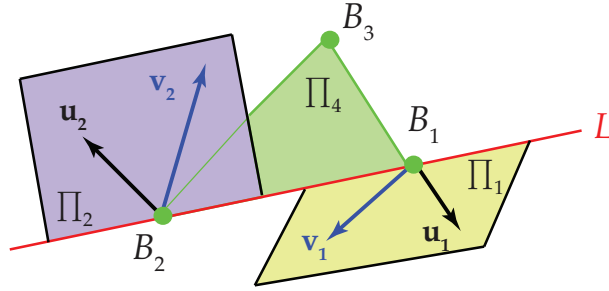


Figure 4.7 – Can two sides and base of the characteristic tetrahedron of the 3-RPS-3-SPR S-PM meet in a line?

must be satisfied and is expressed by the following equations:

$$\begin{aligned} \mathbf{r}_{B_1} \cdot ([w_{02}, \mathbf{w}_2]) &= 0 \implies \\ -2\sqrt{3}c_1c_2f_1 - 2\sqrt{3}c_1f_1f_2 + 3c_1^2f_1 + 3f_1^2c_1 - 3f_2^2c_1 - 3c_2^2f_1 - 3c_1 - 3f_1 &= 0 \end{aligned} \quad (4.34)$$

$$\begin{aligned} \mathbf{r}_{B_2} \cdot ([w_{01}, \mathbf{w}_1]) &= 0 \implies \\ -4\sqrt{3}c_1c_2f_2 - 4\sqrt{3}c_2f_1f_2 + 4c_2c_1f_1 + 4f_2c_1f_1 + c_1\sqrt{3} + \sqrt{3}f_1 - 3c_2 - 3f_2 &= 0 \end{aligned} \quad (4.35)$$

Finding the Groebner basis of the polynomials in Eqs. (4.34) and (4.35) with a graded reverse lexicographic ordering (*tdeg* in Maple) of the parameters  $c_1 <_{grlex} c_2 <_{grlex} f_1 <_{grlex} f_2$ , results in a basis of four polynomials. The four equations can then be solved for  $c_1, c_2, f_1$  and  $f_2$ . Two solutions are obtained, the first one turns out to be a complex solution and the second one is exactly the last case of (4.24). The second solution should also be rejected since it is assumed for this analysis that none of the faces of the characteristic tetrahedron degenerates into a line. Also for other combinations of sides and their intersections with the base plane, the following equations are solved for the parameters:

$$\begin{aligned} \mathbf{r}_{B_2} \cdot ([w_{03}, \mathbf{w}_3]) &= 0 \implies \\ 3c_1^2f_2 - 2c_1c_2f_1 - 2c_1f_1f_2 - 3c_2^2f_2 + 3c_2f_1^2 - 3c_2f_2^2 + 3c_2 + 3f_2 &= 0 \end{aligned} \quad (4.36)$$

$$\begin{aligned} \mathbf{r}_{B_3} \cdot ([w_{02}, \mathbf{w}_2]) &= 0 \implies \\ c_1^2f_1 - 2c_1c_2f_2 + c_1f_1^2 - c_1f_2^2 - c_2^2f_1 - 2c_2f_1f_2 + c_1 + f_1 &= 0 \end{aligned} \quad (4.37)$$

$$\begin{aligned} \mathbf{r}_{B_1} \cdot ([w_{03}, \mathbf{w}_3]) &= 0 \implies \\ -4\sqrt{3}c_1c_2f_2 - 4\sqrt{3}c_2f_1f_2 - 4c_1c_2f_1 - 4c_1f_1f_2 + c_1\sqrt{3} + \sqrt{3}f_1 + 3c_2 + 3f_2 &= 0 \end{aligned} \quad (4.38)$$

$$\begin{aligned} \mathbf{r}_{B_3} \cdot ([w_{01}, \mathbf{w}_1]) &= 0 \implies \\ 2\sqrt{3}c_1c_2f_1 + 2\sqrt{3}c_1f_1f_2 + 3c_1^2f_1 + 3c_1f_1^2 - 3c_1f_2^2 - 3c_2^2f_1 - 3c_1 - 3f_1 &= 0 \end{aligned} \quad (4.39)$$

In each case, the solutions obtained are either complex or correspond to the last case of (4.24), showing that the S-PM at hand cannot have a configuration in which any two sides and the base of its characteristic tetrahedron meet in a line.

Another approach to solve this case is by finding the condition for incidence of an intersection line between two sides and the base [PW01]:

$$L_{ij} : (\mathbf{l}_{ij}, \bar{\mathbf{l}}_{ij}) = (\mathbf{w}_i \times \mathbf{w}_j, w_{0i}\mathbf{w}_j - w_{0j}\mathbf{w}_i) \quad (4.40)$$

$$\Pi_4 \wedge L_{ij} = 0 : \mathbf{w}_4 \cdot \mathbf{l}_{ij} = 0, \quad -w_{03}\mathbf{l}_{ij} + \mathbf{w}_4 \times \bar{\mathbf{l}}_{ij} = 0, \quad i = 1, 2, 3 \quad (4.41)$$

Equation (4.41) does not yield any real or non-trivial solutions. As a result, it is proved by contradiction that the 3-RPS-3-SPR S-PM cannot have a serial singular configuration in which any two sides and the base of the characteristic tetrahedron meet in a line.

**Cases 4 and above** The remaining cases in Table 1 of [EULL02] include two sides meet in a plane, one side and base meet in a plane, two sides and base meet in a plane, two faces meet in a plane. Since the S-PM cannot attain a configuration of Case 3, it is certain that it cannot reach any configuration corresponding to the remaining cases. For example, if two sides could meet in a plane, this case should have appeared as a solution to Eqs. (4.34) and (4.35) and in which case, there definitely would have existed a line of intersection between the meeting plane and the base.

To this end, all possible serial singularities are listed in Tab. 4.1

Geometrical condition	Algebraic expression	Instantaneous <i>dof</i>	An example configuration
<b>Parallel revolute joints</b>			
i. ${}^0\mathbf{u}_1 \parallel {}^0\mathbf{v}_1$	$c_1 = 0, f_1 = 0$	5	Fig. 4.3a
ii. ${}^0\mathbf{u}_2 \parallel {}^0\mathbf{v}_2$	$c_1 = -\sqrt{3}c_2, f_1 = -\sqrt{3}f_2$	5	Fig. 4.3b
iii. ${}^0\mathbf{u}_3 \parallel {}^0\mathbf{v}_3$	$c_1 = \sqrt{3}c_2, f_1 = \sqrt{3}f_2$	5	Fig. 4.3c
iv. parallel base and platform (platform pure translation) ${}^0\mathbf{u}_i \parallel {}^0\mathbf{v}_i \quad \forall i = 1, 2, 3$	$c_1 = -f_1, c_2 = -f_2$	3	Fig. 4.3d
<b>Degeneracy of the characteristic tetrahedron [EULL02]</b>			
v. 4 faces meet in a point (general linear complex [Mer89])			
a. a real point	$p^7(c_1, c_2, f_1, f_2) = 0$ (Eq. (4.26))	5	Fig. 4.5a
b. a point at infinity	$c_1 = -\frac{f_1}{f_1^2 + f_2^2}, c_2 = -\frac{f_2}{f_1^2 + f_2^2}$	5	Fig. 4.5b
vi. 3 sides meet in a line (special linear complex)			
a. a real line	$c_1 f_1 + c_2 f_2 - 1 = 0$	5	Fig. 4.6a
b. a line at infinity parallel base and platform (rotation about $z_0$ -axis)	$c_1 = \frac{f_1}{f_1^2 + f_2^2}, c_2 = \frac{f_2}{f_1^2 + f_2^2}$	5	Fig. 4.6b

Table 4.1 – Enumeration of serial singularities for the 3-RPS-3-SPR S-PM

It is recalled here that the singularity analysis performed in this section is by considering both modules in the operation mode corresponding to  $c_3 = f_3 = 0$ . In fact, there are three

other possibilities,  $c_0 = f_0 = 0$ ,  $c_0 = f_3 = 0$  and  $c_3 = f_0 = 0$ . For these cases, the algebraic expressions for serial singularities can be obtained by the following replacements to the ones listed in Tab. 4.1. These replacements hold true only for the orientation parameters. Favorably, the serial singular configurations for  $f_3 = c_3 = 0$  expressed in Tab. 4.1 are only functions of orientation parameters  $c_i, f_i, i = 1, 2$  as shown below:

$$\begin{aligned}
\text{Case } a. \quad & c_3 = f_3 = 0 : \text{Listed in Tab. 4.1} \\
\text{Case } b. \quad & c_0 = f_0 = 0 : f_2 \rightarrow -f_1, f_1 \rightarrow f_2, c_1 \rightarrow -c_2, c_2 \rightarrow c_1 \\
\text{Case } c. \quad & c_0 = f_3 = 0 : c_1 \rightarrow -c_2, c_2 \rightarrow c_1 \\
\text{Case } d. \quad & c_0 = f_3 = 0 : f_2 \rightarrow -f_1, f_1 \rightarrow f_2
\end{aligned} \tag{4.42}$$

*Proof:* For the 3-RPS ( $f_i, i = 0, 1, 2, 3$ ) and the 3-SPR ( $c_i, i = 0, 1, 2, 3$ ) parallel manipulator modules, the orientation Study parameters can be expressed in terms of the *Tilt and Torsion* angles [BZG02], azimuth ( $\phi$ ), tilt ( $\theta$ ) and torsion ( $\sigma$ ) as follows:

$$\begin{aligned}
f_0 &= \cos\left(\frac{\theta_1}{2}\right) \cos\left(\frac{\sigma_1}{2}\right) & c_0 &= \cos\left(\frac{\theta_2}{2}\right) \cos\left(\frac{\sigma_2}{2}\right) \\
f_1 &= \sin\left(\frac{\theta_1}{2}\right) \cos\left(\phi_1 - \frac{\sigma_1}{2}\right) & c_1 &= -\sin\left(\frac{\theta_2}{2}\right) \cos\left(\phi_2 - \frac{\sigma_2}{2}\right) \\
f_2 &= \sin\left(\frac{\theta_1}{2}\right) \sin\left(\phi_1 - \frac{\sigma_1}{2}\right) & c_2 &= -\sin\left(\frac{\theta_2}{2}\right) \sin\left(\phi_2 - \frac{\sigma_2}{2}\right) \\
f_3 &= \cos\left(\frac{\theta_1}{2}\right) \sin\left(\frac{\sigma_1}{2}\right) & c_3 &= -\cos\left(\frac{\theta_2}{2}\right) \sin\left(\frac{\sigma_2}{2}\right)
\end{aligned} \tag{4.43}$$

The operation mode  $c_0 = 0$  or  $f_0 = 0$  renders the torsion angle  $\sigma_1 = 0$  or  $\sigma_2 = 0$  and if  $f_3 = 0$  or  $c_3 = 0$ ,  $\sigma_1 = 180^\circ$  or  $\sigma_2 = 180^\circ$ , respectively. Furthermore, if, for instance in the operation mode corresponding to  $f_0 = 0$ , the 3-RPS PM can never have  $f_3 = 0$ , thus the parameters  $f_i, i = 0, 1, 2, 3$  can be normalized by forcing  $f_3 = 1$ . Consequently, the operation modes (OM) as functions of tilt and azimuth angles can be represented for each module as follows:

<p>3-RPS OM-1</p> $ \begin{aligned} f_0 &= 1 \\ f_1 &= \tan\left(\frac{\theta_1}{2}\right) \cos(\phi_1) \\ f_2 &= \tan\left(\frac{\theta_1}{2}\right) \sin(\phi_1) \\ f_3 &= 0 \end{aligned} $	<p>3-SPR OM-1</p> $ \begin{aligned} c_0 &= 1 \\ c_1 &= -\tan\left(\frac{\theta_2}{2}\right) \cos(\phi_2) \\ c_2 &= -\tan\left(\frac{\theta_2}{2}\right) \sin(\phi_2) \\ c_3 &= 0 \end{aligned} $
<p>3-RPS OM-2</p> $ \begin{aligned} f_0 &= 0 \\ f_1 &= \tan\left(\frac{\theta_1}{2}\right) \sin(\phi_1) \\ f_2 &= -\tan\left(\frac{\theta_1}{2}\right) \cos(\phi_1) \\ f_3 &= 1 \end{aligned} $	<p>3-SPR OM-2</p> $ \begin{aligned} c_0 &= 0 \\ c_1 &= -\tan\left(\frac{\theta_2}{2}\right) \sin(\phi_2) \\ c_2 &= \tan\left(\frac{\theta_2}{2}\right) \cos(\phi_2) \\ c_3 &= 1 \end{aligned} $

(4.44)

Thus, it is obvious that for the 3-RPS PM, algebraic expressions in OM-2 can be obtained from those in OM-1 replacing  $f_2$  by  $-f_1$  and  $f_1$  by  $f_2$ . For the 3-SPR PM, these replacements will be

$c_2$  by  $c_1$  and  $c_1$  by  $-c_2$ . Accordingly, all the serial singular configurations of the 3-RPS-3-SPR PM can be enumerated starting from *Case a* (where both modules are in OM-1) of Eq. (4.42).

#### 4.4 Direct Kinematics Model(DKM)

The six prismatic joints of the 3-RPS-3-SPR S-PM are assumed to be actuated. The direct kinematics model gives the pose, i.e., the position and orientation, of the moving platform for given prismatic joint lengths. For the 3-RPS and the 3-SPR PMs, the prismatic joint lengths are named  $p_1, p_2, p_3$  and  $q_1, q_2, q_3$ , respectively. If Study parameters  $x_0, x_1, x_2, x_3, y_0, y_1, y_2$  and  $y_3$  represent the pose of the moving platform relative to the base, the direct kinematics problem aims to find  $x_i$  and  $y_i$ ,  $i = 0, 1, 2, 3$  given  $p_j$  and  $q_j$ ,  $j = 1, 2, 3$ .

As mentioned in Sec. 4.2, the transformation matrix between the fixed base and the moving platform,  $\mathbf{T}$  is determined to be a function of  $f_1, f_2, g_1, c_1, c_2$  and  $d_1$  for the case  $c_3 = f_3 = 0$ . Therefore, the sphere constraint equations [Sch+14] for each module after factoring out the non-zero terms are expressed as follows:

$$\begin{aligned} \|\mathbf{0} \mathbf{r}_{B_i} - \mathbf{0} \mathbf{r}_{A_i}\|^2 &= p_i^2 \quad i = 1, 2, 3 \implies \\ S_1 &:= \left(-p_1^2 + h_0^2 - 4h_0h_1 + 4h_1^2\right) f_1^4 f_2^2 + 4f_1^4 g_1^2 + 4h_1 f_1^4 g_1 + h_1^2 f_1^4 \\ &\quad + (-2p_1^2 + 2h_0^2 - 8h_1^2) f_1^2 f_2^4 + 8f_1^2 f_2^2 g_1^2 - 8h_1 f_1^2 f_2^2 g_1 + (-2p_1^2 \\ &\quad + 2h_0^2 - 6h_0h_1 - 2h_1^2) f_1^2 f_2^2 + 8f_1^2 g_1^2 + 4h_1 f_1^2 g_1 + (-p_1^2 + h_0^2 \\ &\quad + 4h_0h_1 + 4h_1^2) f_2^6 + 4f_2^4 g_1^2 - 12h_1 f_2^4 g_1 + (-2p_1^2 + 2h_0^2 + 2h_0h_1 \\ &\quad + 5h_1^2) f_2^4 + 8f_2^2 g_1^2 - 12h_1 f_2^2 g_1 + \left(-p_1^2 + h_0^2 - 2h_0h_1 + h_1^2\right) f_2^2 \\ &\quad + 4g_1^2 = 0 \end{aligned} \tag{4.45a}$$

$$\begin{aligned} S_2 &:= \left(4h_0^2 + 8h_0h_1 + 4h_1^2 - 4p_2^2\right) f_1^4 f_2^2 + 16f_1^4 g_1^2 + 16h_1 f_1^4 g_1 + 4h_1^2 f_1^4 \\ &\quad + \left(16\sqrt{3}h_0h_1 + 16\sqrt{3}h_1^2\right) f_1^3 f_2^3 + 16\sqrt{3}f_1^3 f_2 g_1 h_1 + 8\sqrt{3}f_1^3 f_2 h_1^2 \\ &\quad + \left(8h_0^2 + 40h_1^2 - 8p_2^2\right) f_1^2 f_2^4 + 32f_1^2 f_2^2 g_1^2 + 16h_1 f_1^2 f_2^2 g_1 + (8h_0^2 \\ &\quad + 4h_1^2 - 8p_2^2) f_1^2 f_2^2 + 32f_1^2 g_1^2 + 16h_1 f_1^2 g_1 + (16\sqrt{3}h_0h_1 \\ &\quad - 16\sqrt{3}h_1^2) f_1 f_2^5 + 16\sqrt{3}f_1 f_2^3 g_1 h_1 + \left(16\sqrt{3}h_0h_1 - 16\sqrt{3}h_1^2\right) f_1 f_2^3 \\ &\quad + 16\sqrt{3}f_1 f_2 g_1 h_1 + \left(4h_0^2 - 8h_0h_1 + 4h_1^2 - 4p_2^2\right) f_2^6 + 16f_2^4 g_1^2 \\ &\quad + \left(8h_0^2 - 16h_0h_1 + 8h_1^2 - 8p_2^2\right) f_2^4 + 32f_2^2 g_1^2 + (4h_0^2 - 8h_0h_1 \\ &\quad + 4h_1^2 - 4p_2^2) f_2^2 + 16g_1^2 = 0 \end{aligned} \tag{4.45b}$$

$$\begin{aligned} S_3 &:= \left(4h_0^2 + 8h_0h_1 + 4h_1^2 - 4p_3^2\right) f_1^4 f_2^2 + 16f_1^4 g_1^2 + 16h_1 f_1^4 g_1 + 4h_1^2 f_1^4 \\ &\quad + \left(-16\sqrt{3}h_0h_1 - 16\sqrt{3}h_1^2\right) f_1^3 f_2^3 - 16\sqrt{3}f_1^3 f_2 g_1 h_1 - 8\sqrt{3}f_1^3 f_2 h_1^2 \\ &\quad + \left(8h_0^2 + 40h_1^2 - 8p_3^2\right) f_1^2 f_2^4 + 32f_1^2 f_2^2 g_1^2 + 16h_1 f_1^2 f_2^2 g_1 + (8h_0^2 \\ &\quad + 4h_1^2 - 8p_3^2) f_1^2 f_2^2 + 32f_1^2 g_1^2 + 16h_1 f_1^2 g_1 + (-16\sqrt{3}h_0h_1 \\ &\quad + 16\sqrt{3}h_1^2) f_1 f_2^5 - 16\sqrt{3}f_1 f_2^3 g_1 h_1 + \left(-16\sqrt{3}h_0h_1 + 16\sqrt{3}h_1^2\right) f_1 f_2^3 \\ &\quad - 16\sqrt{3}f_1 f_2 g_1 h_1 + \left(4h_0^2 - 8h_0h_1 + 4h_1^2 - 4p_3^2\right) f_2^6 + 16f_2^4 g_1^2 \end{aligned}$$



$$\begin{aligned}
& + (8h_0^2 - 16h_0h_1 + 8h_1^2 - 8p_3^2) f_2^4 + 32 f_2^2 g_1^2 + (4h_0^2 - 8h_0h_1 \\
& + 4h_1^2 - 4p_3^2) f_2^2 + 16g_1^2 = 0
\end{aligned} \tag{4.45c}$$

$$\|{}^0\mathbf{r}_{C_i} - {}^0\mathbf{r}_{B_i}\|^2 = q_i^2 \quad i = 1, 2, 3 \implies$$

$$\begin{aligned}
S_4 := & (4h_1^2 - 4h_1h_2 + h_2^2 - q_1^2) c_1^4 c_2^2 + 4c_1^4 d_1^2 - 4c_1^4 d_1 h_1 + c_1^4 h_1^2 \\
& + (-8h_1^2 + 2h_2^2 - 2q_1^2) c_1^2 c_2^4 + 8c_1^2 c_2^2 d_1^2 + 8c_1^2 c_2^2 d_1 h_1 + (-2h_1^2 \\
& - 6h_1h_2 + 2h_2^2 - 2q_1^2) c_1^2 c_2^2 + 8c_1^2 d_1^2 - 4c_1^2 d_1 h_1 + (4h_1^2 + 4h_1h_2 \\
& + h_2^2 - q_1^2) c_2^6 + 4c_2^4 d_1^2 + 12c_2^4 d_1 h_1 + (5h_1^2 + 2h_1h_2 + 2h_2^2 \\
& - 2q_1^2) c_2^4 + 8c_2^2 d_1^2 + 12c_2^2 d_1 h_1 + (h_1^2 - 2h_1h_2 + h_2^2 - q_1^2) c_2^2 \\
& + 4d_1^2 = 0
\end{aligned} \tag{4.46a}$$

$$\begin{aligned}
S_5 := & (h_1^2 + 2h_1h_2 + h_2^2 - q_2^2) c_1^4 c_2^2 + 4c_1^4 d_1^2 - 4c_1^4 d_1 h_1 + c_1^4 h_1^2 \\
& + (4\sqrt{3}h_1^2 + 4\sqrt{3}h_1h_2) c_1^3 c_2^3 - 4\sqrt{3}c_1^3 c_2 d_1 h_1 + 2\sqrt{3}c_1^3 c_2 h_1^2 \\
& + (10h_1^2 + 2h_2^2 - 2q_2^2) c_1^2 c_2^4 + 8c_1^2 c_2^2 d_1^2 - 4c_1^2 c_2^2 d_1 h_1 + (h_1^2 \\
& + 2h_2^2 - 2q_2^2) c_1^2 c_2^2 + 8c_1^2 d_1^2 - 4c_1^2 d_1 h_1 + (-4\sqrt{3}h_1^2 \\
& + 4\sqrt{3}h_1h_2) c_1 c_2^5 - 4\sqrt{3}c_1 c_2^3 d_1 h_1 + (-4\sqrt{3}h_1^2 + 4\sqrt{3}h_1h_2) c_1 c_2^3 \\
& - 4\sqrt{3}c_1 c_2 d_1 h_1 + (h_1^2 - 2h_1h_2 + h_2^2 - q_2^2) c_2^6 + 4c_2^4 d_1^2 + (2h_1^2 \\
& - 4h_1h_2 + 2h_2^2 - 2q_2^2) c_2^4 + 8c_2^2 d_1^2 + (h_1^2 - 2h_1h_2 + h_2^2 - q_2^2) c_2^2 \\
& + 4d_1^2 = 0
\end{aligned} \tag{4.46b}$$

$$\begin{aligned}
S_6 := & (-h_1^2 - 2h_1h_2 - h_2^2 + q_3^2) c_1^4 c_2^2 - 4c_1^4 d_1^2 + 4c_1^4 d_1 h_1 - c_1^4 h_1^2 \\
& + (4\sqrt{3}h_1^2 + 4\sqrt{3}h_1h_2) c_1^3 c_2^3 - 4\sqrt{3}c_1^3 c_2 d_1 h_1 + 2\sqrt{3}c_1^3 c_2 h_1^2 \\
& + (-10h_1^2 - 2h_2^2 + 2q_3^2) c_1^2 c_2^4 - 8c_1^2 c_2^2 d_1^2 + 4c_1^2 c_2^2 d_1 h_1 + (-h_1^2 \\
& - 2h_2^2 + 2q_3^2) c_1^2 c_2^2 - 8c_1^2 d_1^2 + 4c_1^2 d_1 h_1 + (-4\sqrt{3}h_1^2 \\
& + 4\sqrt{3}h_1h_2) c_1 c_2^5 - 4\sqrt{3}c_1 c_2^3 d_1 h_1 + (-4\sqrt{3}h_1^2 + 4\sqrt{3}h_1h_2) c_1 c_2^3 \\
& - 4\sqrt{3}c_1 c_2 d_1 h_1 + (-h_1^2 + 2h_1h_2 - h_2^2 + q_3^2) c_2^6 - 4c_2^4 d_1^2 + (-2h_1^2 \\
& + 4h_1h_2 - 2h_2^2 + 2q_3^2) c_2^4 - 8c_2^2 d_1^2 + (-h_1^2 + 2h_1h_2 - h_2^2 + q_3^2) c_2^2 \\
& - 4d_1^2 = 0
\end{aligned} \tag{4.46c}$$

By substituting the prismatic joint lengths  $p_i$  and  $q_i$ , Eqs. (4.45a) to (4.46c) can be solved for the parameters  $f_1, f_2, g_1, c_1, c_2$  and  $d_1$ . Since each module can have up to eight direct kinematics solutions [Sch+14; Nay+17b] in each operation mode, the 3-RPS-3-SPR S-PM can have up to 64 solutions for its direct kinematics problem in each case of Eq. (4.42). The transformation matrix between the fixed frame  $\mathcal{F}_0$  and the moving platform frame  $\mathcal{F}_2$  is established as  $\mathbf{T}$  in Sec. 4.2. By expressing this matrix in dual quaternion form or mapping it to a point in  $\mathbb{P}^7$  leads to the representation of the S-PM at hand in terms of the orientation Study parameters

$x_i$ ,  $i = 0, 1, 2, 3$  as follows:

$$\begin{bmatrix} x_0 \\ x_1 \\ x_2 \\ x_3 \end{bmatrix} = \begin{bmatrix} c_1 f_1 + c_2 f_2 - 1 \\ -c_1 - f_1 \\ -c_2 - f_2 \\ c_1 f_2 - c_2 f_1 \end{bmatrix} \quad (4.47)$$

The expressions for the translational Study parameters  $y_i$ ,  $i = 0, 1, 2, 3$  as functions of  $f_1, f_2, g_1, c_1, c_2$  and  $d_1$  are shown in the Appendix of [NCW18c]. Note that every term in the right-hand side of Eq. (4.47) is divided by  $c_1 f_1 + c_2 f_2 - 1 \neq 0$ . The case  $c_1 f_1 + c_2 f_2 - 1 = 0$  is a particular singularity condition identified as the case vi. a. in Table 4.1. It is easy to verify from Eq. (4.47) and the expressions of  $y_i$  that the Study parameters  $x_i, y_i$ ,  $i = 0, 1, 2, 3$  satisfy the Study's quadric equation:

$$x_0 y_0 + x_1 y_1 + x_2 y_2 + x_3 y_3 = 0 \quad (4.48)$$

The Plücker coordinates ( $p_{01}, p_{02}, p_{03}, p_{23}, p_{31}, p_{12}$ ) of the corresponding *Finite Screw Axis* (FSA) are given by [Wei35]

$$\begin{aligned} p_{01} &= (-x_1^2 - x_2^2 - x_3^2)x_1, & p_{23} &= x_0 y_0 x_1 - (-x_1^2 - x_2^2 - x_3^2)y_1 \\ p_{02} &= (-x_1^2 - x_2^2 - x_3^2)x_2, & p_{31} &= x_0 y_0 x_2 - (-x_1^2 - x_2^2 - x_3^2)y_2 \\ p_{03} &= (-x_1^2 - x_2^2 - x_3^2)x_3, & p_{12} &= x_0 y_0 x_3 - (-x_1^2 - x_2^2 - x_3^2)y_3 \end{aligned} \quad (4.49)$$

The following conclusions are drawn from Eqs. (4.47) and (4.49):

- $x_0 = 0$  implies that the transformation is a finite screw motion [Sch+14] with an angle of  $180^\circ$ , also called as a  $\pi$  screw by Study. It corresponds to the singularity condition vi. a. in Tab. 4.1.
- $x_1 = x_2 = 0$  makes  $p_{01} = p_{02} = 0$ , implying that the direction of the FSA is vertical. It corresponds to the singularity condition iv. in Tab. 4.1 where the platform and the base are parallel to each other.
- $x_3 = 0$  makes  $p_{03} = 0$ , implying that the FSA is parallel to the  $x_0 y_0$  plane. In this case,  $c_1 f_2 = c_2 f_1$ . If  $c_1 = 0$ , then it corresponds to the singular configuration i. in Tab. 4.1.

In fact, the direct kinematics problem is solved by first calculating the parameters  $f_1, f_2, g_1, c_1, c_2, d_1$  and then finding the Study parameters  $x_i, y_i$ ,  $i = 0, 1, 2, 3$  of the whole series-parallel manipulator. To derive six equations in input prismatic joint lengths  $p_j, q_j$ ,  $j = 1, 2, 3$  and output Study parameters  $x_i, y_i$ ,  $i = 0, 1, 2, 3$  is algebraically cumbersome and is still an open problem.

## 4.5 Inverse Kinematics Model (IKM)

The inverse kinematics problem of the manipulator under study aims at finding the prismatic joint lengths as functions of the moving platform pose. Given the Study parameters,  $x_i, y_i$ ,  $i = 0, 1, 2, 3$  representing the transformation between the moving platform and the fixed base, the prismatic joint lengths  $p_j, q_j$ ,  $j = 1, 2, 3$  must be determined. In other words, given points  $C_i$  and  $A_i$ , point  $B_i$ ,  $i = 1, 2, 3$  (refer Fig. 4.1) must be determined.

Let the given transformation matrix between the fixed frame  $\mathcal{F}_0$  and the moving platform frame  $\mathcal{F}_2$  be  $\mathbf{M}$ . Thus, the coordinates of point  $C_i$  expressed in  $\mathcal{F}_2$  as shown in Eq. (4.13) can be represented in  $\mathcal{F}_0$  as  ${}^0\mathbf{r}_{C_i} = \mathbf{M}^2 \mathbf{r}_{C_i}$ . Let the homogeneous coordinates of point  $B_i$  expressed in coordinate frame  $\mathcal{F}_0$  be  ${}^0\mathbf{r}_{B_i} = [1, Bx_i, By_i, Bz_i]$ . The homogeneous coordinates of planes  $\alpha_i$

and  $\beta_i$  shown in Fig. 4.1 are:

$$\begin{aligned}\alpha_i &: [-\mathbf{r}_{A_i}^T \mathbf{u}_i, \mathbf{u}_i^T] \\ \beta_i &: [-\mathbf{r}_{C_i}^T \mathbf{v}_i, \mathbf{v}_i^T]\end{aligned}$$

where all the vectors are expressed in frame  $\mathcal{F}_0$ . To determine the points  $B_i$ , the constraints to be respected are: point  $B_i$  must lie in the plane  $\alpha_i$  and  $\beta_i$  simultaneously and the distance between points  $B_i$  and  $B_j$ ,  $i \neq j = 1, 2, 3$  must be equal to the side length of the coupler triangular platform,  $\sqrt{3}h_1$ ,  $h_1$  being the circum-radius. Three constraints in each leg lead to a total of nine algebraic constraint equations:

Point  $B_i$  belongs to plane  $\alpha_i$ :

$$F_1 := By_1 = 0 \quad (4.50)$$

$$F_2 := -\sqrt{3}Bx_2 - By_2 \quad (4.51)$$

$$F_3 := \sqrt{3}Bx_3 - By_3 \quad (4.52)$$

Point  $B_i$  belongs to plane  $\beta_i$ :

$$\begin{aligned}F_4 &:= (-2x_0x_3 + 2x_1x_2)Bx_1 + (x_0^2 - x_1^2 + x_2^2 - x_3^2)By_1 + (2x_0x_1 + \\ &2x_2x_3)Bz_1 + 2x_0y_2 + 2x_1y_3 - 2x_2y_0 - 2x_3y_1 = 0\end{aligned} \quad (4.53)$$

$$\begin{aligned}F_5 &:= (-\sqrt{3}x_0^2 - \sqrt{3}x_1^2 + \sqrt{3}x_2^2 + \sqrt{3}x_3^2 + 2x_0x_3 - 2x_1x_2)Bx_2 + (-2\sqrt{3}x_0x_3 \\ &- 2\sqrt{3}x_1x_2 - x_0^2 + x_1^2 - x_2^2 + x_3^2)By_2 + (2\sqrt{3}x_0x_2 - 2\sqrt{3}x_1x_3 - 2x_0x_1 \\ &- 2x_2x_3)Bz_2 - 2\sqrt{3}x_0y_1 + 2\sqrt{3}x_1y_0 + 2\sqrt{3}x_2y_3 - 2\sqrt{3}x_3y_2 - 2x_0y_2 - 2x_1y_3 \\ &+ 2x_2y_0 + 2x_3y_1 = 0\end{aligned} \quad (4.54)$$

$$\begin{aligned}F_6 &:= (\sqrt{3}x_0^2 + \sqrt{3}x_1^2 - \sqrt{3}x_2^2 - \sqrt{3}x_3^2 + 2x_0x_3 - 2x_1x_2)Bx_3 + (2\sqrt{3}x_0x_3 \\ &+ 2\sqrt{3}x_1x_2 - x_0^2 + x_1^2 - x_2^2 + x_3^2)By_3 + (-2\sqrt{3}x_0x_2 + 2\sqrt{3}x_1x_3 - 2x_0x_1 \\ &- 2x_2x_3)Bz_3 + 2\sqrt{3}x_0y_1 - 2\sqrt{3}x_1y_0 - 2\sqrt{3}x_2y_3 + 2\sqrt{3}x_3y_2 - 2x_0y_2 - 2x_1y_3 \\ &+ 2x_2y_0 + 2x_3y_1\end{aligned} \quad (4.55)$$

$$\|\mathbf{r}_{B_i} - \mathbf{r}_{B_j}\|^2 = 3h_1^2 \quad i \neq j = 1, 2, 3 \implies$$

$$F_7 := (Bx_1 - Bx_2)^2 + (By_1 - By_2)^2 + (Bz_1 - Bz_2)^2 - 3h_1^2 = 0 \quad (4.56)$$

$$F_8 := (Bx_1 - Bx_3)^2 + (By_1 - By_3)^2 + (Bz_1 - Bz_3)^2 - 3h_1^2 = 0 \quad (4.57)$$

$$F_9 := (Bx_2 - Bx_3)^2 + (By_2 - By_3)^2 + (Bz_2 - Bz_3)^2 - 3h_1^2 = 0 \quad (4.58)$$

$F_i$ ,  $i = 1, \dots, 9$  can be solved for the nine parameters  $Bx_j$ ,  $By_j$  and  $Bz_j$ ,  $j = 1, 2, 3$  to further obtain the prismatic joint lengths.

After substituting the Study parameters and the design parameters, a Groebner basis of the constraint polynomials can be obtained over the ring  $\mathbb{C}[h_0, h_1, h_2]$  as a function of  $Bx_j$ ,  $By_j$  and  $Bz_j$ ,  $j = 1, 2, 3$ . A graded reverse lexicographic ordering of these variables results in a univariate polynomial of degree eight in any variable  $Bx_j$ ,  $By_j$  or  $Bz_j$ . It shows that the inverse kinematics problem of the S-PM at hand has a maximum number of eight solutions. This is not surprising because the problem can be considered as placing three points  $B_i$  on three skew lines  $L_i$ ,  $i = 1, 2, 3$ , where  $L_i$  is the line of intersection of planes  $\alpha_i$  and  $\beta_i$  shown in Fig. 4.1. This is a classical geometrical problem and it has been proven [ZMG09] that the maximum number of solutions is indeed eight with a minimal octic univariate polynomial. The interesting feature

of the inverse kinematics of the 3-RPS-3-SPR S-PM is that the univariate polynomial factors into four quadratic polynomials. Further examination reveals that the four factors belong to four different combinations of the operation modes of each module like the four cases shown in Eq. (4.42). Since the transition between two operation modes is a constraint singularity, one of the singularities separating the IKM solutions is a constraint singularity [Sch+14] in each module.

The IKM is solved for an example with Study parameters:  $(x_0 : x_1 : x_2 : x_3 : y_0 : y_1 : y_2 : y_3) = (2.8215 : -1.2912 : -0.3348 : 1.2434 : 2.1837 : 1.1542 : 1.6012 : -3.3256)$ . The design parameters are chosen to be  $h_0 = 2, h_1 = 1, h_2 = 2$ . Eight real solutions to IKM are found as shown in Table 4.2. The corresponding configurations of the S-PM are displayed in Fig. 4.8.

IKM solution	$Bx_1$	$By_1$	$Bz_1$	$Bx_2$	$By_2$	$Bz_2$	$Bx_3$	$By_3$	$Bz_3$
1	1.190	0.0	1.095	0.922	-1.597	1.710	-0.398	-0.689	1.051
2	-0.385	0.0	2.289	-0.049	0.084	3.986	-0.773	-1.339	3.317
3	-0.867	0.0	2.650	0.562	-0.972	2.550	-0.412	-0.712	1.140
4	-1.500	0.0	3.130	0.169	-0.293	3.470	-0.564	-0.976	2.060
5	0.893	0.0	1.320	0.991	-1.710	1.540	-0.517	-0.895	1.780
6	-1.080	0.0	2.810	0.461	-0.797	2.790	-0.841	-1.450	3.720
7	1.210	0.0	1.080	0.724	-1.250	2.170	-0.384	-0.665	0.975
8	-1.600	0.0	3.210	-0.032	0.055	3.940	-0.845	-1.460	3.750

Table 4.2 – Solutions to inverse kinematics of the 3-RPS-3-SPR S-PM when  $h_0 = 2, h_1 = 1, h_2 = 2$  and  $(x_0 : x_1 : x_2 : x_3 : y_0 : y_1 : y_2 : y_3) = (2.822 : -1.291 : -0.335 : 1.243 : 2.184 : 1.154 : 1.601 : -3.326)$ .

Moreover, the operation mode (OM) of each module is mentioned by recalling the cases from Eq. (4.42):

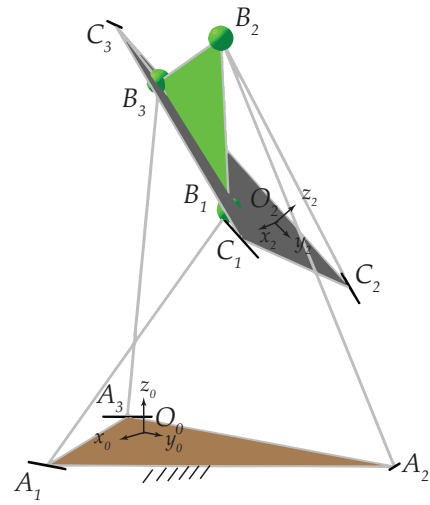
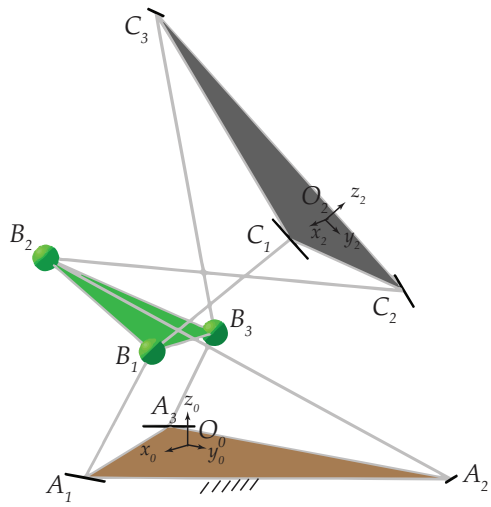
- Case a. (IKM solutions 1 and 2 in Table 4.2)  $c_3 = f_3 = 0 \implies 3\text{-RPS}_{OM1} - 3\text{-SPR}_{OM1}$
- Case b. (IKM solutions 3 and 4 in Table 4.2)  $c_0 = f_0 = 0 \implies 3\text{-RPS}_{OM2} - 3\text{-SPR}_{OM2}$
- Case c. (IKM solutions 5 and 6 in Table 4.2)  $c_0 = f_3 = 0 \implies 3\text{-RPS}_{OM2} - 3\text{-SPR}_{OM1}$
- Case d. (IKM solutions 7 and 8 in Table 4.2)  $c_3 = f_0 = 0 \implies 3\text{-RPS}_{OM1} - 3\text{-SPR}_{OM2}$

There are two inverse kinematic solutions in each of these cases. How these two solutions are separated is still an open issue and is the subject of future work. Figure 4.9 presents the eight solutions to the inverse kinematics problem of the manipulator as eight possibilities to locate the three points,  $B_i$  on three skew lines  $L_i : \alpha_i \wedge \beta_i, i = 1, 2, 3$ .

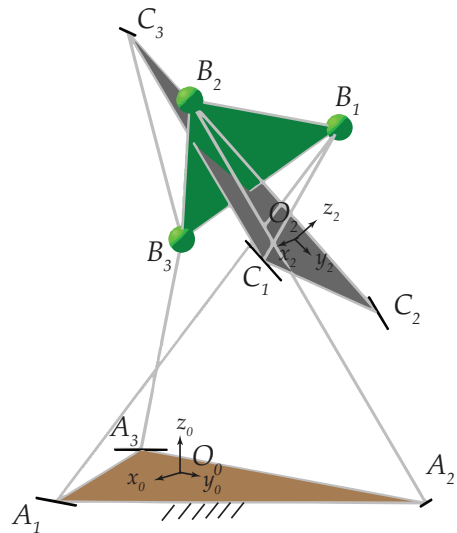
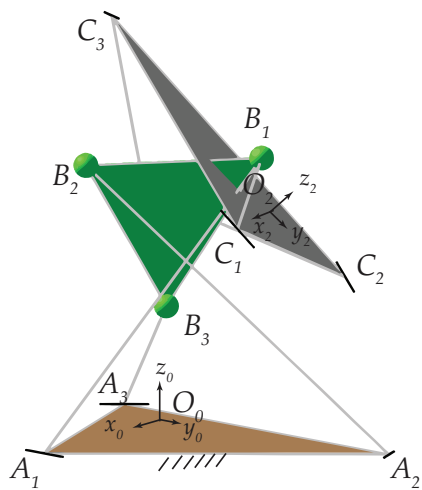
## 4.6 Conclusions

Although the S-PM under study might never see the light of an industrial application, it poses many interesting theoretical problems to be solved especially due to the coupled *dof* of its constituent modules, giving rise to parasitic motions. Moreover, the singularity analysis of this kind of S-PMs is generally ignored in the literature. Therefore, the focus of this chapter was on the determination of its mobility and serial singularities, the latter using an approach that was centered only on PMs.

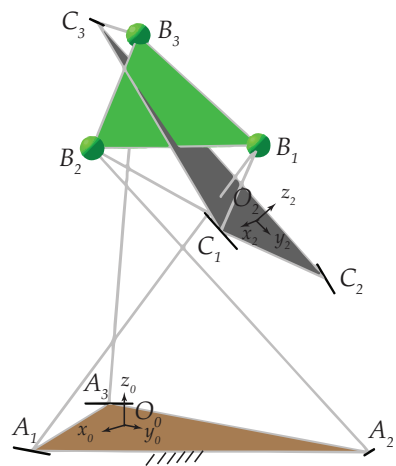
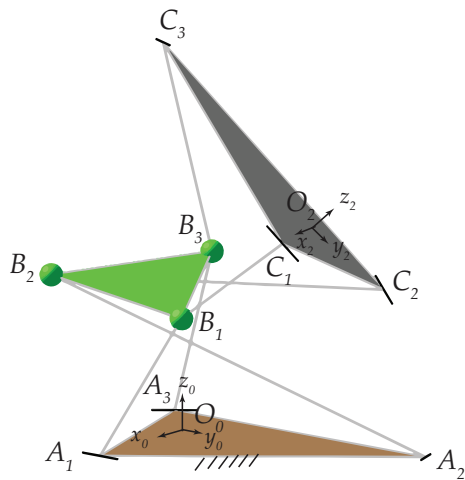
Study parametrization of individual modules of the 3-RPS-3-SPR Series-Parallel Manipulator (S-PM) was used to determine six parameters that characterize the manipulator. The kinematic



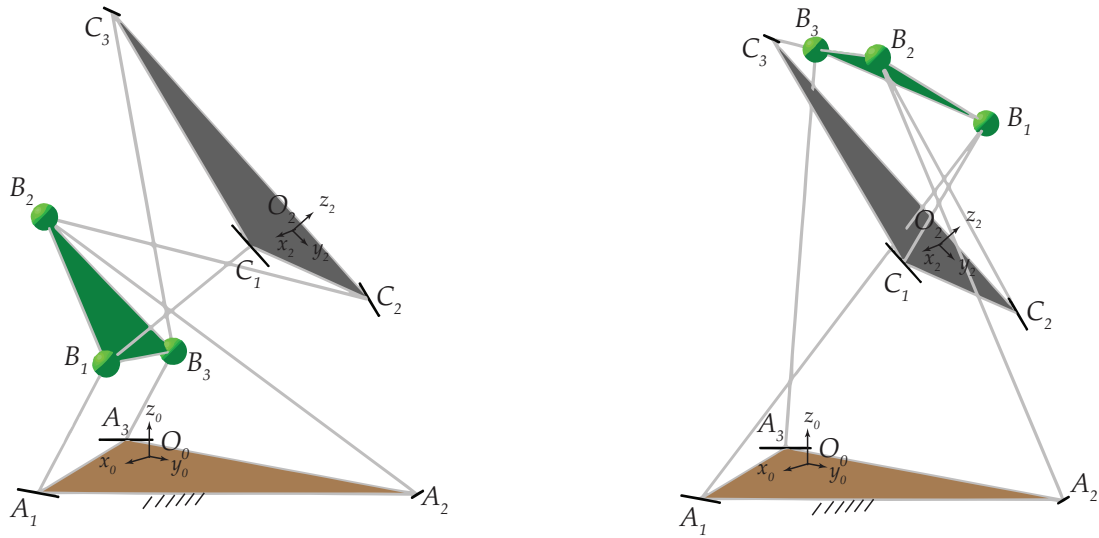
(a) *Case a.*



(b) *Case b.*



(c) *Case c.*



(d) Case d.

Figure 4.8 – Eight inverse kinematic solutions for the 3-RPS-3-SPR S-PM when  $h_0 = 2, h_1 = 1, h_2 = 2$  and  $(x_0 : x_1 : x_2 : x_3 : y_0 : y_1 : y_2 : y_3) = (2.8215 : -1.2912 : -0.3348 : 1.2434 : 2.1837 : 1.1542 : 1.6012 : -3.3256)$ .

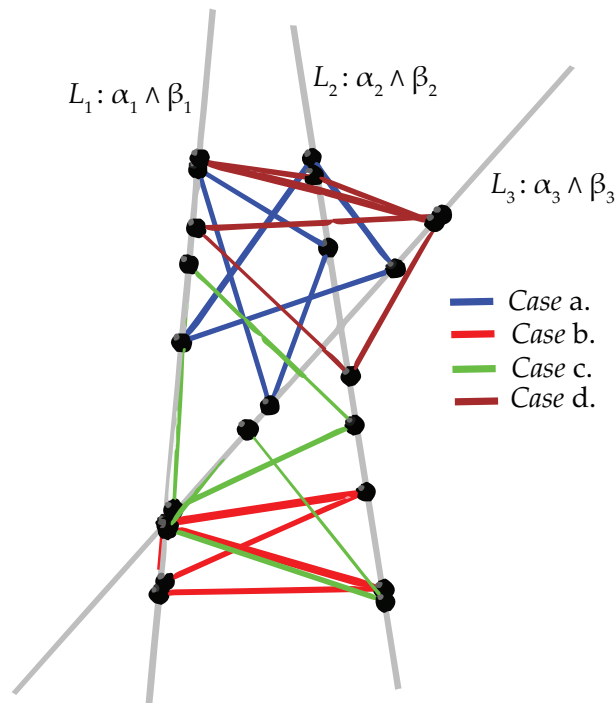


Figure 4.9 – Eight solutions to IKM as locating 3 points on 3 lines problem

Jacobian matrix was derived and can be used to numerically determine whether a manipulator configuration is singular or not. Moreover, the serial singularities that arise due to the stacking of the two parallel modules were enumerated by mapping these singularities to the degeneracy of the characteristic tetrahedron of the S-PM. Both geometric conditions and algebraic expressions for the serial singularities were established and listed in Table 4.1. The Direct Kinematics Model (DKM) of the 3-RPS-3-SPR S-PM was solved to find out that the maximum number of solutions to the DKM was the product of the maximum number of solutions to the DKM of each module. When each module is restricted to lie in one of the operation modes, the maximum number of assembly modes is up to 64. Furthermore, the Inverse Kinematics Model (IKM) was solved to find out that the univariate polynomial splits into four factors based on the operation mode in which each module lies. The maximum number of solutions to the IKM was found to be eight and an example was shown to depict those eight solutions.

## Chapter 5

# Synthesis of compliant mechanisms based on constraint singularities of parallel manipulators

In the context of this doctoral thesis, synthesis through rigid-body displacement is advantageous due to the extensive choice of existing rigid-body mechanisms and their modeling tools. Parallel or closed-loop rigid-body architectures gain an upper hand here as their intrinsic properties favor the characteristics of compliant mechanisms like compactness, symmetry to reduce parasitic motions, low stiffness along the desired degrees of freedom (DOF) and high stiffness in other directions. Moreover, compliant mechanisms usually work around a given position for small range of motions and hence they can be designed by considering existing parallel manipulators in parallel singular configurations. Rubbert *et al.* used an actuation singularity for type-synthesis of a compliant medical device [Rub+14b; Rub+14a].

Another interesting kind of parallel singularity for a parallel manipulator that does not depend on the choice of actuation is a constraint singularity [ZBG02a]. It divides the workspace of a parallel manipulator into different operation modes resulting in a reconfigurable mechanism. Algebraic geometry tools have proved to be efficient in performing global analysis of parallel manipulators and recognizing their operation modes leading to mobility-reconfiguration [Hus+07; Nur+16; He+16]. Though there are abundant reconfigurable rigid-body mechanisms in the literature, the study of reconfigurable compliant mechanisms is limited. Hao studied the mobility and structure reconfiguration of compliant mechanisms [Hao16] while Hao and Li introduced a position-space-based structure reconfiguration (PSR) approach to the reconfiguration of compliant mechanisms and to minimize parasitic motions [HLK16; LH15].

In this chapter, a planar equilateral four-bar linkage is considered at a constraint singularity configuration to synthesize a reconfigurable compliant four-bar mechanism [Nay+17a]. A reconfigurable compliant gripper is further designed that can exhibit multiple grasping modes [Hao+18].

### 5.1 Constraint singularities of an equilateral four-bar mechanism

The operation modes of an equilateral four-bar linkage were determined in Chapter 2 and are shown in Figs. 2.3, 2.4 and 2.5. These operation modes are separated by two similar constraint singularities shown in Fig. 5.1.



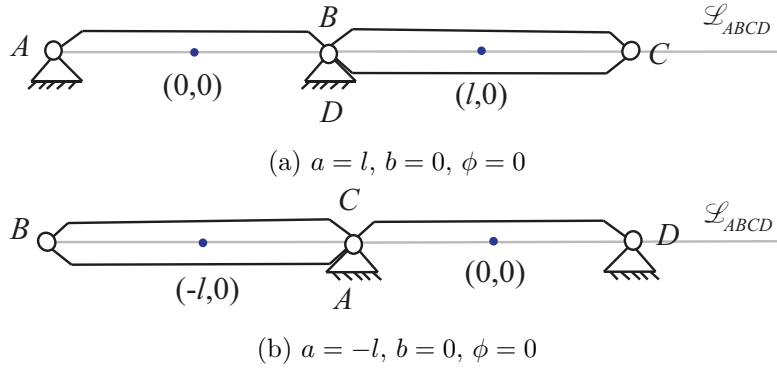


Figure 5.1 – Constraint singularities of the four-bar mechanism.

They can be algebraically represented by  $x_1 = x_3 = 4x_2^2 - l^2x_4^2 = 0$ . From Eqn. (2.4), these singularities occur when  $b = 0$ ,  $\phi = 0$  and  $a = \pm l$ . These two configurations correspond to the two points  $Q_1$  and  $Q_2$  in the image space shown in Fig. 2.2. At a constraint singularity, any mechanism gains one or more degrees of freedom. Therefore, in case of the four-bar linkage with equal link lengths, the DOF at a constraint singularity is equal 2. In this configuration, points  $A$ ,  $B$ ,  $C$  and  $D$  are collinear and the corresponding motion type is a translational motion along the normal to the line  $\mathcal{L}_{ABCD}$  passing through the four points  $A$ ,  $B$ ,  $C$  and  $D$  combined with a rotation about an axis directed along  $z_0$  and passing through  $\mathcal{L}_{ABCD}$ . Eventually, it is noteworthy that two actuators are required in order to control the end-effector in those constraint singularities in order to manage the operation mode changing.

## 5.2 Design and analysis of a compliant four-bar mechanism

In this section, two compliant four-bar mechanisms, compliant four-bar mechanism-1 and compliant four-bar mechanism-2, are proposed based on the operation modes and constraint singularities of the four-bar rigid-body mechanism shown in Fig. 5.1b. Moreover, the desired motion characteristics of the compliant four-bar mechanism-2 are verified by nonlinear FEA simulations.

Based on the constraint singularity configuration of the four-bar rigid-body mechanism represented in Fig. 5.1, a compliant four-bar mechanism can be designed through kinematically replacing the rigid rotational joints with compliant rotational joints [HLK16]. Each of the compliant rotational joints can be any type compliant rotational joint such as cross-spring rotational joint, notch rotational joint and cartwheel rotational joint [How01]. As shown in Fig. 5.2, a compliant four-bar mechanism, termed as the compliant four-bar mechanism-1, has been designed by replacing the four rigid rotational joints with three cross-spring rotational joints (RJ-0, RJ-1 and RJ-3) and one leaf-type isosceles-trapezoidal rotational joint that provides remote rotation centre (RJ-2).

For small motion ranges, the compliant four-bar mechanism-1 has the same operation modes as the four-bar rigid-body mechanism shown in Fig. 5.1, via controlling the rotations of the Bar-1 and Bar-3. Moreover, both the compliant four-bar mechanism-1 and the four-bar rigid-body mechanism are plane motion mechanisms. Additionally, the three cross-spring rotational joints in the compliant four-bar mechanism-1 can be replaced by other types of rotational joints, which can form different compliant four-bar mechanisms. In this paper, cross-spring rotational joints

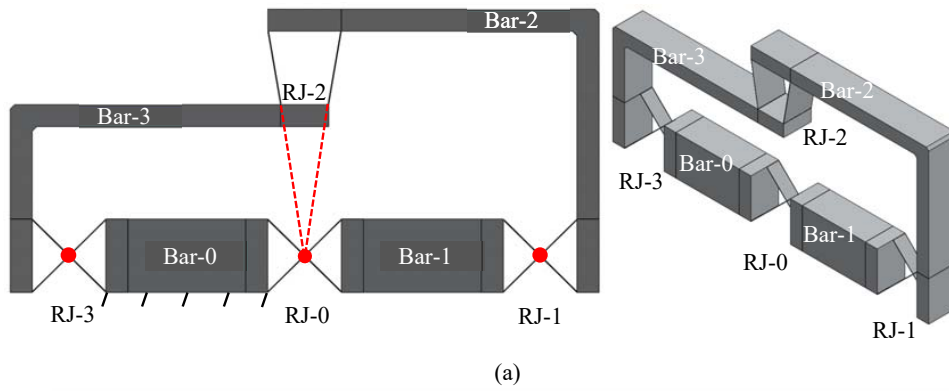


Figure 5.2 – Compliant four-bar mechanism-1.

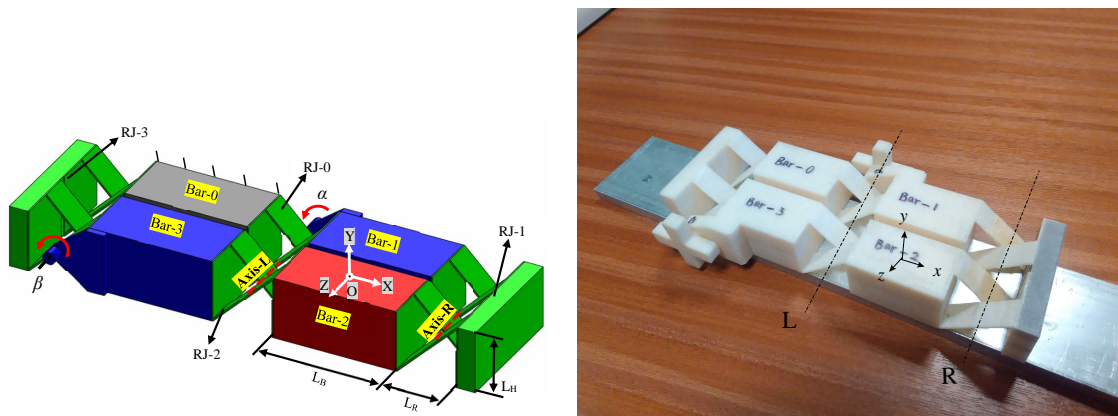


Figure 5.3 – CAD model and prototype of the compliant four-bar mechanism-2.

are employed due to their large motion ranges while small rotation centre shifts. However, the leaf-type isosceles-trapezoidal rotational joint in the compliant four-bar mechanism-1 performs larger rotation centre shifts compared with the cross-spring rotational joint. Therefore, the compliant four-bar mechanism-1 can be improved by replacing the leaf-type isosceles-trapezoidal rotational joint with a cross-spring rotational joint. Such an improved design can be seen in Fig. 5.3, which is termed as the compliant four-bar mechanism-2. Note that, in Fig. 5.3, the RJ-0 and RJ-2, are traditional cross-spring rotational joints, while both the RJ-1 and the RJ-3 are double cross-spring joints introduced in this paper. Each of the rotational joints, RJ-1 and RJ-3, consists of two traditional cross-spring rotational joints in series. We specify that the Bar-0 is fixed to the ground and the Bar-2 is the output motion stage, also named *coupler*. The main body including rigid bars and compliant joints of the proposed compliant four-bar mechanism-2 can be fabricated monolithically using a CNC milling machine. It can also be 3D printed, and a 3D-printed prototype is shown in Fig. 5.3. The bars of the prototype have many small through holes, which can reduce material consumption and improve dynamic performance. Additionally, two cross-shaped parts are added to the actuated bars, which are used to actuate the mechanism by hands. The operation modes of the compliant four-bar mechanism-2 as output stage are analyzed in the following sections.

### 5.2.1 Operation modes of the compliant four-bar mechanism-2

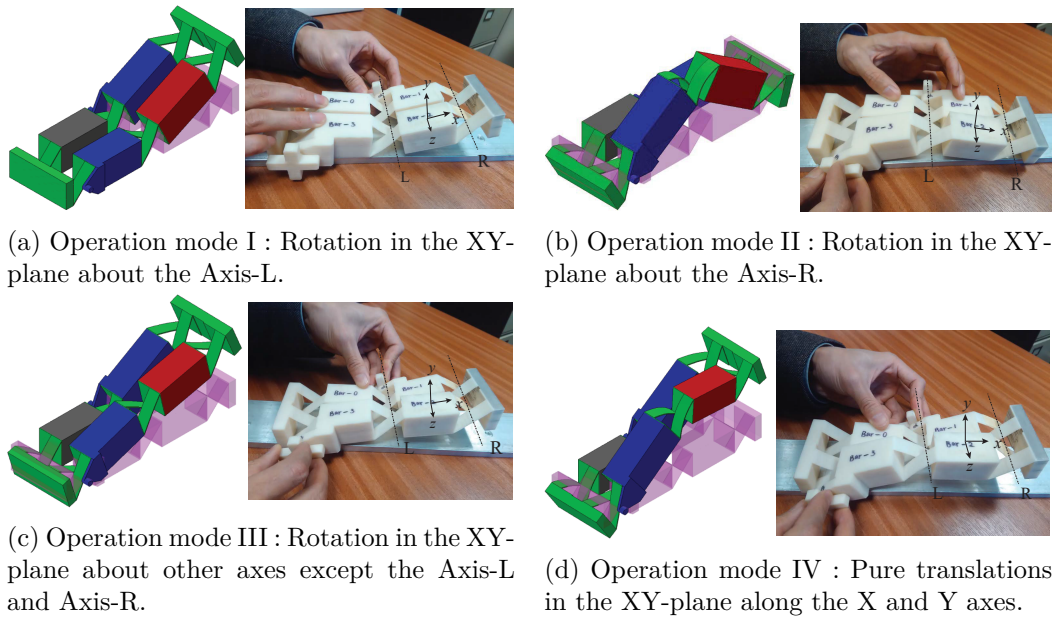


Figure 5.4 – Operation modes of the compliant four-bar mechanism-2.

Like the four-bar rigid-body mechanism shown in Fig. 5.1b, the output motion stage (Bar 2) of the compliant four-bar mechanism-2 has multiple operation modes under two rotational actuations (controlled by input displacements  $\alpha$  and  $\beta$ ), as shown in Fig. 5.3. However, the compliant four-bar mechanism-2 has more operation modes than the rigid counterpart. In order to simplify the analysis, let  $\alpha$  and  $\beta$  be non-negative. A coordinate system is defined in Fig. 5.3, which is located on Bar 2. Based on this assumption, operation modes of the compliant four-bar mechanism-2 are listed below :

1. Operation mode I : Rotation in the XY-plane about the Axis-L, when  $\alpha > 0$  and  $\beta = 0$ , as shown in Fig. 5.4a,
2. Operation mode II : Rotation in the XY-plane about the Axis-R when  $\alpha = 0$  and  $\beta > 0$ , as shown in Fig. 5.4b,
3. Operation mode III : Rotation in the XY-plane about other axes except the Axis-L and Axis-R, when  $\alpha \neq \beta > 0$ , as shown in Fig. 5.4c, and
4. Operation mode IV : Pure translations in the XY-plane along the X- and Y-axes, when  $\alpha = \beta > 0$ , as shown in Fig. 5.4d.

These operation modes are also highlighted through the printed prototype in Fig. 5.4. The primary motions of output motion stage (Bar-2) are the rotation in the XY plane and the translations along the X-and Y-axes; while the rotations in the XZ and YZ planes and translational motion along the Z-axis are the parasitic motions that are not the interest of this paper. Moreover, the rotation angle in the XY-plane and the Y-axis translational motion can be estimated analytically using Eqs. (5.1) and (5.2). However, the X-axis translational motion cannot be accurately estimated in such a simple way, because it is heavily affected by the shift of the rotation centres of the two cross-spring rotational joints [ZBY12]. The X-axis translational motion will be analytically studied in our future work, but will be captured by non-linear FEA.

According to the definition of the location and orientation of the Bar-2 (link BC) with respect to the fixed frame, we can have the primary displacement of the Bar-2 as:

$$\phi = \alpha - \beta \quad (5.1)$$

$$b = \frac{1}{2}(L_B + L_R)(\sin \alpha + \sin \beta) \quad (5.2)$$

where  $\phi$  is the rotation about the Z-axis and  $b$  is the translational displacement along the Y-axis.  $L_B$  and  $L_R$  are the geometrical dimensions of the reconfigurable mechanism at hand, as defined in Fig. 5.3.

Using the assumption of small angles, the displacement of the centre of Bar-2 along the X-axis is normally in the second order of magnitude of the rotational angles, which is trivial and can be neglected in this paper. Note that this trivial displacement is also affected by the centre drift of the compliant rotational joints [ZBY12].

A figure here.

The rotational displacement of each compliant rotational joint is expressed below based on the two input rotational angles:

$$\text{RJ-0 : } \theta_0 = \alpha \quad (5.3a)$$

$$\text{RJ-1 : } \theta_1 = \alpha \quad (5.3b)$$

$$\text{RJ-2 : } \theta_2 = 2\beta - \alpha \quad (5.3c)$$

$$\text{RJ-3 : } \theta_0 = \beta \quad (5.3d)$$

### 5.2.2 Simulations of the operation modes

In order to verify the operation modes of the 4R compliant mechanism-2, nonlinear FEA software is employed to simulate the motions of the compliant four-bar mechanism-2. For the FEA simulations, let  $L_B$  be 100 mm,  $L_R$  and  $L_H$  be 50 mm, the beam thickness be 1 mm, the beam width be 23 mm, the Poisson's ratio be 0.33, and the Young's modulus be 6.9 GPa.

Commercial software, COMSOL MULTIPHYSICS, is selected for the nonlinear FEA simulations, using the 10-node tetrahedral element and finer meshing technology (minimum element size 0.2 mm, curvature factor 0.4, and resolution of narrow regions 0.7). Note that the translational displacements of the Bar-2 along the X and Y axes are measured at the centre point of the top surface of the Bar-2 (termed as the interest point), as shown in Fig. 5.3. Results of the simulations are plotted in Figs. 5.5 to 5.8, and the following conclusions are drawn :

1. The maximum difference between the FEA results and the analytical results in terms of the Y-axis translation of the interest point (the centre of the top surface of the Bar-2) is tiny, which is less than 0.5% as shown in Figs. 5.5a, 5.6a, 5.7a and 5.8a.
2. The FEA results of the rotation in the XY-plane match the analytical results very well. The difference is less than  $0.8 \times 10^{-3}$  rad (0.5% of the maximum rotation angle), which is shown in Figs. 5.5b, 5.6b and 5.7b.
3. It can be seen from Figs. 5.5c, 5.6c, 5.7c, 5.8b and 5.8c that the parasitic motions are much smaller compared with the primary motions, for all the operation modes.

Overall, for all the operation modes of the compliant four-bar mechanism-2, the obtained analytical kinematic models are accurate enough to predict the rotation angle in the XY-plane and the translation displacement along the Y-axis, under specific input actuations. Additionally, the parasitic motions are much smaller than the primary motions, which ensures that the tiny effect of the parasitic motions on the primary motions can be ignored in an acceptable way. Therefore, it has been proved that the compliant four-bar mechanism-2 can be operated in the different operation modes with high accuracy.

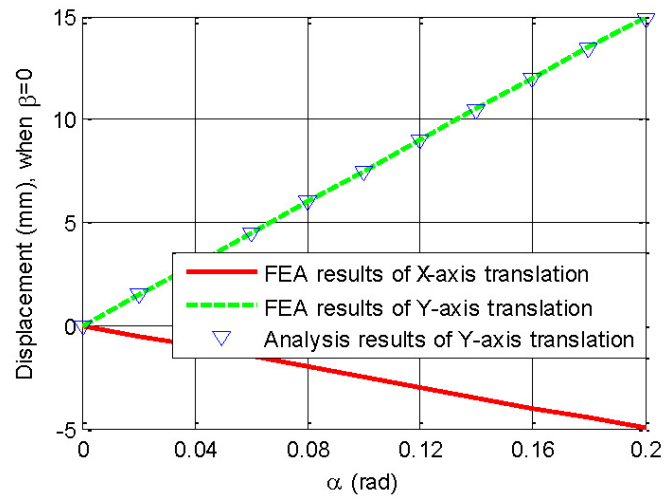
### 5.3 Application as a compliant gripper

The reconfigurable compliant four-bar mechanism-1 shown in Fig. 5.2 is used to design a reconfigurable gripper as shown in Fig. 5.9.

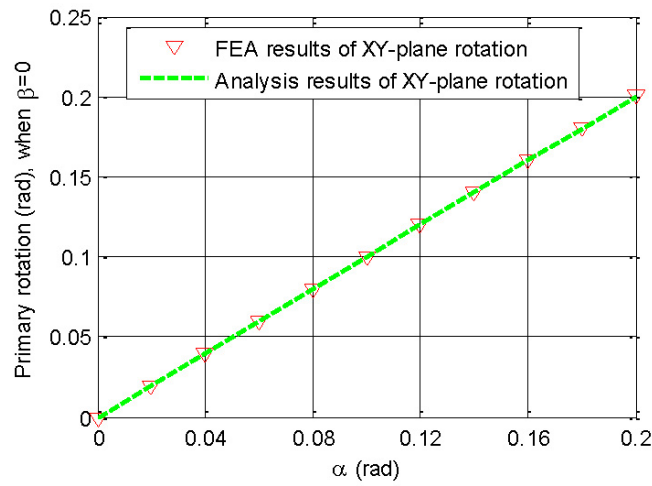
It can exhibit four grasping modes based on the actuation of the linear actuator 1 ( $\pm\alpha$ ) or 2 ( $\pm\beta$ ) as displayed in Fig. 5.11. The first three grasping modes are angular, where the jaws of the gripper rotate about an instantaneous centre of rotation which is different for each grasping mode. The gripper displays an angular grasping mode when  $\alpha \neq 0$ ,  $\beta = 0$  as shown in Fig. 5.11a,  $\alpha = 0$ ,  $\beta \neq 0$  as shown in Fig. 5.11b or when  $\alpha < 0$ ,  $\beta < 0$  as shown in the right Fig. 5.11c. The parallel grasping mode in which the jaws are parallel to one another is achieved when  $\alpha > 0$ ,  $\beta < 0$  as shown in the left Fig. 5.11c. Thus, the reconfigurable compliant gripper at hand unveils an ability to grasp a plethora of shapes unlike other compliant grippers in literature that exhibit only one of these modes of grasping [HH16; HK12]. Potential applications include micromanipulation and grasping lightweight and vulnerable materials like glass, resins, porous composites, etc. in difficult and dangerous environments. In addition, it can be used for medical applications to grasp and manipulate living tissues during surgical operations or as a gripper mounted on a parallel manipulator dedicated to fast and accurate pick-and-place operations. Figure 5.10 shows the prototype of the reconfigurable compliant gripper.

#### 5.3.1 Gripper design 2

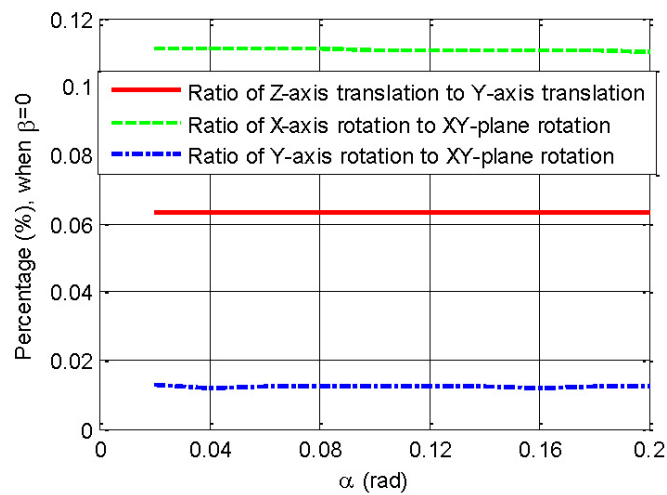
In this section, a multi-operation mode compliant gripper using the compliant four-bar mechanism presented in Fig. 5.3 is proposed as shown in Fig. 5.12. Instead of using the cross-spring joints in the compliant four-bar mechanism, the rectangular short beams (with rotation axis



(a) Translations along the X and Y axes.

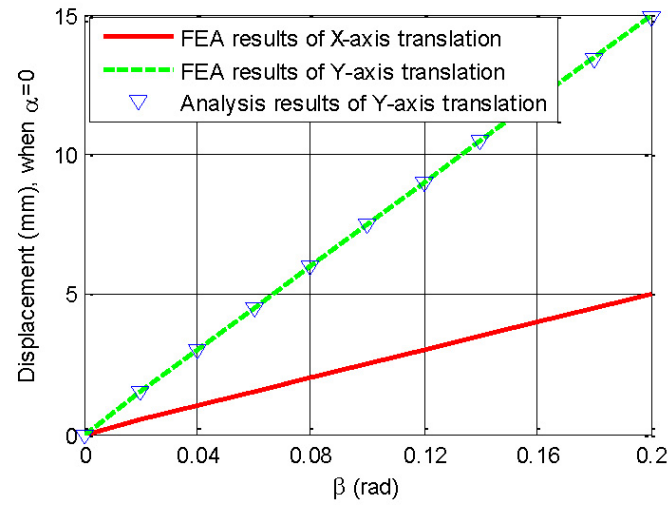


(b) Rotation about the Axis-L.

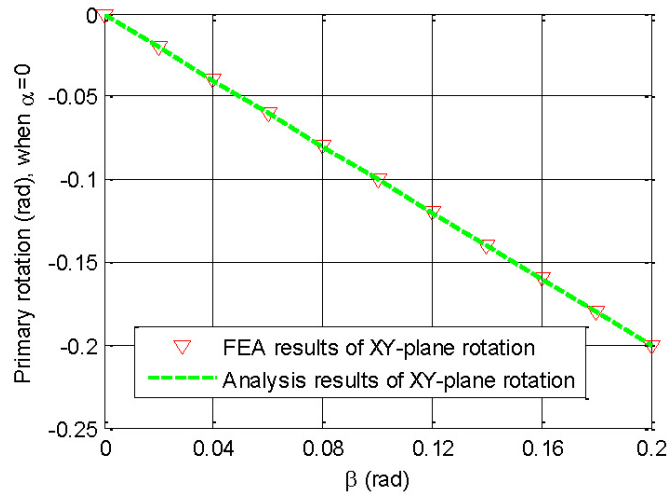


(c) parasitic motions (rotations about the X- and Y-axes and translation along the Z-axis).

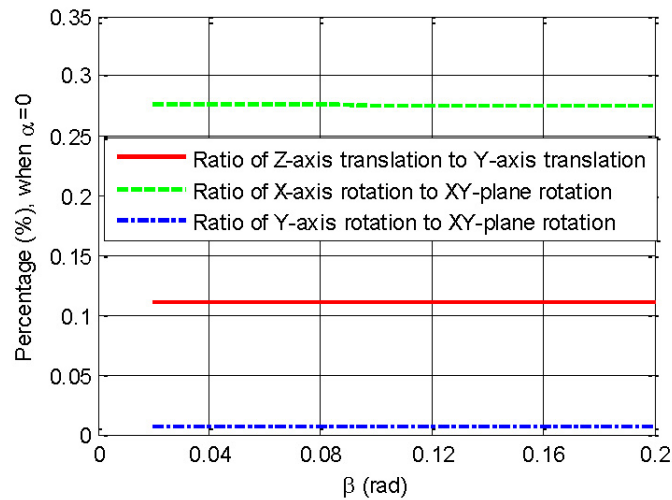
Figure 5.5 – FEA results for operation mode-I.



(a) Translations along the X and Y axes.

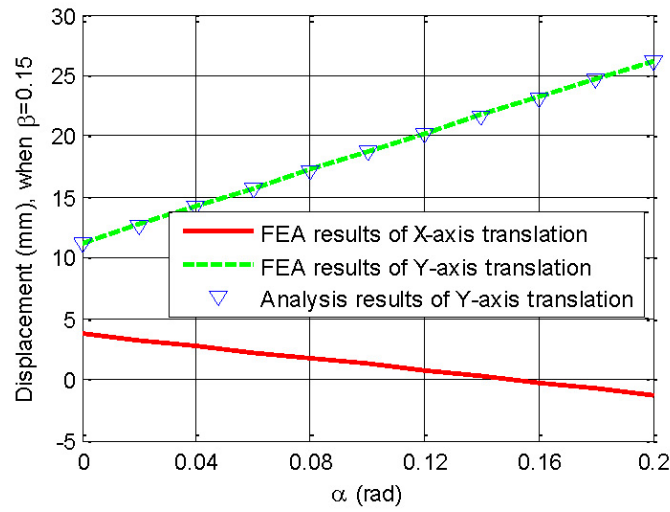


(b) Rotation about the Axis-L.

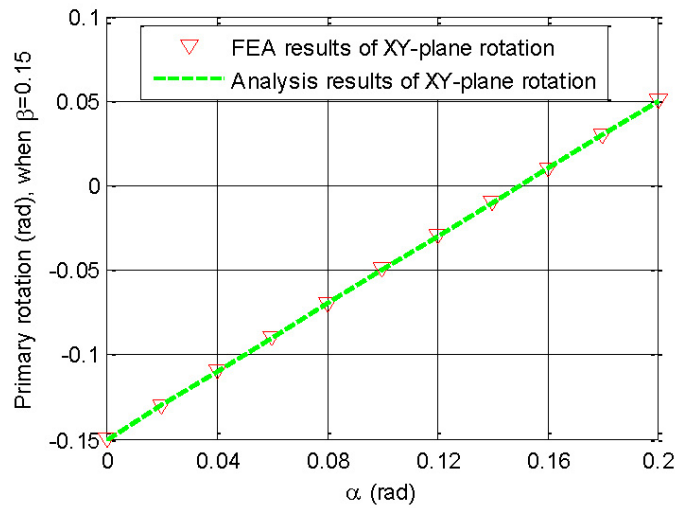


(c) parasitic motions (rotations about the X- and Y-axes and translation along the Z-axis).

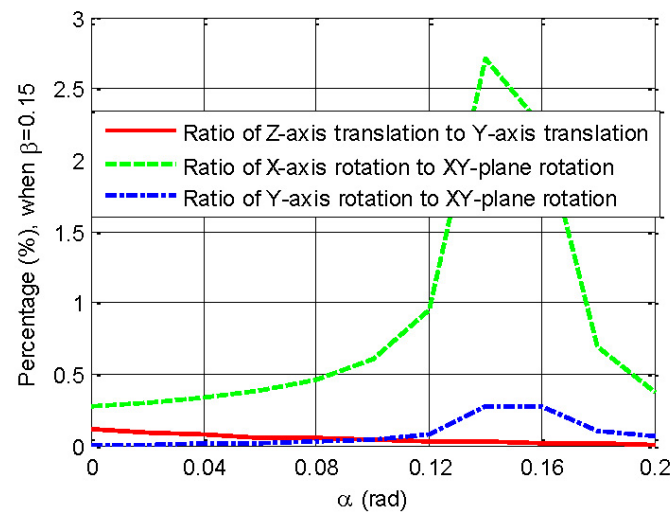
Figure 5.6 – FEA results for operation mode-II.



(a) Translations along the X and Y axes.



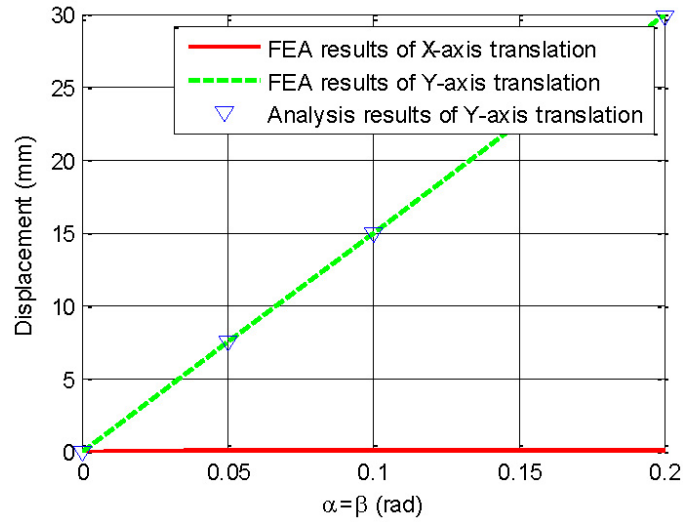
(b) Rotation about the Axis-L.



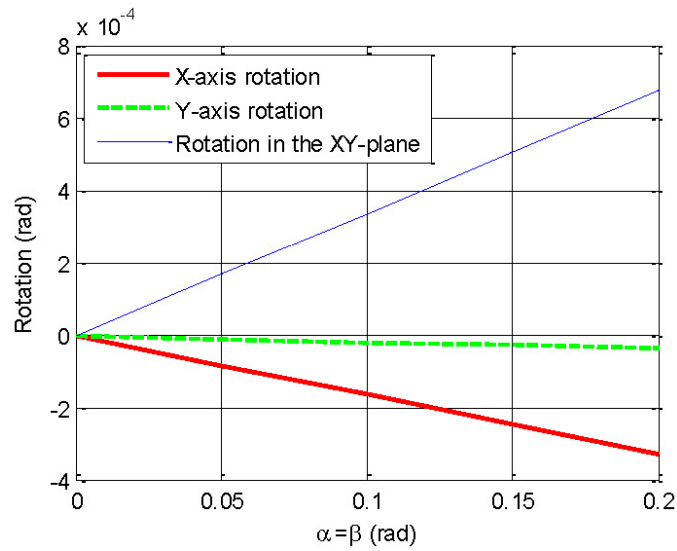
(c) parasitic motions (rotations about the X- and Y-axes and translation along the Z-axis).

Figure 5.7 – FEA results for operation mode-III.

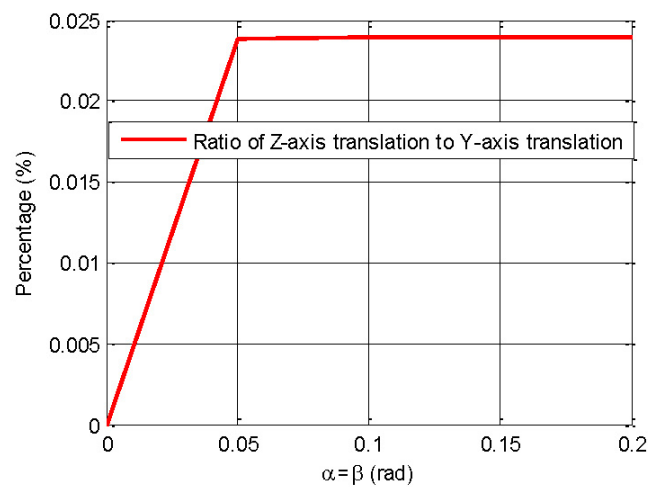




(a) Translations along the X and Y axes.



(b) Rotation about the Axis-L.



(c) parasitic motions (rotations about the X- and Y-axes and translation along the Z-axis).

Figure 5.8 – FEA results for operation mode-IV.

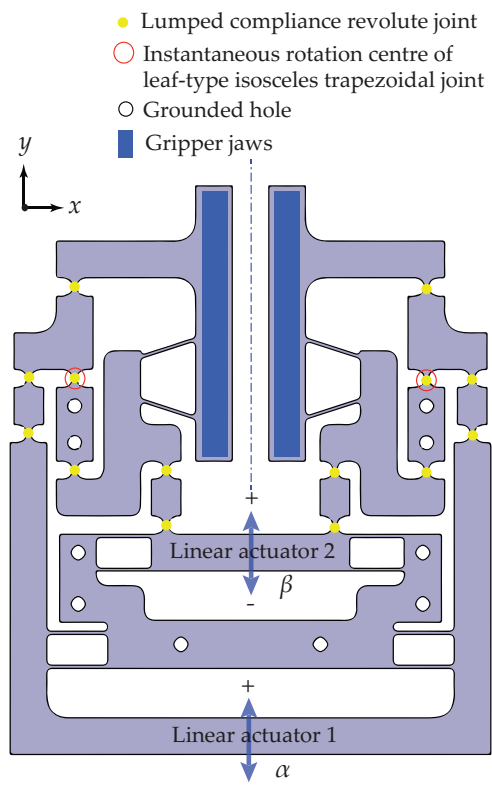


Figure 5.9 – A novel reconfigurable compliant gripper.

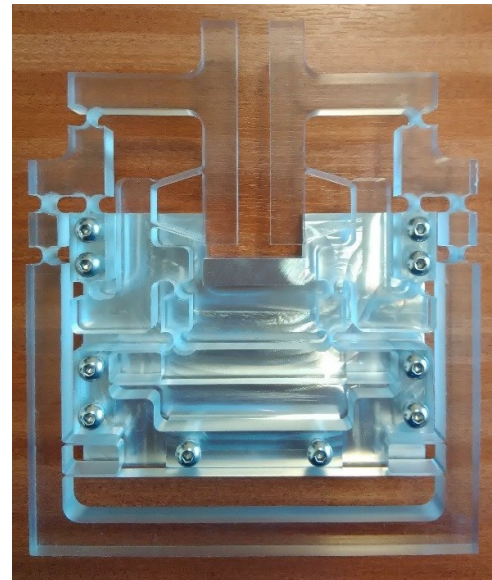


Figure 5.10 – Prototype of the reconfigurable compliant gripper.

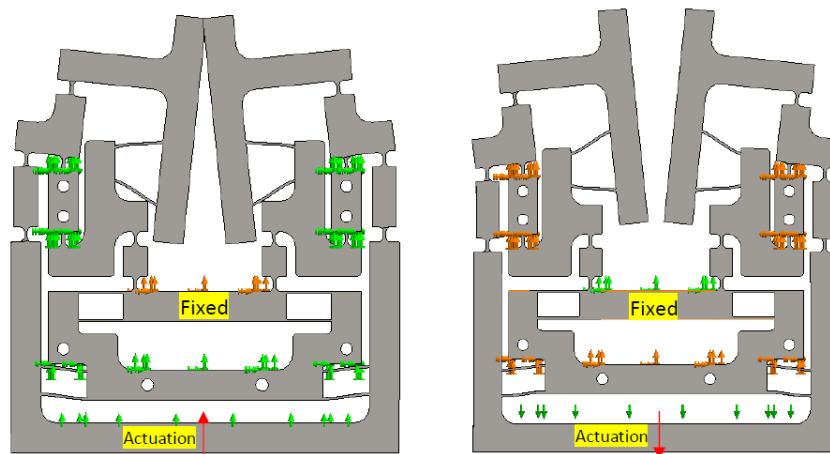
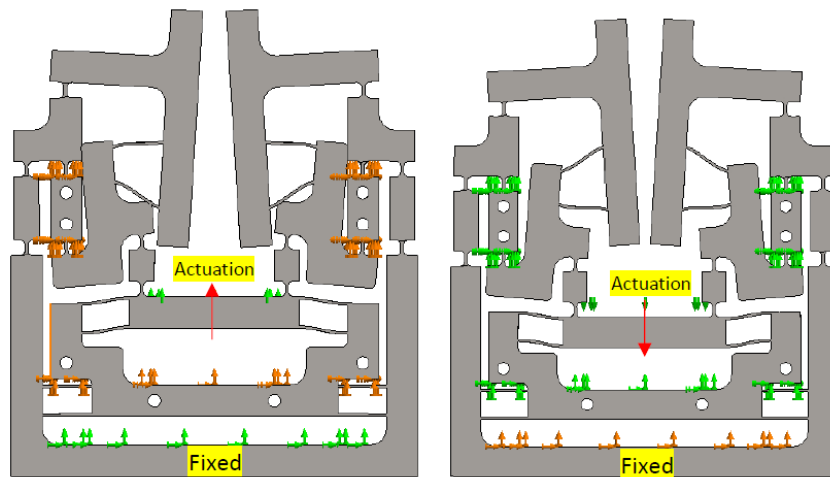
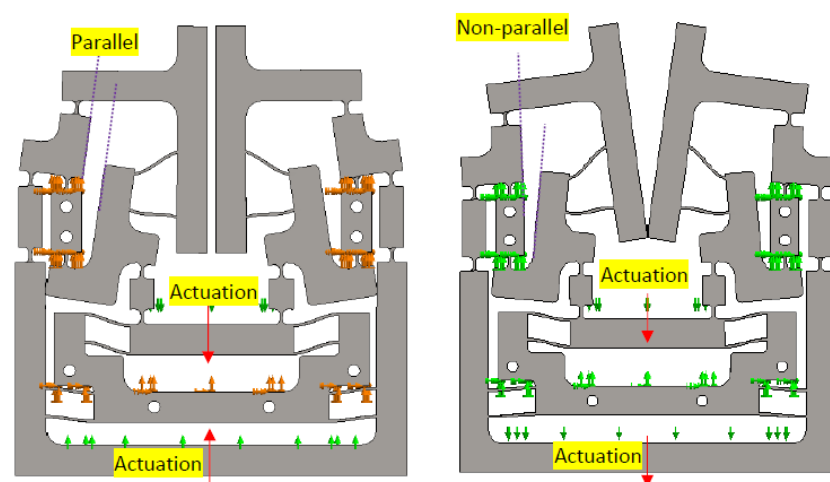
(a) Angular grasping mode 1 :  $\alpha \neq 0$ ,  $\beta = 0$ .(b) Angular grasping mode 2 :  $\alpha = 0$ ,  $\beta \neq 0$ .(c) Left : parallel grasping mode ( $\alpha > 0$ ,  $\beta < 0$ ); Right : angular grasping mode 3 ( $\alpha < 0$ ,  $\beta < 0$ ).

Figure 5.11 – Four grasping modes of the compliant gripper.

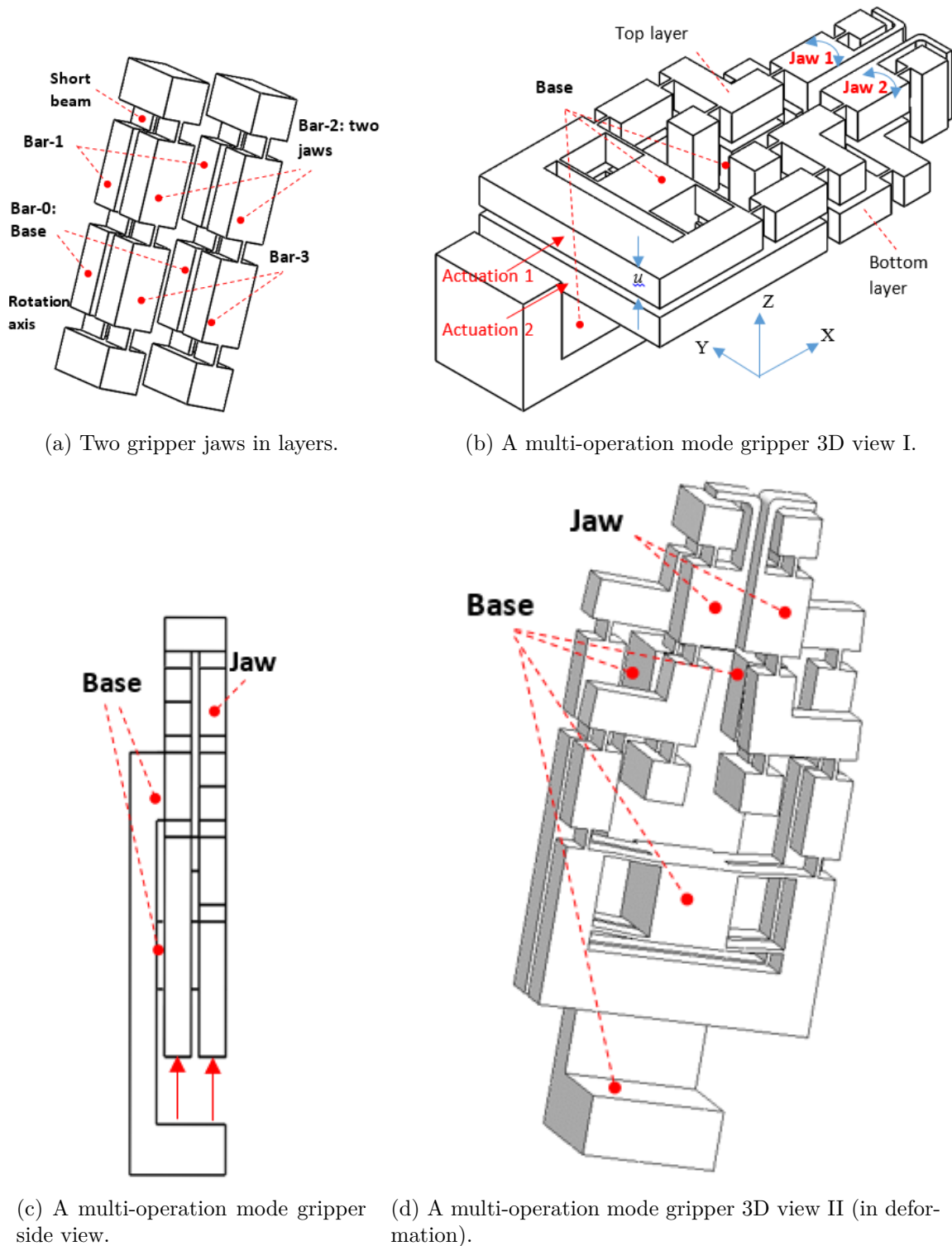


Figure 5.12 – 3D views of the synthesized multi-operation mode compliant gripper-2

approximately in the centre) are adopted as the rotational joints as shown in Fig. 5.12a. The compliant gripper is a two-layer structure with two linear actuators to control the two rotational displacements ( $\alpha$  and  $\beta$ ) in each jaw. The top layer actuator is for actuating  $\beta$  while the bottom layer is for  $\alpha$ .

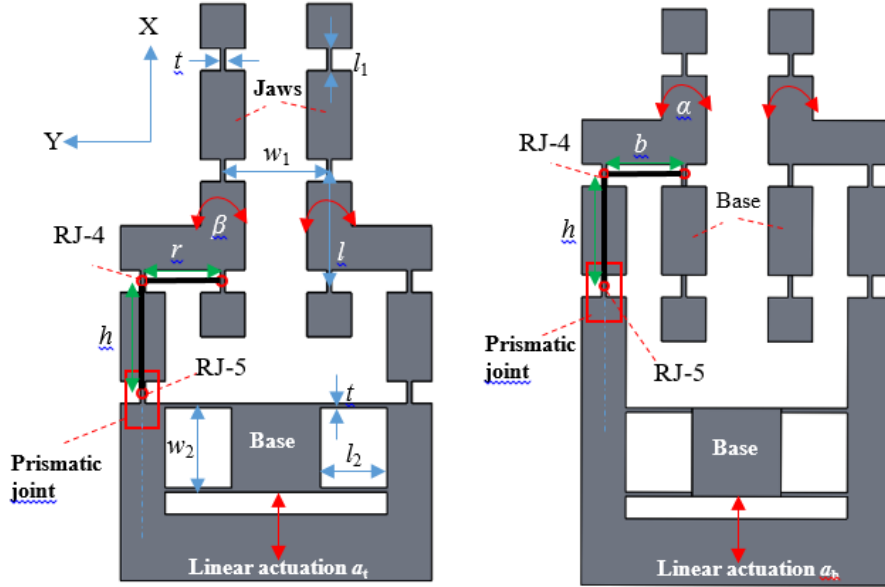


Figure 5.13 – Multi mode compliant gripper consisting of compliant slider-crank mechanisms.

The design of the compliant gripper is further detailed in Fig. 7, with all dominant geometrical parameters labelled except the identical out-of-plane thickness,  $u$  of each layer. A pair of compliant slider-crank mechanism are added in each layer (sharing a revolute joint with the compliant four-bar mechanism), to convert one linear actuation to two simultaneous rotational actuations in two jaws. In both layers, compliant slider-crank mechanisms are identical. All short beams are also identical in the gripper. Figure 5.14 shows the 3D-printed prototype of the gripper with its control scheme.

### 5.3.2 Kinetostatic model

Under the assumption of small rotations, the relationship between the linear actuation and the rotational actuation in the slider-crank mechanism (the left jaw is taken for studying) can be modelled as follows:

$$-a_b = r\alpha \text{ or } \alpha = -\frac{a_b}{r} \quad (5.4)$$

$$-a_t = r\beta \text{ or } \beta = -\frac{a_t}{r} \quad (5.5)$$

where  $a_t$  and  $a_b$  represent the displacements of the top and bottom actuators along the  $X$ -axis, respectively. A minus sign means that the positive linear actuation causes a negative rotational actuation. Here,  $r$  is the lever arm as shown in Fig. 5.13.

The rotational displacement of RJ-4 in the added slider-crank mechanism can be approximately obtained as follows. The rotational displacement of RJ-5 in each layer can be ignored

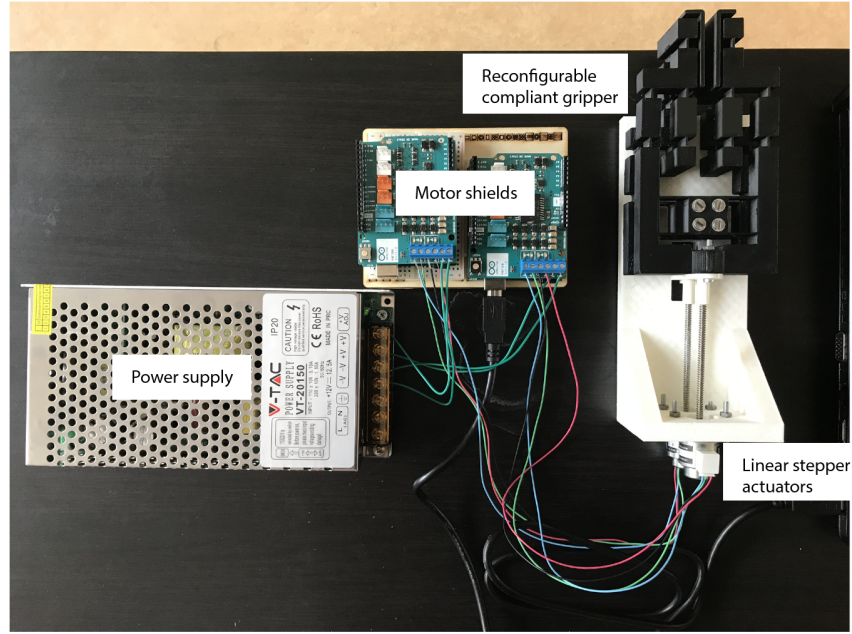


Figure 5.14 – Multi mode compliant gripper prototype

due to the specific configuration of the added slider-crank mechanism.

RJ-4 in the top layer:

$$\theta_{4t} = \beta \quad (5.6)$$

RJ-4 in the bottom layer:

$$\theta_{4b} = \alpha \quad (5.7)$$

From equations (5.1), (5.2) and (5.4), the input-output kinematic equations of the compliant gripper can be obtained as follows:

$$\phi = \frac{a_t - a_b}{r} \quad (5.8)$$

$$b = -\frac{l}{2r}(a_t + a_b) \quad (5.9)$$

Thus, the amplification ratio is a function of design parameter  $r$  denoted in Fig. 5.13. Using the above kinematic equations, the kinetostatic models of the compliant gripper can be derived from the principle of virtual work [How01], with  $a_t$  and  $a_b$  being the generalized coordinates.

$$F_t da_t + F_b da_b = \frac{\partial U}{\partial a_t} da_t + \frac{\partial U}{\partial a_b} da_b \quad (5.10)$$

where  $F_t$  and  $F_b$  represent the actuation forces of the top and bottom linear actuators along the X-axis, corresponding to  $a_t$  and  $a_b$ , respectively. From Eqs. (5.3), (5.6) and (5.7), the total elastic potential energy of the compliant gripper,  $U$  is calculated as follows:

$$\begin{aligned} \frac{U}{2} &= \frac{1}{2}(k_0\theta_0^2 + k_1\theta_1^2 + k_2\theta_2^2 + k_3\theta_3^2 + k_{4t}\theta_{4t}^2 + k_{4b}\theta_{4b}^2 + k_p a_t^2 + k_p a_b^2) \\ &= \frac{1}{2}(k_0 \left(\frac{a_b}{r}\right)^2 + k_1 \left(\frac{a_t}{r}\right)^2 + k_2 \left(\frac{a_b}{r} - 2\frac{a_t}{r}\right)^2 + k_3 \left(\frac{a_t}{r}\right)^2 + k_4 \left(\frac{a_t}{r}\right)^2 + k_4 \left(\frac{a_b}{r}\right)^2 \\ &\quad + k_p a_t^2 + k_p a_b^2) \end{aligned} \quad (5.11)$$

where  $k_0, k_1, k_2, k_3$  correspond to the rotational stiffnesses of RJ-0, RJ-1, RJ-2, RJ-3 in the compliant four-bar mechanism, respectively.  $k_4$  is the rotational stiffness of the RJ-4 in each layer.  $k_p$  is the translational stiffness of the prismatic joint in each layer.

Note that the reaction forces from gripping objects [HH16] can be included in Eq. (5.10), which, however, is not considered in this paper.

Combining the results of Eqs. (5.10) and (5.11) leads to:

$$\begin{aligned} \frac{F_t}{2} &= \frac{\partial U/2}{\partial a_t} = k_1 \left( \frac{a_t}{r} \right) \frac{1}{r} + k_2 \left( \frac{a_b}{r} - 2 \frac{a_t}{r} \right) \left( \frac{-2}{r} \right) + k_3 \left( \frac{a_t}{r} \right) \frac{1}{r} + k_4 \left( \frac{a_t}{r} \right) \frac{1}{r} + k_p a_t \\ \implies F_t &= a_t \left( \frac{2k_1}{r^2} + \frac{8k_2}{r^2} + \frac{2k_3}{r^2} + \frac{2k_4}{r^2} + 2k_p \right) + a_b \left( \frac{-4k_2}{r^2} \right) \end{aligned} \quad (5.12)$$

$$\begin{aligned} \frac{F_b}{2} &= \frac{\partial U/2}{\partial a_b} = k_0 \left( \frac{a_b}{r} \right) \frac{1}{r} + k_2 \left( \frac{a_b}{r} - 2 \frac{a_t}{r} \right) \left( \frac{1}{r} \right) + k_4 \left( \frac{a_b}{r} \right) \frac{1}{r} + k_p a_b \\ \implies F_b &= a_b \left( \frac{2k_0}{r^2} + \frac{2k_2}{r^2} + \frac{2k_4}{r^2} + 2k_p \right) + a_t \left( \frac{-4k_2}{r^2} \right) \end{aligned} \quad (5.13)$$

The aforementioned equations can determine the required forces for given input displacements, which can be rearranged in a matrix form:

$$\begin{bmatrix} F_t \\ F_b \end{bmatrix} = \begin{bmatrix} k_{11} & k_{12} \\ k_{21} & k_{22} \end{bmatrix} \begin{bmatrix} a_t \\ a_b \end{bmatrix} \quad (5.14)$$

where the stiffness coefficients of the system associated with the input forces and input displacements are

$$\begin{aligned} k_{11} &= \frac{2k_1}{r^2} + \frac{8k_2}{r^2} + \frac{2k_3}{r^2} + \frac{2k_4}{r^2} + 2k_p \\ k_{12} &= k_{21} = -\frac{4k_2}{r^2} \\ k_{22} &= \frac{2k_0}{r^2} + \frac{2k_2}{r^2} + \frac{2k_4}{r^2} + 2k_p \end{aligned}$$

Therefore, the input displacements can be represented with regard to the input forces as:

$$\begin{bmatrix} a_t \\ a_b \end{bmatrix} = \begin{bmatrix} c_{11} & c_{12} \\ c_{21} & c_{22} \end{bmatrix} \begin{bmatrix} F_t \\ F_b \end{bmatrix} = \begin{bmatrix} k_{11} & k_{12} \\ k_{21} & k_{22} \end{bmatrix}^{-1} \begin{bmatrix} F_t \\ F_b \end{bmatrix} \quad (5.15)$$

We can further obtain the following stiffness equations for all compliant joints used in [HH17], which can be substituted into Eq. (5.15) to solve the load-displacement equations.

$$\begin{aligned} k_0 &= k_2 = k_4 = \frac{EI}{l_1} = \frac{Eut^3}{12l_1} \\ k_1 &= k_3 = \frac{k_0}{2} = \frac{EI}{2l_1} = \frac{Eut^3}{24l_1} \\ k_p &= \frac{24EI}{l_2^3} = \frac{2Eut^3}{l_2^3} \end{aligned} \quad (5.16)$$

where  $E$  is the Young's modulus of the material and  $I$  is the second moment of inertia of the cross-section areas. With the help of Eqs. (5.9), (5.8) and (5.15), we can have the required output displacements for given input displacements/forces:

$$\begin{bmatrix} b \\ \phi \end{bmatrix} = \begin{bmatrix} -\frac{l}{2r} & -\frac{l}{2r} \\ \frac{1}{r} & -\frac{1}{r} \end{bmatrix} \begin{bmatrix} a_t \\ a_b \end{bmatrix} = \begin{bmatrix} -\frac{l}{2r} & -\frac{l}{2r} \\ \frac{1}{r} & -\frac{1}{r} \end{bmatrix} \begin{bmatrix} k_{11} & k_{12} \\ k_{21} & k_{22} \end{bmatrix}^{-1} \begin{bmatrix} F_t \\ F_b \end{bmatrix} \quad (5.17)$$

### 5.3.3 Case study

In this section, a case study with assigned parameters as shown in Table is presented to verify the analytical models in the previous section. The overall nominal dimension of the compliant gripper is  $130 \text{ mm} \times 70 \text{ mm}$ . The Young's modulus of compliant gripper is given by  $E = 2.4 \text{ GPa}$ , which corresponds to the material of Polycarbonate with Yield Strength of  $\sigma_s > 60 \text{ MPa}$ , and Poisson's Ratio of  $\nu = 0.38$ . Finite element analysis (FEA) simulation was carried out to show

$l$	$t$	$r$	$h$	$l_1$	$l_2$	$w_1$	$w_2$	$u$
25	1	18	25	5	15	24	19	10

Table 5.1 – Geometrical parameters (in mm).

the four operation modes of the compliant gripper (Fig. 5.15). Here, Solidworks 2017, with a meshing size of 1.0 mm and other settings, in default is used for FEA. Figure 5.16 illustrates the kinetostatic analysis of the proposed compliant gripper including the comparisons between the analytical modeling and FEA. It can be observed that linear relations of all figures have been captured where lines in either model are parallel to each other. The FEA results have the same changing trends as the analytical models, but deviate from the analytical models in certain degrees. The discrepancy between the two theoretical models is due to the linear assumption in the analytical modeling as well as the center drift of rotational joints.

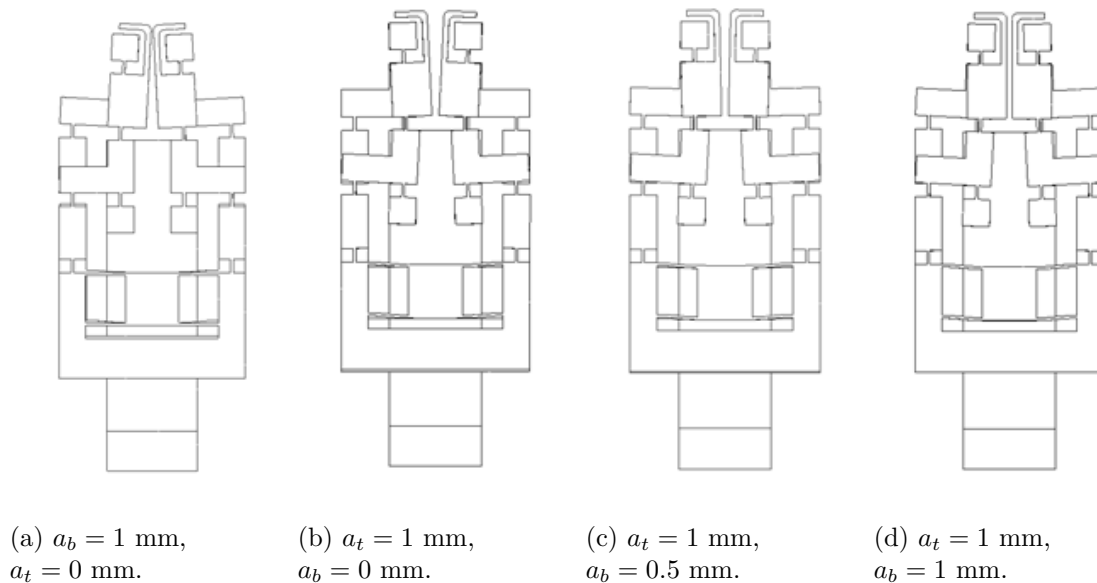
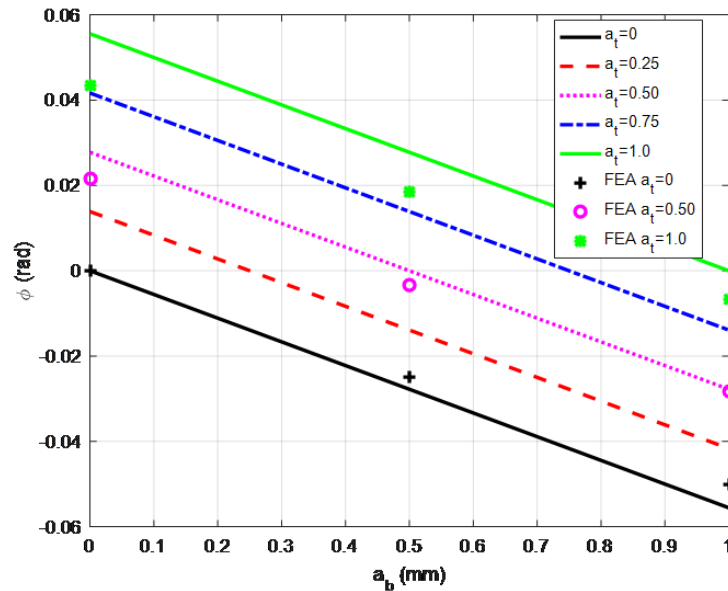


Figure 5.15 – Grasping modes of the compliant gripper.

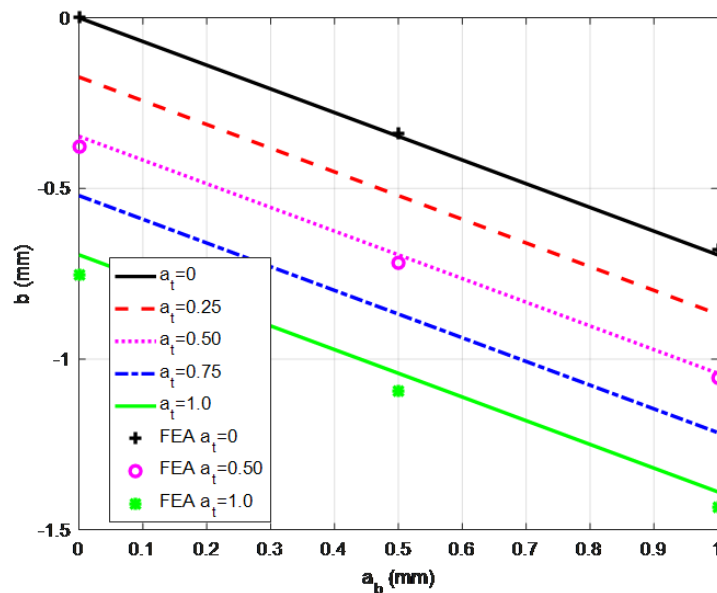
In Fig. 5.16a, with the increase of  $a_b$ , the difference between the two models (analytical and FEA) goes up if  $a_t = 0 \text{ mm}$ , while the difference between the two models decreases if  $a_t = 0.5 \text{ mm}$  and  $1 \text{ mm}$ . This is because of different line slopes of two models. Generally speaking, the larger  $a_t$ , the larger the deviation of two models, where the maximal difference in Fig. 5.16a is about 20%. In Fig. 5.16b, the line slopes of two models are almost same, meaning that the increase of  $a_b$  has no influence of the discrepancy of two models for any value of  $a_t$ . Also, the larger  $a_t$ , the



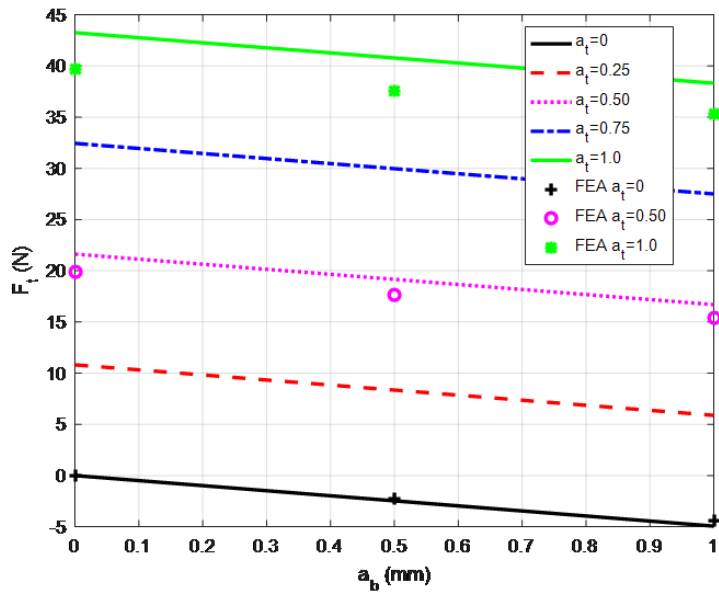
larger the deviation of two theoretical models. Figure 5.16c reveals the same conclusion as that of Fig. 5.16b. Figure 5.16d shows the similar finding to that of Fig. 5.16a, except the larger  $a_t$ , the smaller the deviation of two models. It is clearly shown that in Figs. 5.16b, 5.16c and 5.16d, the general discrepancy of the two models is much lower than that in Fig. 5.16a.



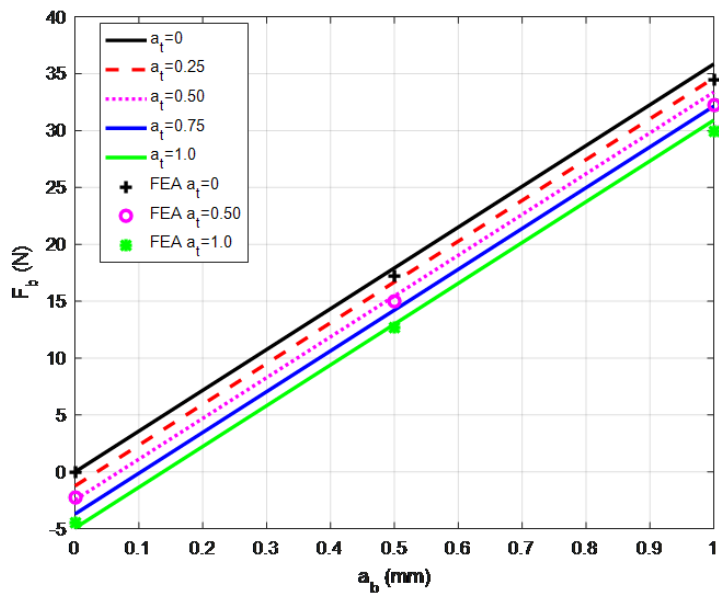
(a) Output rotational angle along the Z-axis.



(b) Output displacement along the Y-axis.



(c) Input force in the top layer.



(d) Input force in the bottom layer.

Figure 5.16 – Analysis and comparison (input displacement non-negative).

## 5.4 Conclusions

A novel idea of designing reconfigurable compliant mechanisms inspired by the constraint singularities of rigid body mechanisms was presented in this chapter [Nay+17a; Hao+18]. A rhombus planar rigid four-bar mechanism was analyzed to identify its three operation modes and two constraint singularities separating those modes. The rigid joints were replaced by compliant joints to obtain two designs of a reconfigurable compliant four-bar mechanism. The second design was found to be more accurate and to provide less parasitic motions than the first one, which is verified by its non-linear FEA simulations in different motion modes. Moreover, the compliant four-bar mechanism was shown to have four operation modes based on the particular actuation strategy unlike its rigid counterpart. A preliminary design of a compliant gripper has been designed based on the reconfigurable compliant four-bar mechanism introduced and studied in this paper.

Additionally, the analytical kinetostatic mode of the multi-mode compliant gripper was derived, which is verified in the case study. It shows that the FEA results comply with the analytical models with acceptable discrepancy. The proposed multiple mode compliant gripper is expected to be applied in extensive applications such as grasping a variety of shapes or adapting to specific requirements.

# Conclusions and future work

## Synopsis

The focus of this doctoral thesis was on the kinematic analysis of some lower mobility parallel manipulators and their derivatives. Geometric constraints were derived with the help of Blaschke mapping for a planar equilateral four-bar linkage and using Study's kinematic mapping for other PMs whose transformation matrices belonged to  $\mathbb{E}^3$ . The geometrical approach and Linear Implicitization Algorithm were used to derive and compare the constraint equations of the 3-RUU PM to finally obtain the same variety.

A global kinematic analysis includes a complete characterization of operation modes which was accomplished using algebraic geometry tools. The equilateral four-bar linkage was found to have three operation modes. The transition between two of them, known as a constraint singularity was later used to design a reconfigurable compliant mechanism. It also led to the conception of a novel reconfigurable compliant gripper with multiple grasping modes.

Furthermore, the 3-[PP]S and 3-S[PP] PMs were found to have two operation modes. The PMs belonging to the 3-[PP]S-Y family were compared on the basis of their singularity-free orientation workspace and parasitic motions, for their different design parameters, operation modes and actuation schemes. However, in this case, the singularities were determined using kinematic Jacobian matrices derived by screw theory. A 3-RPS PM, belonging to the same family is chosen such that the R-joint axes can have any planar orientations and the relations between its design parameters are established such that it has two operation modes. Subsequently, a 3-RPS-3-SPR series-parallel manipulator was analyzed to enumerate the singularities arising due to the serial stacking of two parallel manipulators.

Additionally, a dual reconfigurable 4-rRUU PM was proposed with a novel reconfigurable revolute joint based on the double-Hooke's joint. Its operation modes were determined for some specific orientations of the rR-joint axes. With a goal to build a working prototype of this mechanism for machining application, Pareto-optimal solutions were generated to obtain the optimal design parameters to have the smallest size but the largest singularity and collision-free workspace.

The contributions of this doctoral thesis are epitomized as follows.

## Contributions

### 1. Operation mode analysis of lower-mobility PMs

The operation modes of the following PMs were determined in Chapter 2:

1. Operation mode analysis of an equilateral planar four-bar linkage was done using Blaschke mapping from  $\mathbb{E}^2$  to  $\mathbb{P}^3$ . Its three constraint manifolds corresponding to the three operation

modes were depicted and singular configurations separating them were represented.

2. Operation modes of 3-[PP]S-Y and 3-S[PP]-Y PMs were determined using Study's kinematic mapping from  $\mathbb{E}^3$  to  $\mathbb{P}^7$ . PMs belonging to these families were found to have two operation modes.
3. Constraint equations of a 3-RUU PM were derived using geometrical approach and linear implicitization algorithm to verify that they yield the same variety. However, it was possible to characterize only a translational operation mode.
4. A 4-rRUU dual reconfigurable PM was found to have either a translational operation mode or Schönflies mode depending on the orientations of the R-joint axes attached to the base.

## 2. Influence of design parameters on the number of operation modes

In Chapter 2, the influence of architecture on the operation modes of a PM was explored for the first time for a 3-RPS PM with co-planar R-joint axes. Initially, the relations between the design parameters were established for the PM to have two operation modes. Those relations were further physically interpreted to state a theorem with proof that relates the necessary and sufficient geometric conditions so that the PM at hand can exhibit two operation modes. It was also shown how a simple change of design can avoid the constraint singularities.

## 3. Comparison of a family of zero-torsion parallel manipulators

The PMs belonging to the 3-[PP]S-Y family were considered in Chapter 3 with different sizes of their fixed bases and moving platforms, operation modes and actuation schemes. For their comparison, a new performance index, known as the Maximum Inscribed Circle Radius (MICR) was introduced in order to quantify their singularity-free orientation workspaces. To determine the singularities, the kinematic Jacobian matrices were derived using screw theory which proved to be efficient compared to the computationally cumbersome partial differentiation of the constraint equations with respect to Study parameters. *Tilt and Torsion* angles are used to parametrize the orientation workspace since they are well-suited for this family of mechanisms. Consequently, the CAD models of the Pareto optimal designs with the highest MICR and the least parasitic motions were shown. Moreover, a new complexity index was introduced to favor the operation mode with fewer internal collisions and the Pareto optimal designs were ranked based on their complexities.

## 4. Mobility, kinematics and singularity analysis of a series-parallel manipulator

The 3-RPS-3-SPR S-PM was studied in Chapter 4 by dividing its configuration space into four parts, thanks to the two operation modes exhibited by each of its constituent lower-mobility PM modules. The dimension of its constraint variety was calculated to be six proving that the S-PM has a global mobility of six. Therefore, a new parametrization of the Study's quadric was formulated using six parameters, three from each module. Subsequently, screw theory was used to derive its kinematic serial Jacobian matrix which was shown to be applicable to any S-PM including the ones with multiple modules. Along with line geometry, its serial singularities were enumerated by exploiting an existing result for a PM that bijectively maps the wrench singularities to the collapse of its characteristic tetrahedron. Every serial singularity was represented in Table 4.1 by a geometric condition, algebraic expression, instantaneous *dof* and an example

configuration of the S-PM. the instantaneous *dof* was calculated as the rank of the serial Jacobian matrix and the order of the global twist system. Also, the inverse kinematics problem of the S-PM under study was solved as locating 3 points on 3 lines problem.

## 5. Synthesis of reconfigurable compliant mechanisms

A novel idea to synthesize reconfigurable compliant mechanisms based on constraint singularities of PMs was presented in Chapter 5. It was applied on an equilateral planar four-bar linkage already analyzed in Chapter 2. One of its constraint singular configurations was chosen and a reconfigurable compliant mechanism was designed using rigid body replacement method. The designed compliant mechanism was shown to exhibit a translational motion when both of its actuators were in sync, a rotational motion otherwise. Thereafter, a novel reconfigurable compliant gripper was designed displaying multiple grasping modes. Kinetostatic modeling of the gripper was done and the results were found to match the FEA simulation of the gripper. Moreover, multiple prototypes of the reconfigurable compliant mechanism and the gripper were built with a goal to physically comprehend their operation and grasping modes.

## 6. Prototyping of the dual reconfigurable 4-rRUU PM

The kinematic analysis of 4-rRUU PM in Chapter 2 showed that it can exhibit many operation modes due to its property of dual reconfigurability. In order to manufacture a working prototype of this PM for machining applications, a Pareto optimization problem was formulated as shown in Chapter 2 to obtain a design with the biggest singularity- and collision-free workspace and the smallest size.

## Future work

### Complete characterization of operation modes

Due to the complexity of the 3-RUU, a complete characterization of operation modes was not possible and is still an open problem. Similarly, the operation mode analysis of a 4-rRUU PM for any orientation of the base R-joint axis is left for future work.

### Influence of design parameters on operation modes

Influence of design parameters on the number of operation modes was demonstrated for a 3-RPS PM with coplanar R-joint axes in Chapter 2. However, the case of a 3-RPS PM with non-coplanar revolute joints is still an open problem.

Nonetheless, the proof of Theorem 6 in Chapter 2 indicates that a 3-RPS PM with planar or non-coplanar joints will have two operation modes only if there exists a constraint singularity such that the force lines are dependent. This can happen only when they are concurrent and coplanar which is not possible unless the R-joint axes are all parallel to a fixed plane. By this reasoning, the following conjecture can be stated:

**Conjecture 1.** *A general 3-RPS parallel manipulator will have two operation modes if and only if the following geometric conditions are satisfied*

- i. the revolute joint axes belong to a singular linear complex.*
- ii. Moving platform triangle is homothetic to the triangle enclosed by the revolute joint axes.*

iii. *The three planes normal to the three revolute joint axes, respectively, have a common line of intersection.*

The conjecture answers why the 3-RPS cube PM analyzed in [Nur+14] has only one operation mode. Moreover, the conjecture is in accordance with all the 3-RPS PMs analyzed in [NG18] although a rigorous proof of the conjecture is an open problem. It was attempted using the same approach shown in Chapter 2 in vain due to the complexity of the equations. The approach used in [RT18] simplifies the algebraic manipulations to obtain an univariate polynomial of the 3-RPS PM with non-coplanar R-joint axes. This approach seems to be the right candidate to answer the problem at hand.

The same approach in Chapter 2 could be used to examine the influence of design parameters on the operation modes of other PMs.

### Comparison of other PMs based on the approach proposed in Chapter 3

In Chapter 3, the 3-[PP]S-Y family of PMs were compared. Future work can include a comparison between 3-[PP]S- $\Delta$  and 3-[PP]S-cube PMs for different actuation schemes. Furthermore, the comparison can be done while taking into account joint limits and self collisions. Additionally, MICR, parasitic motions and proposed complexity indices can be used as a basis of comparison for other lower mobility PMs.

### Kinematics and singularity analyses of other S-PMs

The singularity analysis done in Chapter 4 is confined only to the 3-RPS-3-SPR S-PM with coincident spherical joints in each limb or any other manipulator where one can realize a characteristic tetrahedron. Nonetheless, when the spherical joints are placed apart, the singularity analysis is similar to that of a Gough-Stewart platform in which case, the S-PM is singular if the constraint force lines belong to a linear line complex.

A generalized approach to determine the singularities of any S-PM can be done as follows: The overall transformation matrix of the S-PM can still be derived by

$$\mathbf{T} = \mathbf{T}_1 \mathbf{F} \mathbf{T}_2 \quad (5.18)$$

where,  $\mathbf{T}_1$  and  $\mathbf{T}_2$  are the transformation matrices of the proximal and the distal modules, respectively and  $\mathbf{F}$  is the fixed transformation matrix between the moving platform of the proximal module (where three of the spherical joints are located) and the base of the distal module (where the remaining three spherical joints lie). Study parameters can be extracted from  $\mathbf{T}$  and they can be differentiated with respect to the  $m$ -parameters describing the motion of the lower module and  $m$ -parameters corresponding to the upper module of the S-PM to obtain the  $8 \times m + n$  Jacobian matrix. The simultaneous vanishing of the  $\binom{8}{m+n}$  minors of this Jacobian matrix gives the algebraic singularity conditions of the S-PM. This approach was verified for the 3-RPS-3-SPR S-PM by calculating its tangent space yielding an  $8 \times 6$  Jacobian matrix. There remain only 10 non-zero minors that yield all the algebraic singularity conditions listed in Table 4.1. However, to obtain the correct instantaneous *dof*, it is important not to dismiss the parametrization singularities.

On the other hand, the future work can deal with writing the constraint equations of the whole S-PM only as a function of input and output parameters in order to solve the DKM directly instead of splitting it into two stages as shown in Chapter 4 of this doctoral thesis. Moreover, the workspace of the S-PM can be plotted and the singularities separating the solutions to IKM can be explored.

## **Synthesis of reconfigurable compliant mechanisms based on constraint singularities of PMs**

Despite the work mentioned in Chapter 5, there are other aspects to be considered in the future, including but not limited to the following:

1. Extending the proposed approach to synthesize reconfigurable compliant mechanisms based on the constraint singularities of spatial rigid body mechanisms.
2. An analytical nonlinear model for a more accurate kinetostatic modelling of the compliant gripper proposed herein.
3. Design optimization of the compliant gripper and prototyping based on a specific application.
4. Physical testing to verify the established analytical model.
5. Work on the control strategies for the compliant gripper.



# Personal publications

## Journal publications

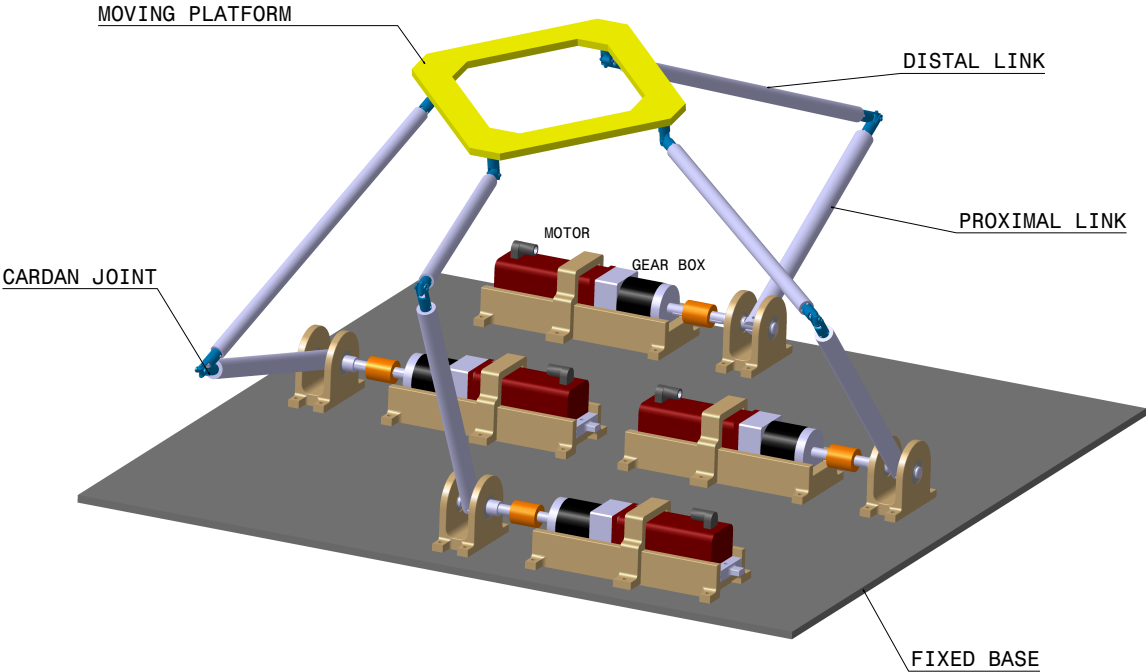
- [1] Abhilash Nayak, Stéphane Caro and Philippe Wenger, *Comparison of 3-[PP]S Parallel Manipulators based on their Singularity Free Orientation Workspace, Parasitic Motions and Complexity*, Mechanism and Machine Theory, **129**, 293-315, 2018.
- [2] Abhilash Nayak, Stéphane Caro and Philippe Wenger, *Kinematic analysis of the 3-RPS-3-SPR series-parallel manipulator*, Robotica, , 1-27, 2018.
- [3] Abhilash Nayak, Thomas Stigger, Manfred L. Husty, Philippe Wenger and Stéphane Caro, *Operation mode analysis of 3-RPS parallel manipulators based on their design parameters*, Computer Aided Geometric Design, **63**, 122-134, 2018.
- [4] Guangbo Hao, Haiyang Li, Abhilash Nayak and Stéphane Caro, *Design of a Compliant Gripper With Multimode Jaws*, ASME Journal of Mechanisms and Robotics, **10(3)**, 031005-031005-12, 2018.

## Conference publications

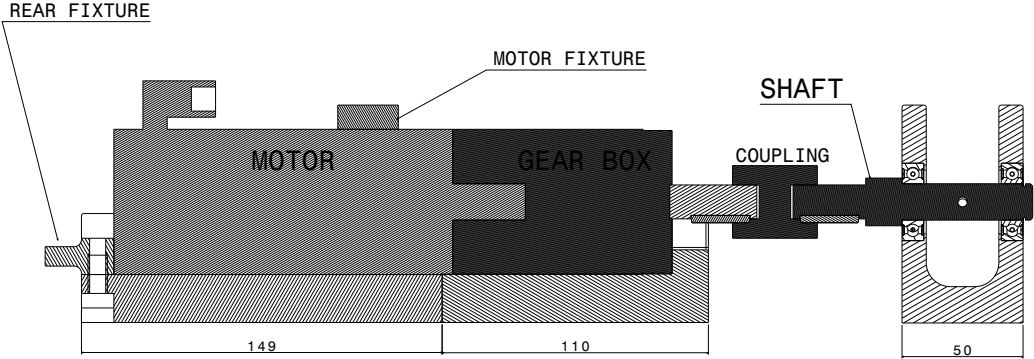
- [1] Abhilash Nayak, Latifah Nurahmi, Philippe Wenger and Stéphane Caro, *Comparison of 3-RPS and 3-SPR Parallel Manipulators Based on Their Maximum Inscribed Singularity-Free Circle*, In: New Trends in Mechanism and Machine Science: Theory and Industrial Applications. Ed. by Philippe Wenger and Paulo Flores, Springer International Publishing, 2017, pp. 121–130.
- [2] Abhilash Nayak, Haiyang Li, Guangbo Hao, and Stéphane Caro, *A Reconfigurable Compliant Four-Bar Mechanism with Multiple Operation Modes*, In: The ASME 2017 International Design Engineering Technical Conferences & Computers and Information in Engineering Conference IDETC/CIE 2017. Cleveland, United States, Aug. 2017.
- [3] Abhilash Nayak, Stéphane Caro and Philippe Wenger, *Local and Full-Cycle Mobility Analysis of a 3-RPS-3-SPR Series-Parallel Manipulator*, In: Computational Kinematics: Proceedings of the 7th International Workshop on Computational Kinematics that was held at Futuroscope-Poitiers, France, Ed. by Saïd Zeghloul, Lotfi Romdhane, and Med Amine Laribi. Cham: Springer International Publishing, 2018, pp. 499-507.

- [4] Abhilash Nayak, Stéphane Caro and Philippe Wenger, *A dual reconfigurable 4-rRUU parallel manipulator*, The 4th IEEE/IFToMM International conference on Reconfigurable Mechanisms and Robots (ReMAR2018), Jun 2018.
- [5] Thomas Stigger, Abhilash Nayak, Stéphane Caro, Philippe Wenger, Martin Pfurner and Manfred L. Husty, *Algebraic Analysis of a 3-RUU Parallel Manipulator*, In: *Advances in Robot Kinematics 2018*, Springer International Publishing, Ed. by Jadran Lenarcic and Vincenzo Parenti-Castelli, 2019, pp. 141-149.

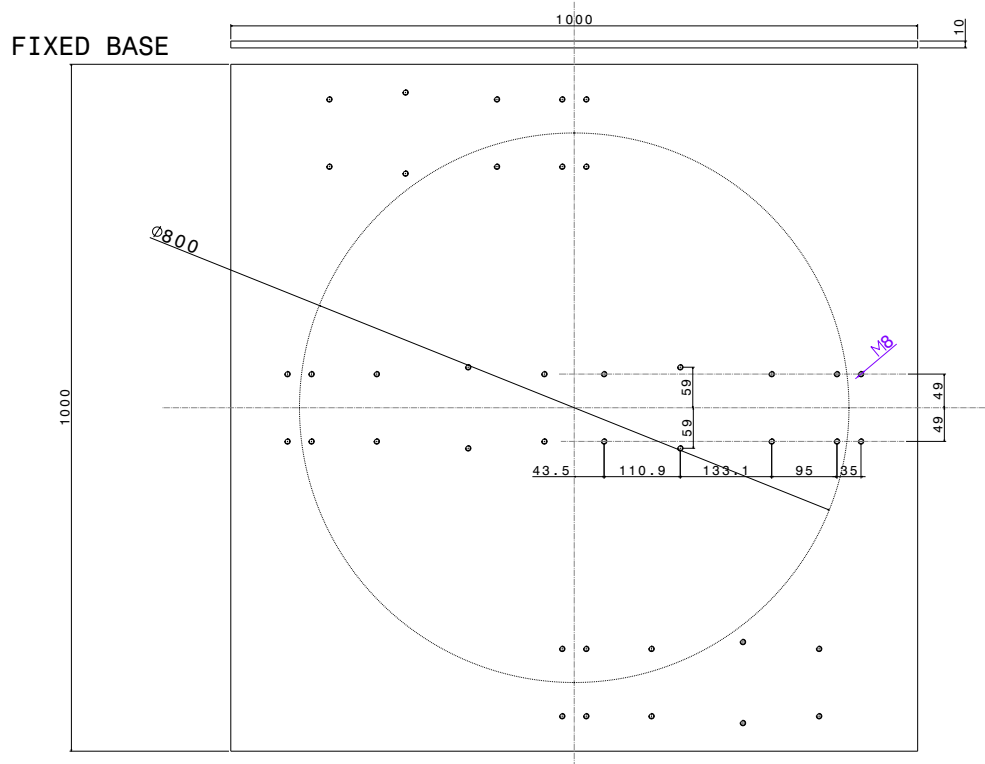
# Appendix A: Manufacturing drawings



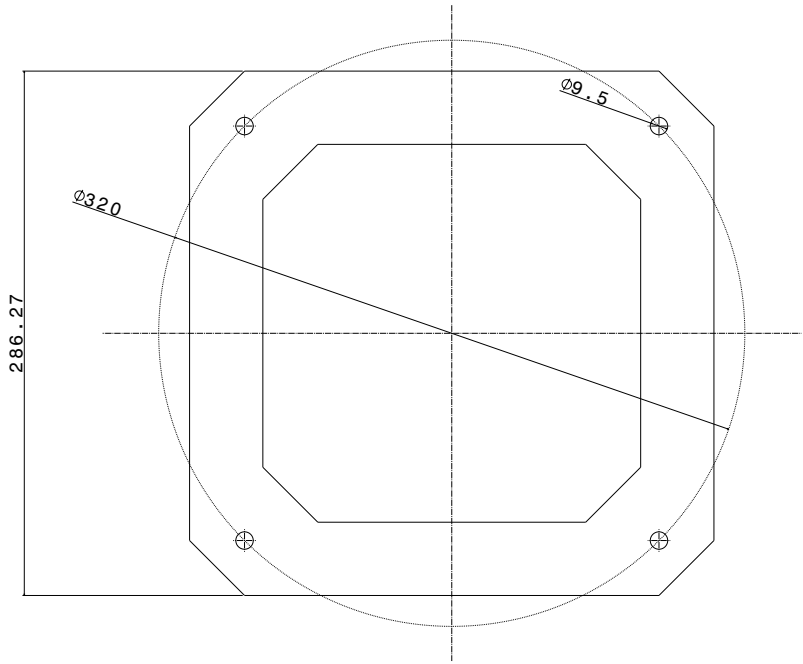
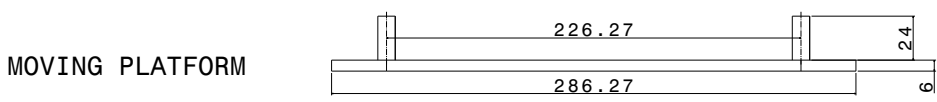
Isometric drawing of the 4-R<sub>x</sub>UU prototype



Cross-section view of the support

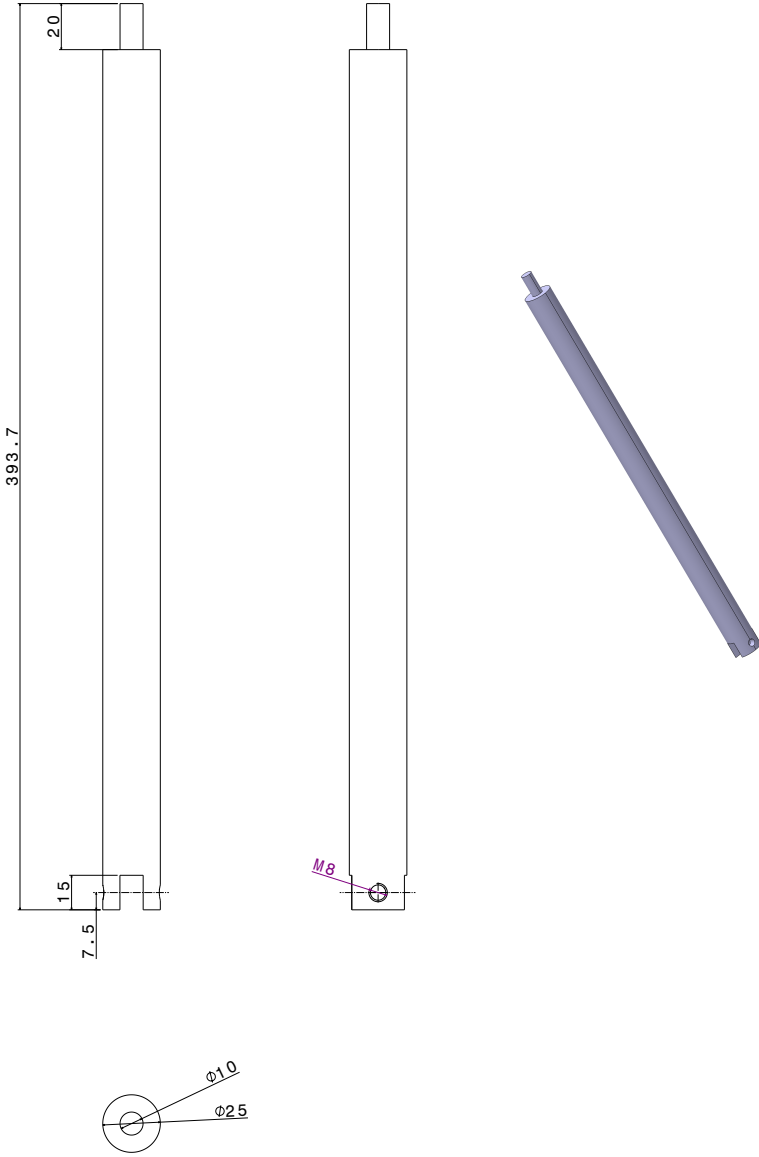


Fixed base



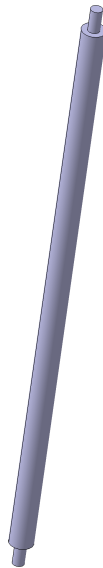
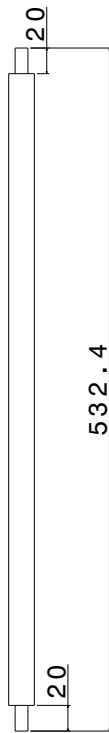
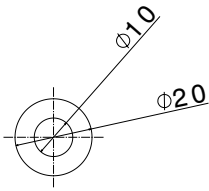
Moving platform

PROXIMAL LINK



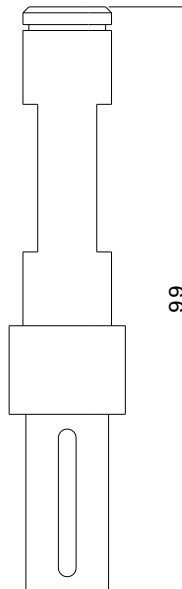
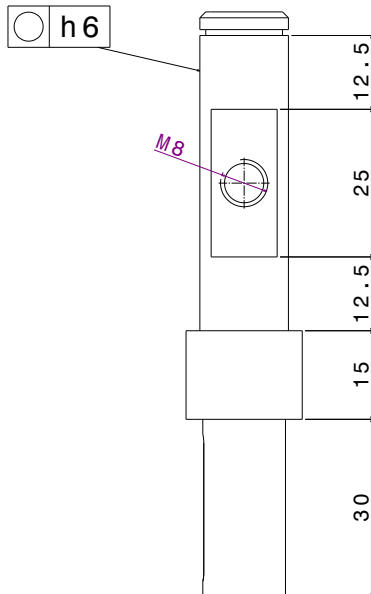
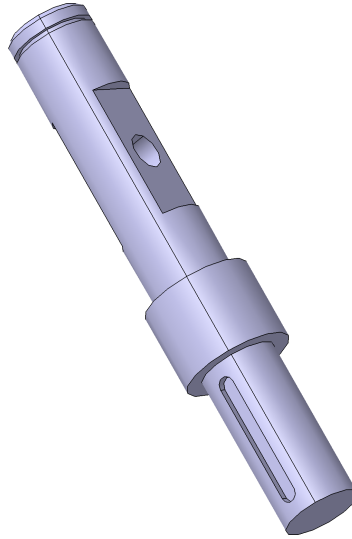
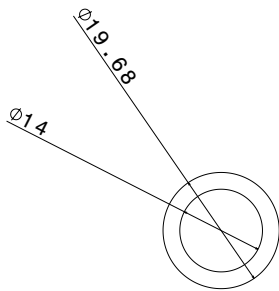
Proximal link

# DISTAL LINK



Distal link

# SHAFT



Input shaft

# Bibliography

- [AMC16] Semaan Amine, Ossama Mokhiamar, and Stéphane Caro. “Classification of 3T1R Parallel Manipulators Based on Their Wrench Graph”. In: *Journal of Mechanisms and Robotics* 9.1 (2016), pp. 011003–011003–10.
- [Ami+12a] Semaan Amine, Stéphane Caro, Philippe Wenger, and Daniel Kanaan. “Singularity analysis of the H4 robot using Grassmann–Cayley algebra”. In: *Robotica* 30.7 (2012), pp. 1109–1118.
- [Ami+12b] Semaan Amine, Mehdi Tale Masouleh, Stéphane Caro, Philippe Wenger, and Clément Gosselin. “Singularity Conditions of 3T1R Parallel Manipulators With Identical Limb Structures”. In: *Journal of Mechanisms and Robotics* 4.1 (2012), pp. 011011–011011–11.
- [Ami11] Semaan Amine. “Lower-mobility parallel manipulators : geometric analysis, singularities and conceptual design”. PhD thesis. Ecole Centrale de Nantes, 2011.
- [Ang13] Jorge Angeles. *Fundamentals of Robotic Mechanical Systems: Theory, Methods, and Algorithms (Mechanical Engineering Series)*. 4th ed. 2014. Springer Publishing Company, Incorporated, 2013. ISBN: 3319018507, 9783319018508.
- [Ang94] Jorge Angeles. “Computer-Aided Analysis of Rigid and Flexible Mechanical Systems”. In: ed. by Manuel F. O. Seabra Pereira and Jorge A. C. Ambrósio. Dordrecht: Springer Netherlands, 1994. Chap. On Twist and Wrench Generators and Annihilators, pp. 379–411.
- [Bak02] J.Eddie Baker. “Displacement–closure equations of the unspecialised double-Hooke’s-joint linkage”. In: *Mechanism and Machine Theory* 37.10 (2002), pp. 1127–1144. ISSN: 0094-114X.
- [Bal00] R. A. Ball. *Treatise on the theory of screws*. Cambridge: Cambridge University Press, 1900, pp. 1–30.
- [BB08] S. Briot and I. A. Bonev. “Singularity analysis of zero-torsion parallel mechanisms”. In: *2008 IEEE/RSJ International Conference on Intelligent Robots and Systems*. 2008, pp. 1952–1957.
- [BCW07] Ilian A. Bonev, Damien Chablat, and Philippe Wenger. “Working and Assembly Modes of the Agile Eye”. In: *IEEE International Conference on Robotics and Automation, Orlando, Florida abs/0708.3936* (2007).
- [Bea85] Millard F. Beatty. *Principles of Engineering Mechanics Volume 1, Kinematics the Geometry of Motion*. Newyork: Plenum Press, 1985, p. 5.
- [BHS06] P. Ben-Horin and M. Shoham. “Singularity condition of six-degree-of-freedom three-legged parallel robots based on grassmann-cayley algebra”. In: *IEEE Transactions on Robotics* 22.4 (2006), pp. 577–590.



- [BHS09] Patricia Ben-Horin and Moshe Shoham. “Application of Grassmann—Cayley Algebra to Geometrical Interpretation of Parallel Robot Singularities”. In: *The International Journal of Robotics Research* 28.1 (2009), pp. 127–141.
- [Bon03] Ilian Bonev. *The True Origins of Parallel Robots, The Parallel Mechanisms Information Center (ParalleMIC)*. 2003. URL: <http://www.parallemic.org/Reviews/Review007p.html>.
- [BR79] Oene Bottema and Bernard Roth. *Theoretical Kinematics*. 1st. Dover Publications, Inc. New York, 1979, et al. ISBN: 0-486-66346-9.
- [BR99] Ilian A Bonev and Jeha Ryu. “Orientation workspace analysis of 6-DOF parallel manipulators”. In: *Proceedings of the ASME*. 1999.
- [BZG02] I.A. Bonev, D. Zlatanov., and C.M. Gosselin. “Advantages of the Modified Euler Angles in the Design and Control of PKMs”. In: *Parallel Kinematic Machines International Conference*. 2002, pp. 171–188.
- [BZG03] Ilian A. Bonev, Dimiter Zlatanov, and Clément M. Gosselin. “Singularity Analysis of 3-DOF Planar Parallel Mechanisms via Screw Theory”. In: *Journal of Mechanical Design* 125.3 (2003), pp. 573–581.
- [Cap67] K.L. Cappel. *Motion Simulator*. US Patent 3295224. 1967.
- [Car+10a] Stéphane Caro, Guillaume Moroz, Thibault Gayral, Damien Chablat, and Chao Chen. “Singularity Analysis of a Six-dof Parallel Manipulator using Grassmann-Cayley Algebra and Gröbner Bases”. In: *Proceedings of an International Symposium on the Occasion of the 25th Anniversary of the McGill University Centre for Intelligent Machines*. 11 pages. Montréal, Canada, Nov. 2010, pp. 341–352.
- [Car+10b] Stéphane Caro, Waseem Ahmad Khan, Damiano Pasini, and Jorge Angeles. “The rule-based conceptual design of the architecture of serial Schönflies-motion generators”. In: *Mechanism and Machine Theory* 45.2 (2010), pp. 251–260.
- [Car+14] L. Carbonari, M. Callegari, G. Palmieri, and M.-C. Palpacelli. “A new class of reconfigurable parallel kinematic machines”. In: *Mechanism and Machine Theory* 79 (2014), pp. 173–183.
- [Car+97] J.A. Carretero, M. Nahon, C.M. Gosselin, and B. Buckham. “Kinematic analysis of a three-dof parallel mechanism for telescope applications”. In: *Proceedings of the 1997 ASME Design Engineering Technical Conferences*. 1997.
- [Car+99] J. A. Carretero, R. P. Podhorodeski, M. A. Nahon, and C. M. Gosselin. “Kinematic Analysis and Optimization of a New Three Degree-of-Freedom Spatial Parallel Manipulator”. In: vol. 122. 1. ASME, 1999, pp. 17–24.
- [Car05] Marco Carricato. “Fully Isotropic Four-Degrees-of-Freedom Parallel Mechanisms for Schoenflies Motion.” In: *I. J. Robotic Res.* 24.5 (2005), pp. 397–414.
- [CC08] Michele Conconi and Marco Carricato. “A New Assessment of Singularities of Parallel Kinematic Chains”. In: *Advances in Robot Kinematics: Analysis and Design*. Ed. by Jadran Lenarčič and Philippe Wenger. Dordrecht: Springer Netherlands, 2008, pp. 3–12.
- [Cha+14] Damien Chablat, Ranjan Jha, Fabrice Rouillier, and Guillaume Moroz. “Workspace and joint space analysis of the 3-RPS parallel robot”. In: *ASME 2013 International Design Engineering Technical Conferences and Computers and Information in Engineering Conference*. Vol. 5A. 2014, pp. 1–10.

- [Cha90] S. Charentus. “Modélisation et commande d’un robot manipulateur redondant composé de plusieurs plate-formes.” PhD thesis. Université Paul Sabatier, Toulouse, 1990.
- [Che+95] H. H. Cheng, J. J. Lee, and R. Penkar. “Kinematics of a hybrid (parallel–serial) robot manipulator”. In: *International Journal of Robotics & Automation* 10.4 (1995), pp. 159–166.
- [Cla88] R. Clavel. “DELTA, a fast robot with parallel geometry”. In: *Proc of the 18th International Symposium on Industrial Robots*. Ed. by C. W. Burckhardt. New York: Springer-Verlag, 1988, pp. 91–100.
- [Cla90] R. Clavel. *Device for the Movement and Positioning of an Element in Space*. US Patent 4976582. 1990.
- [Cle69] M. Clemens. *Improvement in apparatus for transmitting rotary motion*. US Patent 96395. 1869.
- [CLO07] David A. Cox, John Little, and Donal O’Shea. *Ideals, Varieties, and Algorithms: An Introduction to Computational Algebraic Geometry and Commutative Algebra, Undergraduate Texts in Mathematics*. Secaucus, NJ, USA: Springer-Verlag New York, Inc., 2007.
- [CS04] Juan Cortés and Thierry Siméon. “Sampling-Based Motion Planning under Kinematic Loop-Closure Constraints”. In: *In 6th International Workshop on Algorithmic Foundations of Robotics*. Springer-Verlag, 2004, pp. 59–74.
- [CW98] D. Chablat and P. Wenger. “Working modes and aspects in fully parallel manipulators”. In: *Proceedings. 1998 IEEE International Conference on Robotics and Automation*. Vol. 3. 1998, 1964–1969 vol.3.
- [CZ14] Marco Carricato and Dimiter Zlatanov. “Persistent screw systems”. In: *Mechanism and Machine Theory* 73 (2014), pp. 296 –313.
- [CZL14] Gianmarc Coppola, Dan Zhang, and Kefu Liu. “A 6-DOF Reconfigurable Hybrid Parallel Manipulator”. In: *Robot. Comput.-Integr. Manuf.* 30.2 (Apr. 2014), pp. 99–106. ISSN: 0736-5845.
- [Dec+18] Wolfram Decker, Gert-Martin Greuel, Gerhard Pfister, and Hans Schönemann. *SINGULAR 4-1-1 — A computer algebra system for polynomial computations*. <http://www.singular.uni-kl.de>. 2018.
- [Die95] P. Dietmaier. “Simply overconstrained mechanisms with rotational joints”. Habilitation thesis. Graz University of Technology, 1995.
- [DRJ99] J. S. Dai and J. Rees Jones. “Mobility in Metamorphic Mechanisms of Foldable/Erectable Kinds”. In: *Journal of Mechanical Design* 121.3 (1999), pp. 375–382.
- [Duf82] J. Duffy. *The screw theory and its application*. Gainesville: Class note of University of Florida, 1982, p. 10.
- [Ebe07] David H. Eberly. “Chapter 15 - Intersection Methods”. In: *3D Game Engine Design (Second Edition)*. Ed. by David H. Eberly. Second Edition. The Morgan Kaufmann Series in Interactive 3D Technology. San Francisco: Morgan Kaufmann, 2007, pp. 681 –717. ISBN: 978-0-12-229063-3.

- [EK16] M. Reza Emami and Jason A. Kereluk. *System, method and computer program for autonomously emulating robot manipulators of continuously-varying configurations*. US Patent 9358687. 2016.
- [EULL02] I. Ebert-Uphoff, J. K. Lee, and H. Lipkin. “Characteristic tetrahedron of wrench singularities for parallel manipulators with three legs”. In: *Proceedings of the Institution of Mechanical Engineers, Part C: Journal of Mechanical Engineering Science* 216.1 (2002), pp. 81–93.
- [GA+08] Jaime Gallardo-Alvarado, Carlos R. Aguilar-Nájera, Luis Casique-Rosas, José M. Rico-Martínez, and Md. Nazrul Islam. “Kinematics and dynamics of 2(3-RPS) manipulators by means of screw theory and the principle of virtual work”. In: *Mechanism and Machine Theory* 43.10 (2008), pp. 1281–1294.
- [GA+15] Jaime Gallardo-Alvarado, Luciano Pérez-González, Gilberto Ruiz-Mondragón, Héctor Rojas-Garduño, and Antonio Tinoco-Villagómez. “Mobility and velocity analysis of a limited-dof series-parallel manipulator”. In: *Conference : XVII COMRob 2015, Mexican Robotics Congress*. 2015.
- [GA89] C. Gosselin and J. Angeles. “The Optimum Kinematic Design of a Spherical Three-Degree-of-Freedom Parallel Manipulator”. In: *Journal of Mechanisms, Transmissions, and Automation in Design* 111.2 (1989), pp. 202–207.
- [GA90] C. Gosselin and J. Angeles. “Singularity analysis of closed-loop kinematic chains”. In: *IEEE Transactions on Robotics and Automation* 6.3 (1990), pp. 281–290.
- [GOR08] Jaime Gallardo, Horacio Orozco, and José M. Rico. “Kinematics of 3-RPS parallel manipulators by means of screw theory”. In: *The International Journal of Advanced Manufacturing Technology* 36.5 (2008), pp. 598–605.
- [GW62] V.E. Gough and S.G. Whitehall. “Universal tyre test machine”. In: *Proceedings of the FISITA Ninth International Technical Congress*. 1962, pp. 117–137.
- [Gwi31] J.E. Gwinnett. *Amusement Device*. US Patent 1789680. 1931.
- [Hao+18] Guangbo Hao, Haiyang Li, Abhilash Nayak, and Stephane Caro. “Design of a Compliant Gripper With Multimode Jaws”. In: *Journal of Mechanisms and Robotics* 10.3 (2018), pp. 031005–031005–12.
- [Hao16] Guangbo Hao. “Mobility and Structure Re-Configurability of Compliant Mechanisms”. In: *Advances in Reconfigurable Mechanisms and Robots II*. Ed. by Xilun Ding, Xianwen Kong, and Jian S. Dai. Cham: Springer International Publishing, 2016, pp. 49–60.
- [HC10a] Jonathan B. Hopkins and Martin L. Culpepper. “Synthesis of multi-degree of freedom, parallel flexure system concepts via Freedom and Constraint Topology (FACT) – Part I: Principles”. In: *Precision Engineering* 34.2 (2010), pp. 259–270.
- [HC10b] Jonathan B. Hopkins and Martin L. Culpepper. “Synthesis of multi-degree of freedom, parallel flexure system concepts via freedom and constraint topology (FACT). Part II: Practice”. In: *Precision Engineering* 34.2 (2010), pp. 271–278.
- [He+16] Xiuyun He, Xianwen Kong, Guangbo Hao, and James Ritchie. “Design and Analysis of a New 7R Single-Loop Mechanism with 4R, 6R and 7R Operation Modes”. In: *Advances in Reconfigurable Mechanisms and Robots II*. Ed. by Xilun Ding, Xianwen Kong, and Jian S. Dai. Cham: Springer International Publishing, 2016, pp. 27–37.

- [Her+08] Alfonso Hernández, Oscar Altuzarra, Charles Pinto, and Enrique Amezua. “Transitions in the velocity pattern of lower mobility parallel manipulators”. In: *Mechanism and Machine Theory* 43 (2008), pp. 738–753.
- [HF95] Z. Huang and Y. Fang. “Motion Characteristics and Rotational Axis Analysis of Three DOF Parallel Robot Mechanisms”. In: *IEEE International Conference on Systems, Man and Cybernetics. Intelligent Systems for the 21st Century, Vancouver, BC, Canada, Oct. 22-25.* 1995, pp. 67–71. DOI: [10.1109/SMC.1995.492713](https://doi.org/10.1109/SMC.1995.492713).
- [HH16] Guangbo Hao and Ronan Brendan Hand. “Design and static testing of a compact distributed-compliance gripper based on flexure motion”. In: *Archives of Civil and Mechanical Engineering* 16.4 (2016), pp. 708–716. ISSN: 1644-9665.
- [HH17] Guangbo Hao and Xiuyun He. “Designing a monolithic tip-tilt-piston flexure manipulator”. In: *Archives of Civil and Mechanical Engineering* 17.4 (2017), pp. 871–879.
- [HK12] Guangbo Hao and Xianwen Kong. *Conceptual Design and Modelling of a Self-Adaptive Compliant Parallel Gripper for High-Precision Manipulation.* 2012.
- [HL15] Guangbo Hao and Haiyang Li. “Conceptual designs of multi-degree of freedom compliant parallel manipulators composed of wire-beam based compliant mechanisms”. In: *Proceedings of the Institution of Mechanical Engineers, Part C: Journal of Mechanical Engineering Science* 229.3 (2015), pp. 538–555.
- [HLK16] Guangbo Hao, Haiyang Li, and Richard C. Kavanagh. “Position-Space-Based Compliant Mechanism Reconfiguration Approach and Its Application in the Reduction of Parasitic Motion.” In: *ASME. J. Mech. Des.* 138.9 (2016), pp. 092301–092301–13.
- [HLYZ12] B. Hu, J. J. Yu L. Yi, and S. Zhuang. “Analyses of Inverse Kinematics, Statics and Workspace of a Novel 3-RPS-3-SPR Serial-Parallel Manipulator”. In: *Journal of Mechanical Engineering* 6.M1 (2012), pp. 65–72.
- [HMO13] Larry L. Howell, Spencer P. Magleby, and Brian M. Olsen(Editors). *Handbook of Compliant Mechanisms.* John Wiley & Sons Ltd., 2013. ISBN: 9781119953456.
- [Hop10] Jonathan B. Hopkins. “Design of flexure-based motion stages for mechatronic systems via freedom, actuation and constraint topologies (FACT).” PhD thesis. Massachusetts Institute of Technology, 2010.
- [How01] Larry L Howell. *Compliant mechanisms.* 2001.
- [HS08] Manfred L. Husty and Hans-Peter Schröcker. “A proposal for a new definition of the degree of freedom of a mechanism.” In: *Interdisciplinary Applications of Kinematics.* Ed. by A. Kecskeméthy, V. Potkonjak, and Müller V. Cham: Springer International Publishing, 2008, pp. 109–117.
- [HS10] Manfred L. Husty and Hans-Peter Schröcker. “Algebraic Geometry and Kinematics”. In: *Nonlinear Computational Geometry.* Ed. by Ioannis Z. Emiris, Frank Sottile, and Thorsten Theobald. NY: Springer New York, 2010, pp. 85–107. ISBN: 978-1-4419-0999-2.
- [HS13] Manfred L. Husty and Hans Peter Schröcker. “21st Century Kinematics”. In: ed. by J. Michael McCarthy. London: Springer-Verlag London, 2013. Chap. Kinematics and Algebraic Geometry, pp. 85–123.

- [Hu+12] Bo Hu, Jingjing Yu, Yi Lu, Chunping Sui, and Jianda Han. “Statics and Stiffness Model of Serial-Parallel Manipulator Formed by  $k$  Parallel Manipulators Connected in Series”. In: *Journal of Mechanisms and Robotics* 4.2 (2012), pp. 021012–021012–8.
- [Hu14] Bo Hu. “Formulation of unified Jacobian for serial-parallel manipulators”. In: *Robotics and Computer-Integrated Manufacturing* 30.5 (2014), pp. 460–467.
- [Hun83] K. H. Hunt. “Structural Kinematics of In-Parallel-Actuated Robot-Arms”. In: *Journal of Mechanisms, Transmissions, and Automation in Design*. ASME 105.4 (Dec. 1983), pp. 705–712.
- [Hun87] K. H. Hunt. *Kinematic Geometry of Mechanisms*. Clarendon Press, 1987.
- [Hus+07] Manfred L. Husty, Martin Pfurner, Hans-Peter Schröcker, and Katrin Brunthaler. “Algebraic Methods in Mechanism Analysis and Synthesis”. In: *Robotica* 25.6 (Nov. 2007), pp. 661–675.
- [Hus+97] Manfred Husty, Adolf Karger, Hans Sachs, and Waldemar Steinhilper. *Kinematik und Robotik*. 1st. Springer Berlin Heidelberg New York, 1997, et. al. ISBN: 978-3-642-63822-0.
- [IW05] Carlo Innocenti and Philippe Wenger. “Position Analysis of the RRP-3(SS) Multi-Loop Spatial Structure”. In: *Journal of Mechanical Design* 128.1 (2005), pp. 272–278.
- [JT02] Sameer A. Joshi and Lung-Wen Tsai. “Jacobian Analysis of Limited-DOF Parallel Manipulators”. In: *Journal of Mechanical Design* 124.2 (2002), pp. 254–258.
- [Kal+15] Rohit Kalla, Latifah Nurahmi, Sandipan Bandyopadhyay, Stéphane Caro, and Philippe Wenger. “A Study of  $\Sigma^2$  Singularities in the 3-RPS Parallel Manipulator.” In: *2nd International and 17th National Conference on Machines and Mechanisms, India*. 2015.
- [Kan+09] Daniel Kanaan, Philippe Wenger, Stéphane Caro, and Damien Chablat. “Singularity Analysis of Lower-Mobility Parallel Manipulators Using Grassmann-Cayley Algebra”. In: *IEEE Transactions on Robotics* 25.5 (Oct. 2009), pp. 995–1004.
- [Kar03] M. Karouia. “Conception structurale de mecanismes parallèles sphériques”. PhD thesis. Ecole Centrale de Paris, 2003.
- [KG07] Xianwen Kong and Clément Gosselin. *Type Synthesis of Parallel Mechanisms*. *Springer Tracts in Advanced Robotics*. Ed. by Frans Groen Bruno Siciliano Oussama Khatib. Vol. 33. Springer Berlin Heidelberg New York, 2007, p. 26.
- [KGR06] Xianwen Kong, Clément M. Gosselin, and Pierre-Luc Richard. *Type Synthesis of Parallel Mechanisms With Multiple Operation Modes*. 2006.
- [Kha+07] W. A. Khan, S. Caro, J. Angeles, and D. Pasini. *A Formulation of Complexity-Based Rules for the Preliminary Design Stage of Robotic Architectures*, *International Conference on Engineering Design, ICED07, August 28-31, Paris*. France, 2007.
- [KMK08] Charles J. Kim, Yong-Mo Moon, and Sridhar Kota. “A Building Block Approach to the Conceptual Synthesis of Compliant Mechanisms Utilizing Compliance and Stiffness Ellipsoids”. In: *Journal of Mechanical Design* 130.2 (2008), pp. 022308–022308–11.

- [Kon14] Xianwen Kong. “Reconfiguration analysis of a 3-DOF parallel mechanism using Euler parameter quaternions and algebraic geometry method”. In: *Mechanism and Machine Theory* 74 (2014), pp. 188–201. ISSN: 0094-114X.
- [LB08] Xin-Jun Liu and Ilian A. Bonev. “Orientation Capability, Error Analysis, and Dimensional Optimization of Two Articulated Tool Heads With Parallel Kinematics”. In: *Journal of Manufacturing Science and Engineering* 130.1 (2008), pp. 011015–011015–9.
- [LH03] Q. C. Li and Z. Huang. “A Family of Symmetrical Lower-Mobility Parallel Mechanisms with Spherical and Parallel Subchains”. In: *Journal of Robotic Systems* 20.6 (2003), pp. 297–305.
- [LH10] Qinchuan Li and Jacques Marie Hervé. “1T2R parallel mechanisms without parasitic motion”. In: *IEEE Transactions on Robotics* 26.3 (2010), pp. 401–410.
- [LH15] Haiyang Li and Guangbo Hao. “Compliant Mechanism Reconfiguration Based on Position Space Concept for Reducing Parasitic Motion.” In: *ASME. International Design Engineering Technical Conferences and Computers and Information in Engineering Conference*. Vol. 5A. 39th Mechanisms and Robotics Conference. 2015, pp. 475–489.
- [LHY09] Yi Lu, Bo Hu, and JianPing Yu. “Analysis of kinematics/statics and workspace of a 2(SP+SPR+SPU) serial-parallel manipulator”. In: *Multibody System Dynamics* 21.4 (2009), p. 361.
- [Li+11] Qinchuan Li, Zhi Chen, Qiaohong Chen, Chuanyu Wu, and Xudong Hu. “Parasitic motion comparison of 3-PRS parallel mechanism with different limb arrangements”. In: *Robotics and Computer-Integrated Manufacturing* 27.2 (2011), pp. 389–396.
- [LR14] Juan David López and Carlos Francisco Rodríguez. “Design of a Boat Simulator Using Two Parallel Manipulators”. In: *Proceedings of ASME 2014 International Mechanical Engineering Congress and Exposition IMECE, November 14-20, 2014, Montreal, Canada*. 46476. 2014, V04AT04A030.
- [LS88] K. M. Lee and D. K. Shah. “Kinematic analysis of a three-degrees-of-freedom in-parallel actuated manipulator”. In: *IEEE Journal on Robotics and Automation* 4.3 (1988), pp. 354–360.
- [Man+13] Tom Mannheim, Martin Riedel, Mathias Hüsing, and Burkhard Corves. “A New Way of Grasping: PARAGRIP—The Fusion of Gripper and Robot”. In: *Grasping in Robotics*. Ed. by Giuseppe Carbone. London: Springer London, 2013, pp. 433–464.
- [McC86] J.M. McCarthy. “Kinematic Mapping and Robotics”. In: *International Conference on Robotics and Automation*. Vol. 20. IEEE, 1986, pp. 1168–1173.
- [Mer10] J. P. Merlet. *Parallel Robots*. 2nd. Springer Publishing Company, Incorporated, 2010. ISBN: 9048170532, 9789048170531.
- [Mer89] Jean-Pierre Merlet. “Singular configurations of parallel manipulators and grassmann geometry”. In: *Geometry and Robotics*. Ed. by J. D. Boissonnat and J. P. Laumond. Berlin, Heidelberg: Springer Berlin Heidelberg, 1989, pp. 194–212.
- [MG08] Jean Pierre Merlet and Clement Gosselin. *Handbook of Robotics*. Springer, Heidelberg, 2008.

- [MHM04] Christopher A. Mattson, Larry L. Howell, and Spencer P. Magleby. “Development of Commercially Viable Compliant Mechanisms Using the Pseudo-Rigid-Body Model: Case Studies of Parallel Mechanisms”. In: *Journal of Intelligent Material Systems and Structures* 15.3 (2004), pp. 195–202.
- [MNC16] Sidharth Maraje, Latifah Nurahmi, and Stéphane Caro. “Operation Modes Comparison of a Reconfigurable 3-PRS Parallel Manipulator based on Kinematic Performance.” In: *Proceedings of the ASME 2016 International Design Engineering Technical Conferences and Computers and Information in Engineering Conference*. 2016, pp. 21–24.
- [MR95] C. Mavroidis and B. Roth. “Analysis of Overconstrained Mechanisms”. In: *Journal of Mechanical Design* 117.1 (1995), pp. 69–74.
- [Nad13] Oriol Bohigas Nadal. “Numerical Computation and Avoidance of Manipulator Singularities”. PhD thesis. Universitat Politècnica de Catalunya, 2013.
- [Nay+17a] Abhilash Nayak, Haiyang Li, Guangbo Hao, and Stéphane Caro. “A Reconfigurable Compliant Four-Bar Mechanism with Multiple Operation Modes”. In: *The ASME 2017 International Design Engineering Technical Conferences & Computers and Information in Engineering Conference IDETC/CIE 2017*. Cleveland, United States, Aug. 2017. URL: <https://hal.archives-ouvertes.fr/hal-01757797>.
- [Nay+17b] Abhilash Nayak, Latifah Nurahmi, Philippe Wenger, and Stéphane Caro. “Comparison of 3-RPS and 3-SPR Parallel Manipulators Based on Their Maximum Inscribed Singularity-Free Circle”. In: *New Trends in Mechanism and Machine Science: Theory and Industrial Applications*. Ed. by Philippe Wenger and Paulo Flores. Springer International Publishing, 2017, pp. 121–130. ISBN: 978-3-319-44156-6.
- [Nay+18] Abhilash Nayak, Thomas Stigger, Manfred L. Husty, Philippe Wenger, and Stéphane Caro. “Operation Mode Analysis of 3-RPS Parallel Manipulators based on their Design Parameters”. In: *Computer Aided Geometric Design: Special Issue on New Progress in Geometry for Applications*. Ed. by Miroslav Lávička, Maria Lucia Sampoli, and Hans-Peter Schröcker. 2018.
- [NC15] Latifah Nurahmi and Stéphane Caro. “Dimensionally Homogeneous Extended Jacobian and Condition Number.” In: *The 2nd International Conference on Mechanical Engineering (ICOME 2015)*. 2015, pp. 3–5.
- [NCW15a] Latifah Nurahmi, Stéphane Caro, and Philippe Wenger. “Operation Modes and Singularities of 3-PRS Parallel Manipulators With Different Arrangements of P-Joints”. In: *ASME 2015 International Design Engineering Technical Conferences and Computers and Information in Engineering Conference*. American Society of Mechanical Engineers. 2015, V05CT08A015–V05CT08A015.
- [NCW15b] Latifah Nurahmi, Stéphane Caro, and Philippe Wenger. “Design of 3-RPS Parallel Manipulators based on Operation Modes”. In: *Proceedings of the 14th IFTOMM World Congress, October 25-30, 2015, Taipei, Taiwan*. IFTOMM, 2015.
- [NCW18a] Abhilash Nayak, Stéphane Caro, and Philippe Wenger. “A Dual Reconfigurable 4-rRUU Parallel Manipulator”. In: *The 4th IEEE/IFTOMM International conference on Reconfigurable Mechanisms and Robots (ReMAR2018)*. Delft, Netherlands, 2018.

- [NCW18b] Abhilash Nayak, Stéphane Caro, and Philippe Wenger. “Comparison of 3-[PP]S Parallel Manipulators based on their Singularity Free Orientation Workspace, Parasitic Motions and Complexity”. In: *Mechanism and Machine Theory* 129 (2018), pp. 293–315.
- [NCW18c] Abhilash Nayak, Stéphane Caro, and Philippe Wenger. “Kinematic Analysis of the 3-RPS-3-SPR Series-Parallel Manipulator”. In: *Robotica* (2018), pp. 1–27.
- [NCW18d] Abhilash Nayak, Stéphane Caro, and Philippe Wenger. “Local and Full-Cycle Mobility Analysis of a 3-RPS-3-SPR Series-Parallel Manipulator”. In: *Computational Kinematics: Proceedings of the 7th International Workshop on Computational Kinematics that was held at Futuroscope-Poitiers, France, in May 2017*. Ed. by Saïd Zeghloul, Lotfi Romdhane, and Med Amine Laribi. Cham: Springer International Publishing, 2018, pp. 499–507.
- [NG18] Latifah Nurahmi and Dongming Gan. “Workspace transition of 3-rRPS metamorphic parallel mechanism in hyperboloid configuration”. In: *The ASME 2018 International Design Engineering Technical Conferences & Computers and Information in Engineering Conference IDETC/CIE 2018*. Quebec, Canada, Aug. 2018.
- [Nur+14] Latifah Nurahmi, Josef Schadlbauer, Manfred Husty, Philippe Wenger, and Stéphane Caro. “Kinematic Analysis of the 3-RPS Cube Parallel Manipulator. International Design Engineering Technical Conferences and Computers and Information in Engineering Conference”. In: *38th Mechanisms and Robotics Conference*. Vol. 5B. 2014. ISBN: 123-234-345-6.
- [Nur+15] Latifah Nurahmi, Josef Schadlbauer, Stéphane Caro, Manfred Husty, and Philippe Wenger. “Kinematic Analysis of the 3-RPS Cube Parallel Manipulator”. In: *Journal of Mechanisms and Robotics* 7.1 (2015), pp. 011008–011008–11.
- [Nur+16] Latifah Nurahmi, Stéphane Caro, Philippe Wenger, Josef Schadlbauer, and Manfred Husty. “Reconfiguration analysis of a 4-RUU parallel manipulator”. In: *Mechanism and Machine Theory* 96, Part 2 (2016), pp. 269–289.
- [Nur15] Latifah Nurahmi. “Kinematic analysis and design of parallel manipulators with multiple operation modes”. PhD thesis. Ecole Centrale de Nantes, 2015.
- [Ols+10] Brian M. Olsen, Yanal Issac, Larry L. Howell, and Spencer P. Magleby. “Utilizing a Classification Scheme to Facilitate Rigid-Body Replacement for Compliant Mechanism Design.” In: *ASME. International Design Engineering Technical Conferences and Computers and Information in Engineering Conference*. Vol. 2. 34th Annual Mechanisms and Robotics Conference, Parts A and B. 2010, pp. 475–489.
- [PBK96] Christiaan J. J. Paredis, H. Benjamin Brown, and Pradeep K. Khosla. “A rapidly deployable manipulator system”. In: *Robotics and Autonomous Systems* 21 (1996), pp. 289–304.
- [PC07] Geoffrey Pond and Juan A. Carretero. “Quantitative dexterous workspace comparison of parallel manipulators”. In: *Mechanism and Machine Theory* 42.10 (2007), pp. 1388–1400.
- [Pfu06] Martin Pfurner. “Analysis of spatial serial manipulators using kinematic mapping”. Doctoral Thesis. University Innsbruck, 2006, p. 153.
- [Phi84] Jack Phillips. *Freedom in machinery*. Cambridge: Cambridge University Press, 1984, pp. 6,10.



- [Plu65] J. Plucker. “On a New Geometry of Space”. In: *Philosophical Transactions of the Royal Society of London* 155 (1865), pp. 725–791.
- [Pol42] WLG Pollard. *Spray painting machine*. US Patent 2213108. 1942.
- [PW01] Helmut Pottmann and Johannes Wallner. *Computational Line Geometry*. Springer-Verlag New York, Inc., 2001.
- [Rom99] L Romdhane. “Design and analysis of a hybrid serial-parallel manipulator”. In: *Mechanism and Machine Theory* 34.7 (1999), pp. 1037–1055.
- [Rot67] B. Roth. “On the screw axes and other special lines associated of a rigid body”. In: *J Eng Ind* 89 (1967), pp. 102–109.
- [Roz14] George IN Rozvany. *Topology optimization in structural mechanics*. Vol. 374. Springer, 2014.
- [RT18] Nicolas Rojas and Federico Thomas. “Forward Kinematics of the General Triple-Arm Robot Using a Distance-Based Formulation”. In: *Computational Kinematics*. Ed. by Saïd Zegloul, Lotfi Romdhane, and Med Amine Laribi. Cham: Springer International Publishing, 2018, pp. 257–264.
- [Rub+14a] Lennart Rubbert, Pierre Renaud, Stéphane Caro, and Jacques Gangloff. “Design of a compensation mechanism for an active cardiac stabilizer based on an assembly of planar compliant mechanisms”. In: *Mechanics & Industry* 15.2 (2014), pp. 147–151.
- [Rub+14b] Lennart Rubbert, Stéphane Caro, Jacques Gangloff, and Pierre Renaud. “Using Singularities of Parallel Manipulators for Enhancing the Rigid-body Replacement Design Method of Compliant Mechanisms”. In: *ASME Journal of Mechanical Design* 136 (2014), pp. 051010–1–051010–9.
- [SB13] R. Arun Srivatsan and Sandipan Bandyopadhyay. “On the position kinematic analysis of MaPaMan: a reconfigurable three-degrees-of-freedom spatial parallel manipulator”. In: *Mechanism and Machine Theory* 62 (2013), pp. 150–165.
- [Sch+13] J. Schadlbauer, M.L. Husty, S. Caro, and P. Wenger. “Self-Motions of 3-RPS Manipulators”. In: *Frontiers of Mechanical Engineering*. Serie 8(1) (2013), pp. 62–69.
- [Sch+14] J. Schadlbauer, D.R. Walter, M.L. Husty, J. Schadlbauer, D.R. Walter, and M.L. Husty. “The 3-RPS parallel manipulator from an algebraic viewpoint”. In: *Mechanism and Machine Theory* 75.Complete (2014), pp. 161–176.
- [Sch+15] Josef Schadlbauer, Latifah Nurahmi, Manfred Husty, Philippe Wenger, and Stéphane Caro. “Operation Modes in Lower-Mobility Parallel Manipulators”. In: *Interdisciplinary Applications of Kinematics: Proceedings of the International Conference, Lima, Peru, September 9-11, 2013*. Ed. by Andrés Kecskeméthy and Francisco Geu Flores. Cham: Springer International Publishing, 2015, pp. 1–9. ISBN: 978-3-319-10723-3.
- [Sch14] Josef Schadlbauer. “Algebraic Methods in Kinematics and Line Geometry”. PhD thesis. University of Innsbruck, 2014.
- [SF07] C. Stechert and H. J. Franke. “Requirement-oriented Configuration of Parallel Robotic Systems”. In: *The Future of Product Development*. Ed. by Frank-Lothar Krause. Berlin, Heidelberg: Springer Berlin Heidelberg, 2007, pp. 259–268.

- [SH18] Thomas Stigger and Manfred L. Husty. “Constraint Equations of Inverted Kinematic Chains”. In: *Computational Kinematics*. Ed. by Saïd Zeghloul, Lotfi Romdhane, and Med Amine Laribi. Cham: Springer International Publishing, 2018, pp. 491–498.
- [Sha95] M. Shahinpoor. “Kinematics of a parallel-serial (Hybrid) manipulator”. In: *Journal of Robotic Systems* 9.1 (1995), pp. 17–36.
- [SL04a] R. M. Setchi and N. Lagos. “Reconfigurability and reconfigurable manufacturing systems: state-of-the-art review”. In: *Industrial Informatics, 2004. INDIN '04. 2004 2nd IEEE International Conference on*. 2004, pp. 529–535.
- [SL04b] PKMtricept SL. <http://www.pkmtricept.com/empresa/index.php?id=en>. 2004.
- [SPH19] Thomas Stigger, Martin Pfulner, and Manfred Husty. “Workspace and Singularity Analysis of a 3-RUU Parallel Manipulator”. In: *EuCoMeS 2018*. Ed. by Burkhard Corves, Philippe Wenger, and Mathias Hüsing. Cham: Springer International Publishing, 2019, pp. 325–332.
- [Ste65] D. Stewart. “A Platform with Six Degrees of Freedom”. In: *Proceedings of the Institution of Mechanical Engineers* 180.1 (1965), pp. 371–386.
- [Sti+19] Thomas Stigger, Abhilash Nayak, Stéphane Caro, Philippe Wenger, Martin Pfulner, and Manfred L. Husty. “Algebraic Analysis of a 3-RUU Parallel Manipulator”. In: *Advances in Robot Kinematics 2018*. Ed. by Jadran Lenarcic and Vincenzo Parenti-Castelli. Cham: Springer International Publishing, 2019, pp. 141–149.
- [SWH12] J. Schadlbauer, D.R. Walter, and M.L. Husty. “A complete kinematic analysis of the 3-RPS parallel manipulator”. In: *Machines and Mechanisms*. Narosa Publishing House, New Delhi, India, 2012, pp. 410–419. ISBN: 978-81-8487-192-0.
- [SZ95] Shin-Min Song and Ming-Dons Zhang. “A Study of Reactional Force Compensation Based on Three-Degree-of Freedom Parallel Platforms”. In: *Journal of Robotic Systems* 12.12 (1995), pp. 783–794.
- [Tan00] Tanio K Tanev. “Kinematics of a hybrid (parallel–serial) robot manipulator”. In: *Mechanism and Machine Theory* 35.9 (2000), pp. 1183–1196.
- [Tet+16] Halil Tetik, Rohit Kalla, Gokhan Kiper, and Sandipan Bandyopadhyay. “Position Kinematics of a 3-RRS Parallel Manipulator”. In: *ROMANSY 21 - Robot Design, Dynamics and Control: Proceedings of the 21st CISM-IFTOMM Symposium, June 20-23, Udine, Italy*. Ed. by Vincenzo Parenti-Castelli and Werner Schiehlen. Cham: Springer International Publishing, 2016, pp. 65–72.
- [TGK99] HK Tönshoff, H Grendel, and R Kaak. “Structure and characteristics of the hybrid manipulator Georg V”. In: *Parallel Kinematic Machines*. Springer, 1999, pp. 365–376.
- [Tho88] G. S. Thornton. “The GEC Tetrabot—a new serial-parallel assembly robot”. In: *Proceedings. 1988 IEEE International Conference on Robotics and Automation*. 1988, 437–439 vol.1.
- [TJ01] L. W. Tsai and S. Joshi. “Comparison study of architectures of four 3 degree-of-freedom translational parallel manipulators”. In: *Proceedings 2001 ICRA. IEEE International Conference on Robotics and Automation (Cat. No.01CH37164)*. Vol. 2. 2001, 1283–1288 vol.2.

- [Tos+10] D. Tosi, G. Legnani, N. Pedrocchi, P. Righettini, and H. Giberti. “Cheope: A new reconfigurable redundant manipulator”. In: *Mechanism and Machine Theory* 45.4 (2010), pp. 611–626.
- [Tsa96] Lung-Wen Tsai. “Kinematics of A Three-Dof Platform with Three Extensible Limbs”. In: *Recent Advances in Robot Kinematics*. Ed. by Jadran Lenarčič and Vincenzo Parenti-Castelli. Dordrecht: Springer Netherlands, 1996, pp. 401–410. ISBN: 978-94-009-1718-7.
- [Tsa99] L.-W. Tsai. *Robot Analysis*. John Wiley and Sons, Inc., 1999.
- [Ver+09] D. Verde, S. D. Stan, M. Manic, R. Balan, and V. Matie. “Kinematics analysis, workspace, design and control of 3-RPS and TRIGLIDE medical parallel robots”. In: *2009 2nd Conference on Human System Interactions*. 2009, pp. 103–108.
- [Wah02] Joachim Wahl. *Articulated tool head*. US Patent 6,431,802. 2002.
- [Wal66] K. J. Waldron. “The constraint analysis of mechanisms”. In: *Journal of mechanisms* (1966), pp. 101–114.
- [WC98] Philippe Wenger and Damien Chablat. “Workspace and Assembly modes in Fully-Parallel Manipulators : A Descriptive Study”. In: *ARK*. Austria: Kluwer Academic Publishers, 1998, pp. 117–126.
- [Wei35] E. A. Weiss. *Einführung in die Liniengeometrie und Kinematik*. B. G. Teubner, Leipzig, 1935.
- [WH10] Dominic R. Walter and Manfred L. Husty. “On Implicitization of Kinematic Constraint Equations”. In: *Machine Design and Research* 26 (2010), pp. 218–226.
- [WH11] Dominic R. Walter and Manfred L. Husty. “Kinematic Analysis of the TSAI-3UPU Parallel Manipulator using Algebraic Methods”. In: *Thirteenth World Congress in Mechanism and Machine Science, Guanajuato, México*. 2011, pp. 1–9.
- [WHP09] Dominic R. Walter, Manfred L. Husty, and Martin Pfulner. “A complete kinematic analysis of the SNU 3-UPU parallel robot”. In: *Contemporary Mathematics* 496 (2009), p. 331.
- [Woh96] Karl Wohlhart. “Kinematotropic Linkages”. In: *Recent Advance in Robot Kinematics*. Ed. by Jadran Lenarčič and Vincenzo Parenti-Castelli. Springer Netherlands, 1996, pp. 359–368.
- [WRR89] K. J. Waldron, M. Raghavan, and B. Roth. “Kinematics of a Hybrid Series-Parallel Manipulation System”. In: *Journal of Dynamic Systems, Measurement, and Control* 111.2 (1989), pp. 211–221.
- [Yan+11] G. Yang, T. J. Teo, I. M. Chen, and W. Lin. “Analysis and design of a 3-DOF flexure-based zero-torsion parallel manipulator for nano-alignment applications”. In: *2011 IEEE International Conference on Robotics and Automation*. 2011, pp. 2751–2756.
- [ZBG02a] Dimitar Zlatanov, Ilian A. Bonev, and Clément M. Gosselin. “Constraint Singularities as C-Space Singularities”. In: *Advances in Robot Kinematics: Theory and Applications*. Ed. by J. Lenarčič and F. Thomas. Dordrecht: Springer Netherlands, 2002, pp. 183–192.

- [ZBG02b] Dimiter Zlatanov, Ilian A Bonev, and Clement M Gosselin. “Constraint singularities of parallel mechanisms”. In: *2002 IEEE International Conference on Robotics and Automation (ICRA’02)*. Vol. 1. IEEE. 2002, pp. 496–502.
- [ZBL04] XZ Zheng, HZ Bin, and YG Luo. “Kinematic analysis of a hybrid serial-parallel manipulator”. In: *The International Journal of Advanced Manufacturing Technology* 23.11-12 (2004), pp. 925–930.
- [ZBY12] Hongzhe Zhao, Shusheng Bi, and Jingjun Yu. “A novel compliant linear-motion mechanism based on parasitic motion compensation”. In: *Mechanism and Machine Theory* 50 (2012), pp. 15–28. ISSN: 0094-114X.
- [ZD09] Liping Zhang and Jian S Dai. “An overview of the development on reconfiguration of metamorphic mechanisms”. In: *Reconfigurable Mechanisms and Robots, 2009. ReMAR 2009. ASME/IFTOMM International Conference on*. IEEE. 2009, pp. 8–12.
- [ZFB95a] D. Zlatanov, R. G. Fenton, and B. Benhabib. “A Unifying Framework for Classification and Interpretation of Mechanism Singularities”. In: *Journal of Mechanical Design* 117.4 (1995), pp. 566–572.
- [ZFB95b] D. Zlatanov, R. G. Fenton, and B. Benhabib. “Identification and Classification of the Singular Configurations of Mechanisms”. In: *Computational Kinematics ’95*. Ed. by Jean-Pierre Merlet and Bahram Ravani. Dordrecht: Springer Netherlands, 1995, pp. 163–172.
- [ZMG09] P. J. Zsombor-Murray and A. Gferrer. *On Three-Legged Six Degree of Freedom Double Triangular Manipulator Direct Kinematics*. 2009.
- [ZS94] C. Zhang and S-M. Song. “Geometry and Position Analysis of a Novel Class of Hybrid Manipulators.” In: *ASME. International Design Engineering Technical Conferences and Computers and Information in Engineering Conference*. 1994, pp. 1–9.
- [ZZM06] Matteo Zoppi, Dimiter Zlatanov, and Rezia Molino. “On the velocity analysis of interconnected chains mechanisms”. In: *Mechanism and machine theory* 41.11 (2006), pp. 1346–1358.

---

**Titre :** L'analyse cinématique de manipulateurs parallèles et reconfigurables.

**Mots clés :** manipulateurs parallèles, manipulateurs série-parallèle, mécanismes conformes, transformation de Study, singularités.

**Résumé :** Un manipulateur parallèle à mobilité réduite a moins de six degrés de liberté et présente généralement différents types de mouvement connus sous le nom de modes d'opération.

Ainsi, ce type de manipulateur peut être classifié comme reconfigurable selon sa capacité de transition entre les différents modes d'opération. Cette thèse de doctorat s'articule principalement autour de l'analyse cinématique de manipulateurs parallèles à mobilité réduite, de manipulateurs parallèles en série obtenus à partir de leur empilement en série et de mécanismes conformes conçus à partir de leurs configurations singulières à contraintes.

La transformation cinématique de Study est utilisée pour dériver les équations algébriques de contraintes. Ensuite, elles sont interprétées à l'aide d'outils de géométrie algébrique pour effectuer des analyses de mobilité, de cinématique et de singularité. Les techniques de "screw theory" et "line geometry" sont utilisées à côté de l'approche algébrique au besoin.

---

**Title :** Kinematic analysis of reconfigurable parallel manipulators.

**Keywords :** parallel manipulators, series-parallel manipulators, compliant mechanisms, Study's kinematic mapping, singularities.

**Abstract :** A lower mobility parallel manipulator has less than six degrees of freedom and usually exhibits different motion types known as operation modes.

Thus, it can be classified as reconfigurable on account of its ability to transition between different operation modes. This doctoral thesis mainly revolves around the kinematic analysis of some lower-mobility parallel manipulators, series-parallel manipulators obtained from their serial stacking and compliant mechanisms designed using their constraint singular configurations.

Study's kinematic mapping is used to derive the algebraic constraint equations. They are further interpreted using algebraic geometry tools to perform mobility, kinematic and singularity analysis. Screw theory and line geometry techniques are used adjacent to algebraic approach wherever necessary.